

SEDIMENTOLOGY, STRATIGRAPHY, AND ORGANIC GEOCHEMISTRY OF THE  
RED PINE SHALE, UINTA MOUNTAINS, UTAH: A PROGRADING DELTAIC  
SYSTEM IN A MID-NEOPROTEROZOIC INTERIOR SEAWAY

by

Caroline A. Myer

A thesis submitted in partial fulfillment  
of the requirements for the degree

of

MASTER OF SCIENCE

in

Geology

Approved:

---

Dr. Carol M. Dehler  
Major Advisor

---

Dr. W. David Liddell  
Committee Member

---

Dr. Peter T. Kolesar  
Committee Member

---

Dr. Byron R. Burnham  
Dean of Graduate Studies

UTAH STATE UNIVERSITY

Logan, Utah

2008

## ABSTRACT

Sedimentology, Stratigraphy, and Organic Geochemistry of the Red Pine Shale,  
Uinta Mountains, Utah: A Prograding Deltaic System  
in a Mid-Neoproterozoic Interior Seaway

by

Caroline A. Myer, Master of Science

Utah State University, 2008

Major Professor: Dr. Carol M. Dehler

Department: Geology

The Red Pine Shale (RPS; ~1120m thick), uppermost formation of the Neoproterozoic Uinta Mountain Group, Utah, is an organic-rich sedimentary succession interpreted as a marine deltaic system that delivered immature sediment from the north that mixed with mature sediment from the east. Multiple data sets suggest regional climate and sea-level changes associated with changing organic-carbon burial rates.

Six facies were identified and represent wave-, tidal-, and river-influenced parts of the distal prodelta to delta front in a marine system. These include the shale facies and associated concretion facies (distal prodelta), the shale-sandstone facies (proximal prodelta to delta front), the slump fold facies (proximal prodelta to delta front), and the sandstone facies and associated pebbly sandstone facies (delta front).

C-isotope values from organic-rich shale range from -29.46‰ to -16.91‰ PDB and TOC values range from 0.04% to 5.91%. The composite C-isotope curve for the RPS shows less negative values near the base, followed by a long decline to a thick interval of lower values. Combined H/C, TOC, and local-regional isotopic correlations suggest that these values represent C-isotope composition of Neoproterozoic seawater.

Provenance data sets show two distinct detrital zircon signatures. An arkosic sample shows an Archean population, most likely from the Wyoming Craton to the north. Data from two quartz arenite samples show a mixed Proterozoic/Archean population from the east-southeast. Correlation of measured sections show north to south delta progradation with a proximal source to the north and a mature source to the east. The composite section comprises one low-order regressive cycle and ~11 high-order cycles.

There is a relationship between C-isotope values, shale geochemistry, and lithostratigraphy. Relatively positive C-isotope values correspond with increased kaolinite abundance and more distal depofacies indicating an increase in organic-carbon burial and chemical weathering rates, and a rise in sea level. Relatively negative C-isotope values correspond with lower kaolinite abundances and more proximal depofacies indicating a decrease in organic-carbon burial and chemical weathering rates, and sea-level fall. Similar relationships are seen in the correlative Chuar Group, Arizona, suggesting a regional or possibly global control on these related processes.

This paper meets the requirements to revise the RPS as a formalized unit in accordance with the Stratigraphic Code guidelines.

## ACKNOWLEDGMENTS

First of all I would like to thank my parents. My mom, Amelia Myer, has been a constant role model for me. Not only has she supported and loved me throughout my life, but she has also taught me how to support and love myself. From her I learned self-confidence. I would like to thank her for always encouraging me to be a strong and clever woman, like her. My dad, William Myer, has been my inspiration. Not only has he inspired me to be a science lover, but he has also inspired me to become a scientist. He taught me how to be happy in what I do, and, when there are hurdles to jump, he has taught me that family and a strong will can take me anywhere. I also want to thank Walt and Lil Gillette, my Georgetown family. They took care of me and gave me direction in so many ways. You were a comfort to me when I needed it the most. And thank you to Tanner. He has been an amazing companion and a good friend over the last few months.

Secondly, I would like to thank my advisor, Carol Dehler. Thank you for being so understanding of my bizarre schedule and of my distance from Utah. She has been a wonderful teacher and an inspiring woman scientist. Not only did I learn sedimentology from her, but I also learned how to live a cleaner, less wasteful, and healthier life. Thanks to Carol, I now reuse plastic bags until they fall apart. I would also like to thank Carol for the chance to come to Utah and work for her; otherwise I would never have met my husband. I am truly thankful for the opportunities you have given me, not only in my career, but in many other aspects of my life. Thank you to my committee members, Dave Liddell and Pete Kolesar, for taking the time to help me with me research and for working with my schedule. Thank you for your different points of view and input; my

thesis is a better and more interesting project because of your help.

Thirdly, I would like to thank my field assistants, Andy Brehm, Stephanie Davi, and Dan Rybczynski. Thank you, Andy, for taking time out from your own thesis writing to help me collect many, many bags of shale. Dan, you hiked over so many shaley slopes and under so many trees to help me in the field. Thank you for your hard work ethic and company. I would finally like to thank, Stephanie, for helping me carry sandstone samples and cooking amazing food for me. Thank you all for your assistance and friendship.

Finally, I would like to thank my best friends, Emily Myer and Andy Brehm. Emily has been a wonderful sister and friend and I know I could not have survived these last few years without her help. Thank you for your shoulder and your ear. I can always rely on you, comrade! Andy, my husband, I cannot thank enough for everything he has done for me. Thank you for being so patient with me and thank you for encouraging me to finish this work. You have supported me through many difficult times in our short time together, and I hope you know how that has helped me. I am a happier person because of you and I owe the completion of this thesis mostly to you.

Financial aid for this research was provided by the Geological Society of America, the Association of Women Geoscientists (Salt Lake City chapter), the Wyoming Geological Association, and the J. Stewart Williams Fellowship of the Utah State University Geology Department. Thank you also to the Department of Earth and Planetary Sciences at the University of New Mexico for use of their facilities.

Callie Myer

## CONTENTS

|                                                               | Page |
|---------------------------------------------------------------|------|
| ABSTRACT.....                                                 | ii   |
| ACKNOWLEDGMENTS.....                                          | iv   |
| LIST OF TABLES.....                                           | ix   |
| LIST OF FIGURES.....                                          | x    |
| CHAPTER                                                       |      |
| 1. INTRODUCTION AND GEOLOGIC BACKGROUND.....                  | 1    |
| 1.1 - Introduction and Significance.....                      | 1    |
| 1.2 - Geologic Background - The Uinta Mountain Group.....     | 4    |
| 1.3 - Geologic Background - Eastern Uinta Mountain Group..... | 5    |
| 1.4 - Western Uinta Mountain Group.....                       | 7    |
| 2. PREVIOUS WORK ON THE RED PINE SHALE.....                   | 10   |
| 2.1 - Stratigraphy and Mapping.....                           | 10   |
| 2.2 - Facies Analysis.....                                    | 11   |
| 2.3 - Depositional Environment.....                           | 12   |
| 2.4 - Age.....                                                | 13   |
| 2.5 - Correlations.....                                       | 14   |
| 2.6 - Geochemistry.....                                       | 15   |
| 2.7 - Paleontology.....                                       | 16   |
| 3. METHODS.....                                               | 18   |
| 3.1 - Field Methods.....                                      | 18   |
| 3.2 - Lab Methods.....                                        | 19   |

|    |                                                         |    |
|----|---------------------------------------------------------|----|
| 4. | FACIES ANALYSIS .....                                   | 21 |
|    | 4.1 - Introduction and Subdivision.....                 | 21 |
|    | 4.2 - Facies 1: Shale .....                             | 21 |
|    | 4.2.1 – Description .....                               | 21 |
|    | 4.2.2 – Interpretation.....                             | 27 |
|    | 4.3 - Facies 2: Concretion .....                        | 29 |
|    | 4.3.1 – Description .....                               | 29 |
|    | 4.3.2 – Interpretation.....                             | 30 |
|    | 4.4 - Facies 3: Shale-and-Sandstone .....               | 32 |
|    | 4.4.1 – Description .....                               | 32 |
|    | 4.4.2 – Interpretation.....                             | 34 |
|    | 4.5 - Facies 4: Slump fold .....                        | 35 |
|    | 4.5.1 – Description .....                               | 35 |
|    | 4.5.2 – Interpretation.....                             | 37 |
|    | 4.6 - Facies 5: Sandstone .....                         | 37 |
|    | 4.6.1 – Description .....                               | 37 |
|    | 4.6.2 – Interpretation.....                             | 41 |
|    | 4.7 - Facies 6: Pebbly sandstone .....                  | 42 |
|    | 4.7.1 – Description .....                               | 42 |
|    | 4.7.2 – Interpretation.....                             | 42 |
| 5. | GEOCHEMISTRY AND PETROGRAPHY RESULTS .....              | 46 |
|    | 5.1 - Trends in C-isotope and TOC Curves .....          | 46 |
|    | 5.2 - Petrographic Analysis and Sandstone Textures..... | 54 |
|    | 5.3 - Sandstone Composition and Petrographic Data ..... | 55 |
|    | 5.4 - Detrital Zircon Data.....                         | 57 |
| 6. | STRATIGRAPHIC RESULTS.....                              | 59 |
|    | 6.1 - Introduction and Study Sites.....                 | 59 |
|    | 6.2 - Physical and Chemical Stratigraphy.....           | 63 |
|    | 6.3 - Sequence Stratigraphy .....                       | 67 |

|    |                                                                |     |
|----|----------------------------------------------------------------|-----|
| 7. | DISCUSSION.....                                                | 70  |
|    | 7.1 - Paleogeography of the Red Pine Basin.....                | 70  |
|    | 7.2 - Controls on Cycles.....                                  | 74  |
|    | 7.3 - Controls on C-Isotope Composition and Stratigraphy ..... | 75  |
| 8. | CONCLUSIONS.....                                               | 80  |
|    | REFERENCES .....                                               | 82  |
|    | APPENDICES .....                                               | 89  |
|    | Appendix A: Geologic Maps of Measured Sections.....            | 90  |
|    | Appendix B: C-Isotope Data Tables .....                        | 97  |
|    | Appendix C: Raw Point Count Data Tables .....                  | 106 |
|    | Appendix D: Other Point Count Data Table.....                  | 119 |
|    | Appendix E: Detailed Stratigraphic Columns.....                | 123 |
|    | Appendix F: Measured Section Localities and Descriptions.....  | 199 |



## LIST OF TABLES

| Table |                                         | Page |
|-------|-----------------------------------------|------|
| 1     | Paleontology of Red Pine Shale.....     | 17   |
| 2     | Facies descriptions.....                | 22   |
| 3     | Ranges of C-isotope and TOC values..... | 46   |

## LIST OF FIGURES

| Figure |                                                                                                        | Page |
|--------|--------------------------------------------------------------------------------------------------------|------|
| 1      | Geologic map of the Uinta Mountains.....                                                               | 2    |
| 2      | Stratigraphic columns of the eastern and western Uinta Mountain Groups .....                           | 3    |
| 3a     | Ternary diagrams with normalized point count data from sandstone samples.....                          | 24   |
| 3b     | Ternary diagrams with normalized point count data from sandstone samples.....                          | 25   |
| 3c     | Ternary diagrams with normalized point count data from sandstone samples.....                          | 25   |
| 4      | Illustration showing facies positions in a deltaic setting.....                                        | 26   |
| 5      | Photograph of shale facies.....                                                                        | 28   |
| 6      | Photograph of Photograph of <i>Bavlinella faviolata</i> in concretion facies.....                      | 31   |
| 7      | Photograph of shale-and-sandstone facies.....                                                          | 33   |
| 8      | Photograph of slump fold facies.....                                                                   | 36   |
| 9      | Photograph showing planar-tabular foresets in the sandstone facies .....                               | 38   |
| 10     | Photomicrographs of sandstone facies.....                                                              | 39   |
| 11     | Photograph of accreted and amalgamated trough crossbeds in sandstone facies..                          | 40   |
| 12     | Photograph of pebbly sandstone facies.....                                                             | 43   |
| 13     | Stratigraphy, facies, C-isotope, TOC, and petrographic data for the type section.....                  | 47   |
| 14     | Stratigraphy, facies, C-isotope, TOC, and petrographic data for the Hades Creek composite section..... | 48   |
| 15     | Stratigraphy, facies, C-isotope, and petrographic data for the Ashley Creek section.....               | 49   |
| 16     | Stratigraphy, facies, C-isotope, and petrographic data for the Henry's Fork Creek section.....         | 50   |

|    |                                                                                                                        |    |
|----|------------------------------------------------------------------------------------------------------------------------|----|
| 17 | Photograph of partial Hades Creek sections that have been correlated to create composite Hades Creek section .....     | 61 |
| 18 | Correlation of type, Hades composite, Henry's Fork, and Ashley Creek measured sections.....                            | 64 |
| 19 | Correlation between the north and south flank measured sections (Hades Creek and type sections).....                   | 66 |
| 20 | Composite stratigraphic column, mineralogy, C-isotope, TOC, and sea level graphs of Red Pine Shale.....                | 69 |
| 21 | Paleogeographic model of Uinta Mountain and Big Cottonwood basin during deposition of the lower Red Pine sediment..... | 71 |
| 22 | Stratigraphy and C-isotope data from the Chuar Group and Uinta Mountain Group showing correlation.....                 | 77 |

## CHAPTER 1

### INTRODUCTION AND GEOLOGIC BACKGROUND

#### *1.1 – Introduction and Significance*

Recent Precambrian research has raised many questions about Neoproterozoic climate change, biologic evolution, and the rifting of Rodinia (e.g., Dalziel, 1997; Colpron et al., 2002; Hoffman and Schrag, 2002; Knoll, 2003). The ability to test current hypotheses begins with the fundamental understanding of Neoproterozoic successions that capture this time period. The Red Pine Shale of the Uinta Mountain Group is a mid-Neoproterozoic succession that records some of these phenomena and, at a minimum, the resulting data will contribute to an understanding of this unique time in Earth history.

The Red Pine Shale is the uppermost formation of the Neoproterozoic Uinta Mountain Group in northeastern Utah (Figs. 1 and 2) and is now measured to ~1120m thick. This unit is an organic-rich sedimentary succession that was formally named by Williams (1953), and, until now has not been formally described using Stratigraphic Code guidelines (NACSM, 1983). Nevertheless, a number of workers have studied the Red Pine Shale and interpreted it to represent a variety of depositional environments and paleogeographic settings.

The Uinta Mountains are an east-west trending range that spans about 190 km from northeastern Utah to northwestern Colorado (Fig. 1). They are flanked by the North Flank and South Flank fault systems, two Laramide-age high-angle reverse faults that have kilometers of displacement (Hansen, 1965; Wallace and Crittenden,

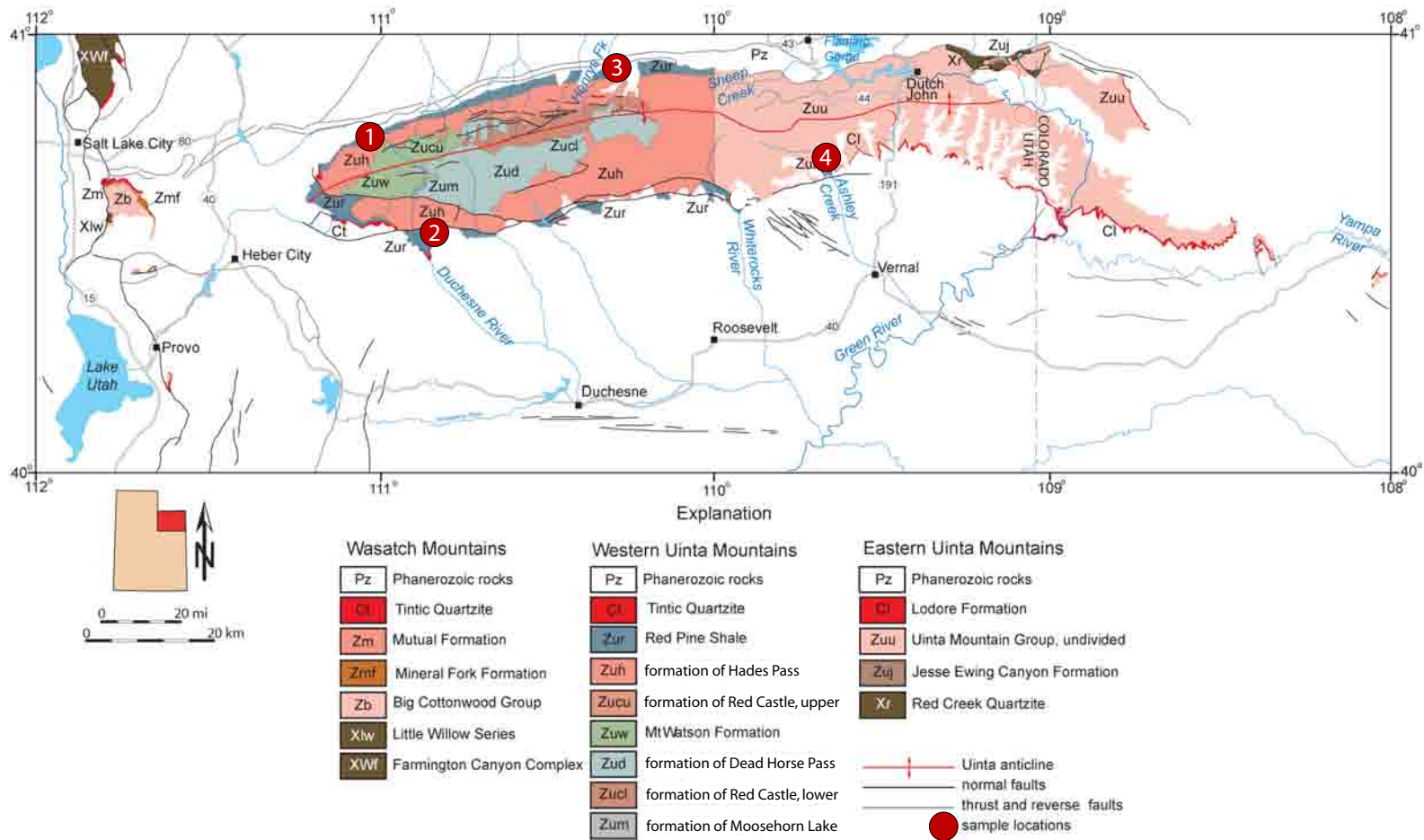


Figure 1. Geologic map of Uinta Mountains, northeastern Utah, showing mapped extent of Red Pine Shale and four study site locations. Site 1: type section and Mud Lake Flat Road section; Site 2: Hades Creek section; Site 3: Henry's Fork section; Site 4: Ashley Creek section. (Modified from Dehler et al., 2007)

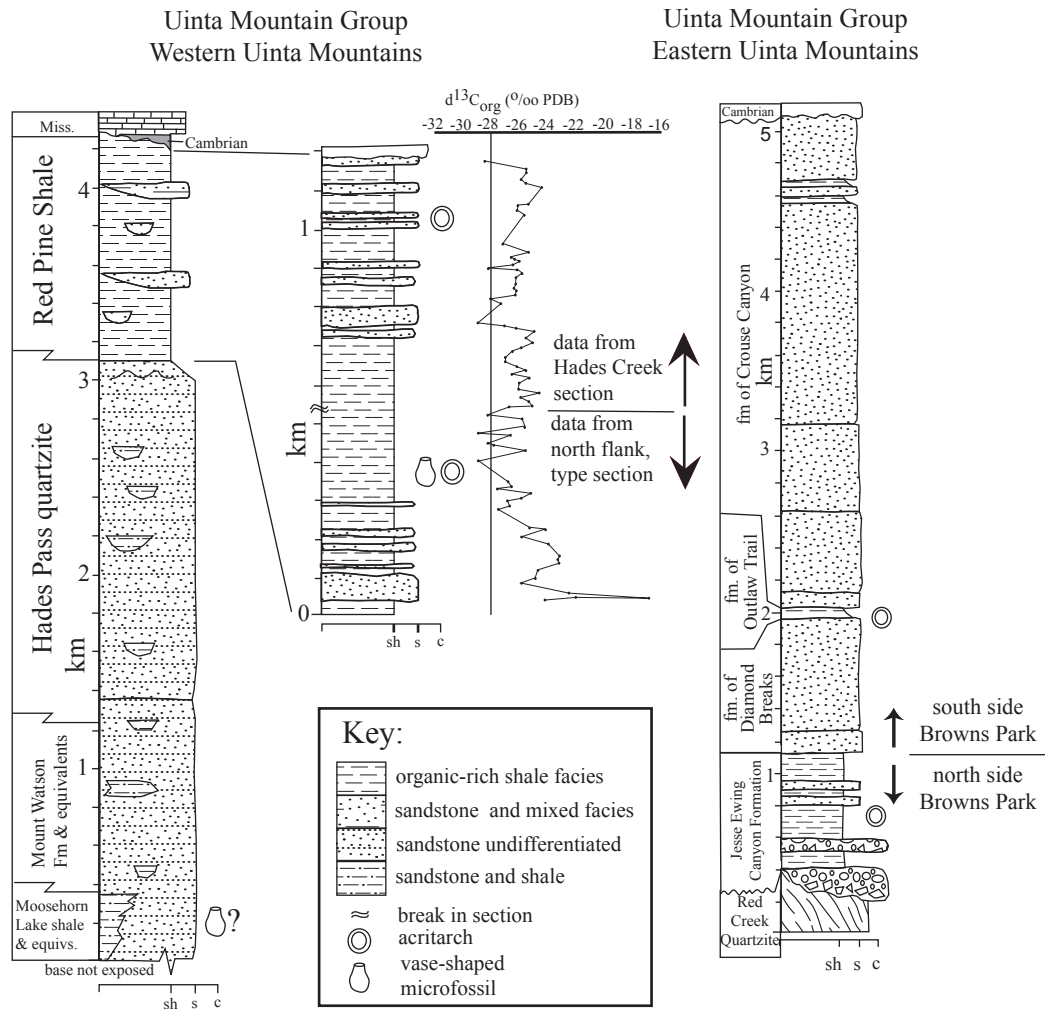


Figure 2. Stratigraphic columns of the eastern and western Uinta Mountain Groups and a more detailed composite section of the Red Pine Shale with corresponding C-isotope curve. Note that the Red Pine Shale composite section is from the two localities that will be the focus of this research. (Modified from Dehler et al., 2007)

1969). The related Uinta anticline spans the length of the range and is about 50 km wide (Hansen, 1965). The core of the Uinta Mountains is occupied by the Uinta Mountain Group. The Red Pine Shale has only been mapped in the western part of these mountains. East of 110° longitude this unit may undergo facies changes in combination with partial truncation by an angular unconformity and overlying Paleozoic units (Sprinkel, 2002; Kowallis, pers comm., 2008).

The objectives of this paper are twofold: to characterize and interpret the Red Pine Shale in detail using stratigraphy, facies analysis, geochemistry, and petrography; and to fulfill the requirements to revise the Red Pine Shale as a formal unit in accordance with the Stratigraphic Code (NACSM, 1983). In this paper, it is hypothesized that the Red Pine Shale represents a deltaic system in a marine intracratonic seaway at ~750 Ma. It is further hypothesized that this unit correlates with the Chuar Group and middle Pahrump Group, and perhaps the Big Cottonwood Formation (Dehler, 2008). Finally, it is suggested that this unit is important for continued studies on the Pre-Sturtian (~750 Ma) Earth system.

## ***1.2 – Geologic Background - The Uinta Mountain Group***

The Uinta Mountain Group is one of the few well preserved mid-Neoproterozoic successions in North America. It is a thick siliciclastic succession of mostly shale, sandstone, and orthoquartzite, yet is unmetamorphosed (Wallace and Crittenden, 1969). It is unclear how the eastern and western Uinta Mountain Group correlate, but it has been documented that strata in the northern part of the range are dominated by deposits derived from the Wyoming craton, and strata from the southern part are dominated by deposits

from Paleoproterozoic and Mesoproterozoic sources to the east (Fig. 2; e.g., Sanderson, 1984; Ball and Farmer, 1998; Condie et al., 2001; Mueller et al., 2007).

### ***1.3 - Geologic Background - Eastern Uinta Mountain Group***

The eastern Uinta Mountain Group is over 7 km thick and is separated from the western Uinta Mountain Group by latitude 110°W (Hansen, 1965). These strata have received less attention than the western Uinta Mountain Group, due to their apparent homogeneous sandy nature. The eastern Uinta Mountain Group unconformably rests on the Paleoproterozoic-Archean(?) Red Creek Quartzite metamorphic complex and is overlain by the Cambrian Lodore Formation (e.g., Sprinkel, 2002). The formations present on this side of the range include the basal Jesse Ewing Canyon Formation, the formations of Diamond Breaks, Outlaw Trail, and Crouse Canyon, and sections of undivided Uinta Mountain Group (Dehler and Sprinkel, 2005, and references therein).

The Jesse Ewing Canyon Formation is >1000 m thick (Brehm, 2007) and is the basal unit of the eastern Uinta Mountain Group, unconformably overlying the Red Creek Quartzite. It consists of two members: a lower member dominated by clast-supported conglomerate and breccia, and an upper member dominated by red to black shale with lesser mixed-composition arenite (Brehm, 2007). Sediment sources for this formation are to the north, east, and south (Sanderson and Wiley, 1986; Brehm, 2007). Fossils in the Jesse Ewing Canyon Formation include *Leiosphaeridia* sp. and filament fragments (Nagy and Porter, 2005; Sprinkel and Waanders, 2005). This unit is interpreted to represent alluvial fan and fan delta deposition along a wave-affected marine shoreline (Sanderson and Wiley, 1986; Dehler et al., 2007).



Conformably (?) above the Jesse Ewing Canyon Formation is ~6 km of undivided Uinta Mountain Group. This section consists of massive and crossbedded sandstone interbedded with intervals of red-to-green shale and conglomerate. This undifferentiated Uinta Mountain Group is interpreted to represent shallow marine to subaerial environments within a trough that was rapidly subsiding (Hansen, 1965).

In some areas, the undifferentiated Uinta Mountain Group has been subdivided into three informal units (DeGrey, 2005). The formation of Diamond Breaks is the lowermost unit and has been measured to between 500 and 1000m thick, though the base is not exposed. This unit is dominantly quartz arenite with lesser arkosic arenite, subarkosic arenite, and shale. It is conformably (?) overlain by the formation of Outlaw Trail and is considered to represent a braided river system flowing to the southwest. (DeGrey, 2005)

The formation of Outlaw Trail is a <300 m thick unit dominated by thick green to gray to red shale with subordinate sandstone intervals (DeGrey, 2005; Rybczynski, in prep). These shale intervals are laminated to thinly bedded and the interbeds of arkosic and quartz sandstone and siltstone exhibit thin to thick beds. Fossils include *Leiosphaeridia* sp. and filament fragments (Sprinkel and Waanders, 2005). It is interpreted to represent a fluvio-estuarine setting (Dehler et al., 2007; Rybczynski, in prep).

The formation of Crouse Canyon is estimated to be ~3200m to 5km thick (DeGrey and Dehler, 2005; Rybczynski, in prep). This formation is similar to the formation of Diamond Breaks and is suggested to represent a similar environment of deposition: a

braided river environment flowing to the southwest indicating an increase in energy from the formation of Outlaw Trail (De Grey, 2005)

#### ***1.4 - Western Uinta Mountain Group***

The western Uinta Mountain Group totals over 4 km thick and, although the base is not exposed, has been subdivided into 7 units (Fig. 2): the formation of Red Castle, the formation of Moosehorn Lake, the formation of Dead Horse Pass, the Mount Watson Formation, the formation of Hades Pass (Wallace, 1972; Sanderson, 1984), and the Red Pine Shale (Williams, 1953).

The basal unit of the western Uinta Mountain Group is the formation of Red Castle (~750). It is dominantly an arkosic arenite with lesser quartz and subarkosic arenite. Sedimentary structures include planar crossbeds, trough crossbeds, ripples, mudcracks, and mud chips. The formation of Red Castle is interpreted to represent a braided stream with sources from the north and east succeeded by a tidal system with flood tide paleoflow from the south (Wallace and Crittenden, 1969; Kingsbury, 2008). This unit is unconformably overlain by the formation of Deadhorse Pass, or possibly the Hades Pass quartzite, and possibly interfingers laterally with the formation of Moosehorn Lake (Kingsbury, 2008) The formation of Moosehorn Lake is ~150 to 300m thick and comprises green shale interbedded with pebbly to coarse-grained arkosic arenite. It contains ripples, soft sediment deformation, and mud cracks. This unit includes organic fragments and siliceous casts that are suggestive of vase-shaped microfossils, though they are not conclusive (Nyberg, 1982; Dehler et al., 2007). This unit is interpreted to represent various marine environments that laterally relate to the fluvial environment of

the formation of Red Castle (Wallace and Crittenden, 1969; Wallace, 1972).

The Mount Watson Formation is from 550 to 1000m thick and is dominantly quartz arenite with some subarkosic arenite, arkosic arenite, and green shale. The most common sedimentary structures are planar and trough cross-beds, soft sediment deformation, ripples, and parting lineations (Wallace and Crittenden, 1969). It has been interpreted to be fluvial (Sanderson, 1984) or a combination of fluvial, deltaic, and marine environments (Wallace and Crittenden, 1969; Wallace, 1972). The Mount Watson Formation grades laterally into the formation of Dead Horse Pass and grades upward (?) into the formation of Hades Pass (Wallace and Crittenden, 1969).

The formation of Dead Horse Pass is ~900m thick and comprises quartz arenite and orthoquartzite with lesser gray to red shale and siltstone. The most common sedimentary structures are trough and planar cross-beds, soft sediment deformation, ripples, and mudchips (Wallace, 1972), although hummocky-cross stratification and planar beds are also present (Kingsbury, 2008). To the west, this unit grades laterally into the Mount Watson Formation (Wallace, 1972). Similar to the Mount Watson Formation, the formation of Dead Horse Pass is interpreted to be a fluvial environment (Sanderson, 1984) or fluvial and marine (Wallace, 1972).

Overlying the formation of Red Castle, the Mount Watson Formation, and formation of Dead Horse Pass is the formation of Hades Pass. It is composed of quartz arenite, subarkosic arenite, and arkosic arenite with lesser shale intervals and ranges in thickness from 1825 to 3000m. This reddish sandstone is dominated by crossbedding and soft-sediment deformation (Wallace and Crittenden, 1969; Wallace, 1972). It is interpreted to

represent a fluvial environment with a dominantly eastern source (Wallace and Crittenden, 1969; Wallace, 1972), although it likely has a marginal marine component at the top due to the gradational upper contact with the hypothesized marine-deltaic Red Pine Shale (Dehler et al., 2007).

## CHAPTER 2

### PREVIOUS WORK ON THE RED PINE SHALE

#### *2.1 – Stratigraphy and mapping*

In 1953, Williams differentiated the Red Pine Shale from the Ophir shale, stating that it was upper Precambrian and not Cambrian. He based his decision upon finding an angular unconformity between the two shale units. Williams found a nice exposure that became the type section of this Precambrian shale in Red Pine Canyon, which is a tributary of Smith and Morehouse Creek. He formally named the Red Pine Shale based on this location.

In 1954, Larsen wrote a masters thesis on the Precambrian geology of the western Uinta Mountain, in which he compiled a history of research on the Red Pine Shale. He describes the stratigraphy of this unit and its relationships with adjacent units and also summarizes Williams' (1953) work and agreed with his findings. He reported a maximum thickness of the Red Pine Shale as >900m. Wallace and Crittenden (1969), also gave a general stratigraphic description of the Red Pine Shale and the adjacent units. They described the lower contact between the Red Pine Shale and what is now referred to as the Hades Pass quartzite, as gradational. They stated that the Red Pine Shale is the most likely Uinta Mountain Group unit to contain fossils. Then in 1972, Wallace produced a more detailed description of the stratigraphy of the Red Pine Shale and a new maximum thickness of 1830m. Wallace (1972) also mapped all known locations of the Red Pine Shale in the western Uinta Mountains. More recently, Bryant (1992) created a geologic map of the Salt Lake City 1° x 2° quadrangle. This included all locations of the

Red Pine Shale as well as a brief description of this unit; much of his mapping of the Uinta Mountain Group was based upon Wallace's original mapping. Sprinkel (2002) mapped the Red Pine Shale in the Dutch John 30° x 60° sheet, extending its known outcrop belt east of the 110°W longitude line, and as far east as Ashley Creek.

Dehler et al. (2007) studied the Red Pine Shale in reconnaissance fashion. The main two sections they studied were the type section (~550 m) and the Hades Creek locality (Fig. 1; Appendix A). This latter locale consists of five partial measured sections (upper Hades Creek, Hades Creek A, B, C, and lower Hades Creek) ranging from ~ 69 m to 370 m in thickness (Appendix A). Only the thickest partial section is used in the composite general section of Fig. 2. Other localities included in the reconnaissance work of Dehler et al., (2007) included: Ashley Creek, Henry's Fork (Fig. 1; Appendix A), and White Rocks canyon.

## ***2.2 - Facies Analysis***

Three main facies were proposed for the Red Pine Shale by Dehler et al. (2007). The first is a shale facies that consists of organic-rich gray to black siltshale, mudshale, and clayshale. This facies is between 1 and 100 m thick and is considered to be about 70% of the composite section. The second facies is the shale-and-sandstone facies that is composed of organic-rich shale (similar to the previous facies) interbedded with fine- to coarse-grained quartz arenite to arkosic arenite in thin to very thin beds. This facies comprises about 20% of the composite section and can be found in intervals between 1 and 10 m thick. The third facies is sandstone, which is mostly fine-grained to granule quartz arenite to arkosic arenite. Sedimentary structures are present and include graded

bedding, hummocky cross-stratification, ripples, and load structures. (Dehler et al., 2007)

### ***2.3 - Depositional Environment***

The depositional environment of the Red Pine Shale is interpreted as mud flat, fluvial, or marine deltaic (Wallace and Crittenden, 1969; Link et al., 1993; Condie et al., 2001; Dehler et al., 2007). Contrasting paleogeographic models suggest either deposition in an east-west-trending intracratonic trough that was dominated by fluvial systems (Condie et al., 2001), or a marine system that was open to the west and south (Wallace and Crittenden, 1969; Dehler et al., 2001).

Though Wallace and Crittenden (1969) do not commit to a depositional environment for the Red Pine Shale, they do tentatively offer ideas that are consistent with their interpretations for the rest of the Uinta Mountain Group. Based on its similarity to other shale units in the Uinta Mountain Group, they suggest that this was an environment of shallow water, a restricted basin, or a mudflat. Preliminary paleocurrent data collected from the lower western Uinta Mountain Group suggest that transport of sediment was to the south and the west, simultaneously. Wallace and Crittenden (1969) also document a gradational lower contact with a fluvial succession of the Hades Pass quartzite. Based on these data, Wallace and Crittenden (1969) developed a paleogeographic model that represented a shallow marine environment that was open to the south and southwest, though they generally address the western Uinta Mountain Group as a whole.

Condie et al. (2001) assert that the Uinta Mountain Group was deposited in an east-west-trending intracratonic trough that opened into a shallow sea to the west and was dominated by an axial fluvial system, although their work was dominantly geochemical

and emphasized provenance, not depositional environments. Based on the estimated age of the Uinta Mountain Group, Condie et al. (2001) suggest that this was a rift basin associated with the breakup of Rodinia, but that it was not an aulocogen due to the location of this deposit 500 km from the Proterozoic edge of the craton in Nevada and the fact that the Uinta Mountain Group rests on continental crust.

Dehler et al. (2007) hypothesize that the Red Pine Shale was deposited in a deltaic environment in a marine basin associated with the breakup of Rodinia. The C-isotope data used in this study showed variability similar to that of known C-isotope curves from mid- to late Neoproterozoic marine successions. Marine microfossils found in the Red Pine Shale were used to further support the claim that this was a marine environment. The similarity of many data sets in the Red Pine Shale and the Chuar and middle Pahrump groups suggest an intracratonic seaway connecting separate rift basins at ~750 Ma (ChUMP hypothesis of Dehler, 2008).

#### **2.4 - Age**

Dating Techniques used for this unit include microfossils, Rb/Sr and U/Pb dating, and correlation of carbon isotopes and fossils. Crittenden and Peterman (1975) reported an age for the Red Pine Shale of 950 Ma using whole rock Rb/Sr dating on shale, which fits within the bracketed age given by Hedge et al. (1986) for the entire Uinta Mountain Group (1.4 – 0.9 Ga). These ages contradict the age suggested by the microfossil assemblage found in the Red Pine Shale. Vase-shaped microfossils and *Bavlinella faveolata* have been identified, as well as a variety of acritarchs (Vidal and Ford, 1985; Horodyski, 1993; Dehler et al., 2007). *Bavlinella faveolata* first appears in the



sedimentary record just before the Sturtian glaciation (750 to 700 Ma) (Vidal, 1976; Knoll and Swett, 1985), while the vase-shaped microfossils have yet to be found in rocks that are post-Sturtian (Porter and Knoll, 2000). These data suggest that the Red Pine Shale was deposited before or during the Sturtian glaciation (Dehler et al., 2007). These microfossil data, in conjunction with C-isotope data from the Red Pine Shale, suggest that this unit correlates with the Chuar Group of Arizona (Dehler et al., 2001; Dehler et al., 2007). The Chuar Group is ~770 to 742 Ma (Karlstrom et al., 2000, Dehler et al., 2005), suggesting a similar age for the Red Pine Shale. The formation of Outlaw Trail of the middle-lower eastern Uinta Mountain Group has yielded a population of grains ( $n=4/128$ ) which indicate a maximum depositional age of  $766\pm 4$  Ma (Dehler et al., in review). Though the relationship between the Red Pine Shale and the formation of Outlaw Trail is not completely understood, the Red Pine Shale is most likely stratigraphically above the formation of Outlaw Trail (Dehler et al., 2007). Therefore, the best constraints on the Red Pine Shale indicate that it is between ~770 Ma and 742 Ma.

### ***2.5 – Correlations***

The Uinta Mountain Group is hypothesized to correlate with the Big Cottonwood Formation west of the Uinta Mountains (see Fig. 1), the Pahrump Group in Death Valley, California, and, as mentioned, the Chuar Group of Grand Canyon, Arizona (Link et al., 1993; Dehler et al., 2007). These correlations are based on combined lithologic, microfossil, and C-isotope data (Link et al., 1993; Dehler et al., 2007). The Big Cottonwood Formation has been correlated with the Uinta Mountain Group using lithology and a preliminary paleomagnetic direction and pole data (Link et al., 1993;

Ehlers and Chan, 1999). New detrital zircon data from the Red Pine Shale and the Big Cottonwood Group show two identical population distributions and suggest this correlation is robust (Dehler et al., in review). The Chuar and Uinta Mountain groups have been correlated by paleomagnetic data, chemostratigraphy and paleontology (e.g., Dehler et al., 2005; Weil et al., 2006). Lithologic characteristics and some paleontology of the Pahrump Group have been correlated to the Uinta Mountain Group (Link et al., 1993; Dehler, 2008).

## **2.6 – Geochemistry**

Condie et al. (2001) used geochemical and Nd isotopic analyses to understand provenance and paleogeography of the western Uinta Mountain Group and the Big Cottonwood Group. They found that Th values within Red Pine Shale samples range from 15 to 40 ppm Th. These values are considered unusually high relative to most Phanerozoic shale samples (<20 ppm Th) (Condie, 1993). Chemical index of alteration (CIA) values within the Red Pine Shale were found to be high and in conjunction with  $\text{Al}_2\text{O}_3$ ,  $\text{CaO} + \text{Na}_2\text{O}$ , and  $\text{K}_2\text{O}$  molecular values, they suggest paleoweathering conditions. They suggest that the Uinta Mountain and Big Cottonwood groups were deposited during subtropical to tropical climates. Nd isotopes and geochemical analyses from this study also suggest that the sediment of the Uinta Mountain Group was derived from a mixing of Archean and Paleoproterozoic sources.

Preliminary C-isotope data by Dehler et al. (2007) are shown in Fig. 2. This curve is a composite of the thickest partial section of the Hades Creek locality (upper part) and the type section (lower part). Although some C-isotope variability is expressed, the pilot data

are low resolution (average spacing of ~20 m). Preliminary TOC data for the Red Pine Shale range from 0.32 to 5.9%, but represent only a subset of the samples previously analyzed for isotopic composition (Dehler et al., 2007).

## **2.7 – Paleontology**

Vidal and Ford (1985) conducted some of the earliest paleontologic work on samples from the Uinta Mountain Group. They identified multiple microfossils within the Red Pine Shale including *Chuarina circularis*, *Leiosphaeridia* sp., other acritarchs, and filaments. They also identified rare examples of more complex fossils such as *Melanocyrrillium* (vase-shaped microfossils), *Valeria lophostriata*, cf. *Stictosphaeridium*, *Trachysphaeridium* sp. A, *T. laminaritum*, *T. laufeldi*, and *Tasmanitesrifeiicus*.

Current paleontologic studies of the Red Pine Shale are revealing an interesting assemblage of fossilized eukaryotes. These microfossils include vase-shaped microfossils, *Bavlinella faveolata*, *Leiosphaeridia* sp., ornamented acritarchs, assorted filaments, and rare *Chuarina circularis* (e.g., Nagy and Porter, 2005; Dehler et al., 2007). The evidence of early heterotrophic protists found in the Red Pine Shale indicates not only an increase in food web complexity by this time, but has implications for prokaryotic and eukaryotic evolution prior to the Cambrian explosion (Porter and Knoll, 2000; Dehler et al., 2007).

The microfossil assemblages dominated by *Bavlinella faveolata* have been found in the Red Pine Shale near Hoop Lake, White Rocks, and the Hades Creek locale (Fig. 1, Table 1) (Nagy and Porter, 2005). These fossils are about 5-20  $\mu\text{m}$  in diameter and are frequently accompanied by *Leiosphaeridia* sp. and acritarch envelopes (Nagy and Porter,

2005; Dehler et al., 2007). Some *Bavlinella faveolata* specimens (e.g. White Rocks locale) appear to have been pyritized. Assemblages of vase-shaped microfossils and occasional acritarchs have been found in the Red Pine Shale at the type section (Vidal and Ford, 1985; Dehler et al., 2007). Vase-shaped microfossils are found in silicified mudstone nodules as casts (Porter et al., 2003; Dehler et al., 2007).

| Table 1: Paleontology of the Red Pine Shale       |      |          |                                                           |
|---------------------------------------------------|------|----------|-----------------------------------------------------------|
| Locale                                            | Year | Sample   | Fossil(s)                                                 |
| Henry's Fork                                      | 2002 | HF-3     | <i>Satka colonialica</i> ; filaments                      |
| Henry' Fork                                       | 2002 | HF-7     | <i>Leiosphaeridia</i> sp.; filaments; possible VSMs       |
| Ashley Creek                                      | 2002 | AC-1     | <i>Leiosphaeridia</i> sp.; filaments                      |
| Type Section                                      | 2004 | RP04-3   | <i>Leiosphaeridia</i> sp.; filaments                      |
| Type Section                                      | 2004 | RP04-10  | <i>Leiosphaeridia</i> sp.; filaments                      |
| Type Section                                      | 2000 | RP00B-8  | <i>Leiosphaeridia</i> sp.                                 |
| Type Section                                      | 2000 | RP00B-32 | <i>Leiosphaeridia</i> sp.                                 |
| Type Section                                      | 2000 | RP00B-40 | VSMs                                                      |
| Hades B                                           | 2003 | RP03B-24 | <i>Chuarina circularis</i>                                |
| Hades B                                           | 2003 | RP03B-25 | <i>Leiosphaeridia</i> sp.                                 |
| Lower Hades                                       | 2001 | RP01A-50 | <i>Leiosphaeridia</i> sp.; filaments; <i>B. faveolata</i> |
| Lower Hades                                       | 2001 | RP01A-63 | <i>Leiosphaeridia</i> sp.; filaments                      |
| Lower Hades                                       | 2001 | RP01A-68 | <i>Leiosphaeridia</i> sp.; filaments                      |
| Lower Hades                                       | 2001 | RP01A-70 | <i>Leiosphaeridia</i> sp.; filaments                      |
| Lower Hades                                       | 2001 | RP01A-85 | <i>B. faveolata</i>                                       |
| <i>B. faveolata</i> : <i>Bavlinella faveolata</i> |      |          |                                                           |
| VSM : vase-shaped microfossil                     |      |          |                                                           |
| <i>from Nagy and Porter, 2005</i>                 |      |          |                                                           |

## CHAPTER 3

### METHODS

Both field and laboratory methods were applied to address the proposed hypotheses of this research. The multiple techniques used include measuring of sections, facies analysis, petrography, carbon-isotope stratigraphy, and shale geochemistry.

#### *3.1 - Field Methods*

Measuring of section and minor geologic mapping were necessary to help in the overall characterization of the Red Pine Shale. Geologic mapping was done to locate, as well as to locally correlate, measured sections. Sedimentologic studies of the Red Pine Shale involved facies analyses including the identification of facies as well as description of sedimentary features and structures seen within these facies. Paleocurrent analyses were attempted, yet appropriate sedimentary structures are limited. The stratigraphic framework of this unit is based on identified marker beds, facies changes, and correlation between measured sections. Two main localities (type section and Hades Creek locales), and three others, were previously identified and preliminary data were collected by C. Dehler in these areas. These localities are the focus of this study.

Samples were collected throughout each measured section using both a uniform and a stratified sampling method. Specific strategic intervals were also sampled for collaborative paleontologic and geochronologic studies (U-Pb and Re-Os dating). A total of 320 shale samples were collected and analyzed for C-isotope ratios and TOC in the University of New Mexico's stable isotope lab. Sixty-nine sandstone samples were

collected and made into thin sections by Quality Thin Sections in Tucson, Arizona. This field work and high resolution sampling was the first step in the interpretation of the depositional system, provenance, and age of the Red Pine Shale.

### ***3.2 - Lab Methods***

Sample collection and preparation procedures for shale followed those used by Dehler et al. (2005). About 20g of shale chips was chosen from samples to be cleaned with 10% HCl solution. After drying, samples were crushed in a zirconium shatter box to ~200 mesh and were again digested in 10% HCl solution until all carbonate was dissolved. Samples were then rinsed with deionized water until pH reached 5.5. Samples from the shale facies were analyzed for organic  $\delta^{13}\text{C}$  and TOC using the mass spectrometer at the University of New Mexico, with some trial work at Brigham Young University. C-isotopic data are reported relative to the Pee Dee belemnite (PDB) standard. Precision for these analyses is 0.1‰ based on multiple analyses of international standards and duplicate samples. TOC was determined by evolved  $\text{CO}_2$  volume (Strauss et al., 1992).

Each of the 69 thin sections was point counted using the traditional method and a sampling target of 300 points per slide. The categories were limited to the following: monocrystalline quartz, undulatory quartz, polycrystalline quartz, plagioclase, potassium feldspar, weathered feldspar, muscovite, chlorite, mudstone fragment, siltstone fragment, matrix, and other lithics. For each sample average grain size, rounding, sorting, and additional features were described. All petrographic analysis was done at the University of New Mexico. Detrital zircon analyses were conducted by Mark Fanning at the

Australian National University, Canberra, Australia, using a sensitive high resolution ion microprobe (SHRIMP); see Dehler et al. (in review) for methodology. Some of these detrital zircon results were published in Fanning and Dehler (2005) and Dehler et al. (in review).

## CHAPTER 4

### FACIES ANALYSIS

#### *4.1 - Introduction and subdivision*

Six facies were identified within the Red Pine Shale. This analysis builds on the work of Dehler et al. (2007) by adding three new facies (concretion, slump fold, pebble sandstone) and expanding the descriptions and interpretations of the previously identified three facies (shale, shale-and-sandstone, sandstone). Facies are defined by grain size, bed thickness and packaging, and sedimentary structures (Table 2). Normalized point count data from sandstone samples were plotted on QFL ternary diagrams to aid in facies descriptions (Fig. 3). Delta terminology is used to describe these facies, though the defining delta shape cannot be seen in the exposed Red Pine Shale due to the lack of laterally extensive exposure. This decision is based on the gradational transition from the underlying Hades Pass quartzite, which represents braided fluvial deposition (Wallace and Crittenden, 1969; this study), and, more generally, on the idea that transverse and axial streams fed the Uinta Mountain Group basin (e.g., Wallace, 1972). Fig. 4 shows the interpreted depositional setting for each facies in a deltaic system.

#### *4.2 - Facies 1: Shale*

##### *4.2.1 – Description*

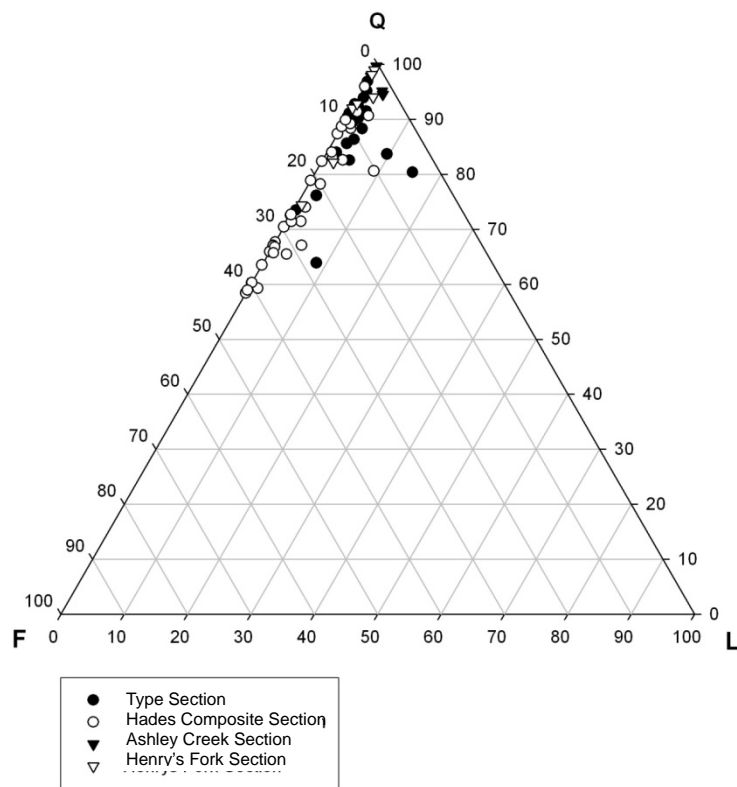
This facies, originally identified by Dehler et al. (2007) is dominated by organic-rich



| Table 2: Summary of Red Pine Shale Facies Descriptions and Interpretations |                                                                                                                                                                                                                                                                                                                                                                                                                                                                                                                                                  |                                                                                                       |                              |
|----------------------------------------------------------------------------|--------------------------------------------------------------------------------------------------------------------------------------------------------------------------------------------------------------------------------------------------------------------------------------------------------------------------------------------------------------------------------------------------------------------------------------------------------------------------------------------------------------------------------------------------|-------------------------------------------------------------------------------------------------------|------------------------------|
| Facies                                                                     | Description                                                                                                                                                                                                                                                                                                                                                                                                                                                                                                                                      | Facies Definition                                                                                     | Environmental Interpretation |
| 1: Shale                                                                   | Gray to black claystone to siltstone, thin to thick beds, organic-rich, contains <i>Bavlinella faveolata</i> and acritarch fossils, and rare 10cm to 1m thick tabular fine sandstone beds; sandstone is quartz arenite to arkosic arenite, usually weathered and oxidized with siltstone lenses, graded bedding, ripple and parallel laminations, hummocky-cross stratification, swaly bedding, tool marks, symmetric and interference ripples.                                                                                                  | Mostly clay to siltstone with few 10cm to 1m thick fine sandstone beds. Shale beds 5m to 310m thick.  | Distal prodelta              |
| 2: Concretion                                                              | Silt to medium sand, usually gray to black shale, some thin sandy interbeds with silty lenses, graded bedding, ripple to parallel laminations, vase-shaped microfossils, and multiple silica concretions.                                                                                                                                                                                                                                                                                                                                        | 1-4m thick siltstone with some medium sandstone beds. Distinguishing features are silica concretions. | Distal prodelta              |
| 3: Shale-and-Sandstone                                                     | Shale interbedded with sandstone. Shale is claystone to siltstone, gray to black, some maroon with parallel laminations, silty lenses, acritarch fossils; sandstone is fine- to coarse-grained, moderately sorted quartz to arkosic arenite, thin to medium beds, graded bedding, planar-tabular, swaley, and hummocky cross-bedding, ripple-cross and parallel laminations, and climbing and symmetric ripples, siltstone rip-ups, scoured contacts, and cut-and-fill structures with coarse sand fining upward to silt, many beds are massive. | Interbedded sandstone beds <2m with shale beds <5m thick. This combination is from 3-16m thick.       | Delta front, prodelta        |
|                                                                            |                                                                                                                                                                                                                                                                                                                                                                                                                                                                                                                                                  |                                                                                                       | <i>continued</i>             |

Table 2: Summary of Red Pine Shale Facies Descriptions and Interpretations (*continued*)

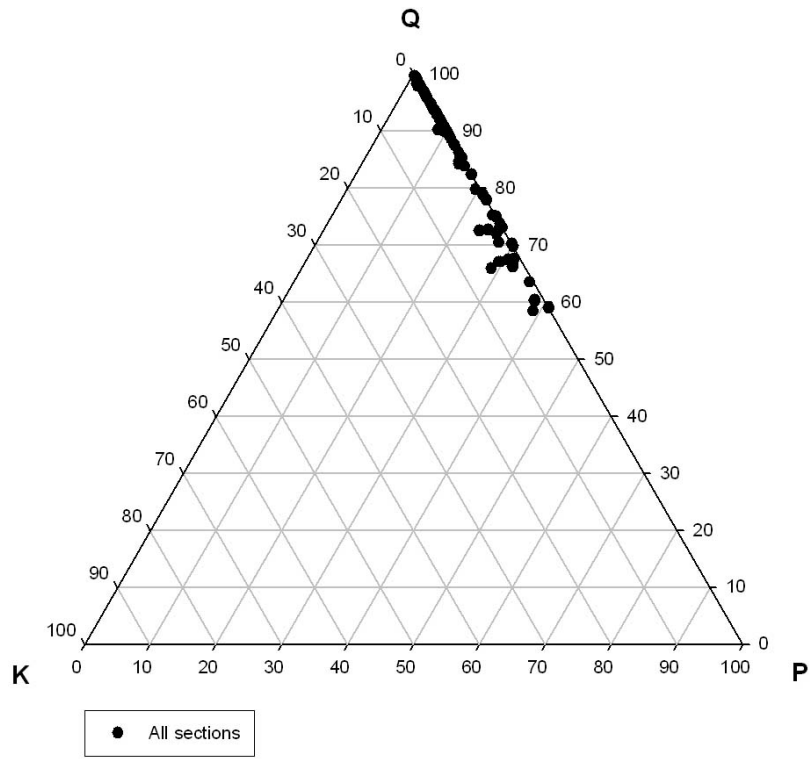
| Facies              | Description                                                                                                                                                                                                                                                                                                                                                                                                                                                                                                                              | Facies Definition                                                                                         | Environmental Interpretation   |
|---------------------|------------------------------------------------------------------------------------------------------------------------------------------------------------------------------------------------------------------------------------------------------------------------------------------------------------------------------------------------------------------------------------------------------------------------------------------------------------------------------------------------------------------------------------------|-----------------------------------------------------------------------------------------------------------|--------------------------------|
| 4: Slump Fold       | Gray to black mudstone with some sandstone beds. Sandstone is fine-grained quartz to arkosic arenite with symmetric ripples, ripple laminations, hummocky-cross stratification up to 1m x 20cm, slump folds up to 1m x 30cm.                                                                                                                                                                                                                                                                                                             | Usually mudstone with some fine sandstone interbeds, 1-4m thick. Distinguishing feature is slump folding. | Proximal prodelta, delta front |
| 5: Sandstone        | Fine- to coarse-grained sandstone, subarkosic to arkosic, some quartz arenite, muscovite and rare chlorite, mudstone intraclasts angular to subrounded grains, poorly to well sorted, tabular, undulatory to planar beds, thin to medium bedding, normal to reverse grading, symmetric ripples, granule sandstone lenses, cut and fill structures, laminations within thin shale interbeds, mudstone rip-ups, parallel and ripple-cross laminations, hummocky- and swaley cross stratification, and planar and tangential cross-bedding. | Sandstone ranging in thickness from 2-17m thick.                                                          | Delta front                    |
| 6: Pebble Sandstone | Fine to coarse pebbly sandstone, quartzite to sub lithic or subarkosic, angular to subangular, moderate to poor sorting, undulatory to tabular thin to medium beds with normal and reverse grading, maroon siltstone rip-ups, and pebbles up to 5mm in diameter.                                                                                                                                                                                                                                                                         | Granule to pebble sandstone <10m thick, from 0.5-7m thick.                                                | Delta front                    |



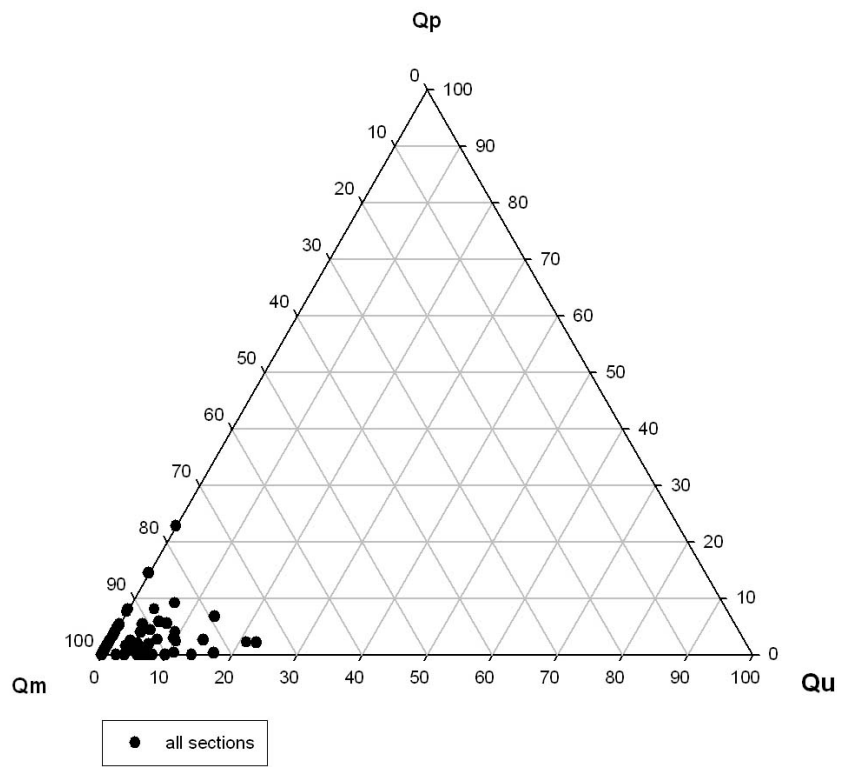
a.

Figure 3. Ternary diagrams with normalized point count data from sandstone samples.

- Quartz-feldspar-lithic (QFL) ternary diagram of all sandstone samples.
- Quartz-potassium feldspar-plagioclase (QKP) ternary diagram with weathered grains excluded.
- Polycrystalline-monocrystalline-undulatory quartz (QpQmQu) ternary diagram of sandstone samples from all sections.









b.



c.

## Facies Key

|                                                                                   |                  |                                                                                   |                     |
|-----------------------------------------------------------------------------------|------------------|-----------------------------------------------------------------------------------|---------------------|
|  | pebble sandstone |  | shale-and-sandstone |
|  | sandstone        |  | shale               |
|  | slump fold       |  | concretion          |

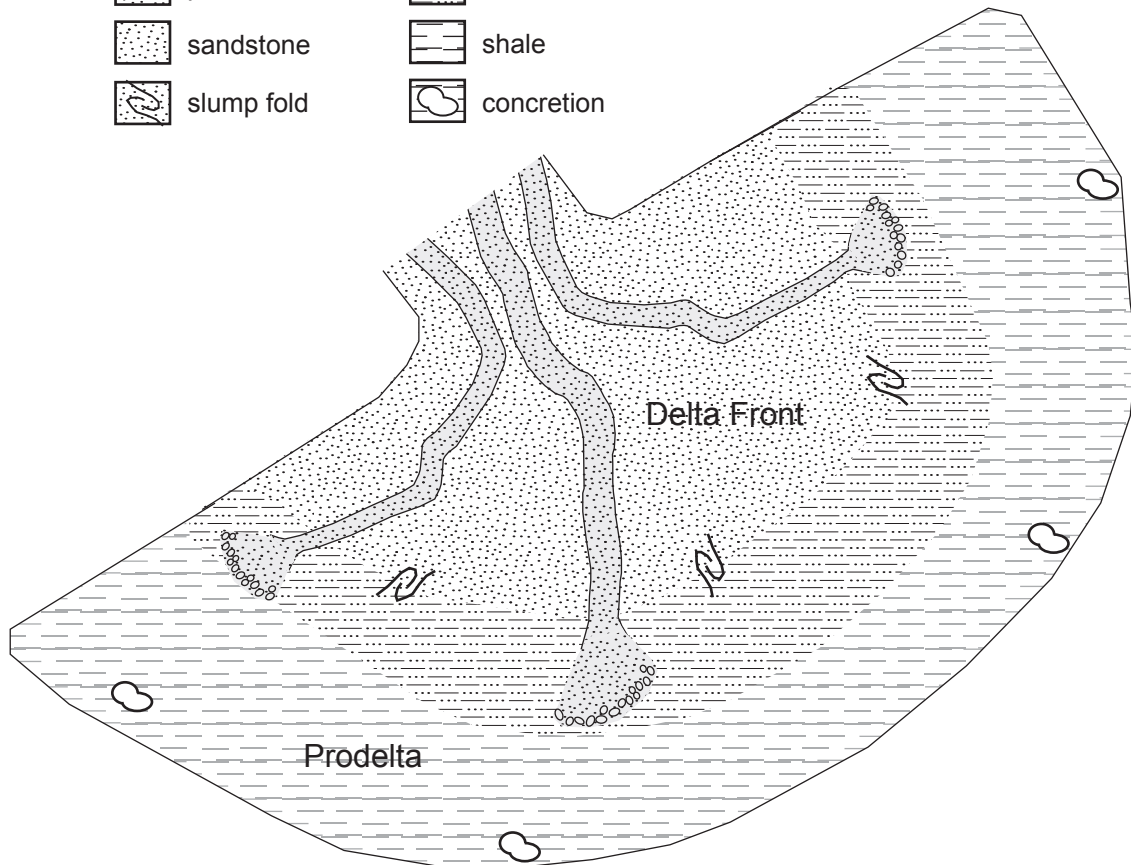


Figure 4. Illustration showing facies positions in a deltaic setting. Six facies are identified and depositional settings are interpreted as follows: shale facies - distal prodelta; concretion facies – distal prodelta; shale-and-sandstone facies - proximal prodelta to delta front; slump fold facies - proximal prodelta or delta front; sandstone facies - delta front; pebbly sandstone facies - delta front.

gray to black siltshale, mudshale, and clayshale (Fig. 5). The shale facies is defined as any shale interval > 5m thick. Outcrops of this facies are present at all study sites. The shale facies is the most common of all facies found within the Red Pine Shale.

The shale facies ranges in thickness from 5 to 310 m thick and is composed of clay- to silt-sized particles in thin to thick beds with subordinate sandstone beds. Centimeter- to 1-m-thick tabular beds of fine-grained quartz and arkosic sandstone are present within this facies. The sandstone beds are typically oxidized. Aside from laminations in the shale, the majority of sedimentary structures are present in the sandstone beds. These include graded bedding, ripple and parallel laminae, hummocky-cross stratification, swaley bedding, tool marks, symmetric and interference ripples, and cm-scale siltstone to sandstone lenses. Both *Bavlinella faveolata* and acritarch microfossils are present (Nagy and Porter, 2005). The shale facies is most often in association with the shale-and-sandstone facies and less frequently with the sandstone facies.

#### 4.2.2 - Interpretation

The shale facies represents a wave-affected distal prodelta in a marine setting, which is in agreement with the interpretations of Dehler et al. (2007) (Fig. 4). The supporting evidence specifically suggests a combination of suspension settling and punctuated dilute density currents, indicating deposition predominantly below storm wave base.

Based on the thickness, continuity, and lack of subaerial sedimentary features of this shale, it was most likely deposited in an extensive, low energy subaqueous environment where processes are dominated by suspension settling. Thick intervals of parallel-



Figure 5. Photograph looking north of the shale facies from Hades Creek A locale. Shale slopes are photographed from across Hades Creek drainage. Slope is ~30m in height and is near the base of Hades A.

laminations in the shale support deposition from suspension, much of which was below storm wave base (Prothero and Schwab, 1996). Discrete changes in grain size within some laminae, ripple laminations, graded beds, and tool marks indicate intermittent weak, dilute density currents affected the bottom bed at times (Collinson and Thompson, 1982). Hummocky-cross stratification and swaley bedding indicate combined-flow at or near fair-weather wave base (Harms et al., 1975). The silty and sandy lenses also represent scour and deposition likely caused by storm waves. Symmetric ripples are consistent with these features and also represent wave-generated currents near fair-weather wave base. The presence of *Bavlinella faveolata* and acritarch microfossils suggests deep- to shallow-water marine environments (Knoll et al., 1981; Nagy and Porter, 2005). Relatively high TOC content (up to 2.29%) (Appendix B) in the shale facies is characteristic of prodelta settings (Bhattacharya and Walker, 1991).

### **4.3 - Facies 2: Concretion**

#### **4.3.1 - Description**

The concretion facies is very similar to the shale facies and is characterized by meter-scale intervals of shale or sandstone with multiple silica concretions. This facies is only seen in outcrop at the type section (Appendix A).

The concretion facies is 1 to 4 m thick and consists of siltstone to medium-grained sandstone. Though it is usually composed of gray to black shale, there are thin sandy interbeds with some silty lenses. Sedimentary structures found within this facies are ripple and parallel laminae with graded bedding. The concretions within this facies are typically <10cm in diameter, have ovular to spherical shape, and are composed of



silicified shale. They are significant because they contain vase-shaped microfossils (Dehler et al., 2007). One unusual pair of these fossils was preserved in a position suggesting they were asexually reproducing (Fig. 6). This facies is typically found in association with the shale facies, but it is also seen less often in contact with the shale-and-sandstone facies.

#### *4.3.2 - Interpretation*

The similarity to, and association with, the shale facies indicate that the concretion facies was also deposited in a distal prodelta setting (Fig. 4). This facies, however, lacks significant sandstone and hence, the associated sedimentary structures representing higher energy currents. Parallel laminae likely represent a combination of suspension settling and weak dilute density currents. Graded bedding within some lamina and thin beds also indicate deposition by weak density currents. Ripple laminae could also be deposited by waning weak density currents, or could indicate reworking by weak storm waves (Prothero and Schwab, 1996; Nichols, 2001). The majority of sedimentary structures in this facies reflect density current deposits that have survived reworking and therefore were likely deposited below storm wave base (Prothero and Schwab, 1996). The lack of sedimentary structures indicating higher energy currents suggests that this facies represents the deepest water setting in the Red Pine Shale. It is most commonly associated with the shale facies, and less so with the shale-and-sandstone facies, suggesting an overall proximal to dominantly distal prodelta setting. This is consistent with observations that, in delta deposits, concretions are most likely to be found in the prodelta (Prothero and Schwab, 1996; Bhattacharya, 2006).

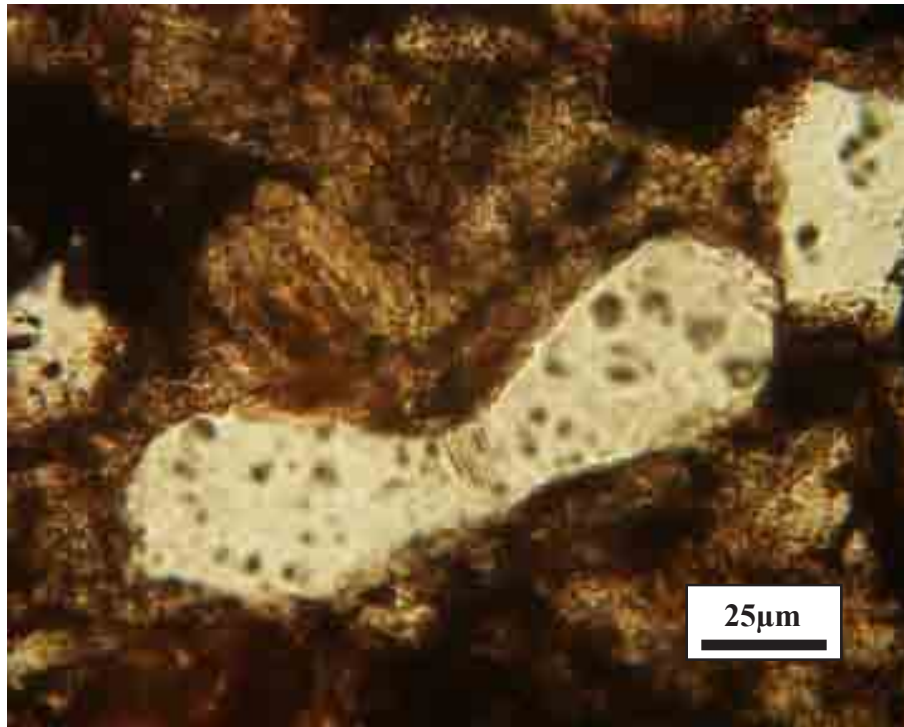


Figure 6. Photograph of *Bavlinella faviolata* performing asexual reproduction at time of death. These microfossils were found within the concretion facies near the base of the type section measured section. Each microfossil is  $\sim 75 \mu\text{m}$  in length. (From Porter and Knoll, 2000 and Dehler et al., 2007)

The presence of vase-shaped microfossils in this subtidal facies may indicate that they have a broader environmental range. Prior to recent studies on the Red Pine Shale, vase-shaped microfossils were thought to represent only tidal-flat and lagoonal environments (Porter and Knoll, 2000). These organisms have preservable tests that can be deposited immediately or can be transported by currents before deposition. Though it cannot be ruled out, it is unlikely that these tests were transported due to their low concentration within the silica concretions of the Red Pine Shale (Dehler et al., 2007). Porter and Knoll (2000) found that the tests of modern testate amoeba are typically found in dense concentrations when transported. This is consistent with exceptionally high concentrations of vase-shaped microfossils found within dolomite nodules of the upper Walcott Member of the Chuar Group, which were interpreted to have been transported by storms (Porter and Knoll, 2000).

#### ***4.4 - Facies 3: Shale-and-Sandstone***

##### *4.4.1 - Description*

The shale-and-sandstone facies (Fig. 7), originally defined by Dehler et al. (2007), is composed of organic-rich shale (similar to the shale facies) interbedded with fine- to coarse-grained sandstone. To be considered part of the shale-and-sandstone facies, the sandstone intervals must be <2m thick and interbedded with shale intervals that must be <5m thick. Outcrops of this facies are found in all of the study areas. This facies can be found in intervals between 3 and 16m thick. The shale intervals of this facies are similar in composition to those of the shale facies and are slightly more common than the intervals of sandstone. The shale intervals are usually gray to black and, less frequently,



Figure 7. Photograph of the shale-and-sandstone facies near the base of the Henry's Fork section. The thickest sandstone beds are ~10cm thick.

maroon in color. These beds are composed of claystone to siltstone with parallel laminations and common silty lenses. Acritarch fossils are found in these shale units (Nagy and Porter, 2005).

The sandstone is fine- to coarse-grained, moderately sorted quartz to arkosic arenite in thin to medium beds. Sedimentary structures include graded bedding, planar-tabular, swaley, and hummocky cross-bedding, ripple-cross and parallel laminations, and climbing and symmetric ripples. Many beds are massive. There are also siltstone rip-ups, scoured contacts, and cut-and-fill structures with coarse sand fining upward to silt.

#### *4.4.2 - Interpretation*

Similar to the previous two facies, the shale-sandstone-facies also represents suspension settling punctuated by density currents and wave action. Despite their similarities, this facies shows an increase in sand percentage and displays sedimentary features that suggest a more proximal position on the delta (proximal prodelta to delta front environment; Fig. 4).

The shale of this facies is similar to that of the shale and concretion facies. The combination of parallel laminations and silty lenses indicate suspension settling interrupted by weak density currents and some reworking of sediment by waves, near storm wave base (Prothero and Schwab, 1996). Acritarch fossils found in this facies are interpreted to represent deep- and shallow-water marine environments (Knoll et al., 1981; Nagy and Porter, 2005), consistent with our interpretation.

The sandstone of the shale-and-sandstone facies represents the shift to a higher energy environment of deposition. Sedimentary structures indicate that two main

currents influenced these deposits; density currents and storm waves. The higher frequency of sandstone within this facies represents a shift towards a more proximal prodelta or even delta front environment (Prothero and Schwab, 1996; Bhattacharya, 2006). Density currents are responsible for generating the graded beds, scours, and parallel laminations in sandstones (planar beds). Climbing ripples can also form in density currents when the rate of sedimentation is comparable to that of ripple migration (e.g., Nichols, 2001). Storm events are represented in these sandstones by siltstone rip-ups, hummocky and swaley crossbedding, and symmetric ripples. Siltstone rip-ups require that the silt was cohesive enough to endure transport by storm-wave-generated currents. In summary, this facies indicates deposition from near fair weather wave base to near storm wave base by suspension settling, density, and storm wave currents in the prodelta and delta front settings.

#### ***4.5 - Facies 4: Slump fold***

##### *4.5.1 - Description*

The slump fold facies (1 to 4 m thick; Fig. 8) is primarily a mudstone unit with some fine sandstone interbeds, and is similar to the shale-and-sandstone facies. This facies is defined by meter-scale beds distinguished by slump folding. Outcrops of this facies can be found in the Hades Creek and Ashley Creek locales.

This facies is usually associated with the shale-and-sandstone facies and less frequently is found with the shale facies. The sandstone beds are typically composed of fine-grained quartz to arkosic arenite with symmetric ripples and ripple laminations. Hummocky-cross stratification is rare but can be up to ~1m wide by ~20cm high. The



Figure 8. Photograph of slump fold facies within the Hades Creek B section. Arrow on notecard is 10 cm in height.

slump folds are up to 30cm in height and 1m in length and are generally isoclinal (Fig. 8).

#### *4.5.2 - Interpretation*

The slump fold facies is similar to, and associated with, the shale-and-sandstone facies and likely represents a similar environment on the delta (Fig. 4). Symmetric ripples and ripple laminations represent an environment that was influenced by waves. Hummocky-cross stratification suggests deposition in an area affected by storm waves. These sedimentary structures together suggest deposition above storm wave base and near, but below fair-weather wave base (Prothero and Schwab, 1996; Nichols, 2001).

Slump folds typically form in unconsolidated fine-grained sediment on unstable slopes (Collinson and Thompson, 1982). Elevated pore-fluid pressure in certain layers, in combination with high sedimentation rates, often causes the instability; these processes are followed by gravity-driven movement downslope as a coherent mass. Slump folds commonly form on over-steepened and overloaded slopes in the delta front and the proximal prodelta settings (Prothero and Schwab, 1996; Bhattacharya, 2006).

### **4.6 - Facies 5: Sandstone**

#### *4.6.1 - Description*

The sandstone facies (Fig. 9) is characterized by sandstone intervals >2m thick. Outcrops of this facies are present in all four study locales. The sandstone facies is fine- to coarse-grained sandstone that ranges in thickness from 2 to 17m. It is mostly subarkosic to arkosic with some quartz arenite present (see Fig. 10). There are also muscovite and rare chlorite grains present, as well as mudstone intraclasts. Sandstone grains are angular to subrounded and poorly to well sorted within tabular, undulatory to





Figure 9. Photograph showing planar-tabular foresets in the sandstone facies. Although measureable crossbed sets are rare, these foresets in White Rocks Canyon indicate paleoflow to the south. Rock hammer for scale.

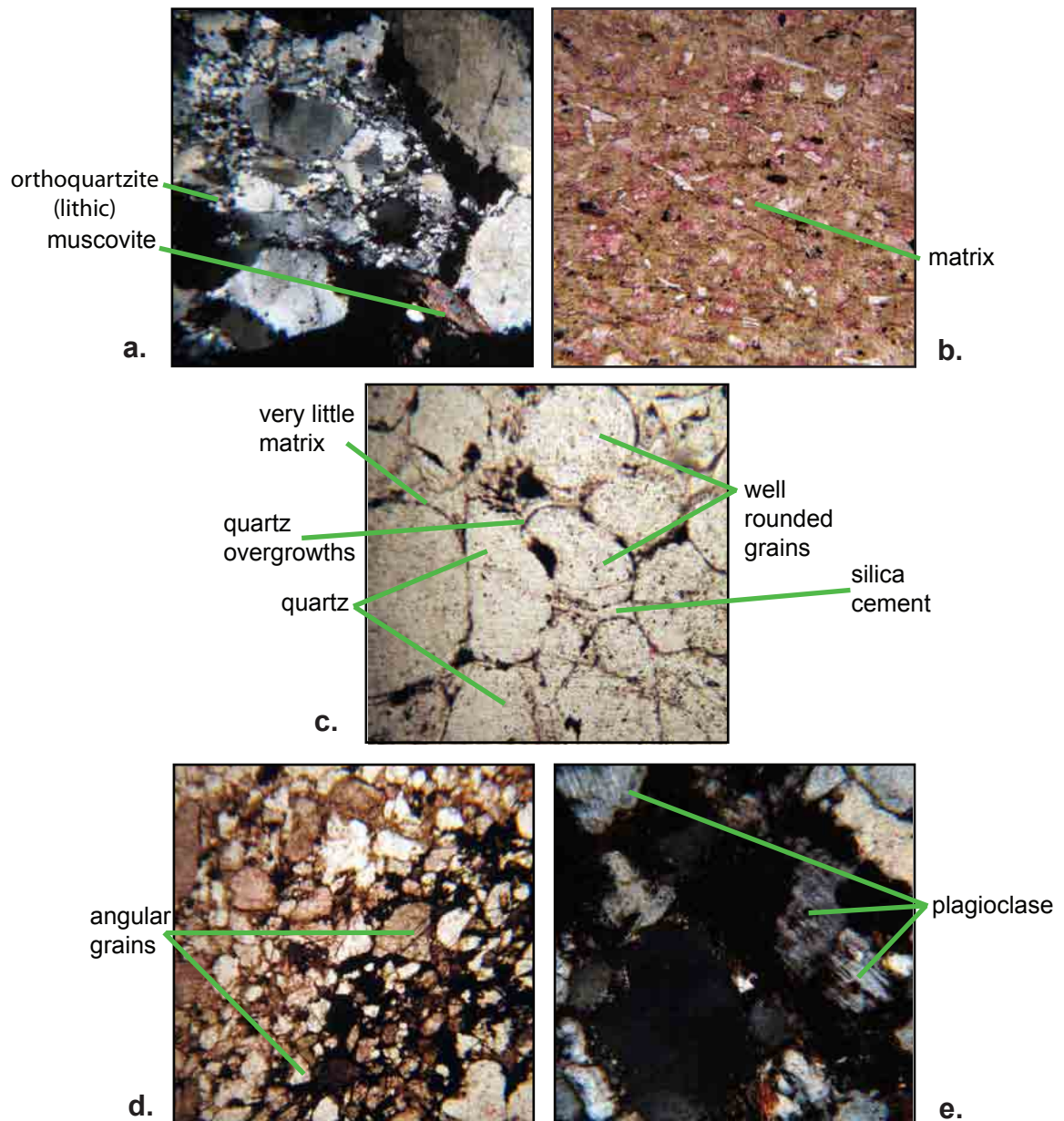


Figure 10. Photomicrographs taken at 10x magnification showing textures and grains from petrographic analysis.

- RP0B-23 – sublithic sandstone showing grains of orthoquartzite and muscovite
- RP0B-30 – subarkosic sandstone showing high matrix content
- AC04-7 – quartz arenite sandstone showing examples of well rounded quartz grains, silica cement, quartz overgrowths, and very little matrix content
- Hades 2 – arkosic sandstone showing angular grains
- Hades 10 – subarkosic sandstone showing examples of plagioclase grains

planar beds. The sandstone facies usually has thin to medium bedding with rare massive bedding and normal to reverse grading. There are symmetric ripples, granule sandstone lenses, cut and fill structures, laminations within thin shale interbeds, and mudstone rip-ups. Sedimentary structures also include parallel and ripple-cross laminations, hummocky- and swaley cross stratification, planar tabular crossbedding, and trough crossbeds with mud drapes in amalgamated and accreted sets (Fig. 11). TOC values in this facies from the Hades C measured section were the highest values found in the Red Pine Shale. They range from 1.33 – 5.91%.



Figure 11. Accreted and amalgamated trough crossbeds with black shale partings from Hades Creek C section indicating migrating bars in the mouth bar area of the delta front. These mud-draped crossbeds suggest a tidal influence. Rock pick for scale.

#### *4.6.2 - Interpretation*

This facies represents a change towards a higher energy environment, in this case the delta front (Fig. 4). Sedimentary structures present show evidence of a mixed-influenced deltaic setting that was near to above fair weather wave base. Interpretations of other facies suggest a wave-dominated delta, though the sedimentary features of this facies suggest a combination of fluvial and marine (wave and tidal) processes.

Common sedimentary structures in the delta front environment are cross bedding, cut-and-fill structures, and ripple marks. Symmetric ripples indicate oscillatory flow from wave refraction (e.g., Prothero and Schwab, 1996). Granule sandstone lenses found in this facies are common in a river-dominated deltaic setting in the delta front, as are cut-and-fill structures (Prothero and Schwab, 1996; Nichols, 2001; Bhattacharya, 2006). Shale partings seen draping cross-beds are suggestive of deposition from suspension during the short time of slack water between tidal reversals (Prothero and Schwab, 1996). Though this delta may not have been tidal-dominated, tides may have had an effect. Planar and amalgamated and accreted tangential crossbedding indicate subaqueous dunes and bars above fair-weather wave base, likely in a distributary mouthbar setting (Nichols, 2001). Reverse grading indicates deposition from a grain flow, which is due to instability on the delta; this instability can result from of an overly steep surface or over-loading, which is frequently found in the delta front of river-dominated deltas (Prothero and Schwab, 1996; Bhattacharya, 2006). Hummocky crossbedding is the result of storm waves acting upon sediment that has been deposited at the transition zone between fair-weather wave-base and storm wave-base (Harms et al., 1975; Nichols, 2001). Associated

parallel laminations indicate plane bed conditions generated by storm-wave currents. Preservation of organic matter is often higher in river-dominated delta front settings where sedimentation rates are relatively high and can rapidly bury available organic material (Bhattacharya and Walker, 1991). Overall, the features suggest deposition above to below fair-weather wave-base in a high-energy delta front setting.

#### ***4.7 - Facies 6: Pebbly sandstone***

##### *4.7.1 – Description*

The pebbly sandstone facies (Fig. 12) is characterized by cm- to m-scale beds of granule- to pebble- sandstone. Outcrops of this facies are found in both northern locales: Henry's Fork and the type section (Fig. 1).

The pebbly sandstone facies is between 0.5 and 7m thick and is usually associated with the sandstone facies at the type section and with the shale-and-sandstone facies at the type and Henry's Fork sections. This facies is a fine- to coarse-grained sandstone that is usually quartzite-lithic or subarkosic and contains pebbles of quartzite. These grains are angular to subangular with moderate to poor sorting. This facies is found in undulatory to tabular thin to medium beds with normal and reverse grading, maroon siltstone rip-ups, and pebbles up to 5mm in diameter.

##### *4.7.2 – Interpretation*

The pebbly sandstone facies is representative of a delta front to proximal prodelta setting whereby coarse sediment from the fluvial system fed the delta during storm events. Compared to the sandstone facies, this facies is coarser grained, more arkosic, and is more poorly sorted. This indicates that the pebbly sandstone facies was deposited



Figure 12. Photograph of pebbly sandstone facies near the top of the Henrys Fork section. Lithic grains are dominantly quartzite in composition. Abney level and upper part of Jacob Staff for scale (~0.3 meters).

closer to its source than the sandstone facies or that higher energy processes were occurring in the same depositional setting. The pebbly sandstone facies is found at the two northern-most sampling locales, and not in the southern localities, suggesting that there was a proximal source to the north of these deposits. This is consistent with observations by previous workers that there were transverse streams entering the basin from the north (e.g., Wallace and Crittenden, 1969; Sanderson, 1984; Ball and Farmer, 1998; Condie et al., 2001; Dehler et al., 2007). When compared to the sandstone facies, the pebbly sandstone typically represents deposition in a more specific setting on the delta front (Fig. 4).

Undulatory bedding in conjunction with the pebbles found in this facies suggests that these may be subaqueous distributary mouth bar deposits affected by both marine and fluvial processes (Prothero and Schwab, 1996; Nichols, 2001; Bhattacharya, 2006). Asymmetric ripples support this interpretation while symmetric ripples show that this facies was still in an environment affected by waves. Siltstone rip-ups from nearby cohesive beds were eroded and transported either by wave-generated currents or by fluvial currents, and deposited in the distributary mouth area (Prothero and Schwab, 1996). Reverse grading indicates deposition from a grain or debris flow, due to instability on an overly steep surface or over loading (Prothero and Schwab, 1996; Boggs, 2006; Bhattacharya, 2006). This is frequently found in the delta front of river-dominated deltas (Prothero and Schwab, 1996; Boggs, 2006; Bhattacharya, 2006). In rare cases, the pebbly sandstone beds are found in association with the shale facies and contain reverse grading or siltstone rip-ups. This implies transport from the coarser delta

front into deeper water by higher energy processes (Prothero and Schwab, 1996; Boggs, 2006).



## CHAPTER 5

### GEOCHEMISTRY AND PETROGRAPHY RESULTS

#### *5.1 – Trends in C-isotope and TOC curves*

The ranges of C-isotope and TOC data for each measured section are displayed in Table 3 and all data can be seen in Appendix B. C-isotope data are displayed next to each stratigraphic column in Figs. 13-16 and TOC data are displayed in Figs. 13-14. Isotope data collected and analyzed in 2000 by Dehler are also included, some of which appear in Dehler et al. (2007). The type section contains the least negative C-isotope value and the lowest TOC value within the Red Pine Shale. Ashley Creek and Henry's Fork sections have limited C-isotope data and no TOC data. These data were reported in Dehler et al. (2007), yet they were not put into a stratigraphic context.

Table 3: C-Isotope and TOC Ranges from Each Measured Section

| Measured Section   | C-isotopes (PDB) | TOC            |
|--------------------|------------------|----------------|
| Type Section       | -29.12 to -16.91 | 0.04% to 2.29% |
| Mud Lake Flat Road | -26.03 to -19.74 | 0.15% to 1.16% |
| Hades Creek A      | -29.46 to -23.90 | 0.1% to 3.7%   |
| Hades Creek B      | -27.10 to -24.65 | 0.06% to 0.29% |
| Lower Hades Creek  | -24.87 to -23.99 | 0.20% to 0.54% |
| Hades Creek C      | -29.26 to -27.37 | 1.33% to 5.91% |
| Ashley Creek       | -27.65 to -17.10 | --             |
| Henry's Fork       | -26.47 to -19.55 | --             |

C-isotope values from the type section show significant variability of up to 12‰. The most positive values can be found at the base of the section as well as in the Mud Lake Flat Road section, correlative to the base of the type section. At the base of the type

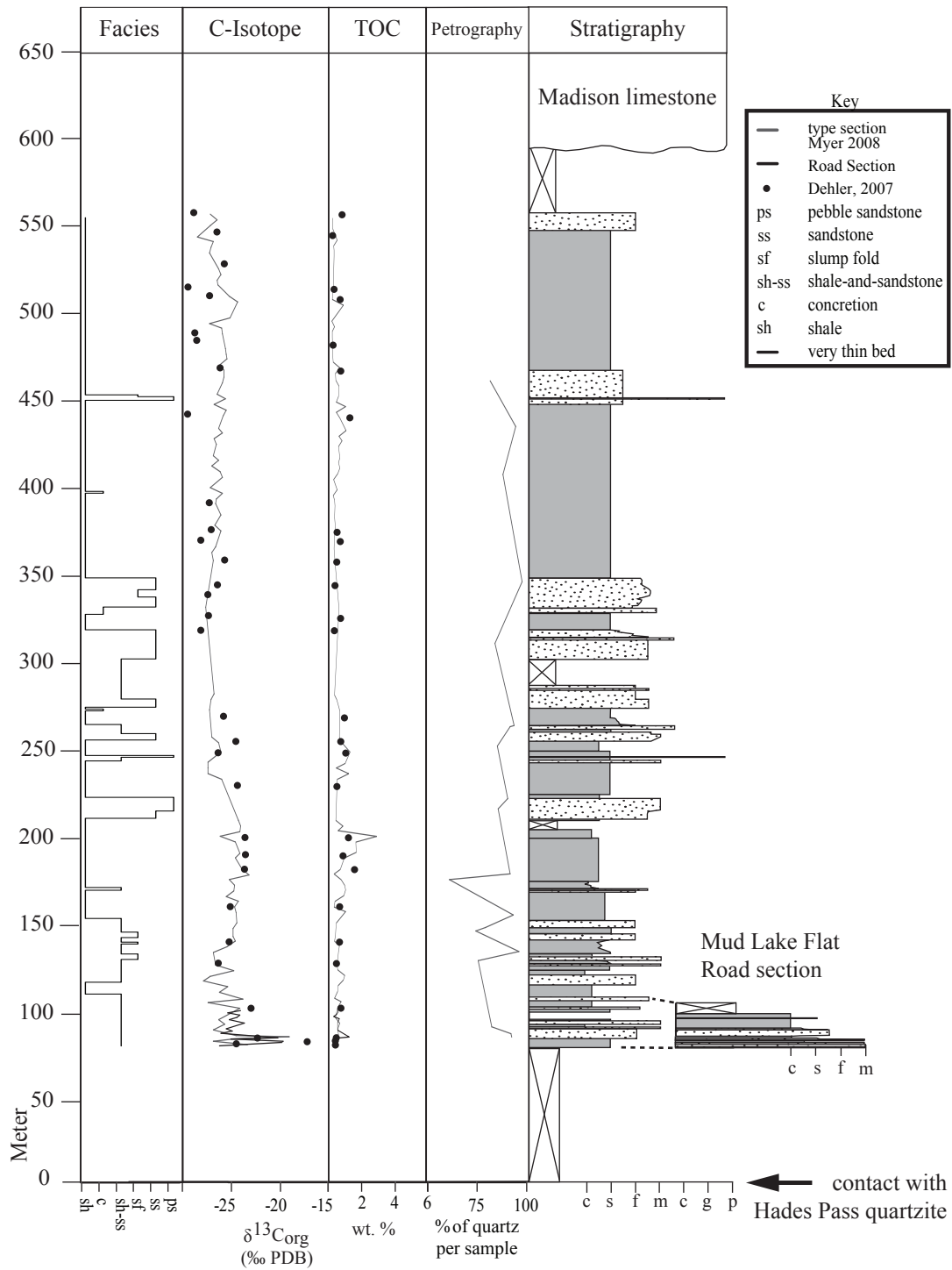


Figure 13. Stratigraphy, facies, C-isotope, TOC, and petrographic data for the type section. Notice correlation with Mud Lake Flat Road measured section. Quartz percentage is shown relative to all other grain types present in sample.

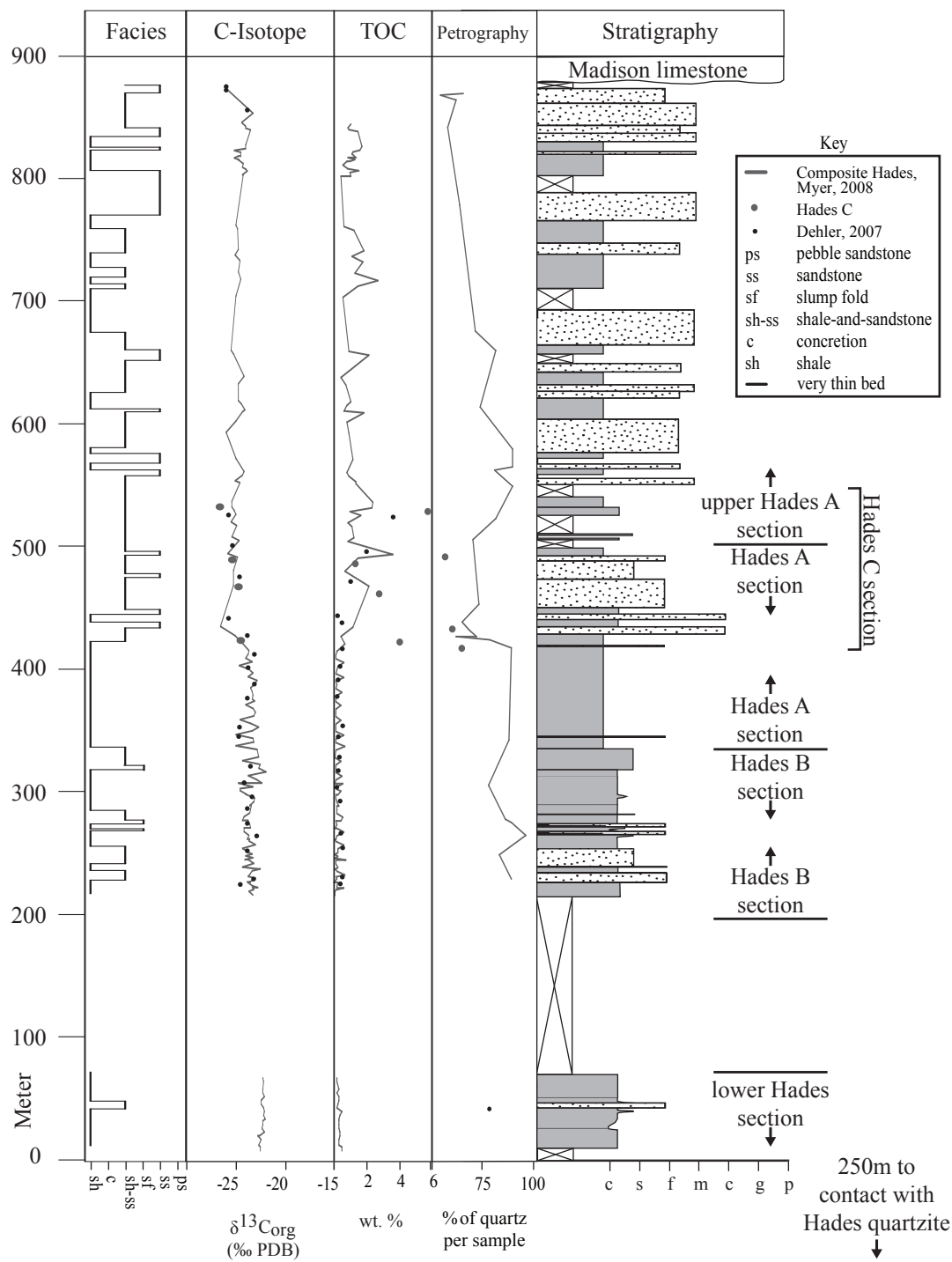


Figure 14. Stratigraphy, facies, C-isotope, TOC, and petrographic data for the composite Hades Creek section. Quartz percentage is shown relative to all other grain types present in sample.

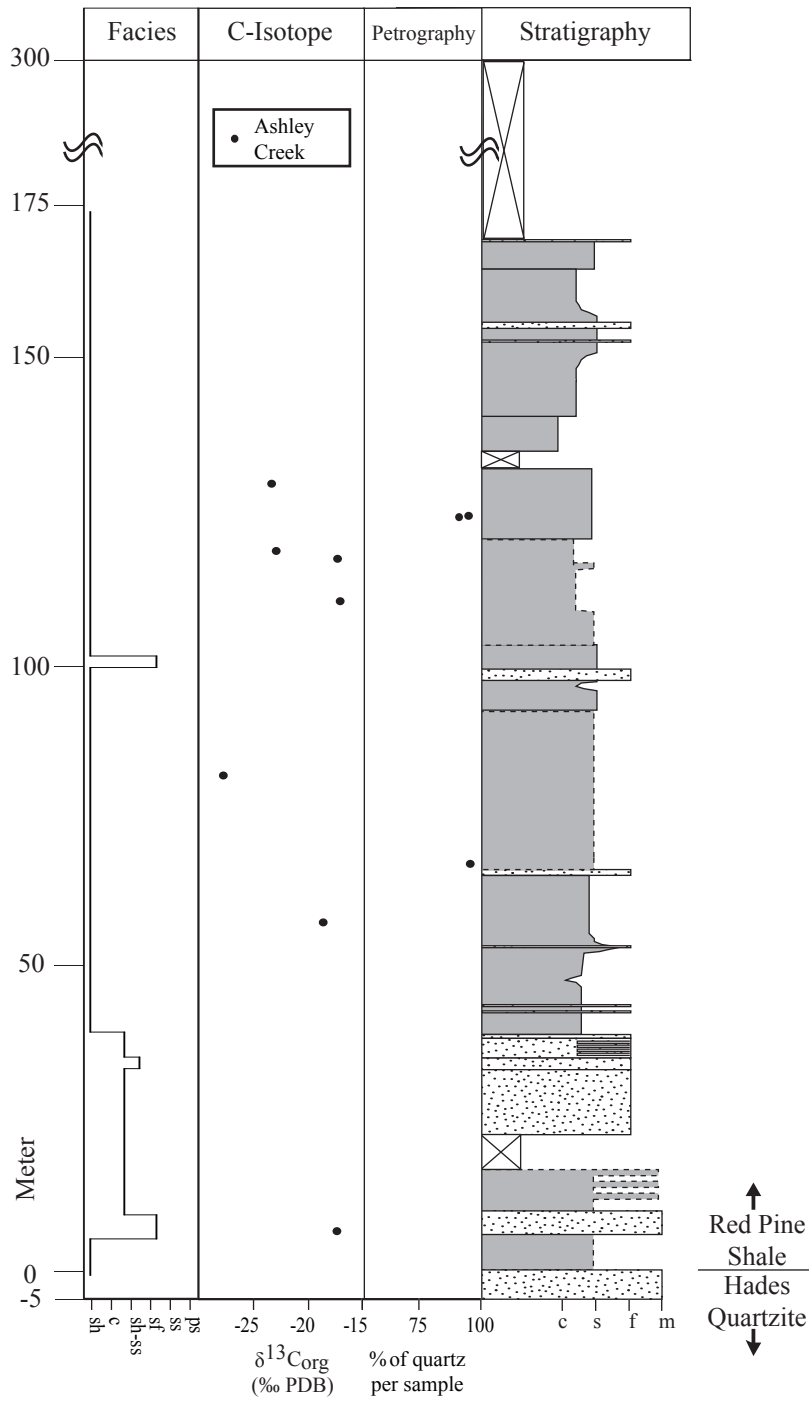


Figure 15. Stratigraphy, facies, C-isotope, and petrographic data for the Ashley Creek section. Quartz percentage is shown relative to all other grain types present in sample. Approximate upper contact with the Mississippian Madison Limestone based on mapping (Sprinkel, 2002). C-isotope data from Dehler et al., 2007.

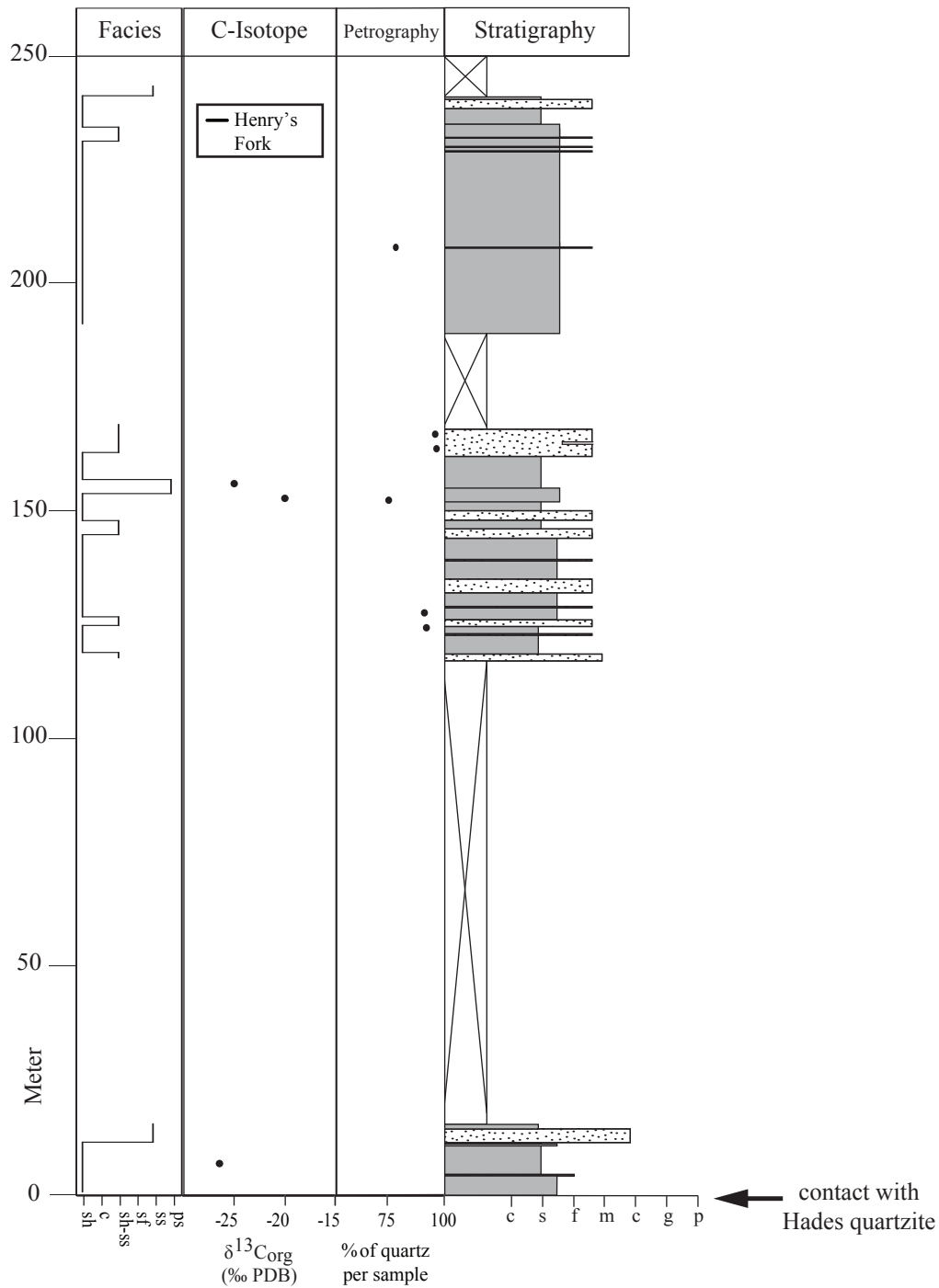


Figure 16. Stratigraphy, facies, C-isotope, and petrographic data for the Henry's Fork section. This continues for ~1500 m above what is shown based on geologic mapping (Bryant, 1992). Quartz percentage is shown relative to all other grain types present in sample. C-isotope data from Dehler et al., 2007.

section the C-isotope curve shows an initial rise from  $\sim 26\text{‰}$  to  $\sim 17\text{‰}$  over 0.5m and a fall over 1m to  $\sim 24\text{‰}$ . This is followed by another positive excursion to  $\sim 18.5\text{‰}$  over 1m. From here, the type section C-isotope curve drops to values as low as  $\sim -27\text{‰}$  over 35m. For the next 60m, the C-isotope values increase to a maximum of  $\sim -22.5\text{‰}$  before dropping to  $\sim -26.5\text{‰}$  for the next 60m. The values then begin a long climb to  $\sim 23.5\text{‰}$  over the next 250m. The values in the final 34 m of the section shift to more negative values again and reach  $\sim -29\text{‰}$ .

The changes within the type section C-isotope curve show a cyclicality that is generally bounded by a maximum of  $\sim -23\text{‰}$  and a minimum of  $\sim -26\text{‰}$ . Generally each drop or rise is over a 35 or 60m section. There is an overall pattern of decreasing C-isotope values up-section with values mostly bounded by  $-27\text{‰}$  to  $-23.5\text{‰}$  in the lower half of the section and by  $-29\text{‰}$  to  $-25\text{‰}$  in the upper half. This excludes the noteworthy cluster of relatively positive values near the base ranging from  $\sim 17\text{‰}$  (Dehler et al., 2007) and  $18.5\text{‰}$  (this research) from the type section to  $\sim 19.5\text{‰}$  from the Mud Flat Lake Road section. The overall decline in this section spans  $\sim 12\text{‰}$ , which is consistent with the findings of Dehler et al. (2007). Though the data patterns are similar, there are some inconsistencies between the C-isotope data from Dehler et al. (2007) and the values obtained by this research. This is most likely due to minor differences in sampling, sample preparation, in the analysis of these samples, or inherent variability.

Using field methods (i.e., mapping and identifying marker beds) the Hades Creek measured sections have been correlated and are now referred to as the “composite Hades Creek section.” These correlations are discussed below and shown in Fig. 14. The

composite Hades Creek section shows a very low variability of the C-isotope values in the lower ~400m, which becomes more variable in the upper part of the section, opposite to what is seen in the type section. The base of the Red Pine Shale is not exposed at this locale, so unfortunately a full comparison of the C-isotope datasets is not possible. This includes the inability to test whether the positive excursion at the base of the type section is present at this locale. The Hades Creek section is also twice as thick as the type section, so these strata inevitably preserve isotopic structure that is not preserved at the type locale.

The composite Hades Creek sections shows similar isotopic variability to the type section, with an average rise or drop in C-isotope values over a 30 to 65m section but also, with a few gradual positive shifts that cover just under 200 m of section (Figs. 13 and 14). Data from the lower Hades Creek section show a short rise of ~1‰ over 24m of section. It is unknown what happens to the C-isotope curve until the Hades Creek B section begins at 225m, where the curve has dropped 2‰ over 165m of covered section. Hades Creek B C-isotope values continue to drop for 30m to ~-27‰. Then there is a rise for 60m to ~-24‰ and a drop to ~-28‰ over the next 30m. This is followed by an increase to ~-25‰ and a decrease to ~-29‰ both over about 45m of section. From here, there is a gradual increase for about 180m to ~-27‰, then a decrease to ~-28 for 45m. There is another gradual rise over 190m to ~-26‰, followed by a final drop for 20m to ~-29‰. This curve also shows a cyclicity similar to the type section with average shifts over about 30-65m. This C-isotope curve also shows a pattern of gradual positive shifts followed by more rapid negative shifts on a larger scale. On a larger scale, this section

has a general pattern of C-isotope values becoming more negative upsection until about 435m where the curve begins to become more positive upsection.

Both Ashley Creek and Henrys Fork also have values that fall within the typical C-isotope value range for the Red Pine Shale between  $\sim -23\text{‰}$  to  $\sim -28\text{‰}$  (Figs. 15 and 16). The less negative values at the base of the type section and Mud Lake Flat Road are also observed in the basal Ashley Creek and Henry's Fork sections. Ashley Creek has the most values that concentrate near  $-17\text{‰}$ . Henry's Fork section has less negative values of  $\sim -19.5\text{‰}$ . In Ashley Creek there are two excursions of C-isotope values near  $-17\text{‰}$ .

Strauss et al. (1992) reported C-isotope values of  $-17.7$  and  $-17.1\text{‰}$  and H/C values of 0.62 and 0.68, respectively, from the Red Pine Shale near the base of the type section. Strauss et al. (1992) regarded an H/C value of 0.2 as a threshold for alteration of organic carbon; the organic component from samples with ratios lower than 0.2 were considered to be thermally altered and isotopic values from these samples would not reflect a primary value. More recently, DesMarais (1997) found that this value was much too high for recording thermal alteration of organic carbon. The relatively high thermal alteration values in the Red Pine Shale of 0.62-0.68 (Strauss et al., 1992) suggest that they were not substantially altered. Strauss et al. (1992) suggest that there is a relationship between higher concentrations of organic matter in shale and better preservation of organic carbon. TOC values in the Red Pine Shale are as high as 5.91%, with an average TOC value of 0.69%. These relatively high TOC values, in combination with the high thermal alteration values of Strauss et al. (1992), and the similarity of isotopic values at all four locales argue that these samples are minimally altered and represent the primary carbon-



isotope composition of Neoproterozoic seawater.

There is an obvious inverse relationship between the C-isotope and TOC data (Figs. 13-16). Nearly all positive shifts in C-isotope values correspond to a negative shift in TOC values. Though these shifts are opposite from one another, the TOC and C-isotope values show similar variability between samples in different parts of the curves. The TOC curve for the type section shows, on average, a higher variability between each data point near the base of the section (~1%) while the data points tend to get tighter higher in the upper section (~0.5%). In the composite Hades Creek section, the TOC data points are tightly bound through the lower Hades Creek and Hades Creek B section (~0.5%), but become, on average, more variable in the upper part of this section (~1%). The same pattern is seen in the C-isotope data curves for these measured sections. For the type section, there is an average variability of ~3‰ near the base of the section whereas, higher in the upper section, it is closer to ~1‰. In the composite Hades Creek section, the C-isotope values through the lower Hades Creek and Hades Creek B section have an average variability of ~1.5‰ and ~4‰ in the upper part of this section. This change in variability corresponds with a positive shift in C-isotope values. There seems to be no relationship between these datasets and the facies data (Figs. 13-16).

## ***5.2 – Petrographic analysis and sandstone textures***

Petrographic analysis of the 69 thin sections revealed an array of textural characteristics. Sandstone samples collected from the type section range from fine to coarse sand, with one sample containing pebble-sized grains; most samples have medium-sized sand grains (Appendix C). They range from poorly to well-sorted but are

usually moderately sorted, and generally are angular to sub-angular with some sub-rounding. The composite Hades Creek section sandstones (Fig. 14) have fine to coarse sand with mostly medium sand. The grains are usually poorly to moderately sorted and rarely well-sorted. They range from very angular to sub-rounded but are mostly sub-angular. Ashley Creek (Fig. 15) samples are very fine- to fine-grained, with one sample of medium to very coarse-grained sand. The grains are sub-angular to well-rounded, but are mostly sub-rounded. These sandstones are poorly to well-sorted and usually are well-sorted. The Henry's Fork (Fig. 16) sandstones are very fine to medium sand to pebble sandstones, with mostly fine sand. The grains are poorly to well-sorted but are usually well-sorted and angular to rounded, usually sub-rounded. There is one sample from the pebbly sandstone facies that is coarser, has more angular grains, and is poorly sorted.

Fig. 10 shows photomicrographs taken to illustrate various categories used for point counting. AC04-7 is a clear example of what was considered well rounded, while Hades 2 shows an example of angular grains. AC04-7 is also an example of a sample with little to no matrix. RP0B-30 demonstrates how some of the Red Pine Shale sandstones contain higher amounts of matrix. The rest of the photomicrographs show examples of various mineral categories used in this petrographic analysis, such as polycrystalline quartz and muscovite in sample RP0B-23, monocrystalline quartz in sample AC04-7, and plagioclase in sample Hades 10.

### ***5.3 – Sandstone composition and petrographic data***

Appendix C and D contains all raw petrographic data. All data collected from the petrographic analysis were normalized for quartz, feldspar, and lithics for compositional

analysis and are displayed on quartz-feldspar-lithic (QFL) ternary diagrams (Fig. 3).

Polycrystalline quartz was included in the “quartz” category as they were likely recycled.

Quartz-potassium feldspar-plagioclase (QKP) and polycrystalline quartz-monocrystalline quartz-undulatory quartz (QpQmQu) ternary diagrams were also generated (Fig. 3).

The sandstone samples from this study contain examples of sublithic, arkosic, subarkosic, and quartz arenite. The type section and composite Hades Creek section sandstone samples, representing the bulk of the Red Pine Shale petrographic analysis, are mostly arkosic or quartz arenite in composition. Though the Ashley Creek and Henry’s Fork sections have far fewer thin sections, they are both represented by mostly quartz arenite. Samples classified as sublithic are >10% lithic and between 10-25% feldspar grains. They are fine to pebbly sandstones with mostly angular grains and are moderately to poorly sorted. These samples are only found within the type section. Sandstones that are compositionally arkosic have >25% feldspar and >25% lithic content. They are dominantly medium sand, sub-angular grains, and are poorly sorted. This composition is found within the composite Hades Creek, Henry’s Fork, and type sections. Samples from subarkosic sandstones have between 10 and 25% feldspar, <10% lithics and are generally medium-grained, sub-angular and moderately sorted. These sandstones are also found within the composite Hades Creek, Henry’s Fork, and type sections. Quartz arenite sandstones are found in each of the locales; composite Hades Creek, Henry’s Fork, type section, and Ashley Creek. The sandstones with this composition are mostly very fine to fine sand, sub-rounded, and well-sorted and are composed of >90% quartz grains. The QpQmQu plot (Fig. 3) shows that quartz grains are dominantly monocrystalline. A

significant number of weathered feldspar grains were found within the Red Pine Shale sandstone samples, which poses a problem when plotting data on a QKP ternary diagram. Though it shows that grains are dominantly quartz, it is unclear if there are more plagioclase or potassium feldspar grains. On average, there are more weathered feldspar grains than plagioclase or potassium feldspar, but discounting the weathered grains, plagioclase is more common (Fig. 3).

The percentage of quartz in each sample was plotted on the QFL ternary diagram (Fig. 3) and for each measured section and can be seen in Figs. 13-16 in the petrographic curves. These curves show the percentage of quartz from each sample relative to combined feldspar and lithic totals. The type section petrographic curve (Fig. 13) shows more compositional variability at the base and becomes consistently more quartz-rich upsection. The sandstone beds in this section also become more fine-grained and are increasingly well-rounded up section, which is consistent with the compositional trends. In the composite Hades Creek section (Fig. 14), the sandstone beds show an increase in arkose farther up section. These sandstone samples also become more angular and are more poorly sorted higher in the section, again consistent with compositional trends. The Ashley Creek section and the Henry's Fork section have too few samples to recognize definitive trends, but the petrographic data are displayed in Figs. 15 and 16 respectively. There does not seem to be a relationship between the petrographic curve and the C-isotope and TOC curves.

#### ***5.4 – Detrital zircon data***

Three detrital zircon samples from the western locales show a diversity of age

populations and distributions. Two of these detrital zircon plots were first reported in Fanning and Dehler (2005) (samples RP03B-2 and 69PL05). Sample 69PL05 is from meter 80 in the type section. Samples RP03B-2 and 135PL02 are from the same 20 m interval at the base of Hades Creek section B (Appendix E). Sample 69PL05 (35 grains) has an exclusively Archean-Paleoproterozoic population, with a peak at 2.6 Ga, and represents direct sourcing of the Wyoming craton to the north. This single population also suggests that this part of the delta system was not mixing with the other sources. Both 135PL02 (58 grains) and RP03B-2 (30 grains) also show a high concentration of grains at 2.6 Ga., yet also have populations at 1.1-1.2 Ga, 1.4 Ga, and 1.7-1.8 Ga. The 1.1-1.2 Ga peak represents the Grenville orogeny and these grains likely came from the east-southeast (Fanning and Dehler, 2005; Mueller et al., 2007). The 1.4 Ga grains are likely derived from mid-continent A-type granites and the 1.7 to 1.8 Ga grains represent a source from the Yavapi-Mazatzal Province, which is to the east and south of the Uinta Mountains (Fanning and Dehler, 2005; Foster et al., 2006). The assortment of grain populations found in these sandstones suggests that the sediments deposited in the Red Pine basin were derived predominantly from the north, east, and possibly southeast. These observations are consistent with facies and petrographic trends in the Red Pine Shale, as well as Nd-isotope and detrital mode studies by Condie et al. (2001) and facies and petrographic studies of Wallace (1972). Though there are no point count data from these three samples, the sample from the type section is an arkosic arenite and the two samples from the Hades section are quartz arenites.

## CHAPTER 6

### STRATIGRAPHIC RESULTS

#### *6.1 - Introduction and Study Sites*

Multiple measured sections (from 18.5 to 662 m thick) from the four study areas were used in this research to stratigraphically characterize the Red Pine Shale: the type section, Mud Lake Flat Road section, Hades Creek A (now combined with upper Hades Creek), Hades Creek B, Hades Creek C, lower Hades Creek, Ashley Creek, and Henry's Fork (Appendix E; Appendix F). The type section and the composite Hades Creek measured sections are considered the main reference sections and jointly will be the composite-stratotype for the Red Pine Shale. The Ashley Creek and Henry's Fork sections are also considered reference sections.

The type section is the only measured section with all six facies present and is the only section that can be easily measured from the base to the top. The sole purpose of measuring and sampling the adjacent and correlative Mud Lake Flat Road partial section was to try to recapture the positive C-isotope excursion recorded near the base of the type section (Fig. 2). The Mud Lake Flat Road section was correlated to the type section by using stratigraphy and C-isotope data.

The Hades Creek locality (Appendices A and B) includes five partial sections previously identified by Dehler et al. (2007) that have now been correlated to form one composite section. The base of the Red Pine Shale is not exposed in this location, so these measured sections do not represent the total thickness of the formation, though a calculated total thickness is possible using new data from a recently drilled well (Richins

and Sons, Inc., 2006). The correlation of the Hades Creek measured sections was done using field methods (i.e. mapping and identification of marker beds) and facies characteristics. The Hades Creek section A was measured to the unconformable contact between the Red Pine Shale and the Mississippian Madison Formation; all other measured sections of the Hades Creek locale are 'floating' partial sections, with no upper or lower contacts. Correlations between generalized measured sections can be seen in Fig. 17. The Hades Creek A and upper Hades Creek sections were measured as two separate sections that stack exactly on top of one another. These sections are now the composite Hades Creek section and represent a continuous section 660m thick. By identifying marker beds within the lower part of section Hades Creek A, it was possible to correlate sections Hades Creek B and lower Hades Creek sections. Beds of fine-sandstone in the slump fold facies in section B from ~51 to 54m and ~59 to 60m correlate to more resistant beds in Hades Creek section A from ~50 to 52m and ~54 to 56m (Fig. 17, Appendix E). This is further supported by the beginning of distinctive cyclic interbedding of mudstone and siltstone to sandstone found beginning at 91.5m in Hades Creek section A and at 100m in Hades Creek section B (Appendix E). The top of the lower Hades Creek section is separated from the Hades Creek section by 156m of cover. Hades Creek section C correlates to the cliffy sandstone unit just below the contact between Hades Creek section A and upper Hades Creek section, at ~235m. Hades Creek section C was more difficult to correlate due to its distance from the other sections, but this is the most likely position for this measured section based on stratigraphic position, facies characteristics, TOC, and C-isotope correlation. The composite measured exposed



Figure 17. Photograph looking southeast of partial Hades Creek sections that have been correlated to create composite Hades Creek section.



thickness of the Hades Creek measured sections is ~890m.

A replacement water well was drilled in July of 2006 by Richins and Sons, Inc. beginning at approximately the base of the measured Hades Creek sections. This drilling penetrated the Red Pine Shale and terminated in a sandy unit interpreted to be Hades Pass quartzite with a contact depth of 231m (Richins and Sons, Inc., 2006). With this added thickness to the base of the composite Hades Creek section, the maximum measured thickness of the Red Pine Shale is now known to be at least 1121m. This is much less than Wallace's (1972) thickness of the Red Pine Shale (1830m).

The Ashley Creek locale, the most southeastern exposure of the Red Pine Shale, has potential for generating a complete measured section, but, due to vegetation and talus cover, it has only been measured as a partial section of 187.5m (Appendices A and E). Though access to this area is difficult and the section is on a very steep slope, this section provides important lateral and vertical faces information. The total map-calculated thickness of this section, from the gradational basal contact between the Red Pine Shale and the Hades Pass quartzite, to the unconformity with the overlying Mississippian Madison Limestone, is ~300 m. Because this area is difficult to access, samples are limited and, therefore, only a few C-isotope values have been obtained.

The Henry's Fork partial section is 248m thick and, though it is not a complete measured section due to accessibility and cover, has the potential to be the thickest overall section of the Red Pine Shale. The total map-calculated thickness is ~1800m (Bryant, 1992). This section also shows the gradational contact between the Red Pine Shale and the Hades Pass quartzite. Due to the high amount of cover in this locale and

lesser exposed black shale, C-isotope analysis has only been done on a few samples thus far.

## ***6.2 – Physical and Chemical Stratigraphy***

Initial correlation of the four measured sections was based on facies associations and the basal contact with the underlying Hades Pass quartzite (Fig. 18). The shale, shale-and-sandstone, and sandstone facies are the three most common facies and all three of these facies are seen in each of the measured sections, yet in varying proportions. The concretion facies is present only in the type section. The slump fold facies is seen in the type, composite Hades Creek, and Ashley Creek sections representing the western, southwestern and southern localities. The pebbly sandstone facies is found only within the two northernmost sections: type and Henry's Fork sections.

Vertical patterns within the type section, Henry's Fork, and Ashley Creek locales are similar. Each of these sections shows a decrease in sandstone percentage upsection. The composite Hades Creek section shows the opposite, an increase in sandstone percentage near the upper contact with the Madison Limestone. Because the type section, Henry's Fork, and Ashley Creek locales are less complete measured sections, it is possible that a coarsening upward sequence, such as the one seen at the Hades Creek locale, either is present and covered, or was present before removal by erosion. The drillers logs from the well at the Hades Creek locale do show an increase in sandstone percentage downwards towards the lower contact with the Hades Pass quartzite (Appendix E), consistent with the other locales.

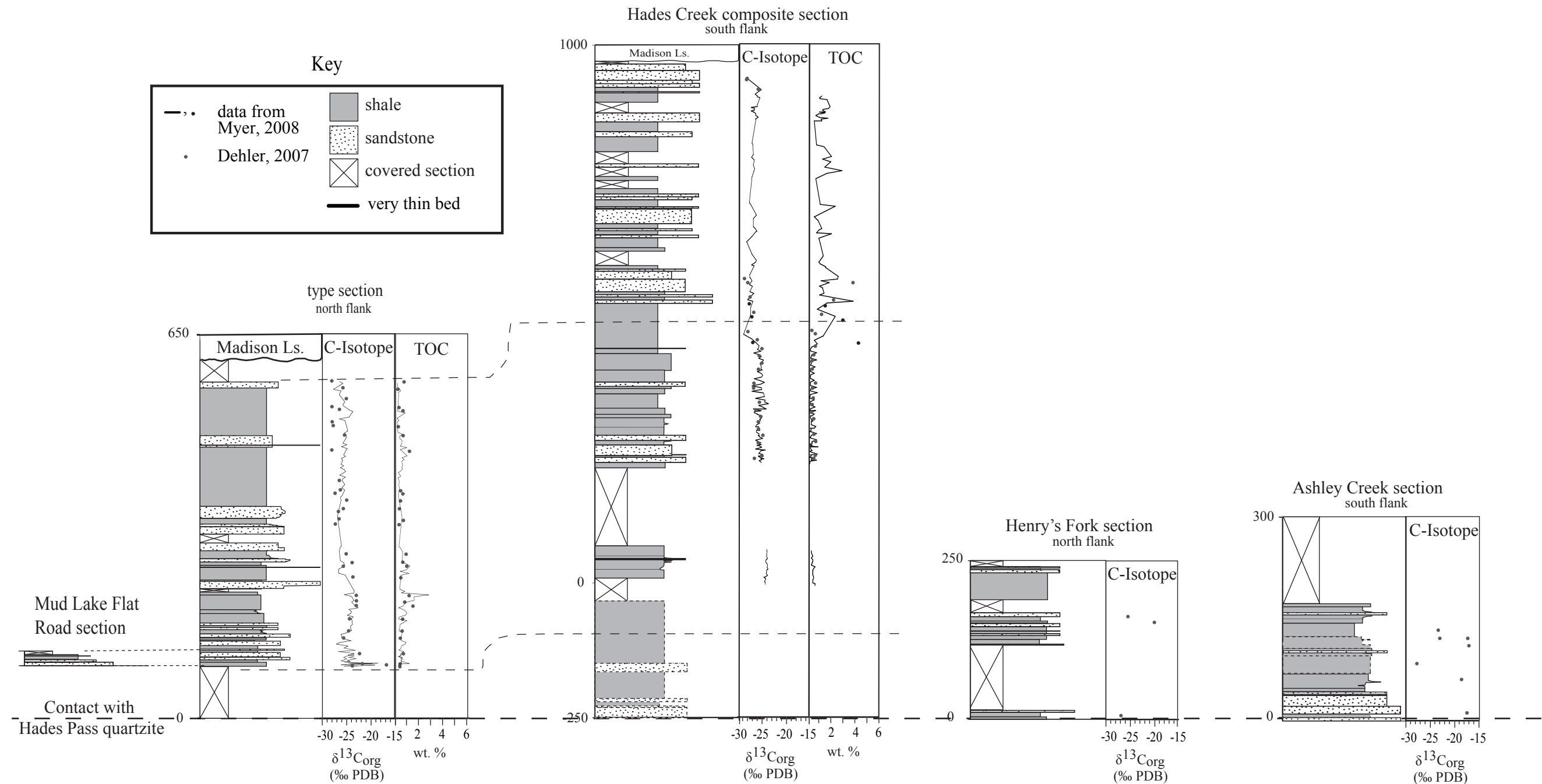


Figure 18. Correlation of type, Hades Creek composite, Henry's Fork, and Ashley Creek measured sections based on their contacts between the Red Pine Shale and the Hades Pass quartzite is gradational, though it is not seen at the Hades Creek locale. Stratigraphy below 0m at this measured section is based on subsurface data. Henry's Fork and Ashley Creek sections are not measured to upper contact with Mississippian Madison limestone because of cover and accessibility issues.

A relationship between the physical stratigraphy and C-isotope values can be seen in both the type and composite Hades Creek sections (Fig. 19). C-isotope values generally become less negative throughout finer grained intervals and become more negative in sandier intervals. The type section has higher concentrations of shale near the base and top of the section, which is also where C-isotope values are relatively less negative. In the center of the section is an interval of dominantly sandstone that has more negative C-isotope values. In the composite Hades Creek section there are relatively less negative C-isotope values in the lower half of the section where there are also higher concentrations of shale. In the upper half of this section, there are relatively more negative C-isotope values and more sandstone. Although there is a general correlation between isotopic values and grain size, there does not appear to be a specific facies dependence with isotopic values. For example, within a single facies, there is isotopic variability, and two different facies can also show similar values.

The most robust correlation is made when combining facies, petrography, C-isotope, and TOC data from the two main sections. The type section is best correlated with the base of the composite Hades Creek section and the subsurface Red Pine Shale below the at the Hades Creek locale. Fig. 19 shows this correlation and illustrates the best fit of the C-isotope and TOC data from each section, and the consistency with the estimated basal contact of the Red Pine Shale in the subsurface. The established correlation makes lateral facies trends recognizable; the type section is coarser (sandier) than the equivalent strata of the Hades Creek composite section, which is supportive of a delta system prograding from the north.

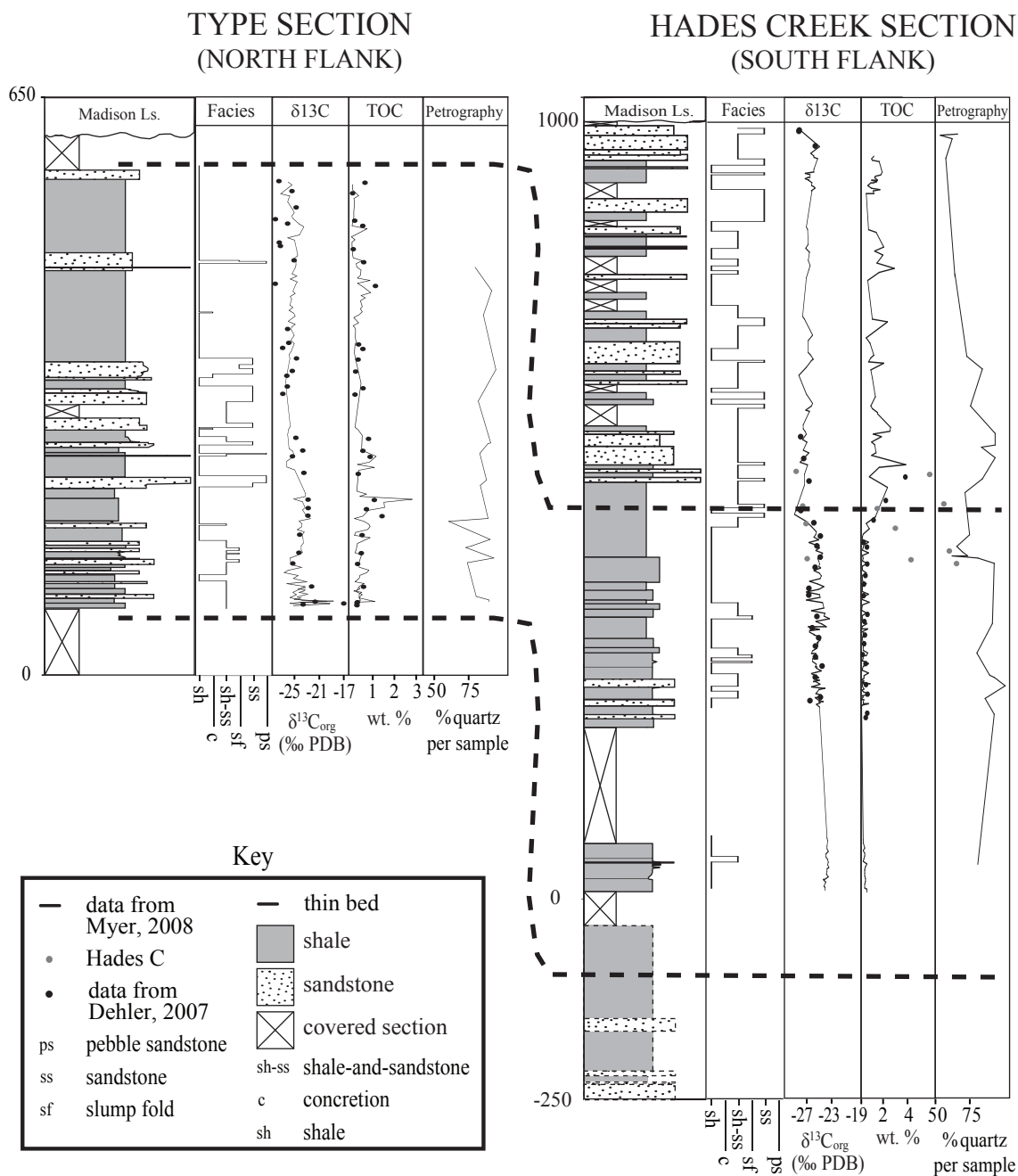


Figure 19. By using stratigraphy, facies, C-isotopes, TOC, and petrography the best fit was found to make a correlation between the north and south flank measured sections.

The Henry's Fork and Ashley Creek locales may exhibit lateral facies changes as compared to the western locales. While both of these measured sections fine upwards, they have a lower sandstone percentage than the two westernmost sections. The base of each of these measured sections contains thin sandstone beds, but relatively more interbedded shale. The composition of these sandstones is also different than those of the type and Hades Creek sections. Both Henry's Fork and Ashley Creek sandstones are more quartz-rich, with finer-grained, more-rounded, and better-sorted sand. This suggests that these two locales received sediment from a distal source, likely to the east based on previous paleogeographic models of the Uinta Mountain Group (Wallace and Crittenden, 1969; Condie et al., 2001). The Henry's Fork measured section does include the pebble facies that is seen in the type section and therefore shows the interaction of a proximal source to the north and a distal source from the east.

### ***6.3 Sequence Stratigraphy***

Generalized sequence stratigraphic terms are applied to these strata, although this application is somewhat difficult and therefore limited due to the lack of continuous vertical and lateral exposure. Because the contact with the underlying Hades Pass quartzite is apparently gradational, sequence stratigraphy of the Red Pine Shale requires consideration of this lower unit. The Hades Pass quartzite (1825-3000 m thick) is an understudied unit, but is generally interpreted as representing dominantly braided fluvial deposits (Wallace and Crittenden, 1969; Wallace, 1972). Kingsbury (2008) places a sequence boundary at the base of the Hades Pass quartzite. It appears that the Hades Pass quartzite and overlying Red Pine Shale package represent a single low order (2<sup>nd</sup>?) cycle

close to 4000 m thick. Considering the age (10s of millions of years) and thickness of the cycle, it is likely 2<sup>nd</sup> order (Prothero and Schwab, 1996). If there is a subtle unconformity at the base of the Red Pine Shale, then it would be considered a single transgressive-regressive cycle, possibly of 3<sup>rd</sup> order or sequence scale. Another possibility is that there is an unconformity at the base of the sandy upper part of the Red Pine Shale. However, no incision was observed and the intimately alternating facies patterns suggest a gradational contact. Also, there is not a significant facies change in this interval.

The Red Pine Shale shows stacking patterns of alternating coarse- and fine-grained intervals on 10-100s m scale and meter-scale that may reflect higher order cyclicity (Fig. 20). Cycles range from 32 to 143 m thick. These are defined by typical coarsening upward trends from shale to sandstone. Cycle tops were chosen above thick intervals (~30-100 m thick) of relatively coarser grained intervals (Fig. 20, Appendix E). Above these coarser grained intervals, the grain size typically decreases abruptly, although in some cases, the top of the coarser-grained interval grades upward into finer facies (Appendix E). Cyclicity in the Hades Creek sandstones was more difficult to assess due to significant cover. Eleven sequences are identified in the composite section, and if the Red Pine Shale represents ~10-20 million years, each sequence would approximate ~ 1 million year in duration, consistent with the duration of many Phanerozoic sequences. Within these potential sequences, higher order cyclicity on a meter to sub-meter scale is also defined by alternating coarse- and fine-grained intervals. There are thick (10-100 m scale) intervals where no higher-order cyclicity is notable, especially in the shale intervals of the type section.

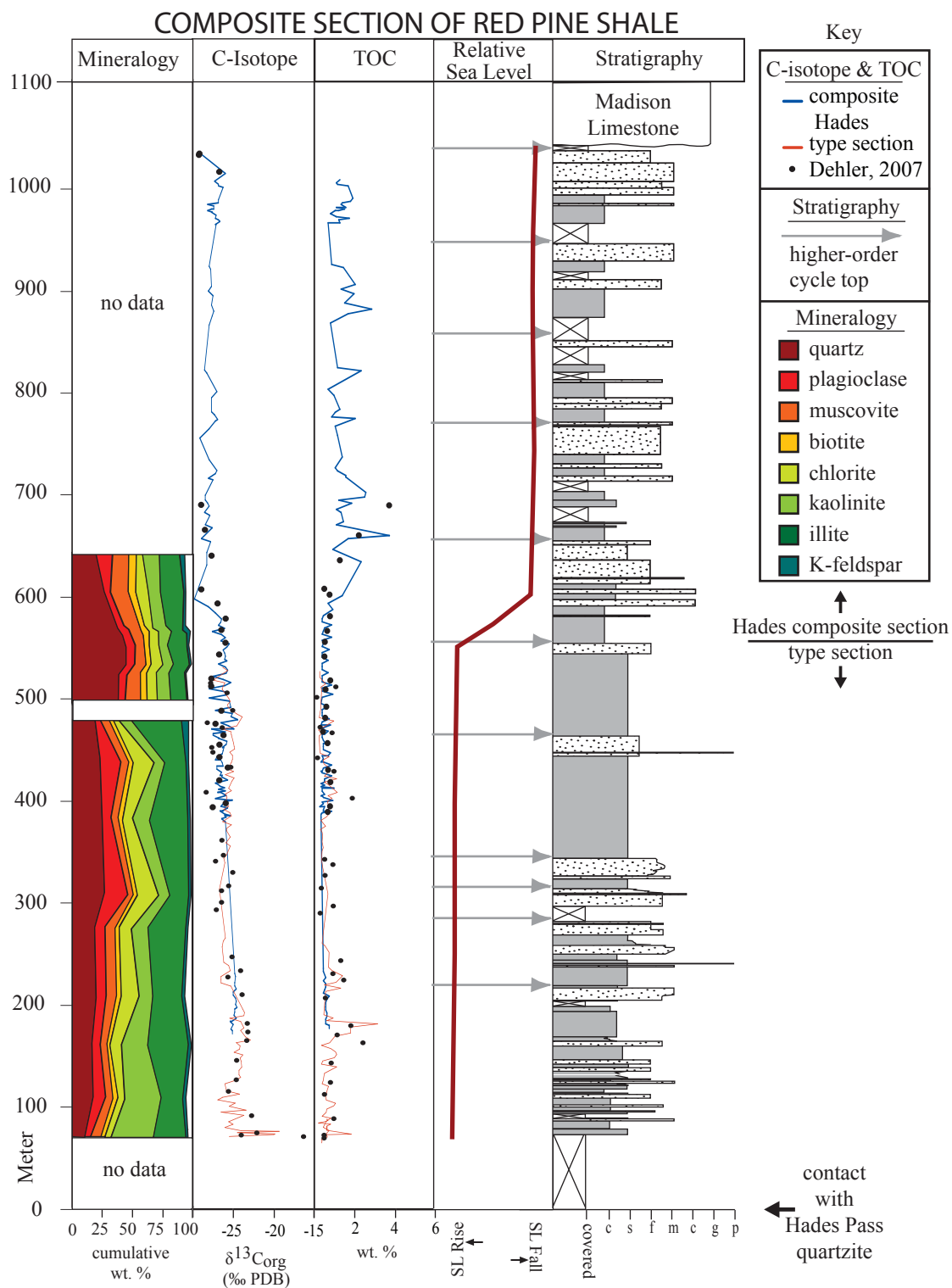


Figure 20. Composite stratigraphic column, mineralogy, C-isotope, TOC, and sea level graphs of Red Pine Shale. Notice upper section is taken from Hades composite section while lower section is taken from type section. (Mineralogy data modified from Block, unpublished data)



## CHAPTER 7

### DISCUSSION

#### *7.1 - Paleogeography of the Red Pine basin*

A combination of evidence from this study and from previous research (Wallace and Crittenden, 1969; Farmer and Ball, 1998; Condie et al., 2001; Dehler et al., 2007) indicate that the Red Pine Shale represents a marine deltaic setting with streams feeding the area from sources to the east and north (Fig. 21). More specifically, the facies show the interrelationship of prodeltaic and delta front environments that were affected at different times by different processes (fluvial, wave, and tide).

Lateral north to south correlation between sections show that the type section strata are relatively sandier than the correlative strata at the Hades Pass section (Fig. 18). Similarly, the basal partial section at Henry's Fork is relatively sandier than the same interval at Ashley Creek section to the south (Fig. 18). These lateral correlations show that the dominant deltaic system was being fed by rivers from the north, providing coarser sediment to the northern part of the basin and finer coeval sediment to the south. It is notable that the two southern localities are relatively finer grained, do not contain pebbles, both have slump folds, and contain a greater percentage of mature sandstone. These similarities suggest that these localities were distal to the immature sediment source and were also receiving sediment from another, more distal source, likely to the east. Another implication of these correlations is that there is still no evidence of a source or basin edge to the south (Condie et al., 2001), yet paleocurrent data from older units in

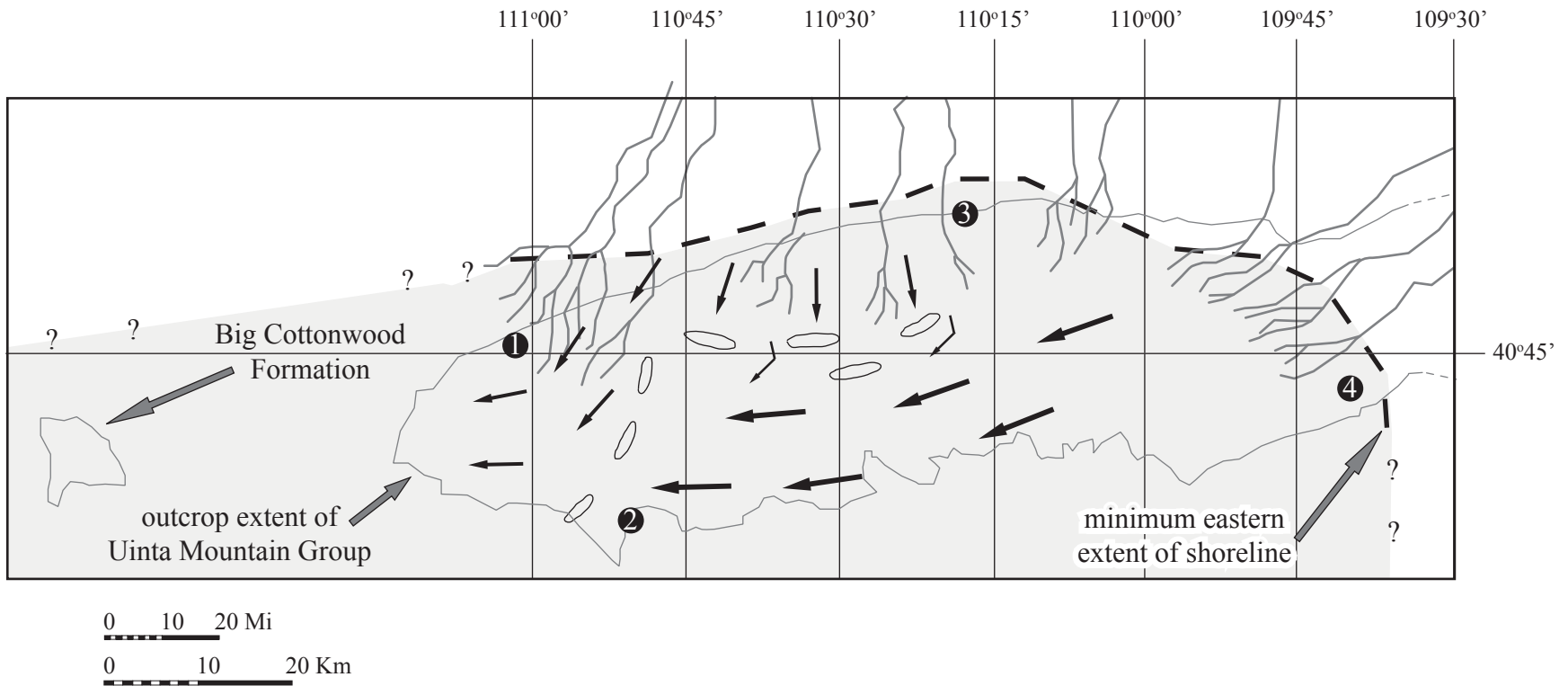


Figure 21. Paleogeographic model of Uinta Mountain and Big Cottonwood basin during deposition of the lower Red Pine sediment. Major transverse stream systems brought sediment from the east and north. 1 - type section, 2 - Hades Creek section, 3 - Henry's Fork section, 4 - Ashley Creek section. (Modified from Wallace and Crittenden, 1969)

the Uinta Mountain Group and correlative Big Cottonwood Formation show a northerly component of paleoflow. This suggests that there were marine currents flowing to the north at times, yet no obvious basin edge coincides with the southern termination of the Uinta Mountain Group outcrop extent (i.e., basin continues past Uinta Mountain Group outcrop extent to south). This is consistent with the ChUMP hypothesis of Dehler (2008), which proposes an interior seaway stretching from the Red Pine basin south to the Chuar and Pahrump group basins in the Grand Canyon and Death Valley regions, respectively.

The petrography of the sandstone-bearing facies in the eastern and southern sections shows a high percentage of quartz arenite, which likely reflects a deltaic system feeding the basin from the east, whereas sandstone facies in the northern and some eastern localities are more arkosic, reflecting the proximal source to the north. This is consistent with petrographic analyses of previous workers (e.g., Wallace, 1972; Condie et al., 2001). Other notable trends are the high concentrations of monocrystalline quartz grains and relatively high plagioclase and lesser orthoclase percentages, collectively suggesting first cycle sediments were derived from, in part, tonalitic and sialic granite sources that were exposed on the Wyoming craton. This research suggests that TTG complexes (tonalite-trondhjemite-granodiorite) were still a major source rock component on the Wyoming Craton (Frost, 1993) and were being exhumed during Uinta Mountain Group time, contrary to Condie et al (2001) who state that there is no record of TTG complexes in the Uinta Mountain Group sandstones because the Wyoming craton had experienced a period of uplift and erosion of the TTGs prior to Uinta Mountain Group time.

The detrital zircon data reflect the petrographic data. The arkosic Red Pine Shale

sample from the north flank shows exclusively Archean grain populations, reflecting a fluvial-dominated part of the delta that was tapping sediment from the Wyoming craton. This indicates that, at times, the delta sediment was not mixing with sediment from other sources and also shows the link between immature composition (and texture) and a locally derived source. Exclusively Archean populations are seen in the basal Red Castle formation (Kingsbury, 2008) and in the basal Big Cottonwood Formation to the west (Dehler et al., in review). This indicates that the fluvial system feeding the greater Uinta Mountain Group and Big Cottonwood basin from the north was sustained throughout the life of the basin and also emphasizes the genetic relationship between the Uinta Mountain Group and the Big Cottonwood Formation. The two quartz-rich samples from the south flank, as expected, show the range of age populations reported by other workers (Mueller et al., 2007; Kingsbury, 2008), except for the 766 Ma population reported by Dehler et al. (in review). These populations show a mixing of Archean grains derived from the north and east, with Proterozoic grains derived from the east-southeast. This shows a link between mature sandstone composition and farther-traveled Proterozoic grains. This spectrum of ages is also seen in a sample from the middle Big Cottonwood Formation (Dehler et al., in review), again emphasizing the relationship between the Uinta Mountain Group and Big Cottonwood Formation, and showing that there was a mixing of sources at times in the Big Cottonwood Formation part of the basin. The detrital zircon age modes from the Red Pine Shale can be used to indicate direction, proximity, and lithology of a source to a certain degree. However, the youngest age population only indicates that the Red Pine Shale has a maximum depositional age of 950 Ma (Crittenden and

Peterman, 1975), whereas it is very likely younger than 766 Ma (Dehler et al., 2007). Furthermore, it is not possible, as was hoped, to tie a certain age spectra to a certain facies type/depositional environment or place in a transgressive-regressive cycle, because the two main sediment sources do not change as the facies do.

### ***7.2-Controls on cycles***

The Hades Pass quartzite-Red Pine Shale low-order (2<sup>nd</sup>?) cycle represents a somewhat symmetrical cycle showing fluvial deposition at the base (lowstand), grading into organic-rich prodelta deposits in the middle (transgression) and followed by coarser delta front (and possibly delta plain) deposits at the top (highstand). This large-scale cycle is likely riddled with hiatal and/or unconformable surfaces, yet, because the strata appear to be genetically related, there is likely no significant time missing (or at least no basin reorganization) in this cycle. It should be noted that there is a similar cycle that makes up the lower western Uinta Mountain Group. The Red Castle formation and equivalents grade up into the Mount Watson Formation and equivalents and are capped by the Hades Pass quartzite. This stratigraphically lower 2<sup>nd</sup> order cycle also represents fluvial deposition grading up to marginal marine and marine deposition and contains higher-order cycles (3<sup>rd</sup>-5<sup>th</sup>) order (Kingsbury, 2008).

Controls on cyclicity in the Red Pine Shale are likely a combination of allogenic and autogenic processes. The lower order (2<sup>nd</sup>?) cyclicity is likely controlled by changes in seafloor spreading rates (Prothero and Schwab, 1996; Nichols, 2001) associated with the breakup of Rodinia. Although there could be local tectonic controls on this order of cyclicity, these alone could not explain marine incursion of ~500 km from the craton

edge. Higher-order cycle controls are difficult to assess due to the lack of lateral exposure of cycles. Local tectonic and deltaic controls likely contributed to (or even dominated) stratal stacking patterns, although glacioeustatic controls cannot be ruled out.

### ***7.3- Controls on C-isotope composition and stratigraphy***

The relationship between the physical stratigraphy and C-isotope values in the Red Pine Shale suggests that there is a common control on sedimentation patterns and organic carbon burial rates during Red Pine deposition. Within intervals of high shale content, the C-isotopes shift to relatively more positive values, and within coarser intervals, the values become relatively more negative. Because changes in sea level are hypothesized to be the cause of the lower order changes in sedimentation patterns in the Red Pine Shale, then it is likely that these changes are also responsible for C-isotope variability.

Many workers have noticed a relationship between C-isotope values and strata indicating sea-level change. Neoproterozoic glacial intervals, which are associated with sea-level fall, are generally associated with a decrease in C-isotope values, whereas strata indicating interglacial times and higher sea level are typically associated with less negative C-isotope values (e.g., Knoll et al., 1986; Kaufman and Knoll, 1995; Kaufman et al., 1997; Dehler et al., 2001; Dehler et al., 2007). Lithostratigraphic cycles in the pre-glacial Neoproterozoic Chuar Group have been attributed to subtle changes in glacioeustasy and concomitant local climate change; the cycles show less negative C-isotope values in relatively deeper-water facies when sea-level is at its highest, and more negative C-isotope values in shallow water and peritidal facies during lowstands (Dehler et al., 2005). These patterns are not limited to the Neoproterozoic; similar relationships

are observed in Phanerozoic deposits. For example, Cretaceous strata also show the relationship between transgressions and positive shifts in C-isotope composition and regressions with negative shifts in C-isotope composition, although excursions are much lower in magnitude (~2 per mil) (Jarvis et al., 2002; Lintnerova and Michalik, 2002). A similar relationship can be seen at the Ordovician-Silurian boundary prior to a short-lived glaciation (Brenchley, 1988; Brenchley et al., 1994). There is a complicated, but clear relationship between transgressions and relatively more positive C-isotope values and regressions with relatively more negative C-isotope values prior to and throughout this glaciation (Brenchley et al. 1994; Underwood et al., 1997).

If changes in the physical and C-isotope stratigraphy in the Red Pine Shale are a regional or global signature, then controls on the Red Pine Shale can be attributed to changes associated with eustasy. There is a possibility that the Red Pine Shale is recording local effects on these sedimentologic and geochemical processes, yet, considering that the isotope variability is similar to mid-Neoproterozoic sections nearby and around the globe, it is hypothesized that the Red Pine Shale records a global signature of sea-level and isotopic change (Dehler et al., 2005; Halverson et al., 2005; Dehler et al., 2007; Dehler, 2008).

Dehler et al. (2005, 2007) suggest that the Red Pine Shale correlates with the Chuar Group of Grand Canyon using, in part, C-isotope curves (Fig. 22). The high-resolution C-curve for the Red Pine Shale from this research adds strength to this correlation by reproducing the large-scale variability in C-isotopes used to make the correlation. This correlation is strengthened by similar microfossil assemblage, facies similarities, and

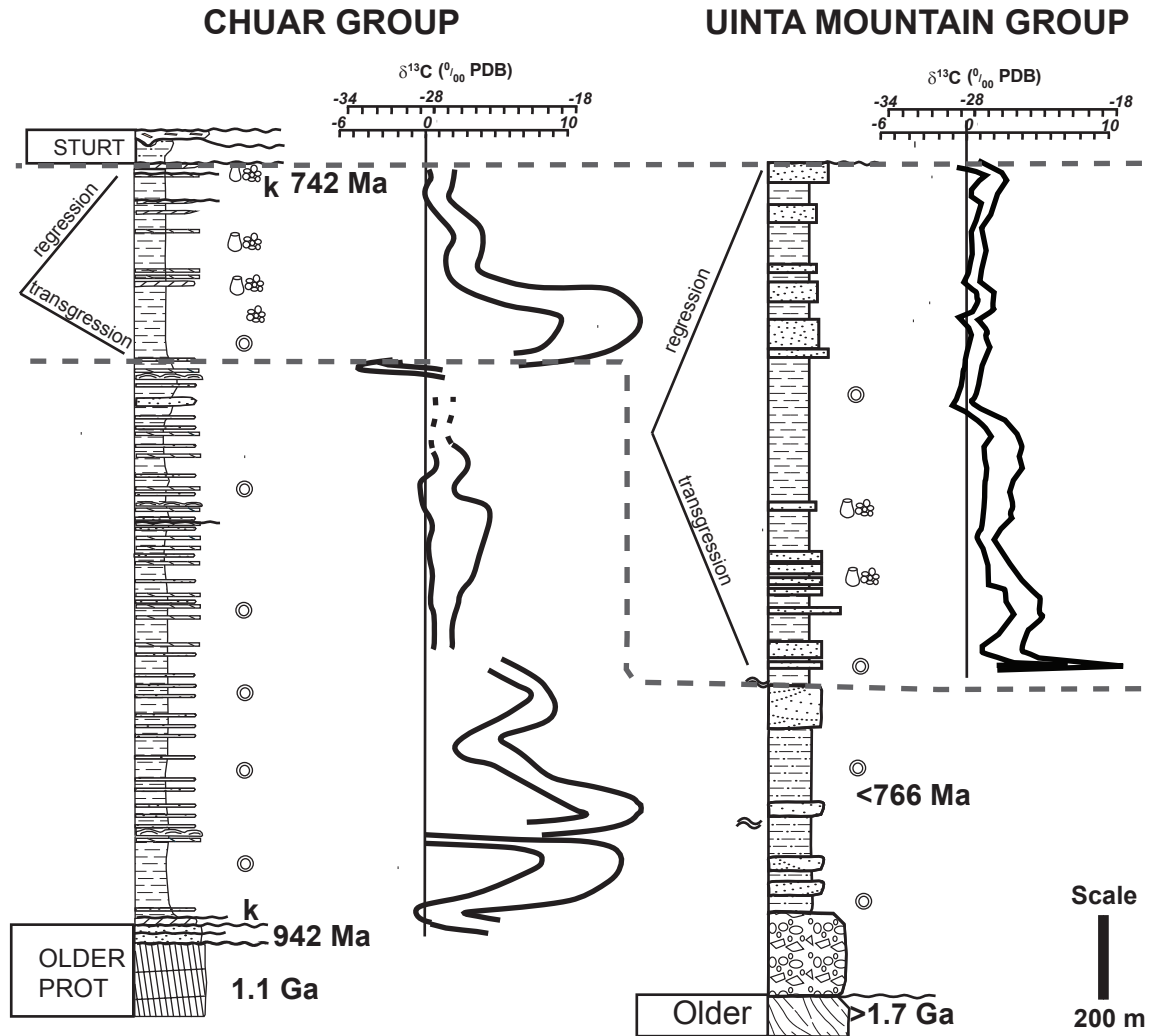


Figure 22. Stratigraphy and C-isotope data from the Chuar Group and Uinta Mountain Group showing Neoproterozoic correlation. The correlation was made based on C-isotope patterns, stratigraphy, and microfossil assemblages. (Modified from Dehler et al., 2008, and Dehler, unpublished data)



depositional ages (Dehler, 2008). Both the Chuar Group and Red Pine Shale show variability on the order of  $\sim 12$  ‰, which is a common magnitude of C-isotope variability just prior to the first of at least two low-latitude glaciations (Halverson et al., 2005), the first of which is thought to have occurred at about 750-700 Ma (Hoffman et al., 1998).

Shale geochemical data show a relationship between kaolinite abundance and C-isotope values (Bloch unpubl data; Fig. 20), which have implications for control on isotopic composition. Where kaolinite percentages are high, C-isotope values are relatively positive, and where kaolinite is less abundant, the C-isotopes values are lower. This independent dataset suggests that there was more weathering and likely greater humidity during times of greater organic-carbon burial rates, and less weathering in the source area and greater aridity during times of lower organic carbon burial rates. Dehler et al. (2005) report the same relationship in the correlative Chuar Group: high C-isotope values associated with high kaolinite abundances (and higher CIA values) and lower C-isotope values with lower kaolinite abundances (and lower CIA values).

This research suggests that the model used by Dehler et al. (2005) to explain the multiple data sets in the Chuar Group can also be used to explain the Red Pine Shale datasets. Relatively more positive C-isotope values associated with higher kaolinite percentages and fine-grained intervals suggest that, during wetter times, sedimentation rates and sea level were higher, hence burying greater amounts of organic carbon. Conversely, more negative C-isotope values associated with coarser grained intervals suggest drier conditions, lower sedimentation rates and lower sea level, and hence less organic carbon burial. Because this is seen in both Red Pine Shale and the coeval Chuar

Group, and these strata are similar to global mid-Neoproterozoic data sets, it is likely that these parameters – climate-driven sedimentation rates and sea level change -- are, in part, responsible for C-isotope variability globally at this time.

The Red Pine and Chuar basins were areas of the craton that were flooded during times of high sea level, likely associated with increased seafloor spreading rates as Rodinia broke apart. These basins were reservoirs for carbon storage, and when productivity rates were likely high due to higher sedimentation rates and related nutrient levels, significant burial would have taken place. If the cratons worldwide were intermittently flooded during the mid-Neoproterozoic, then significant amounts of carbon could be sequestered. This could ultimately lead to CO<sub>2</sub> drawdown and global cooling, which is seen in deposits overlying the Red Pine Shale correlatives: stratigraphic units which record low-latitude glaciations.

## CHAPTER 8

### CONCLUSIONS

1) This study used both field and laboratory techniques to formally characterize the Red Pine Shale. Up until now, although the Red Pine Shale is formally named, it is not formally described. This paper fulfills the requirements to modify the Red Pine Shale (Williams, 1953) in accordance with the Stratigraphic Code (NACSM, 1983). The type section and Hades Creek composite measured sections, the main reference sections, are proposed as the composite-stratotype for the Red Pine Shale. The Henry's Fork and Ashley Creek sections are proposed reference sections.

2) Facies, petrographic, and stratigraphic analyses of the Red Pine Shale indicate that it represents marine deltaic systems being fed by rivers transporting mature sediment from the east and coincident immature sediment from the north. Six facies indicate wave-, storm-, and possibly tidal-influences on prodelta and delta front areas of these delta systems through Red Pine time. The composite measured section of the Red Pine Shale shows overall low order (2<sup>nd</sup>?) transgressive-regressive cycles with ~11 C-isotope cycles within and is evidence for a north-south progradation of deltas from the north. The longer-term low-order cycle must be in part controlled by tectonoeustacy as these marine deposits are hundreds of kilometers inboard from the cratonic edge. Higher-order cycles have mixed controls and, therefore, are harder to discern. This interpretation is consistent with the petrographic data, which show more input from a quartz-rich source at the base of the section with an increasing amount of mixing with a more arkosic source through time; the arkosic sandstone reflects delta progradation from the north. Detrital

zircon analyses also show two major grain population distributions: one from the north consisting of only Archean grains and one from the east showing mixed Proterozoic and Archean populations.

3) The composite C-isotope curve from the type section and correlative Hades section shows high-magnitude variability at the base of the section with declining variability upsection. Local and regional C-isotope correlation, H/C, and TOC values suggest that these values represent primary seawater values.

4) Correlation of C-isotope values with shale geochemistry and facies data suggest common controls on these parameters. Less negative C-isotope values correspond to relatively high sea level and higher kaolinite abundances (humid climate). More negative C-isotope values correspond to relatively lower sea level and lower kaolinite abundances (arid climate). These same relationships are seen in the correlative Chuar Group of Grand Canyon, and suggest that changes in sedimentation rates, driven by climate change, may be in part responsible for the high-magnitude variability in C-values at this time globally and the related CO<sub>2</sub> drawdown responsible for ensuing colder times of the Sturtian episode.

## REFERENCES

- Ball, T. T., and Farmer, G. L., 1998. Infilling history of a Neoproterozoic intracratonic basin, Nd isotope provenance studies of the Uinta Mountain Group, Western United States: *Precambrian Research*, v. 87, no. 1-2, p. 1-18.
- Bhattacharya, J.P., 2006. Terminal distributary channels and delta front architecture of river-dominated delta systems: *Journal of Sedimentary Research*, v. 76, no. 2, p. 212-233.
- Bhattacharya, J.P. and Walker, R.G., 1991. Allostratigraphic subdivision of the Upper Cretaceous Dunvegan, Shaftesbury and Kaskapau formations in the northwestern Alberta subsurface: *Bulletin of Canadian Petroleum Geology*, v. 39, p. 145–164.
- Boggs, S., 2006. *Principles of Sedimentology and Stratigraphy*; Fourth Edition, Columbus, Pearson-Prentice Hall, 688 p.
- Brehm, A. M., 2007. A re-evaluation of the Jesse Ewing Canyon Formation, Uinta Mountain Group, Northeastern Utah: M.S. Thesis. Utah State University, Logan. 232 p.
- Brenchley, P.J., 1988. Environmental changes close to the Ordovician Silurian boundary, *in* Cocks, L.R.M. & Rickards, R.B., eds., *A Global Analysis of the Ordovician-Silurian boundary*: *Bulletin of the British Museum (Natural History). Geology Series*, v. 43, p. 377-385.
- Brenchley, P.J., Marshall, J. D., Carden, G. A. F., Robertson, D. B. R., Long, D. G. F., Meidla, T., Hints, L., and Anderson T. F., 1994. Bathymetric and isotopic evidence for a short-lived late Ordovician glaciation in a greenhouse period: *Geology*, v. 22, p. 295-298.
- Bryant, B., 1992, Geologic and structure maps of the Salt Lake City 1° x 2° quadrangle, Utah and Wyoming: U.S. Geological Survey Miscellaneous Investigations Series Map I-1997, scale 1:250,000.
- Collinson, J.D., and Thompson, D.B., 1982. *Sedimentary Structures*: London, George Allen and Unwin, 194 p.
- Colpron, M., Logan, J.M., and Mortensen, J.K., 2002. U-Pb zircon age constraint for the late Neoproterozoic rifting and initiation of the lower Paleozoic passive margin of western Laurentia: *Canadian Journal of Earth Science*, v. 39, p. 133-143.

- Condie, K. C., 1993. Chemical composition and evolution of the upper continental crust: contrasting results from surface samples and shales: *Chemical Geology*, v. 104, p. 1-37.
- Condie, K.C., Lee, D., and Farmer, G.L., 2001. Tectonic setting and provenance of the Neoproterozoic Uinta Mountain and Big Cottonwood groups, northern Utah. constraints from geochemistry, Nd isotopes, and detrital modes: *Sedimentary Geology*, v. 141, p. 443-464.
- Crittenden, M. D., and Peterman, Z.E., 1975. Provisional Rb/Sr age of the Precambrian Uinta Mountain Group, northeastern Utah, *Utah: Geology*, v. 2, no. 1, p. 75-77.
- Dalziel, I. W. D., 1997. Neoproterozoic-Paleozoic geography and tectonics; review, hypothesis: *Geological Society of America Bulletin*, v. 109, no. 1, p. 16-42.
- DeGrey, L.D., 2005. Geology of the Swallow Canyon 7.5-minute quadrangle, Dagget County, Utah and Moffat County, Colorado-Facies analysis and stratigraphy of the Neoproterozoic eastern Uinta Mountain Group: M.S. Thesis, Idaho State University, Pocatello, 122 p.
- Dehler, C. M., 2008. The Chuar Group-Uinta Mountain Group-Pahrump Group connection revisited: a “snapshot” of the infra-Sturtian earth system: *Geological Society of America Abstracts with Programs*, v. 40, no. 1, p. 36.
- Dehler, C.M., Fanning, C.M., and Link, P.K., in review. 766 Ma Maximum Age for lower Uinta Mountain Group, Utah: SHRIMP Foils the Curse of the Proterozoic Sandstone: Submitted to *Geology*.
- Dehler, C.M., Prave, A.R., Crossey, L.I., Karlstrom, K.E., Atudorei, V., and Porter, S.M., 2001. Linking mid-Neoproterozoic successions in the western U.S.: The Chuar Group Uinta Mountain Group-Pahrump Group connection (ChUMP): *Geological Society of America Abstracts with Programs*, v. 33, no. 5, p. 20-21.
- Dehler, C.M., Elrick, M.E., Bloch, J.D., Karlstrom, K.E., Crossey, L.J., and DesMarais, D., 2005. High-resolution  $\delta^{13}\text{C}$  stratigraphy of the Chuar Group (~770-742 Ma), Grand Canyon: Implications for mid-Neoproterozoic climate change: *Geological Society of America Bulletin*, v. 117, p. 32-45.
- Dehler, C. M., and Sprinkel, D. A., 2005. Revised Stratigraphy and correlation of the Neoproterozoic Uinta Mountain Group, *in* Dehler, C.M., Pederson, J.L., Sprinkel, D.A., and Kowallis, B.J., eds., *Uinta Mountain Geology: Utah Geological Association Publication*, v. 33, p. 17-30.

- Dehler, C.M., Porter, S.M., Sprinkel, D.A., DeGrey, L.D., and Brehm, A., 2007. The Neoproterozoic Uinta Mountain Group revisited: a synthesis of recent work on the Red Pine Shale and undivided clastic strata, northeastern Utah, *in* Link, P.K., & Lewis, R., eds., *Proterozoic Geology of Western North America and Siberia*: SEPM Special Publication 86, p. 151-166.
- Ehlers, T.A., and Chan, M.A., 1999. Tidal cyclicities and estuarine deposition of the Proterozoic Big Cottonwood Formation, Utah: *Journal of Sedimentary Research*, v. 69, no. 6, p. 1169-1180.
- Fanning, M.C., and Dehler, C.M., 2005. Constraining depositional ages for Neoproterozoic siliciclastic sequences through detrital zircon ages: ca. 770 Ma maximum age for the lower Uinta Mountain Group: *Geological Society of America Abstracts with Programs*.
- Foster, D.A., Mueller, P.A., Mogk, D.W., Wooden, J.L., and Vogl, J.J., 2006. Proterozoic evolution of the western margin of the Wyoming craton: implications for the tectonic and magmatic evolution of the northern Rocky Mountains: *Canadian Journal of Earth Sciences*, v. 43, p. 1601-1619.
- Halverson, G.P., Hoffman, P.F., Schrag, D.P., Maloof, A.C., and Rice, A.H.N., 2005. Toward a Neoproterozoic composite carbon-isotope record: *Geological Society of America Bulletin*, v. 117, p. 1181-1207.
- Hansen, W. R., 1965. *Geology of the Flaming Gorge Area, Utah-Colorado-Wyoming*: U.S. Geological Survey, Professional Paper, v. 490, p. 196.
- Harms, J.C., Southard, J.B., Spearing, D.R., and Walker, R.G., 1975. Depositional environments as interpreted from primary sedimentary structures and stratification sequences: *SEPM Short Course #2*, 161 p.
- Hedge, C. E., Houston, R. S., Tweto, O. L., Peterman, Z., Harrison, J. E., and Reid, R. R., 1986. The Precambrian of the Rocky Mountain region, *in* Harrison, J. E. and Peterman, Z. E., eds., *Correlation of Precambrian Rocks of the United States and Mexico*: U.S. Geological Survey Professional Paper 1241-D. 17 p.
- Hoffman, P.F., Kaufman, A.K., Halverson, G.P., Schrag, D.P., 1998. A Neoproterozoic snowball earth: *Science*, v. 281, p. 1342-1346.
- Hoffman, P. F., and D. P. Schrag, 2002. The snowball Earth hypothesis: testing the limits of global change: *Terra Nova*, v. 14, p. 129-155.

- Horodyski R. J., 1993. Paleontology of Proterozoic shales and mudstones. examples from the Belt Supergroup, Chuar Group and Pahrump Group, western USA: *Precambrian Research*, v. 61, p. 241–278.
- Jarvis, I., Mabrouk, A., Moody, R., and De Cabrera, S., 2002. Late Cretaceous (Campanian) carbon isotope events, sea-level change and correlation of the Tethyan and Boreal realms: *Palaeogeography. Palaeoclimatology. Palaeoecology*, v. 188, p. 215-248.
- Karlstrom, Karl E., Bowring, S. A., Dehler, C.M., Knoll, A.H., Porter, S. M., Sharp, Z., Des Marais, D. J., Weil, A.B., Geissman, J. W., Elrick, M., Timmons, M. J., Keefe, K., and Crossey, L. J., 2000. The Chuar Group of the Grand Canyon: Record of break-up of Rodinia, associated change in the global carbon cycle, and ecosystem expansion by 740 Ma: *Geology*, v. 28, p. 619-622.
- Kaufman, A. J., and Knoll, A. H., 1995. Neoproterozoic variations in the C-isotope composition of seawater: stratigraphic and biogeochemical implications: *Precambrian Research*, v. 73, p. 27-49.
- Kingsbury, E.M., 2008. A Neoproterozoic (<770 Ma) shoreline in the high Uintas Wilderness, Uinta Mountain Group, northeastern Utah: Evidence for a pre-Sturtian western interior seaway: M.S. Thesis, Idaho State University, Pocatello.
- Knoll, A.H., 2003. *Life on a Young Planet: The First Three Billion Years of Evolution on Earth*: Princeton, Princeton University Press, 304 p.
- Knoll, A.H., Blick, N., and Awramik, A.M., 1981. Stratigraphic and ecologic implications of late Precambrian microfossils from Utah: *American Journal of Science*, v. 281, p. 247–263.
- Knoll, A.H., Hayes, J.M., Kaufman, A.J., Swett, K., Lambert, I.B., 1986. Secular variation in carbon isotope ratios from Upper Proterozoic successions of Svalbard and East Greenland: *Nature*, v. 321, p. 832-838.
- Larsen, W. N., 1954. *Precambrian Geology of the Western Uinta Mountains, Utah*: M.S. Thesis, University of Utah, Salt Lake City, 53 p.
- Link, P. K., and many others, 1993. Middle and Late Proterozoic stratified rocks of the western U.S. Cordillera, Colorado Plateau, and Basin and Range province, *in* J. Reed, J. C., M. E. Bickford, R. S. Houston, P. K. Link, D. W. Rankin, P. K. Sims, and W. R. Van Schmus, eds., *The Geology of North America: DNAG Volume C-2, Precambrian: Conterminous U.S.*, p. 463-595.



- Lintnerová, O., and Michalík, J., 2002. High resolution Carbon isotope stratigraphy of lower Cretaceous pelagic limestones: *Geologica Carpathica*. 53 p.
- Mueller, P. A., Foster, D. A., Mogk, D. W., Wooden, J. L., Kamenov, G. D., and Vogl, J. J., 2007. Detrital mineral chronology of the Uinta Mountain Group: Implications for the Grenville flood in southwestern Laurentia: *Geology*, v. 35, no. 5, p. 431 – 434.
- Nagy, R.M., and S. M. Porter, 2005. Paleontology of the Neoproterozoic Uinta Mountain Group, *in* Dehler, C.M., Pederson, J.L., Sprinkel, D.A., and Kowallis, B.J., eds., *Uinta Mountain Geology: Utah Geological Association Publication 33*, p. 49-62.
- Nichols, G., 2001. *Sedimentology and stratigraphy*: London, Blackwell Science Ltd., 355 p.
- North American Commission on Stratigraphic Nomenclature (NACSM), Code Committee, Steven S. Oriel, Chairman, 1983. *North American Stratigraphic Code: American Association of Petroleum Geologists Bulletin*, v. 67, no. 5, p. 841-875.
- Nyberg, A.V., 1982. Contributions of micropaleontology; Proterozoic stromatolitic chert and shale-facies microfossil assemblages from the western United States and the Soviet Union; morphology and relationships of the Cretaceous foraminifera Colomia, Cushman, and Bermudez: University of California, Ph.D. dissertation, Los Angeles, 265 p.
- Porter, S. M. and Knoll, A. H., 2000. Testate amoebae in the Neoproterozoic Era: evidence from vase-shaped microfossils in the Chuar Group, Grand Canyon: *Paleobiology*, p. 26, no. 3, p. 360-385.
- Porter, S. M., R. Meisterfeld, R. Knoll, A. H., 2003. Vase-shaped microfossils from the Neoproterozoic Chuar Group, Grand Canyon: a classification guided by modern testate amoebae: *Journal of Paleontology*, p. 77, no. 3, p. 409-429.
- Prothero, D. R. and Schwab, F. 1996. *Sedimentary Geology. An Introduction to Sedimentary Rocks and Stratigraphy*: New York, W. H. Freeman, 575 p.
- Richins and Sons, Inc., “replacement wells completed by driller”, July 8, 2006. Utah Division of Water Rights, January 29, 2008, <[www.waterrights.utah.gov/](http://www.waterrights.utah.gov/)>.
- Rybczynski, D., in prep. Confessions of a Rodinian intracratonic basin: analyzing the undivided eastern Uinta Mountain Group: M.S. Thesis, Utah State University, Logan.

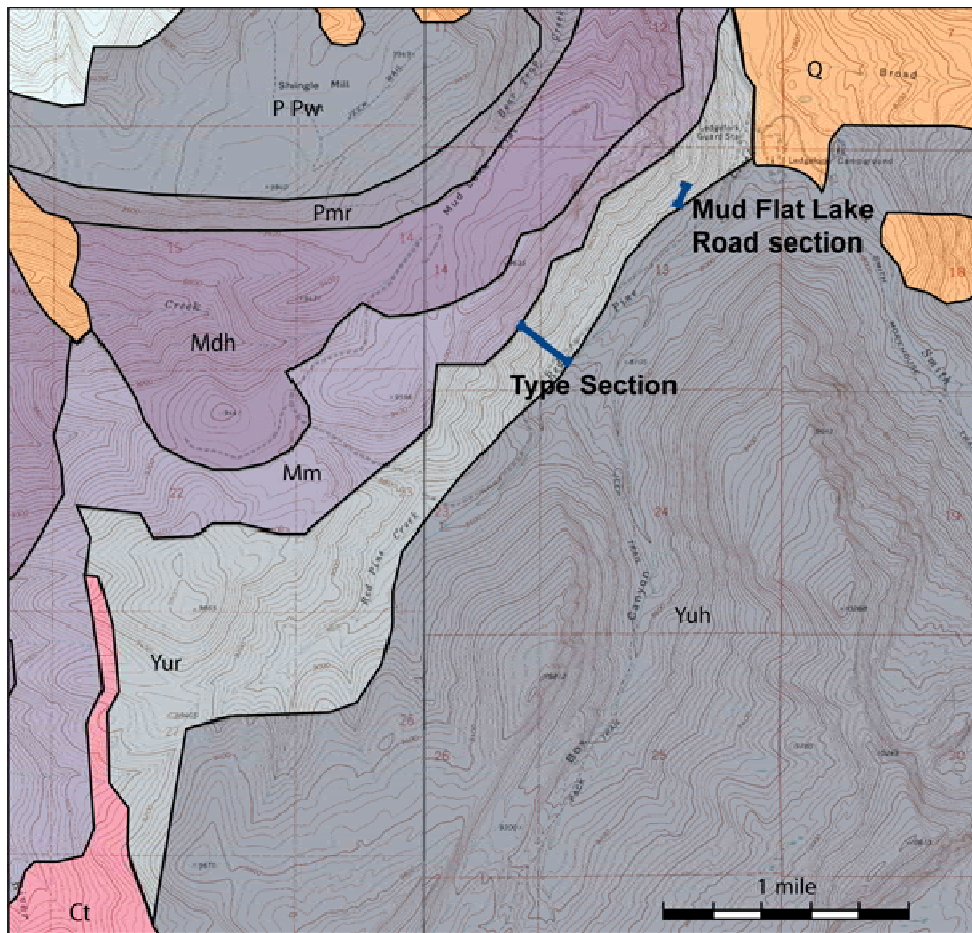
- Sanderson, I. D., 1984. The Mount Watson Formation, an interpreted braided-fluvial deposit in the Uinta Mountain Group (Upper Precambrian), Utah: *The Mountain Geologist*, v. 21, no. 4, p. 157-164.
- Sanderson, I.D., and Wiley, M.T., 1986. The Jesse Ewing Canyon Formation, an interpreted alluvial fan deposit in the basal Uinta Mountain Group (Middle Proterozoic), Utah: *The Mountain Geologist*, v. 23, no. 3, p. 77-89.
- Sprinkel, D.A., 2002. Progress report geologic map of the Dutch John 30' x 60' quadrangle, Utah-Colorado-Wyoming (year 3 of 3): Utah Geological Survey Open-File Report 399. scale 1:62,500.
- Sprinkel, D. A., and Waanders, G., 2005. Stratigraphy, organic microfossils, and thermal maturation of the Neoproterozoic Uinta Mountain Group in the eastern Uinta Mountains, Northeastern Utah, *in* Dehler, C.M., Pederson, J.L., Sprinkel, D.A., and Kowallis, B.J., eds., *Uinta Mountain Geology: Utah Geological Association Publication 33*, p. 63-73.
- Strauss, H., Des Marais, D.J., Summons, R.E., and Hayes, J.M, 1992. Concentrations of Organic Carbon and Maturities and Elemental Compositions of Kerogens, *in*, Schopf, J.W., and Klein, C., eds., *The Proterozoic Biosphere: A Multidisciplinary Study*, Cambridge University Press, New York, NY, p. 95-100.
- Underwood, C .J., Crowley, S .F., Marshall, J .D., and Brenchley, P. J., 1997. High-resolution carbon isotope stratigraphy of the basal Silurian Stratotype (Dob's Linn, Scotland) and its global correlation: *Journal of the Geological Society*. July 1997, v. 16.
- Vidal, G., 1976. Late Precambrian microfossils from the Visingsö beds in southern Sweden: *Fossils and Strata*, v. 9, p. 1-57.
- Vidal, G. and Ford, T. D., 1985. Microbiotas from the Late Proterozoic Chuar Group (Northern Arizona) and Uinta Mountains Group (Utah) and their chronostratigraphic implications: *Precambrian Research*, v. 28, p. 349-389.
- Wallace, C. A., 1972. A basin analysis of the upper Precambrian Uinta Mountain Group, Utah: Ph.D. Dissertation, University of California Santa Barbara. 412 p.
- Wallace, C.A., and Crittenden, M.D., 1969. The Stratigraphy, depositional environment and correlation of the Precambrian Uinta Mountain Group, western Uinta Mountains, Utah, *in* Lindsey, J.B., ed., *Geologic Guidebook of the Uinta Mountains*. Intermountain Association of Geologists 16th Annual Field Conference, p. 127-142.

Weil, A.B., Geissman, J.W., and Ashby, J.M., 2006. A new paleomagnetic pole for the Neoproterozoic Uinta Mountain supergroup, Rocky Mountain States, USA: *Precambrian Research*, v. 147, p. 234–259.

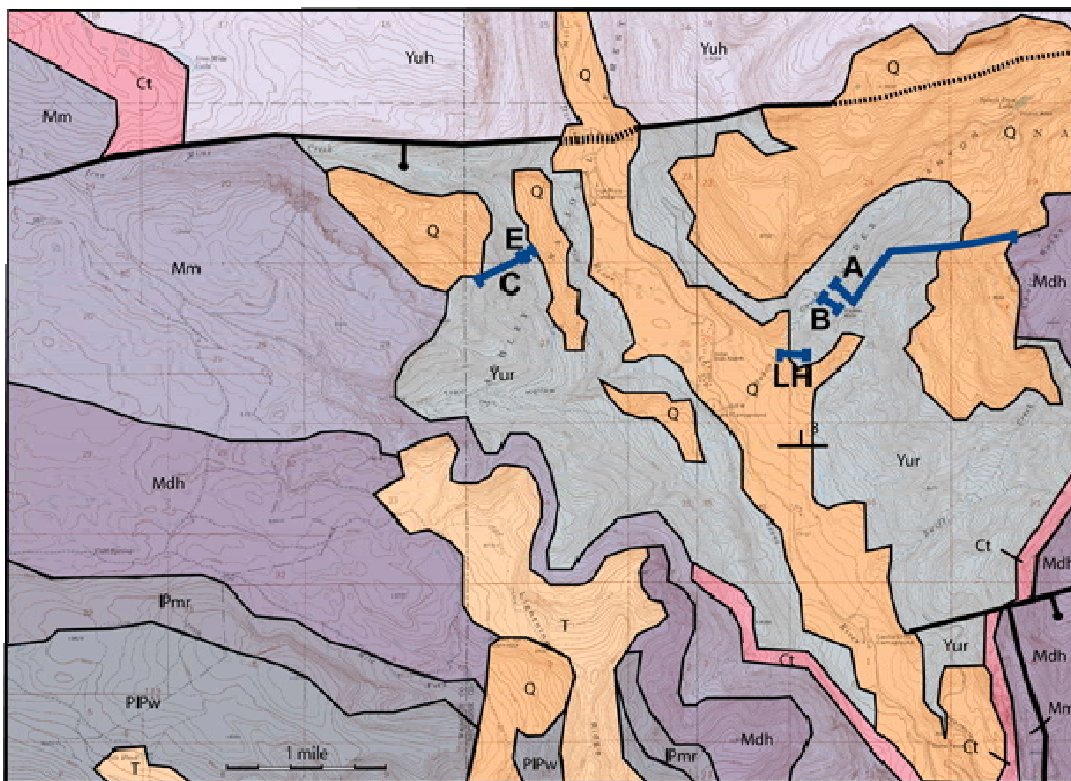
Williams, N., 1953. Late pre-Cambrian and early Paleozoic geology of western Uinta Mountains, Utah: *AAPG Bulletin*, v. 37, no. 12, p. 2734.

APPENDICES

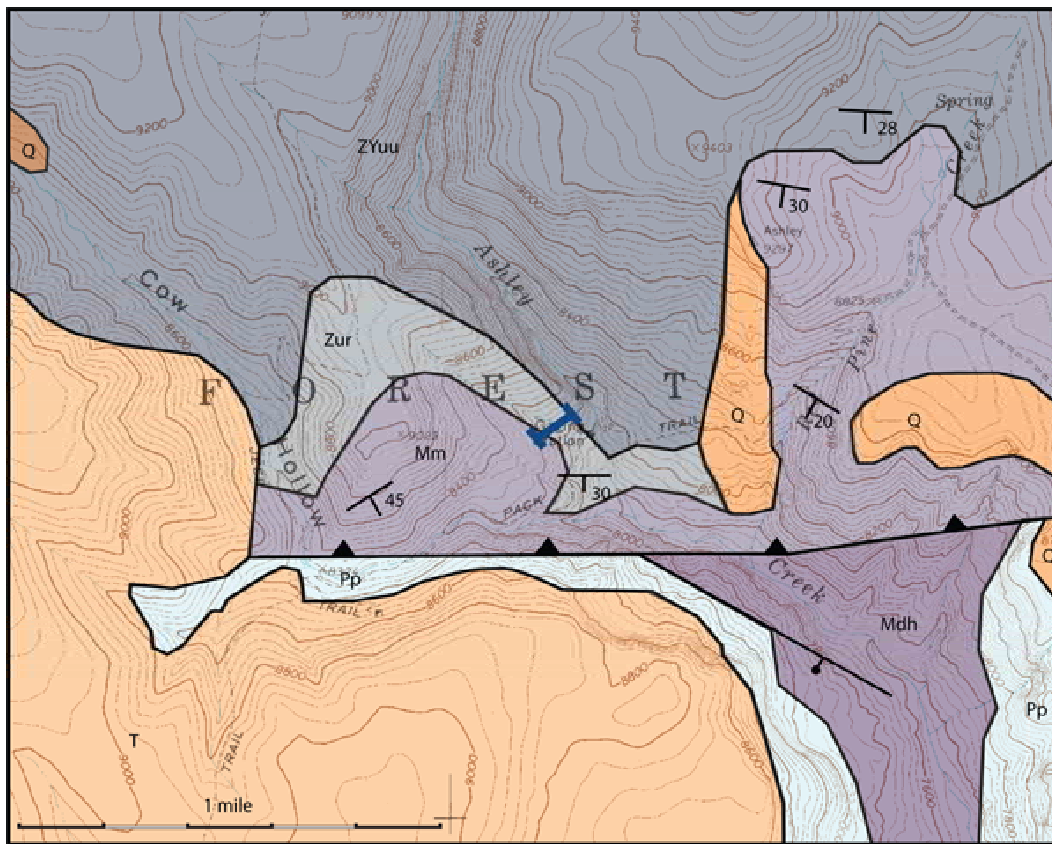
## Appendix A: Maps of measured sections



Geologic map showing location of measured sections at type section locale and surrounding geology. The type section has been previously measured in reconnaissance fashion by Dehler and is a focus of this study. Also shown is the location of the Mud Flat Lake Road potential measured section for understanding facies architecture and diagenesis of organic carbon. (Modified from Bryant, 1992)

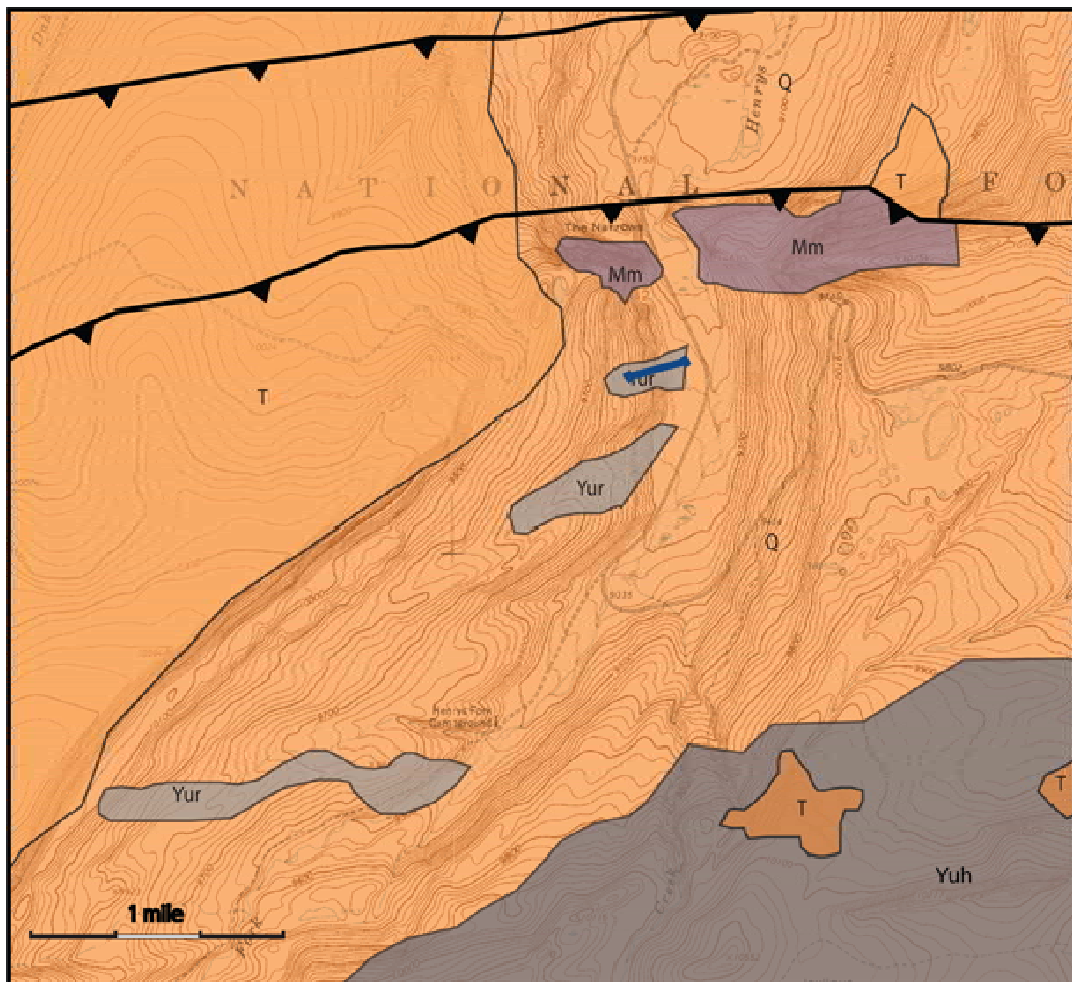


Geologic map of measured sections and surrounding geology at Hades Creek locale. Measured section previously measured by Dehler in reconnaissance fashion. Sections A, B, lower Hades (LH), and C is a major focus of this study. E is a partial measured section that was measured but is not used for this study. (Modified from Bryant, 1992)



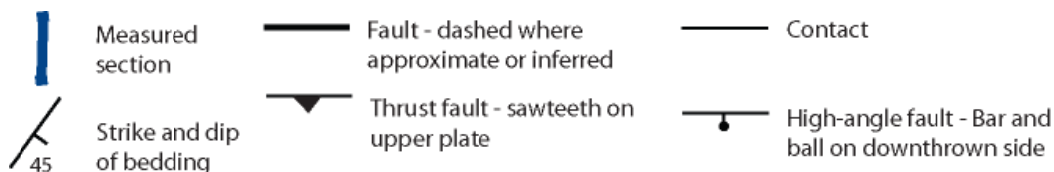
Geologic map of measured section and surrounding geology at Ashley Creek locale. Measured section previously measured by Dehler in reconnaissance fashion. (Modified from Bryant, 1992)





Geologic map of measured section and surrounding geology at Henry's Fork locale. Measured section previously measured by Dehler in reconnaissance fashion. (Modified from Bryant, 1992)

Description of map units and legend. Modified from Bryant, 1992



Q

**Alluvial and debris-fans, landslide deposits, and till of Pindale age (Holocene and Pleistocene) -**

Alluvial and debris-fans - Gravel, sand, and silt; locally bouldery. Crudely bedded to non bedded and poorly sorted. Maximum thickness probably 10m.

Landslide deposits - Poorly sorted; particle size ranges from clay to blocks, depending on material involved in sliding; include mudflow, debris-avalanche, and slump deposits.

Till of Pindale age - Poorly sorted bouldery till that forms prominent moraines. As mapped, may include some colluvium, talus, and landslide debris. A few meters thick except in moraines where maximum thickness is 180 m

T

**Hooper Canyon Formation (Pliocene?) and Conglomerate (Miocene?) -**

Hooper Canyon Formation - Boulder, cobble, and pebbles in a matrix of sand and silt.

Coarse clasts are predominantly subrounded to subangular limestone and quartzite. Caps ridges north of City Creek and lies on erosion surface cut on deformed conglomerate. Maximum thickness 15 m

Conglomerate - Pale-brown and light- to medium-gray, well- to poorly cemented, pebble and cobble conglomerate and sandstone. Generally contains coarse, subrounded to subangular clasts of limestone and quartzite, but near Mill Creek southeast of Bountiful, clasts of metamorphic rocks from the Farmington Canyon Complex are numerous. Thickness greater than 500 m

R

**Thaynes Limestone and Woodside Formation (Lower Triassic) -**

Thaynes Limestone - Light-gray, thin- to thick-bedded limestone and brownish-gray siltstone containing beds of light-gray sandstone, pale-red silty limestone, light-gray shaly limestone, and dark-greenish-gray siltstone and shale. Locally contains pelecypods, gastropods, and ammonites. Thickness ranges from 600 m north of Red Butte Creek to 215 m on northwest flank of Uinta Mountains

Woodside Formation - Grayish-red, grayish-purple, reddish-brown, and moderate-red shale, siltstone, and fine-grained sandstone; thin white limestone beds; and grayish-red siltstone. Locally, a few tens of meters of green or greenish-gray shale and siltstone at the base. Thickness ranges from 120 m north of Red Butte Creek east of Salt Lake City to 300 m near Park City

Pp

**Park City Formation (Permian) -** Fossiliferous and cherty, gray to pinkish-gray limestone, calcareous siltstone, and cherty sandstone; near middle of unit is a dark-gray, phosphatic shale which is about 30 m thick (Meade Peak Phosphatic Shale Member of Phosphoria Formation). Thickness ranges from 200 m at Mill Creek southeast of Salt Lake City to 600 m at South Fork Dry Creek northeast of Salt Lake City

(continued)

Description of map units and legend. Modified from Bryant, 1992. (*continued*)

- PIPw** **Weber Sandstone (Lower Permian to Middle Pennsylvanian)** - Pale-yellowish-gray to white, crossbedded, quartzitic and calcareous sandstone containing a few beds of light-gray to white limestone and dolomite. Thickness generally 300-500 m, but ranges from 150 to 750 m south of City Creek Canyon, where thinned by bedding faults and thickened by folding of fault repetition, and 600 m east of head of American Fork Canyon along the south-central edge of the quadrangle. Upper part may be younger than middle Pennsylvanian
- IPmr** **Morgan Formation and Round Valley Limestone (Lower to Middle Pennsylvanian)** -  
**Morgan Formation** - Grayish-red calcareous siltstone and silty limestone, light-greenish-gray siltstone, gray fossiliferous limestone containing gray, yellowish-gray, reddish-brown, and pinkish-orange chert, and white to light-gray sandstone. Occurs only on flanks of Uinta Mountains. About 100 m thick  
**Round Valley Limestone** - Light-gray-weathering, gray to dark-gray, fossiliferous limestone containing gray and reddish-gray chert and interbeds of gray and light-green shale and siltstone, grayish-red silty shale, and sandstone and sandy limestone. Pale-reddish-orange silicified fossils are characteristic. Thickness ranges from 300 m in Wasatch Range in City Creek area to 60 m on eastern edge of quadrangle
- Mdh** **Doughnut Shale and Humbug Formation (Upper Mississippian)**-Thicknesses of map units is 160-181 m.  
**Doughnut Shale** - Dark-gray shale, with some red shale near base, with beds of coarse sandstone, limestone and coal; shale is slope forming and clayey; 89-91 m thick  
**Humbug Formation** - Light-gray to red, fine-grained to very fine-grained, soft to resistant sandstone interbedded with light-gray limestone and red to black shale; sandstone is locally cross-bedded and hematitic near top of formation; may contain caves and sinkholes along the south flank of the Uinta Mountains; 75-90 m thick
- Mm** **Madison Limestone (Upper and Lower Mississippian)** - Mostly dark-gray, medium to coarse crystalline, cherty limestone; chert is typically light gray; commonly contains numerous caves and sinkholes; 130-300m thick
- Ct** **Tintic Quartzite (Middle and Lower Cambrian)** - Medium- to thick-bedded, fine- to coarse-grained, white, pale-yellowish-gray, and pale-reddish-brown quartzite; conglomeratic beds in lower 100 m. Thickness 250-600 m in Wasatch Range. Discontinuous lenses of unit as much as 100 m thick locally are preserved below pre-Late Devonian unconformity around Uinta Mountains
- Yur** **Red Pine Shale of the Uinta Mountain Group (middle Upper Proterozoic)** - Grayish-black to olive-drab siltstone and shale and thin, discontinuous quartzites and arkose beds. About 900 m thick on South Fork of Weber River.
- Yuh** **Hades Pass (Wallace, 1972; Sanderson, 1984)** - Pale-red, grayish-red, pale-reddish-brown, light-gray, and yellowish-gray quartz sandstone, arkose, and shale; thick, moderate-red, lenticular shale beds on the north flank of the Uinta Mountains and thin, discontinuous shale bed on the south flank. Shale (s) shown were thick and continuous. About 1,800 m thick

## Appendix B: C-isotope data

| Locale      | Sample    | Meter | C-isotope | TOC  | Composite Hades Meter |
|-------------|-----------|-------|-----------|------|-----------------------|
| Lower Hades | LH03-01   | 9     | -24.61    | 0.50 | 9                     |
| Lower Hades | LH03-02   | 12    | -24.60    | 0.54 | 12                    |
| Lower Hades | LH03-03   | 14    | -24.83    | 0.33 | 14                    |
| Lower Hades | LH03-04   | 18    | -24.52    | 0.35 | 18                    |
| Lower Hades | LH03-05a  | 21    | -24.87    | 0.38 | 21                    |
| Lower Hades | LH03-05b  | 21    | -24.70    | 0.40 | 21                    |
| Lower Hades | LH03-06   | 24    | -24.09    | 0.42 | 24                    |
| Lower Hades | LH03-07   | 27    | -24.43    | 0.33 | 27                    |
| Lower Hades | LH03-08   | 30    | -24.26    | 0.32 | 30                    |
| Lower Hades | LH03-09   | 33    | -24.29    | 0.32 | 33                    |
| Lower Hades | LH03-10   | 36    | -23.99    | 0.34 | 36                    |
| Lower Hades | LH03-11   | 39    | -24.21    | 0.40 | 39                    |
| Lower Hades | LH03-12   | 42    | -24.12    | 0.49 | 42                    |
| Lower Hades | LH03-13   | 45    | -24.15    | 0.21 | 45                    |
| Lower Hades | LH03-15   | 48    | -24.47    | 0.29 | 48                    |
| Lower Hades | LH03-16   | 51    | -24.46    | 0.32 | 51                    |
| Lower Hades | LH03-17   | 54    | -24.14    | 0.34 | 54                    |
| Lower Hades | LH03-18   | 57    | -24.30    | 0.24 | 57                    |
| Lower Hades | LH03-19   | 60    | -24.33    | 0.31 | 60                    |
| Lower Hades | LH03-20   | 66    | -24.21    | 0.20 | 66                    |
| Lower Hades | LH03-21   | 69    | -24.34    | 0.23 | 69                    |
| Hades B     | RP01B-01  | 3     | -25.61    | 0.54 | 228                   |
| Hades B     | RP03B-01  | 3     | -25.47    | 0.07 | 228                   |
| Hades B     | RP01B-02  | 6     | -25.58    | 0.27 | 231                   |
| Hades B     | RP03B-03  | 6     | -26.01    | 0.09 | 231                   |
| Hades B     | RP01B-03  | 9     | -24.70    | 0.15 | 234                   |
| Hades B     | RP03B-04  | 9     | -24.86    | 0.21 | 234                   |
| Hades B     | RP03B-05  | 11.5  | -25.38    | 0.11 | 236.5                 |
| Hades B     | RP01B-04  | 12    | -26.71    | 0.33 | 237                   |
| Hades B     | RP03B-07A | 14    | -25.85    | 0.06 | 239                   |
| Hades B     | RP03B-07B | 14    | -25.94    | 0.06 | 239                   |
| Hades B     | RP01B-05  | 15    | -24.44    | 0.23 | 240                   |
| Hades B     | RP01B-06  | 18    | -25.50    | 0.05 | 243                   |
| Hades B     | RP03B-09  | 18    | -26.05    | 0.17 | 243                   |
| Hades B     | RP01B-07  | 21    | -24.87    | 0.07 | 246                   |
| Hades B     | RP03B-10  | 21    | -25.65    | 0.24 | 246                   |
| Hades B     | RP01B-08  | 24    | -30.77    | 0.61 | 249                   |
| Hades B     | RP03B-11A | 24    | -24.65    | 0.14 | 249                   |
| Hades B     | RP03B-11B | 24    | -25.02    | 0.10 | 249                   |
| Hades B     | RP01B-09  | 27    | -26.18    | 0.23 | 252                   |
| Hades B     | RP03B-12  | 27    | -24.53    | 0.15 | 252                   |
| Hades B     | RP01B-10  | 30    | -24.17    | 0.12 | 255                   |
| Hades B     | RP03B-13  | 30    | -25.89    | 0.13 | 255                   |
| Hades B     | RP03B-14  | 33    | -25.46    | 0.12 | 258                   |
| Hades B     | RP01B-12  | 36    | -25.47    | 0.18 | 261                   |
| Hades B     | RP03B-15  | 36    | -25.56    | 0.12 | 261                   |
| Hades B     | RP01B-13  | 39    | -25.81    | 0.52 | 264                   |
| Hades B     | RP03B-16  | 39    | -26.35    | 0.29 | 264                   |
| Hades B     | RP01B-14  | 42    | -25.60    | 0.15 | 267                   |
| Hades B     | RP03B-17  | 42    | -26.07    | 0.21 | 267                   |

| Locale  | Sample    | Meter | C-isotope | TOC  | Composite Hades Meter |
|---------|-----------|-------|-----------|------|-----------------------|
| Hades B | RP01B-15  | 45    | -25.98    | 0.18 | 270                   |
| Hades B | RP01B-16  | 48    | -25.65    | 0.15 | 273                   |
| Hades B | RP03B-18  | 48    | -25.88    | 0.08 | 273                   |
| Hades B | RP03B-19  | 51    | -25.97    | 0.22 | 276                   |
| Hades B | RP01B-18  | 52    | -25.31    | 0.09 | 277                   |
| Hades B | RP01B-19  | 54    | -25.45    | 0.09 | 279                   |
| Hades B | RP01B-19D | 54    | -25.75    | 0.14 | 279                   |
| Hades B | RP01B-20  | 56    | -27.15    | 0.32 | 281                   |
| Hades B | RP03B-20  | 57    | -26.61    | 0.22 | 282                   |
| Hades B | RP03B-21  | 63    | -26.09    | 0.13 | 288                   |
| Hades B | RP03B-22  | 75    | -25.67    | 0.22 | 300                   |
| Hades B | RP03B-23  | 84    | -26.44    | 0.15 | 309                   |
| Hades B | RP03B-24  | 90    | -27.10    | 0.19 | 315                   |
| Hades B | RP03B-25  | 100   | -26.17    | 0.18 | 325                   |
| Hades B | RP03B-26  | 101   | -26.75    | 0.19 | 326                   |
| Hades A | RP01A-01  | 3     | -27.31    | 0.59 | 333                   |
| Hades A | RP01A-02  | 4     | -25.42    | 0.15 | 334                   |
| Hades A | RP01A-04  | 6     | -25.60    | 0.63 | 336                   |
| Hades A | RP01A-05  | 9     | -25.64    | 0.19 | 339                   |
| Hades A | RP01A-06  | 12    | -26.16    | 0.26 | 342                   |
| Hades A | RP01A-07  | 15    | -25.20    | 0.19 | 345                   |
| Hades A | RP01A-08  | 18    | -25.92    | 0.69 | 348                   |
| Hades A | RP01A-09  | 21    | -25.61    | 0.23 | 351                   |
| Hades A | RP01A-10  | 24    | -26.78    | 0.25 | 354                   |
| Hades A | RP01A-11  | 27    | -25.38    | 0.15 | 357                   |
| Hades A | RP01A-11D | 27    | -26.07    | 0.13 | 357                   |
| Hades A | RP01A-12  | 30    | -26.49    | 0.74 | 360                   |
| Hades A | RP01A-13  | 33    | -26.36    | 0.26 | 363                   |
| Hades A | RP01A-14  | 36    | -26.21    | 0.25 | 366                   |
| Hades A | RP01A-15  | 39    | -26.85    | 0.28 | 369                   |
| Hades A | RP01A-16  | 42    | -25.20    | 0.67 | 372                   |
| Hades A | RP01A-17  | 45    | -26.05    | 0.17 | 375                   |
| Hades A | RP01A-18  | 48    | -26.19    | 0.17 | 378                   |
| Hades A | RP01A-20  | 53    | -26.59    | 0.67 | 383                   |
| Hades A | RP01A-21  | 56    | -25.84    | 0.12 | 386                   |
| Hades A | RP01A-22  | 59    | -25.87    | 0.20 | 389                   |
| Hades A | RP01A-24  | 63    | -26.82    | 0.46 | 393                   |
| Hades A | RP01A-25  | 66    | -26.55    | 0.61 | 396                   |
| Hades A | RP01A-27  | 69    | -25.92    | 0.22 | 399                   |
| Hades A | RP01A-28  | 72    | -25.77    | 0.22 | 402                   |
| Hades A | RP01A-29  | 75    | -25.91    | 0.33 | 405                   |
| Hades A | RP01A-30  | 78    | -25.43    | 0.18 | 408                   |
| Hades A | RP01A-31  | 81    | -25.32    | 0.15 | 411                   |
| Hades A | RP01A-32  | 84    | -26.28    | 0.25 | 414                   |
| Hades A | RP01A-33  | 87    | -27.13    | 0.46 | 417                   |
| Hades A | RP01A-34  | 90    | -25.49    | 0.14 | 420                   |
| Hades A | RP01A-35  | 93    | -24.39    | 0.10 | 423                   |
| Hades A | RP01A-36  | 96    | -25.10    | 0.15 | 426                   |
| Hades A | RP01A-37  | 99.5  | -26.09    | 0.52 | 429.5                 |
| Hades A | RP01A-38  | 102   | -23.90    | 0.13 | 432                   |
| Hades A | RP01A-39  | 105   | -24.79    | 0.14 | 435                   |

| Locale  | Sample   | Meter | C-isotope | TOC  | Composite<br>Hades Meter |
|---------|----------|-------|-----------|------|--------------------------|
| Hades A | RP01A-40 | 108   | -24.58    | 0.17 | 438                      |
| Hades A | RP01A-41 | 111   | -26.82    | 0.48 | 441                      |
| Hades A | RP01A-42 | 114   | -24.76    | 0.10 | 444                      |
| Hades A | RP01A-44 | 120   | -25.02    | 0.13 | 450                      |
| Hades A | RP01A-45 | 123   | -27.62    | 0.73 | 453                      |
| Hades A | RP01A-46 | 126   | -25.45    | 0.17 | 456                      |
| Hades A | RP01A-47 | 129   | -25.49    | 0.18 | 459                      |
| Hades A | RP01A-48 | 132   | -27.63    | 0.66 | 462                      |
| Hades A | RP01A-49 | 135   | -25.57    | 0.18 | 465                      |
| Hades A | RP01A-50 | 138   | -24.76    | 0.17 | 468                      |
| Hades A | RP01A-51 | 141   | -25.77    | 0.17 | 471                      |
| Hades A | RP01A-52 | 144   | -27.12    | 0.43 | 474                      |
| Hades A | RP01A-53 | 147   | -25.38    | 0.14 | 477                      |
| Hades A | RP01A-54 | 150   | -25.17    | 0.16 | 480                      |
| Hades A | RP01A-55 | 153   | -25.50    | 0.15 | 483                      |
| Hades A | RP01A-56 | 156   | -26.42    | 0.46 | 486                      |
| Hades A | RP01A-57 | 159   | -25.27    | 0.16 | 489                      |
| Hades A | RP01A-58 | 162   | -25.58    | 0.15 | 492                      |
| Hades A | RP01A-59 | 165   | -25.49    | 0.17 | 495                      |
| Hades A | RP01A-60 | 168   | -25.63    | 0.53 | 498                      |
| Hades A | RP01A-61 | 171   | -25.76    | 0.16 | 501                      |
| Hades A | RP01A-62 | 174   | -25.27    | 0.22 | 504                      |
| Hades A | RP01A-63 | 177   | -24.96    | 0.15 | 507                      |
| Hades A | RP01A-64 | 180   | -26.11    | 0.67 | 510                      |
| Hades A | RP01A-65 | 183   | -25.50    | 0.18 | 513                      |
| Hades A | RP01A-66 | 186   | -26.05    | 0.20 | 516                      |
| Hades A | RP01A-67 | 189   | -27.18    | 0.27 | 519                      |
| Hades A | RP01A-68 | 192   | -25.57    | 0.66 | 522                      |
| Hades A | RP01A-69 | 195   | -26.35    | 0.17 | 525                      |
| Hades A | RP01A-70 | 198   | -26.14    | 0.16 | 528                      |
| Hades A | RP01A-71 | 201   | -26.01    | 0.19 | 531                      |
| Hades A | RP01A-73 | 207   | -26.77    | 0.70 | 537                      |
| Hades A | RP01A-75 | 212.5 | -27.70    | 0.46 | 542.5                    |
| Hades A | RP01A-79 | 220.5 | -29.46    | 1.20 | 550.5                    |
| Hades A | RP01A-81 | 254   | -27.89    | 2.21 | 584                      |
| Hades A | RP01A-82 | 266   | -27.85    | 0.68 | 596                      |
| Hades A | RP01A-84 | 276.5 | -27.44    | 1.52 | 606.5                    |
| Hades A | RP01A-85 | 280.5 | -28.59    | 3.70 | 610.5                    |
| Hades A | Hades 01 | 291   | -27.20    | 0.89 | 621                      |
| Hades A | Hades 03 | 294   | -28.07    | 1.27 | 624                      |
| Hades A | Hades 04 | 303   | -27.52    | 1.12 | 633                      |
| Hades A | Hades 05 | 306   | -28.18    | 0.91 | 636                      |
| Hades A | Hades 06 | 311   | -27.57    | 1.68 | 641                      |
| Hades A | Hades 07 | 315   | -27.82    | 1.02 | 645                      |
| Hades A | Hades 08 | 318   | -28.13    | 2.41 | 648                      |
| Hades A | Hades 09 | 322.5 | -28.08    | 2.46 | 652.5                    |
| Hades A | Hades 11 | 337   | -27.09    | 1.39 | 667                      |
| Hades A | Hades 12 | 339   | -27.72    | 1.40 | 669                      |
| Hades A | Hades 13 | 344   | -26.76    | 0.97 | 674                      |
| Hades A | Hades 14 | 346   | -26.60    | 0.83 | 676                      |

| Locale  | Sample    | Meter | C-isotope | TOC  | Composite Hades Meter |
|---------|-----------|-------|-----------|------|-----------------------|
| Hades A | Hades 16  | 357   | -27.55    | 1.18 | 687                   |
| Hades A | Hades 17  | 379   | -28.78    | 0.97 | 709                   |
| Hades A | Hades 18  | 387   | -27.60    | 0.84 | 717                   |
| Hades A | Hades 19  | 396   | -26.83    | 1.90 | 726                   |
| Hades A | Hades 20  | 397   | -26.50    | 0.67 | 727                   |
| Hades A | Hades 22  | 401   | -26.85    | 0.85 | 731                   |
| Hades A | Hades 23  | 404   | -27.32    | 1.07 | 734                   |
| Hades A | Hades 24  | 417.5 | -27.34    | 0.76 | 747.5                 |
| Hades A | Hades 25  | 424   | -26.63    | 0.46 | 754                   |
| Hades A | Hades 26  | 442   | -27.87    | 2.17 | 772                   |
| Hades A | Hades 27  | 446   | -28.22    | 0.94 | 776                   |
| Hades A | Hades 30  | 489   | -27.62    | 0.59 | 819                   |
| Hades A | Hades 31  | 498   | -27.20    | 1.53 | 828                   |
| Hades A | Hades 32  | 503   | -27.04    | 2.74 | 833                   |
| Hades A | Hades 33  | 510   | -27.33    | 1.32 | 840                   |
| Hades A | Hades 34  | 518   | -27.09    | 1.81 | 848                   |
| Hades A | Hades 35  | 523   | -27.69    | 1.12 | 853                   |
| Hades A | Hades 36  | 528   | -27.35    | 1.89 | 858                   |
| Hades A | Hades 37  | 544   | -27.37    | 1.26 | 874                   |
| Hades A | Hades 38  | 548   | -27.61    | 0.67 | 878                   |
| Hades A | Hades 40  | 588   | -26.71    | 0.49 | 918                   |
| Hades A | Hades 41  | 589   | -26.85    | 1.09 | 919                   |
| Hades A | Hades 42  | 591   | -26.21    | 1.01 | 921                   |
| Hades A | Hades 43  | 592.5 | -26.43    | 1.58 | 922.5                 |
| Hades A | Hades 44  | 594   | -26.83    | 0.90 | 924                   |
| Hades A | Hades 45  | 597   | -26.69    | 0.57 | 927                   |
| Hades A | Hades 46a | 600   | -27.32    | 0.82 | 930                   |
| Hades A | Hades 46b | 600   | -27.19    | 1.04 | 930                   |
| Hades A | Hades 47  | 601.5 | -27.85    | 1.31 | 931.5                 |
| Hades A | Hades 48a | 603   | -27.29    | 0.87 | 933                   |
| Hades A | Hades 48b | 603   | -26.99    | 1.37 | 933                   |
| Hades A | Hades 49  | 607   | -27.00    | 1.13 | 937                   |
| Hades A | Hades 50  | 608   | -27.82    | 1.18 | 938                   |
| Hades A | Hades 51  | 609   | -26.40    | 1.65 | 939                   |
| Hades A | Hades 52  | 612   | -26.43    | 1.77 | 942                   |
| Hades A | Hades 54  | 624.5 | -25.85    | 1.52 | 954.5                 |
| Hades A | Hades 55  | 627   | -26.39    | 0.96 | 957                   |
| Hades A | Hades 57  | 627.2 | -26.35    | 0.91 | 957.2                 |
| Hades A | Hades 58  | 631.5 | -26.94    | 1.10 | 961.5                 |
| Hades A | Hades 59  | 639   | -25.48    | --   | 969                   |
| Hades A | Hades 62  | 657   | -28.54    | --   | 987                   |
| Hades A | Hades 63  | 658   | -28.54    | --   | 988                   |
| Hades C | RP01C-03  | 13.5  | -27.37    | 4.12 | 443.5                 |
| Hades C | RP01C-05  | 54    | -27.73    | 2.75 | 484                   |
| Hades C | RP01C-06  | 78    | -28.24    | 1.33 | 508                   |
| Hades C | RP01C-07  | 121   | -29.26    | 5.91 | 551                   |



| Locale             | Sample           | Meter | C-isotope | TOC  | type section<br>Meter |
|--------------------|------------------|-------|-----------|------|-----------------------|
| Mud Lake Flat Road | Road Section 01  | 0     | -22.68    | 0.35 | 41                    |
| Mud Lake Flat Road | Road Section 02  | 1.5   | -26.03    | 0.29 | 42.5                  |
| Mud Lake Flat Road | Road Section 03  | 3     | -24.08    | 0.39 | 44                    |
| Mud Lake Flat Road | Road Section 04  | 3.5   | -19.74    | 1.16 | 44.5                  |
| Mud Lake Flat Road | Road Section 04D | 3.5   | -20.03    | 0.91 | 44.5                  |
| Mud Lake Flat Road | Road Section 05  | 6     | -25.32    | 0.68 | 47                    |
| Mud Lake Flat Road | Road Section 06  | 7.5   | -24.20    | 0.42 | 48.5                  |
| Mud Lake Flat Road | Road Section 07  | 9     | -24.74    | 0.42 | 50                    |
| Mud Lake Flat Road | Road Section 08  | 12    | -22.97    | 0.41 | 53                    |
| Mud Lake Flat Road | Road Section 09  | 13.5  | -24.47    | 0.53 | 54.5                  |
| Mud Lake Flat Road | Road Section 10  | 15    | -23.74    | 0.15 | 56                    |
| Mud Lake Flat Road | Road Section 11  | 16    | -23.47    | 0.35 | 57                    |
| Mud Lake Flat Road | Road Section 12  | 17.5  | -24.66    | 0.43 | 58.5                  |
| Mud Lake Flat Road | Road Section 13  | 18.5  | -23.39    | 0.40 | 59.5                  |
| type section       | TS-706-01        | 80    | -25.43    | 0.19 |                       |
| type section       | RP00-B-01        | 81.5  | -24.05    | 0.28 |                       |
| type section       | TS-706-02        | 82    | -19.37    | 0.22 |                       |
| type section       | RP00-B-02        | 83    | -16.91    | 0.24 |                       |
| type section       | TS-706-03        | 83    | -19.17    | 0.18 |                       |
| type section       | TS-706-04        | 84    | -24.30    | 0.21 |                       |
| type section       | RP00-B-03        | 84.5  | -22.00    | 0.27 |                       |
| type section       | TS-706-05        | 85    | -18.63    | 0.26 |                       |
| type section       | TS-706-06        | 86    | -23.79    | 0.48 |                       |
| type section       | TS-706-07        | 89    | -26.01    | 0.40 |                       |
| type section       | TS-706-08        | 92    | -24.89    | 0.57 |                       |
| type section       | TS-706-09        | 95    | -25.52    | 0.26 |                       |
| type section       | TS-706-10        | 101   | -23.42    | 0.42 |                       |
| type section       | RP00-B-06        | 101.5 | -22.52    | 0.60 |                       |
| type section       | TS-706-11        | 104   | -26.57    | 0.65 |                       |
| type section       | TS-706-12        | 106   | -23.13    | 0.21 |                       |
| type section       | TS-706-13        | 110   | -25.47    | 0.42 |                       |
| type section       | TS-706-14        | 113   | -24.59    | 0.43 |                       |
| type section       | TS-706-15        | 116   | -26.99    | 0.77 |                       |
| type section       | TS-706-16        | 119   | -26.38    | 0.87 |                       |
| type section       | TS-706-17        | 122   | -24.07    | 0.42 |                       |
| type section       | TS-706-18        | 125   | -25.84    | 0.38 |                       |
| type section       | RP00-B-09        | 128   | -25.80    | 0.30 |                       |
| type section       | TS-706-19        | 132   | -26.02    | 0.46 |                       |
| type section       | TS-706-20        | 135   | -24.73    | 0.51 |                       |
| type section       | TS-706-21        | 138   | -23.91    | 0.21 |                       |
| type section       | RP00-B-11        | 140   | -24.80    | 0.48 |                       |
| type section       | TS-706-22        | 141   | -24.13    | 0.26 |                       |
| type section       | TS-706-23        | 145   | -24.12    | 0.31 |                       |
| type section       | TS-706-24        | 148   | -23.75    | 0.33 |                       |
| type section       | TS-706-25        | 154   | -23.77    | 0.94 |                       |
| type section       | TS-706-25a       | 157   | -23.95    | 0.17 |                       |
| type section       | RP00-B-13        | 160   | -24.60    | 0.51 |                       |

| Locale       | Sample    | Meter | C-isotope | TOC  |
|--------------|-----------|-------|-----------|------|
| type section | TS-706-26 | 160   | -23.56    | 0.24 |
| type section | TS-706-27 | 163   | -24.79    | 0.81 |
| type section | TS-706-28 | 166   | -24.07    | 0.92 |
| type section | TS-706-29 | 169   | -23.99    | 0.86 |
| type section | TS-706-30 | 172   | -24.49    | 0.64 |
| type section | TS-706-31 | 175   | -22.58    | 0.19 |
| type section | TS-706-32 | 178   | -23.18    | 0.60 |
| type section | RP00-B-15 | 181.5 | -23.19    | 1.51 |
| type section | TS-706-33 | 184   | -23.92    | 0.83 |
| type section | TS-706-34 | 187   | -23.41    | 1.61 |
| type section | RP00-B-16 | 190   | -23.22    | 0.71 |
| type section | TS-706-35 | 193   | -23.85    | 1.59 |
| type section | TS-706-36 | 196   | -25.36    | 2.92 |
| type section | TS-706-37 | 199   | -23.45    | 0.43 |
| type section | RP00-B-17 | 200   | -23.12    | 1.11 |
| type section | TS-706-38 | 202   | -23.38    | 0.76 |
| type section | TS-706-39 | 205   | -23.62    | 0.30 |
| type section | TS-706-40 | 228   | -25.23    | 0.38 |
| type section | RP00-B-19 | 230   | -23.90    | 0.33 |
| type section | TS-706-41 | 231   | -26.58    | 1.11 |
| type section | TS-706-42 | 234   | -26.55    | 0.32 |
| type section | TS-706-43 | 237   | -26.57    | 0.89 |
| type section | TS-706-44 | 243   | -25.29    | 1.22 |
| type section | TS-706-45 | 248   | -25.51    | 0.68 |
| type section | RP00-B-20 | 249   | -25.90    | 0.93 |
| type section | TS-706-46 | 251   | -26.16    | 0.53 |
| type section | RP00-B-24 | 255.5 | -24.10    | 0.54 |
| type section | TS-706-47 | 266   | -26.44    | 0.55 |
| type section | RP00-B-25 | 269   | -25.26    | 0.84 |
| type section | TS-706-48 | 272   | -26.24    | 0.36 |
| type section | TS-706-49 | 275   | -25.94    | 0.22 |
| type section | RP00-B-27 | 320   | -27.50    | 0.18 |
| type section | TS-706-50 | 323   | -26.75    | 0.50 |
| type section | RP00-B-28 | 327   | -26.76    | 0.57 |
| type section | RP00-B-32 | 340   | -26.90    | 0.36 |
| type section | RP00-B-33 | 345.5 | -25.87    | 0.25 |
| type section | TS-706-51 | 349   | -26.02    | 0.23 |
| type section | TS-706-52 | 353   | -26.16    | 0.21 |
| type section | TS-706-53 | 356   | -25.83    | 0.18 |
| type section | RP00-B-35 | 359.5 | -25.17    | 0.31 |
| type section | TS-706-55 | 365   | -25.33    | 0.21 |
| type section | TS-706-56 | 368   | -25.91    | 0.27 |
| type section | RP00-B-36 | 371.5 | -27.61    | 0.56 |
| type section | TS-706-57 | 374   | -25.33    | 0.20 |
| type section | RP00-B-37 | 377   | -26.51    | 0.34 |
| type section | TS-706-58 | 380   | -25.81    | 0.25 |
| type section | TS-706-59 | 383   | -25.76    | 0.22 |
| type section | TS-706-60 | 386   | -25.12    | 0.14 |
| type section | TS-706-61 | 389   | -26.34    | 0.38 |

| Locale       | Sample     | Meter | C-isotope | TOC  |
|--------------|------------|-------|-----------|------|
| type section | RP00-B-39  | 393   | -26.75    | 0.52 |
| type section | TS-706-62  | 395   | -25.14    | 0.14 |
| type section | TS-706-63  | 398   | -25.35    | 0.40 |
| type section | TS-706-64  | 401   | -26.18    | 0.55 |
| type section | TS-706-65  | 404   | -25.52    | 0.47 |
| type section | TS-706-66  | 407   | -26.01    | 0.55 |
| type section | TS-706-67  | 413   | -25.78    | 0.46 |
| type section | TS-706-68  | 416   | -25.94    | 0.69 |
| type section | TS-706-69  | 419   | -25.15    | 0.48 |
| type section | TS-706-70  | 422   | -25.54    | 0.97 |
| type section | TS-706-71  | 429   | -25.08    | 0.55 |
| type section | TS-706-72  | 432   | -24.80    | 0.32 |
| type section | TS-706-73  | 435   | -25.97    | 0.92 |
| type section | TS-706-74  | 438   | -24.82    | 0.32 |
| type section | TS-706-75  | 441   | -25.67    | 0.47 |
| type section | RP00-B-43  | 444   | -28.85    | 1.18 |
| type section | TS-706-76  | 447   | -25.13    | 0.51 |
| type section | TS-706-77  | 450   | -25.00    | 0.30 |
| type section | TS-706-78  | 454   | -24.99    | 0.28 |
| type section | TS-706-79  | 457   | -25.40    | 0.55 |
| type section | TS-706-80  | 460   | -24.67    | 0.14 |
| type section | TS-706-81  | 463   | -24.77    | 0.09 |
| type section | TS-706-82  | 466   | -24.85    | 0.08 |
| type section | RP00-B-45  | 470.5 | -25.52    | 0.62 |
| type section | TS-706-83  | 474   | -25.14    | 0.07 |
| type section | TS-706-84  | 477   | -25.23    | 0.08 |
| type section | TS-706-85  | 480   | -26.42    | 0.21 |
| type section | TS-706-86  | 483   | -24.38    | 0.04 |
| type section | RP00-B-46  | 486   | -27.87    | 0.10 |
| type section | RP00-B-47  | 490.5 | -28.16    | 0.15 |
| type section | TS-706-87  | 492   | -23.66    | 0.79 |
| type section | TS-706-88  | 495   | -24.46    | 0.07 |
| type section | TS-706-89  | 501   | -25.63    | 0.12 |
| type section | TS-706-90  | 504   | -25.70    | 0.15 |
| type section | TS-706-91  | 507   | -25.31    | 0.14 |
| type section | TS-706-92  | 510   | -25.55    | 0.17 |
| type section | RP00-B-49  | 512   | -26.67    | 0.55 |
| type section | RP00-B-50  | 517   | -28.93    | 0.17 |
| type section | TS-706-93  | 519   | -26.39    | 0.18 |
| type section | TS-706-94  | 522   | -26.27    | 0.19 |
| type section | TS-706-95  | 525   | -26.02    | 0.15 |
| type section | TS-706-96  | 528   | -27.62    | 0.37 |
| type section | RP00-B-51  | 530   | -25.14    | 0.13 |
| type section | TS-706-97  | 534   | -26.31    | 0.10 |
| type section | TS-706-98  | 537   | -25.64    | 0.10 |
| type section | TS-706-99  | 540   | -26.31    | 0.09 |
| type section | TS-706-100 | 543   | -26.36    | 0.11 |
| type section | TS-706-101 | 546   | -27.01    | 0.19 |
| type section | RP00-B-52  | 548.5 | -25.86    | 0.07 |
| type section | TS-706-102 | 552   | -28.03    | 0.70 |
| type section | TS-706-103 | 555   | -28.31    | 0.58 |
| type section | TS-706-104 | 558   | -29.12    | 1.15 |
| type section | RP00-B-53  | 560   | -28.17    | 0.67 |

| Locale       | Sample | Meter | C-isotope | TOC |
|--------------|--------|-------|-----------|-----|
| Ashley Creek | AC01   | 9     | -17.27    | --  |
| Ashley Creek | AC06   | 59    | -18.81    | --  |
| Ashley Creek | AC09   | 82.5  | -27.65    | --  |
| Ashley Creek | AC12   | 110.5 | -17.11    | --  |
| Ashley Creek | AC13   | 117   | -17.10    | --  |
| Ashley Creek | AC14   | 118.5 | -22.80    | --  |
| Ashley Creek | AC15   | 129   | -23.23    | --  |
| Henry's Fork | HF02   | sub 0 | -25.19    | --  |
| Henry's Fork | HF04   | 7     | -26.47    | --  |
| Henry's Fork | HF11   | 151   | -19.55    | --  |
| Henry's Fork | HF13   | 154   | -24.87    | --  |

Appendix C: Raw point count data tables

| Point Count Raw Data |              |                         |                   |                         |             |
|----------------------|--------------|-------------------------|-------------------|-------------------------|-------------|
| Sample               |              | Mono-crystalline Quartz | Undulatory Quartz | Poly-crystalline Quartz | Plagioclase |
| AC-3                 | <u>Count</u> | 134.00                  | --                | --                      | 3.00        |
|                      | <u>%</u>     | 44.67                   | --                | --                      | 1.00        |
| AC-10                | <u>Count</u> | 265.00                  | --                | 5.00                    | 4.00        |
|                      | <u>%</u>     | 88.33                   | --                | 1.67                    | 1.33        |
| AC-11                | <u>Count</u> | 239.00                  | --                | 1.00                    | 4.00        |
|                      | <u>%</u>     | 79.67                   | --                | 0.33                    | 1.33        |
| AC04-7               | <u>Count</u> | 247.00                  | 51.00             | 1.00                    | 1.00        |
|                      | <u>%</u>     | 82.33                   | 17.00             | 0.33                    | 0.33        |
| RP01A-19.5           | <u>Count</u> | 242.00                  | 18.00             | --                      | 10.00       |
|                      | <u>%</u>     | 80.67                   | 6.00              | --                      | 3.33        |
| RP01A-23             | <u>Count</u> | 207.00                  | 11.00             | 3.00                    | 15.00       |
|                      | <u>%</u>     | 69.00                   | 3.67              | 1.00                    | 5.00        |
| RP01A-26             | <u>Count</u> | 203.00                  | 14.00             | 4.00                    | 25.00       |
|                      | <u>%</u>     | 67.67                   | 4.67              | 1.33                    | 8.33        |
| RP01A-47A            | <u>Count</u> | 204.00                  | 13.00             | 2.00                    | 13.00       |
|                      | <u>%</u>     | 68.00                   | 4.33              | 0.67                    | 4.33        |
| RP01A-72             | <u>Count</u> | 205.00                  | 14.00             | --                      | 9.00        |
|                      | <u>%</u>     | 68.33                   | 4.67              | --                      | 3.00        |
| RP01A-74A            | <u>Count</u> | 196.00                  | 6.00              | 3.00                    | 17.00       |
|                      | <u>%</u>     | 65.33                   | 2.00              | 1.00                    | 5.67        |
| RP01A-76             | <u>Count</u> | 174.00                  | 6.00              | 6.00                    | 78.00       |
|                      | <u>%</u>     | 58.00                   | 2.00              | 2.00                    | 26.00       |
| RP01A-76A            | <u>Count</u> | 155.00                  | --                | 6.00                    | 29.00       |
|                      | <u>%</u>     | 51.67                   | --                | 2.00                    | 9.67        |
| RP01A-77             | <u>Count</u> | 193.00                  | --                | 4.00                    | 18.00       |
|                      | <u>%</u>     | 64.33                   | --                | 1.33                    | 6.00        |
| RP01A-78             | <u>Count</u> | 181.00                  | --                | 7.00                    | 26.00       |
|                      | <u>%</u>     | 60.33                   | --                | 2.33                    | 8.67        |
| RP01A-79a            | <u>Count</u> | 138.00                  | 38.00             | 4.00                    | 33.00       |
|                      | <u>%</u>     | 46.00                   | 12.67             | 1.33                    | 11.00       |
| RP01A-80             | <u>Count</u> | 139.00                  | 42.00             | 4.00                    | 22.00       |
|                      | <u>%</u>     | 46.33                   | 14.00             | 1.33                    | 7.33        |
| Hades 2              | <u>Count</u> | 162.00                  | 28.00             | 5.00                    | 14.00       |
|                      | <u>%</u>     | 54.00                   | 9.33              | 1.67                    | 4.67        |
| Hades 10             | <u>Count</u> | 206.00                  | 33.00             | --                      | 11.00       |
|                      | <u>%</u>     | 68.67                   | 11.00             | --                      | 3.67        |
| Hades 15             | <u>Count</u> | 222.00                  | 26.00             | 6.00                    | 6.00        |
|                      | <u>%</u>     | 74.00                   | 8.67              | 2.00                    | 2.00        |

*continued*

Point Count Raw Data (*continued*)

| Sample     |              | Potassium<br>Feldspar | Weathered<br>Feldspar | Muscovite | Chlorite |
|------------|--------------|-----------------------|-----------------------|-----------|----------|
| AC-3       | <u>Count</u> | --                    | --                    | --        | --       |
|            | <u>%</u>     | --                    | --                    | --        | --       |
| AC-10      | <u>Count</u> | 1.00                  | --                    | 6.00      | 10.00    |
|            | <u>%</u>     | 0.33                  | --                    | 2.00      | 3.33     |
| AC-11      | <u>Count</u> | 1.00                  | --                    | 1.00      | 25.00    |
|            | <u>%</u>     | 0.33                  | --                    | 0.33      | 8.33     |
| AC04-7     | <u>Count</u> | --                    | --                    | --        | --       |
|            | <u>%</u>     | --                    | --                    | --        | --       |
| RP01A-19.5 | <u>Count</u> | --                    | 1.00                  | 8.00      | 3.00     |
|            | <u>%</u>     | --                    | 0.33                  | 2.67      | 1.00     |
| RP01A-23   | <u>Count</u> | --                    | 10.00                 | 5.00      | 5.00     |
|            | <u>%</u>     | --                    | 3.33                  | 1.67      | 1.67     |
| RP01A-26   | <u>Count</u> | --                    | 7.00                  | 5.00      | --       |
|            | <u>%</u>     | --                    | 2.33                  | 1.67      | --       |
| RP01A-47A  | <u>Count</u> | --                    | 12.00                 | 7.00      | 5.00     |
|            | <u>%</u>     | --                    | 4.00                  | 2.33      | 1.67     |
| RP01A-72   | <u>Count</u> | --                    | 19.00                 | 2.00      | 3.00     |
|            | <u>%</u>     | --                    | 6.33                  | 0.67      | 1.00     |
| RP01A-74A  | <u>Count</u> | --                    | 38.00                 | 1.00      | --       |
|            | <u>%</u>     | --                    | 12.67                 | 0.33      | --       |
| RP01A-76   | <u>Count</u> | 2.00                  | 27.00                 | --        | 2.00     |
|            | <u>%</u>     | 0.67                  | 9.00                  | --        | 0.67     |
| RP01A-76A  | <u>Count</u> | 2.00                  | 46.00                 | 6.00      | 34.00    |
|            | <u>%</u>     | 0.67                  | 15.33                 | 2.00      | 11.33    |
| RP01A-77   | <u>Count</u> | 2.00                  | 54.00                 | --        | 9.00     |
|            | <u>%</u>     | 0.67                  | 18.00                 | --        | 3.00     |
| RP01A-78   | <u>Count</u> | 5.00                  | 48.00                 | 2.00      | 2.00     |
|            | <u>%</u>     | 1.67                  | 16.00                 | 0.67      | 0.67     |
| RP01A-79a  | <u>Count</u> | 5.00                  | 49.00                 | 5.00      | 3.00     |
|            | <u>%</u>     | 1.67                  | 16.33                 | 1.67      | 1.00     |
| RP01A-80   | <u>Count</u> | 1.00                  | 38.00                 | 9.00      | 6.00     |
|            | <u>%</u>     | 0.33                  | 12.67                 | 3.00      | 2.00     |
| Hades 2    | <u>Count</u> | --                    | 58.00                 | 5.00      | 11.00    |
|            | <u>%</u>     | --                    | 19.33                 | 1.67      | 3.67     |
| Hades 10   | <u>Count</u> | 3.00                  | 12.00                 | 3.00      | 5.00     |
|            | <u>%</u>     | 1.00                  | 4.00                  | 1.00      | 1.67     |
| Hades 15   | <u>Count</u> | --                    | 15.00                 | 4.00      | 3.00     |
|            | <u>%</u>     | --                    | 5.00                  | 1.33      | 1.00     |

*continued*

Point Count Raw Data (*continued*)

| Sample     |              | Mudstone | Siltstone | Other<br>Lithic | Matrix |
|------------|--------------|----------|-----------|-----------------|--------|
| AC-3       | <u>Count</u> | --       | --        | --              | 163.00 |
|            | <u>%</u>     | --       | --        | --              | 54.33  |
| AC-10      | <u>Count</u> | 9.00     | --        | --              | --     |
|            | <u>%</u>     | 3.00     | --        | --              | --     |
| AC-11      | <u>Count</u> | 9.00     | --        | --              | 20.00  |
|            | <u>%</u>     | 3.00     | --        | --              | 6.67   |
| AC04-7     | <u>Count</u> | --       | --        | --              | --     |
|            | <u>%</u>     | --       | --        | --              | --     |
| RP01A-19.5 | <u>Count</u> | --       | --        | --              | 18.00  |
|            | <u>%</u>     | --       | --        | --              | 6.00   |
| RP01A-23   | <u>Count</u> | --       | --        | --              | 44.00  |
|            | <u>%</u>     | --       | --        | --              | 14.67  |
| RP01A-26   | <u>Count</u> | --       | --        | --              | 42.00  |
|            | <u>%</u>     | --       | --        | --              | 14.00  |
| RP01A-47A  | <u>Count</u> | 4.00     | --        | --              | 40.00  |
|            | <u>%</u>     | 1.33     | --        | --              | 13.33  |
| RP01A-72   | <u>Count</u> | --       | --        | --              | 48.00  |
|            | <u>%</u>     | --       | --        | --              | 16.00  |
| RP01A-74A  | <u>Count</u> | --       | --        | --              | 39.00  |
|            | <u>%</u>     | --       | --        | --              | 13.00  |
| RP01A-76   | <u>Count</u> | --       | --        | --              | 5.00   |
|            | <u>%</u>     | --       | --        | --              | 1.67   |
| RP01A-76A  | <u>Count</u> | --       | --        | --              | 22.00  |
|            | <u>%</u>     | --       | --        | --              | 7.33   |
| RP01A-77   | <u>Count</u> | --       | --        | --              | 20.00  |
|            | <u>%</u>     | --       | --        | --              | 6.67   |
| RP01A-78   | <u>Count</u> | --       | --        | --              | 29.00  |
|            | <u>%</u>     | --       | --        | --              | 9.67   |
| RP01A-79a  | <u>Count</u> | 7.00     | 1.00      | --              | 17.00  |
|            | <u>%</u>     | 2.33     | 0.33      | --              | 5.67   |
| RP01A-80   | <u>Count</u> | 4.00     | --        | --              | 35.00  |
|            | <u>%</u>     | 1.33     | --        | --              | 11.67  |
| Hades 2    | <u>Count</u> | 6.00     | --        | --              | 11.00  |
|            | <u>%</u>     | 2.00     | --        | --              | 3.67   |
| Hades 10   | <u>Count</u> | 2.00     | 1.00      | --              | 24.00  |
|            | <u>%</u>     | 0.67     | 0.33      | --              | 8.00   |
| Hades 15   | <u>Count</u> | 3.00     | --        | --              | 15.00  |
|            | <u>%</u>     | 1.00     | --        | --              | 5.00   |

*continued*



## Point Count Raw Data (continued)

| Sample      |              | Mono-crystalline Quartz | Undulatory Quartz | Poly-crystalline Quartz | Plagioclase |
|-------------|--------------|-------------------------|-------------------|-------------------------|-------------|
| Hades 21    | <u>Count</u> | 165.00                  | 29.00             | 14.00                   | 22.00       |
|             | <u>%</u>     | 55.00                   | 9.67              | 4.67                    | 7.33        |
| Hades 28    | <u>Count</u> | 196.00                  | 21.00             | 9.00                    | 14.00       |
|             | <u>%</u>     | 65.33                   | 7.00              | 3.00                    | 4.67        |
| Hades 29    | <u>Count</u> | 175.00                  | 14.00             | 4.00                    | 26.00       |
|             | <u>%</u>     | 58.33                   | 4.67              | 1.33                    | 8.67        |
| Hades 39    | <u>Count</u> | 165.00                  | 11.00             | 11.00                   | 25.00       |
|             | <u>%</u>     | 55.00                   | 3.67              | 3.67                    | 8.33        |
| Hades 56    | <u>Count</u> | 153.00                  | 6.00              | 9.00                    | 5.00        |
|             | <u>%</u>     | 51.00                   | 2.00              | 3.00                    | 1.67        |
| Hades 60    | <u>Count</u> | 170.00                  | 9.00              | 16.00                   | 21.00       |
|             | <u>%</u>     | 56.67                   | 3.00              | 5.33                    | 7.00        |
| Hades 61    | <u>Count</u> | 166.00                  | 13.00             | 18.00                   | 25.00       |
|             | <u>%</u>     | 55.33                   | 4.33              | 6.00                    | 8.33        |
| Hades 64    | <u>Count</u> | 153.00                  | 7.00              | 14.00                   | 37.00       |
|             | <u>%</u>     | 51.00                   | 2.33              | 4.67                    | 12.33       |
| Hades 06-1  | <u>Count</u> | 228.00                  | 11.00             | 4.00                    | 11.00       |
|             | <u>%</u>     | 76.00                   | 3.67              | 1.33                    | 3.67        |
| Hades 06-2  | <u>Count</u> | 209.00                  | 23.00             | 7.00                    | 24.00       |
|             | <u>%</u>     | 69.67                   | 7.67              | 2.33                    | 8.00        |
| Hades 06-3  | <u>Count</u> | 252.00                  | 12.00             | 2.00                    | 7.00        |
|             | <u>%</u>     | 84.00                   | 4.00              | 0.67                    | 2.33        |
| RP03B-8     | <u>Count</u> | 237.00                  | 8.00              | 6.00                    | 10.00       |
|             | <u>%</u>     | 79.00                   | 2.67              | 2.00                    | 3.33        |
| RP03B-27    | <u>Count</u> | 195.00                  | --                | 8.00                    | 18.00       |
|             | <u>%</u>     | 65.00                   | --                | 2.67                    | 6.00        |
| HadesB 06-1 | <u>Count</u> | 176.00                  | 4.00              | --                      | 4.00        |
|             | <u>%</u>     | 58.67                   | 1.33              | --                      | 1.33        |
| RP01C-1     | <u>Count</u> | 170.00                  | --                | 6.00                    | 24.00       |
|             | <u>%</u>     | 56.67                   | --                | 2.00                    | 8.00        |
| RP01C-4     | <u>Count</u> | 162.00                  | --                | 2.00                    | 33.00       |
|             | <u>%</u>     | 54.00                   | --                | 0.67                    | 11.00       |
| RP01C-8     | <u>Count</u> | 144.00                  | --                | 8.00                    | 24.00       |
|             | <u>%</u>     | 48.00                   | --                | 2.67                    | 8.00        |
| HC06-1      | <u>Count</u> | 156.00                  | --                | 4.00                    | 47.00       |
|             | <u>%</u>     | 52.00                   | --                | 1.33                    | 15.67       |
| HCO6-2      | <u>Count</u> | 169.00                  | --                | 9.00                    | 33.00       |
|             | <u>%</u>     | 56.33                   | --                | 3.00                    | 11.00       |
| HC06-3      | <u>Count</u> | 171.00                  | --                | 15.00                   | 42.00       |
|             | <u>%</u>     | 57.00                   | --                | 5.00                    | 14.00       |
| HC06-4      | <u>Count</u> | 173.00                  | --                | 8.00                    | 36.00       |
|             | <u>%</u>     | 57.67                   | --                | 2.67                    | 12.00       |
| HF-1        | <u>Count</u> | 209.00                  | --                | 3.00                    | 30.00       |
|             | <u>%</u>     | 69.67                   | --                | 1.00                    | 10.00       |
| HF-5        | <u>Count</u> | 246.00                  | --                | 5.00                    | 10.00       |
|             | <u>%</u>     | 82.00                   | --                | 1.67                    | 3.33        |

continued

| Point Count Raw Data ( <i>continued</i> ) |              |                       |                       |           |          |
|-------------------------------------------|--------------|-----------------------|-----------------------|-----------|----------|
| Sample                                    |              | Potassium<br>Feldspar | Weathered<br>Feldspar | Muscovite | Chlorite |
| Hades 21                                  | <u>Count</u> | 2.00                  | 29.00                 | 12.00     | --       |
|                                           | <u>%</u>     | 0.67                  | 9.67                  | 4.00      | --       |
| Hades 28                                  | <u>Count</u> | 2.00                  | 25.00                 | 9.00      | 7.00     |
|                                           | <u>%</u>     | 0.67                  | 8.33                  | 3.00      | 2.33     |
| Hades 29                                  | <u>Count</u> | 10.00                 | 37.00                 | 1.00      | --       |
|                                           | <u>%</u>     | 3.33                  | 12.33                 | 0.33      | --       |
| Hades 39                                  | <u>Count</u> | 10.00                 | 57.00                 | 2.00      | 4.00     |
|                                           | <u>%</u>     | 3.33                  | 19.00                 | 0.67      | 1.33     |
| Hades 56                                  | <u>Count</u> | 2.00                  | 104.00                | 3.00      | 14.00    |
|                                           | <u>%</u>     | 0.67                  | 34.67                 | 1.00      | 4.67     |
| Hades 60                                  | <u>Count</u> | 4.00                  | 71.00                 | 3.00      | 1.00     |
|                                           | <u>%</u>     | 1.33                  | 23.67                 | 1.00      | 0.33     |
| Hades 61                                  | <u>Count</u> | 4.00                  | 48.00                 | 6.00      | 10.00    |
|                                           | <u>%</u>     | 1.33                  | 16.00                 | 2.00      | 3.33     |
| Hades 64                                  | <u>Count</u> | 8.00                  | 79.00                 | --        | --       |
|                                           | <u>%</u>     | 2.67                  | 26.33                 | --        | --       |
| Hades 06-1                                | <u>Count</u> | --                    | 41.00                 | 1.00      | --       |
|                                           | <u>%</u>     | --                    | 13.67                 | 0.33      | --       |
| Hades 06-2                                | <u>Count</u> | 3.00                  | 18.00                 | 6.00      | 3.00     |
|                                           | <u>%</u>     | 1.00                  | 6.00                  | 2.00      | 1.00     |
| Hades 06-3                                | <u>Count</u> | 1.00                  | 22.00                 | 2.00      | --       |
|                                           | <u>%</u>     | 0.33                  | 7.33                  | 0.67      | --       |
| RP03B-8                                   | <u>Count</u> | --                    | 7.00                  | 4.00      | 7.00     |
|                                           | <u>%</u>     | --                    | 2.33                  | 1.33      | 2.33     |
| RP03B-27                                  | <u>Count</u> | 1.00                  | 7.00                  | 7.00      | 1.00     |
|                                           | <u>%</u>     | 0.33                  | 2.33                  | 2.33      | 0.33     |
| HadesB06-1                                | <u>Count</u> | --                    | 27.00                 | 5.00      | 1.00     |
|                                           | <u>%</u>     | --                    | 9.00                  | 1.67      | 0.33     |
| RP01C-1                                   | <u>Count</u> | 14.00                 | 53.00                 | 1.00      | 3.00     |
|                                           | <u>%</u>     | 4.67                  | 17.67                 | 0.33      | 1.00     |
| RP01C-4                                   | <u>Count</u> | 4.00                  | 71.00                 | 2.00      | 1.00     |
|                                           | <u>%</u>     | 1.33                  | 23.67                 | 0.67      | 0.33     |
| RP01C-8                                   | <u>Count</u> | --                    | 82.00                 | 3.00      | 2.00     |
|                                           | <u>%</u>     | --                    | 27.33                 | 1.00      | 0.67     |
| HC06-1                                    | <u>Count</u> | 4.00                  | 55.00                 | --        | 4.00     |
|                                           | <u>%</u>     | 1.33                  | 18.33                 | --        | 1.33     |
| HCO6-2                                    | <u>Count</u> | 5.00                  | 53.00                 | 3.00      | 3.00     |
|                                           | <u>%</u>     | 1.67                  | 17.67                 | 1.00      | 1.00     |
| HC06-3                                    | <u>Count</u> | 6.00                  | 22.00                 | 2.00      | 2.00     |
|                                           | <u>%</u>     | 2.00                  | 7.33                  | 0.67      | 0.67     |
| HC06-4                                    | <u>Count</u> | 9.00                  | 44.00                 | 3.00      | 5.00     |
|                                           | <u>%</u>     | 3.00                  | 14.67                 | 1.00      | 1.67     |
| HF-1                                      | <u>Count</u> | 1.00                  | 10.00                 | 10.00     | 23.00    |
|                                           | <u>%</u>     | 0.33                  | 3.33                  | 3.33      | 7.67     |
| HF-5                                      | <u>Count</u> | --                    | --                    | 3.00      | 4.00     |
|                                           | <u>%</u>     | --                    | --                    | 1.00      | 1.33     |

*continued*

| Point Count Raw Data ( <i>continued</i> ) |              |          |           |                 |        |
|-------------------------------------------|--------------|----------|-----------|-----------------|--------|
| Sample                                    |              | Mudstone | Siltstone | Other<br>Lithic | Matrix |
| Hades 21                                  | <u>Count</u> | 5.00     | --        | --              | 22.00  |
|                                           | <u>%</u>     | 1.67     | --        | --              | 7.33   |
| Hades 28                                  | <u>Count</u> | 2.00     | --        | --              | 15.00  |
|                                           | <u>%</u>     | 0.67     | --        | --              | 5.00   |
| Hades 29                                  | <u>Count</u> | --       | --        | --              | 33.00  |
|                                           | <u>%</u>     | --       | --        | --              | 11.00  |
| Hades 39                                  | <u>Count</u> | --       | --        | --              | 15.00  |
|                                           | <u>%</u>     | --       | --        | --              | 5.00   |
| Hades 56                                  | <u>Count</u> | --       | --        | --              | 4.00   |
|                                           | <u>%</u>     | --       | --        | --              | 1.33   |
| Hades 60                                  | <u>Count</u> | --       | --        | --              | 5.00   |
|                                           | <u>%</u>     | --       | --        | --              | 1.67   |
| Hades 61                                  | <u>Count</u> | 2.00     | --        | --              | 8.00   |
|                                           | <u>%</u>     | 0.67     | --        | --              | 2.67   |
| Hades 64                                  | <u>Count</u> | --       | --        | --              | 2.00   |
|                                           | <u>%</u>     | --       | --        | --              | 0.67   |
| Hades 06-1                                | <u>Count</u> | --       | --        | --              | 4.00   |
|                                           | <u>%</u>     | --       | --        | --              | 1.33   |
| Hades 06-2                                | <u>Count</u> | 4.00     | --        | --              | 3.00   |
|                                           | <u>%</u>     | 1.33     | --        | --              | 1.00   |
| Hades 06-3                                | <u>Count</u> | --       | --        | --              | 2.00   |
|                                           | <u>%</u>     | --       | --        | --              | 0.67   |
| RP03B-8                                   | <u>Count</u> | 9.00     | --        | --              | 12.00  |
|                                           | <u>%</u>     | 3.00     | --        | --              | 4.00   |
| RP03B-27                                  | <u>Count</u> | 23.00    | --        | --              | 40.00  |
|                                           | <u>%</u>     | 7.67     | --        | --              | 13.33  |
| HadesB06-1                                | <u>Count</u> | 7.00     | --        | --              | 76.00  |
|                                           | <u>%</u>     | 2.33     | --        | --              | 25.33  |
| RP01C-1                                   | <u>Count</u> | --       | --        | --              | 29.00  |
|                                           | <u>%</u>     | --       | --        | --              | 9.67   |
| RP01C-4                                   | <u>Count</u> | --       | --        | --              | 25.00  |
|                                           | <u>%</u>     | --       | --        | --              | 8.33   |
| RP01C-8                                   | <u>Count</u> | --       | --        | --              | 37.00  |
|                                           | <u>%</u>     | --       | --        | --              | 12.33  |
| HC06-1                                    | <u>Count</u> | 2.00     | 2.00      | --              | 26.00  |
|                                           | <u>%</u>     | 0.67     | 0.67      | --              | 8.67   |
| HCO6-2                                    | <u>Count</u> | --       | 2.00      | --              | 23.00  |
|                                           | <u>%</u>     | --       | 0.67      | --              | 7.67   |
| HC06-3                                    | <u>Count</u> | --       | --        | --              | 40.00  |
|                                           | <u>%</u>     | --       | --        | --              | 13.33  |
| HC06-4                                    | <u>Count</u> | --       | 1.00      | --              | 21.00  |
|                                           | <u>%</u>     | --       | 0.33      | --              | 7.00   |
| HF-1                                      | <u>Count</u> | 5.00     | --        | --              | 9.00   |
|                                           | <u>%</u>     | 1.67     | --        | --              | 3.00   |
| HF-5                                      | <u>Count</u> | 6.00     | --        | --              | 26.00  |
|                                           | <u>%</u>     | 2.00     | --        | --              | 8.67   |

*continued*

| Point Count Raw Data (continued) |              |                         |                   |                         |             |
|----------------------------------|--------------|-------------------------|-------------------|-------------------------|-------------|
| Sample                           |              | Mono-crystalline Quartz | Undulatory Quartz | Poly-crystalline Quartz | Plagioclase |
| HF-6                             | <u>Count</u> | 228.00                  | --                | 2.00                    | 14.00       |
|                                  | <u>%</u>     | 76.00                   | --                | 0.67                    | 4.67        |
| HF-12                            | <u>Count</u> | 200.00                  | --                | 59.00                   | 15.00       |
|                                  | <u>%</u>     | 66.67                   | --                | 19.67                   | 5.00        |
| HF-14                            | <u>Count</u> | 284.00                  | --                | 2.00                    | 3.00        |
|                                  | <u>%</u>     | 94.67                   | --                | 0.67                    | 1.00        |
| HF-15                            | <u>Count</u> | 258.00                  | --                | 2.00                    | 4.00        |
|                                  | <u>%</u>     | 86.00                   | --                | 0.67                    | 1.33        |
| HF-16                            | <u>Count</u> | 183.00                  | --                | --                      | 56.00       |
|                                  | <u>%</u>     | 61.00                   | --                | --                      | 18.67       |
| LH03-14                          | <u>Count</u> | 202.00                  | --                | 3.00                    | 12.00       |
|                                  | <u>%</u>     | 67.33                   | --                | 1.00                    | 4.00        |
| LH06-1                           | <u>Count</u> | 161.00                  | --                | 4.00                    | 24.00       |
|                                  | <u>%</u>     | 53.67                   | --                | 1.33                    | 8.00        |
| RP00B-2.5                        | <u>Count</u> | 205.00                  | 17.00             | 13.00                   | 14.00       |
|                                  | <u>%</u>     | 68.33                   | 5.67              | 4.30                    | 4.60        |
| RP00B-5                          | <u>Count</u> | 247.00                  | --                | 8.00                    | 16.00       |
|                                  | <u>%</u>     | 82.33                   | --                | 2.67                    | 5.33        |
| RP00B-7                          | <u>Count</u> | 208.00                  | --                | 12.00                   | 12.00       |
|                                  | <u>%</u>     | 69.33                   | --                | 4.00                    | 4.00        |
| RPP00B-10                        | <u>Count</u> | 195.00                  | 9.00              | 3.00                    | 7.00        |
|                                  | <u>%</u>     | 65.00                   | 3.00              | 1.00                    | 2.30        |
| RP00B-12                         | <u>Count</u> | 215.00                  | 18.00             | --                      | 18.00       |
|                                  | <u>%</u>     | 71.60                   | 6.00              | --                      | 6.00        |
| RP00B-17.5                       | <u>Count</u> | 202.00                  | 16.00             | 6.00                    | 9.00        |
|                                  | <u>%</u>     | 67.27                   | 5.33              | 2.00                    | 3.00        |
| RP00B-21                         | <u>Count</u> | 179.00                  | 19.00             | --                      | 8.00        |
|                                  | <u>%</u>     | 58.67                   | 6.33              | --                      | 2.60        |
| RP00B-22a                        | <u>Count</u> | 176.00                  | 24.00             | 2.00                    | 13.00       |
|                                  | <u>%</u>     | 58.60                   | 8.00              | 0.60                    | 4.30        |
| RP00B-22b                        | <u>Count</u> | 184.00                  | 32.00             | 6.00                    | 14.00       |
|                                  | <u>%</u>     | 61.33                   | 10.67             | 2.00                    | 4.60        |
| RP00B-23                         | <u>Count</u> | 231.00                  | --                | 39.00                   | 12.00       |
|                                  | <u>%</u>     | 77.00                   | --                | 13.00                   | 4.00        |
| RP00B-30                         | <u>Count</u> | 85.00                   | --                | 7.00                    | 2.00        |
|                                  | <u>%</u>     | 28.33                   | --                | 2.33                    | 0.67        |
| RP00B-32                         | <u>Count</u> | 203.00                  | 25.00             | 1.00                    | 7.00        |
|                                  | <u>%</u>     | 67.67                   | 8.33              | 0.30                    | 2.30        |
| RP00B-40                         | <u>Count</u> | 180.00                  | 12.00             | 1.00                    | 11.00       |
|                                  | <u>%</u>     | 60.00                   | 4.00              | 0.30                    | 3.60        |
| RP00B-42a                        | <u>Count</u> | 204.00                  | 12.00             | 10.00                   | 14.00       |
|                                  | <u>%</u>     | 68.00                   | 4.00              | 3.30                    | 4.60        |
| RP00B-44                         | <u>Count</u> | 128.00                  | 9.00              | 25.00                   | 2.00        |
|                                  | <u>%</u>     | 42.60                   | 3.00              | 8.30                    | 0.60        |

continued

| Point Count Raw Data ( <i>continued</i> ) |              |                       |                       |           |          |
|-------------------------------------------|--------------|-----------------------|-----------------------|-----------|----------|
| Sample                                    |              | Potassium<br>Feldspar | Weathered<br>Feldspar | Muscovite | Chlorite |
| HF-6                                      | <u>Count</u> | --                    | 6.00                  | 6.00      | 14.00    |
|                                           | <u>%</u>     | --                    | 2.00                  | 2.00      | 4.67     |
| HF-12                                     | <u>Count</u> | --                    | 4.00                  | --        | --       |
|                                           | <u>%</u>     | --                    | 1.33                  | --        | --       |
| HF-14                                     | <u>Count</u> | --                    | --                    | --        | 2.00     |
|                                           | <u>%</u>     | --                    | --                    | --        | 0.67     |
| HF-15                                     | <u>Count</u> | --                    | 1.00                  | 3.00      | 7.00     |
|                                           | <u>%</u>     | --                    | 0.33                  | 1.00      | 2.33     |
| HF-16                                     | <u>Count</u> | --                    | 5.00                  | 7.00      | 26.00    |
|                                           | <u>%</u>     | --                    | 1.67                  | 2.33      | 8.67     |
| LH03-14                                   | <u>Count</u> | --                    | 43.00                 | 2.00      | 2.00     |
|                                           | <u>%</u>     | --                    | 14.33                 | 0.67      | 0.67     |
| LH06-1                                    | <u>Count</u> | --                    | 46.00                 | 2.00      | 7.00     |
|                                           | <u>%</u>     | --                    | 15.33                 | 0.67      | 2.33     |
| RP00B-2.5                                 | <u>Count</u> | --                    | 7.00                  | 6.00      | 12.00    |
|                                           | <u>%</u>     | --                    | 2.30                  | 2.00      | 4.00     |
| RP00B-5                                   | <u>Count</u> | --                    | 4.00                  | 8.00      | 5.00     |
|                                           | <u>%</u>     | --                    | 1.33                  | 2.67      | 1.67     |
| RP00B-7                                   | <u>Count</u> | --                    | 19.00                 | 2.00      | 11.00    |
|                                           | <u>%</u>     | --                    | 6.33                  | 0.67      | 3.67     |
| RPP00B-10                                 | <u>Count</u> | --                    | 5.00                  | 7.00      | 20.00    |
|                                           | <u>%</u>     | --                    | 1.60                  | 2.30      | 6.60     |
| RP00B-12                                  | <u>Count</u> | --                    | 5.00                  | 1.00      | 4.00     |
|                                           | <u>%</u>     | --                    | 1.60                  | 0.30      | 1.30     |
| RP00B-17.5                                | <u>Count</u> | --                    | 12.00                 | 2.00      | 5.00     |
|                                           | <u>%</u>     | --                    | 4.00                  | 0.60      | 1.60     |
| RP00B-21                                  | <u>Count</u> | --                    | 8.00                  | 4.00      | 2.00     |
|                                           | <u>%</u>     | --                    | 2.60                  | 1.30      | 0.30     |
| RP00B-22a                                 | <u>Count</u> | --                    | 8.00                  | 6.00      | 5.00     |
|                                           | <u>%</u>     | --                    | 2.60                  | 2.00      | 1.60     |
| RP00B-22b                                 | <u>Count</u> | --                    | 1.00                  | 5.00      | 3.00     |
|                                           | <u>%</u>     | --                    | 0.30                  | 1.60      | 1.00     |
| RP00B-23                                  | <u>Count</u> | --                    | 11.00                 | --        | 1.00     |
|                                           | <u>%</u>     | --                    | 3.67                  | 0.00      | 0.33     |
| RP00B-30                                  | <u>Count</u> | --                    | 1.00                  | 58.00     | 3.00     |
|                                           | <u>%</u>     | --                    | 0.33                  | 19.33     | 1.00     |
| RP00B-32                                  | <u>Count</u> | --                    | 3.00                  | 11.00     | 3.00     |
|                                           | <u>%</u>     | --                    | 1.00                  | 3.20      | 1.00     |
| RP00B-40                                  | <u>Count</u> | --                    | 13.00                 | 5.00      | 3.00     |
|                                           | <u>%</u>     | --                    | 4.30                  | 1.60      | 1.00     |
| RP00B-42a                                 | <u>Count</u> | --                    | 3.00                  | 2.00      | 0.00     |
|                                           | <u>%</u>     | --                    | 1.00                  | 0.60      | 0.00     |
| RP00B-44                                  | <u>Count</u> | --                    | 7.00                  | 5.00      | 0.00     |
|                                           | <u>%</u>     | --                    | 2.30                  | 1.60      | 0.00     |

*continued*

| Point Count Raw Data ( <i>continued</i> ) |              |          |           |                 |        |
|-------------------------------------------|--------------|----------|-----------|-----------------|--------|
| Sample                                    |              | Mudstone | Siltstone | Other<br>Lithic | Matrix |
| HF-6                                      | <u>Count</u> | --       | --        | --              | 30.00  |
|                                           | <u>%</u>     | --       | --        | --              | 10.00  |
| HF-12                                     | <u>Count</u> | --       | --        | 1.00            | 21.00  |
|                                           | <u>%</u>     | --       | --        | 0.33            | 7.00   |
| HF-14                                     | <u>Count</u> | --       | --        | --              | 9.00   |
|                                           | <u>%</u>     | --       | --        | --              | 3.00   |
| HF-15                                     | <u>Count</u> | --       | --        | --              | 25.00  |
|                                           | <u>%</u>     | --       | --        | --              | 8.33   |
| HF-16                                     | <u>Count</u> | 2.00     | --        | --              | 21.00  |
|                                           | <u>%</u>     | 0.67     | --        | --              | 7.00   |
| LH03-14                                   | <u>Count</u> | --       | --        | --              | 36.00  |
|                                           | <u>%</u>     | --       | --        | --              | 12.00  |
| LH06-1                                    | <u>Count</u> | 8.00     | --        | 3.00            | 45.00  |
|                                           | <u>%</u>     | 2.67     | --        | 1.00            | 15.00  |
| RP00B-2.5                                 | <u>Count</u> | 5.00     | --        | --              | 21.00  |
|                                           | <u>%</u>     | 1.60     | --        | --              | 7.00   |
| RP00B-5                                   | <u>Count</u> | --       | --        | --              | 12.00  |
|                                           | <u>%</u>     | --       | --        | --              | 4.00   |
| RP00B-7                                   | <u>Count</u> | --       | 2.00      | 4.00            | 30.00  |
|                                           | <u>%</u>     | --       | 0.67      | 1.33            | 10.00  |
| RPP00B-10                                 | <u>Count</u> | --       | --        | 2.00            | 52.00  |
|                                           | <u>%</u>     | --       | --        | 0.60            | 17.30  |
| RP00B-12                                  | <u>Count</u> | --       | --        | --              | 39.00  |
|                                           | <u>%</u>     | --       | --        | --              | 13.00  |
| RP00B-17.5                                | <u>Count</u> | 2.00     | --        | 7.00            | 39.00  |
|                                           | <u>%</u>     | 0.60     | --        | 2.30            | 13.00  |
| RP00B-21                                  | <u>Count</u> | 9.00     | --        | 14.00           | 57.00  |
|                                           | <u>%</u>     | 2.90     | --        | 4.60            | 19.00  |
| RP00B-22a                                 | <u>Count</u> | --       | --        | 3.00            | 63.00  |
|                                           | <u>%</u>     | --       | --        | 1.00            | 21.00  |
| RP00B-22b                                 | <u>Count</u> | --       | --        | 6.00            | 49.00  |
|                                           | <u>%</u>     | --       | --        | 2.00            | 16.30  |
| RP00B-23                                  | <u>Count</u> | --       | --        | 4.00            | 2.00   |
|                                           | <u>%</u>     | --       | --        | 1.33            | 0.67   |
| RP00B-30                                  | <u>Count</u> | --       | --        | --              | 144.00 |
|                                           | <u>%</u>     | --       | --        | --              | 48.00  |
| RP00B-32                                  | <u>Count</u> | 1.00     | --        | 1.00            | 45.00  |
|                                           | <u>%</u>     | 0.30     | --        | 0.30            | 15.00  |
| RP00B-40                                  | <u>Count</u> | 3.00     | --        | 4.00            | 68.00  |
|                                           | <u>%</u>     | 1.00     | --        | 1.30            | 22.60  |
| RP00B-42a                                 | <u>Count</u> | --       | --        | 2.00            | 53.00  |
|                                           | <u>%</u>     | --       | --        | 0.60            | 17.60  |
| RP00B-44                                  | <u>Count</u> | 4.00     | --        | 27.00           | 93.00  |
|                                           | <u>%</u>     | 1.30     | --        | 9.00            | 31.00  |

*continued*

| Point Count Raw Data ( <i>continued</i> ) |              |                         |                   |                         |             |
|-------------------------------------------|--------------|-------------------------|-------------------|-------------------------|-------------|
| Sample                                    |              | Mono-crystalline Quartz | Undulatory Quartz | Poly-crystalline Quartz | Plagioclase |
| TS1-SS                                    | <u>Count</u> | 188.00                  | 9.00              | 4.00                    | 16.00       |
|                                           | <u>%</u>     | 62.67                   | 3.00              | 1.33                    | 5.33        |
| TS3-SS                                    | <u>Count</u> | 195.00                  | 7.00              | --                      | 18.00       |
|                                           | <u>%</u>     | 65.00                   | 2.33              | --                      | 6.00        |
| TS5-SS                                    | <u>Count</u> | 161.00                  | 7.00              | 7.00                    | 44.00       |
|                                           | <u>%</u>     | 53.67                   | 2.33              | 2.33                    | 14.67       |
| TS6-SS                                    | <u>Count</u> | 208.00                  | 12.00             | --                      | 21.00       |
|                                           | <u>%</u>     | 69.33                   | 4.00              | --                      | 7.00        |
| TS7-SS                                    | <u>Count</u> | 216.00                  | 16.00             | --                      | 25.00       |
|                                           | <u>%</u>     | 72.00                   | 5.33              | --                      | 8.33        |

*continued*

| Point Count Raw Data ( <i>continued</i> ) |              |                       |                       |           |          |
|-------------------------------------------|--------------|-----------------------|-----------------------|-----------|----------|
| Sample                                    |              | Potassium<br>Feldspar | Weathered<br>Feldspar | Muscovite | Chlorite |
| TS1-SS                                    | <u>Count</u> | --                    | 41.00                 | 13.00     | 18.00    |
|                                           | <u>%</u>     | --                    | 13.67                 | 4.33      | 6.00     |
| TS3-SS                                    | <u>Count</u> | --                    | 54.00                 | 15.00     | 6.00     |
|                                           | <u>%</u>     | --                    | 18.00                 | 5.00      | 2.00     |
| TS5-SS                                    | <u>Count</u> | --                    | 32.00                 | 9.00      | 12.00    |
|                                           | <u>%</u>     | --                    | 10.67                 | 3.00      | 4.00     |
| TS6-SS                                    | <u>Count</u> | --                    | 17.00                 | 19.00     | 10.00    |
|                                           | <u>%</u>     | --                    | 5.67                  | 6.33      | 3.33     |
| TS7-SS                                    | <u>Count</u> | --                    | 12.00                 | 13.00     | 2.00     |
|                                           | <u>%</u>     | --                    | 4.00                  | 4.33      | 0.67     |

*continued*



| <u>Point Count Raw Data (continued)</u> |              |          |           |              |        |
|-----------------------------------------|--------------|----------|-----------|--------------|--------|
| Sample                                  |              | Mudstone | Siltstone | Other Lithic | Matrix |
| TS1-SS                                  | <u>Count</u> | 6.00     | --        | --           | 5.00   |
|                                         | <u>%</u>     | 2.00     | --        | --           | 1.67   |
| TS3-SS                                  | <u>Count</u> | 1.00     | --        | --           | 4.00   |
|                                         | <u>%</u>     | 0.33     | --        | --           | 1.33   |
| TS5-SS                                  | <u>Count</u> | --       | --        | 23.00        | 5.00   |
|                                         | <u>%</u>     | --       | --        | 7.67         | 1.67   |
| TS6-SS                                  | <u>Count</u> | --       | --        | 4.00         | 9.00   |
|                                         | <u>%</u>     | --       | --        | 1.33         | 3.00   |
| TS7-SS                                  | <u>Count</u> | --       | --        | 12.00        | 4.00   |
|                                         | <u>%</u>     | --       | --        | 4.00         | 1.33   |

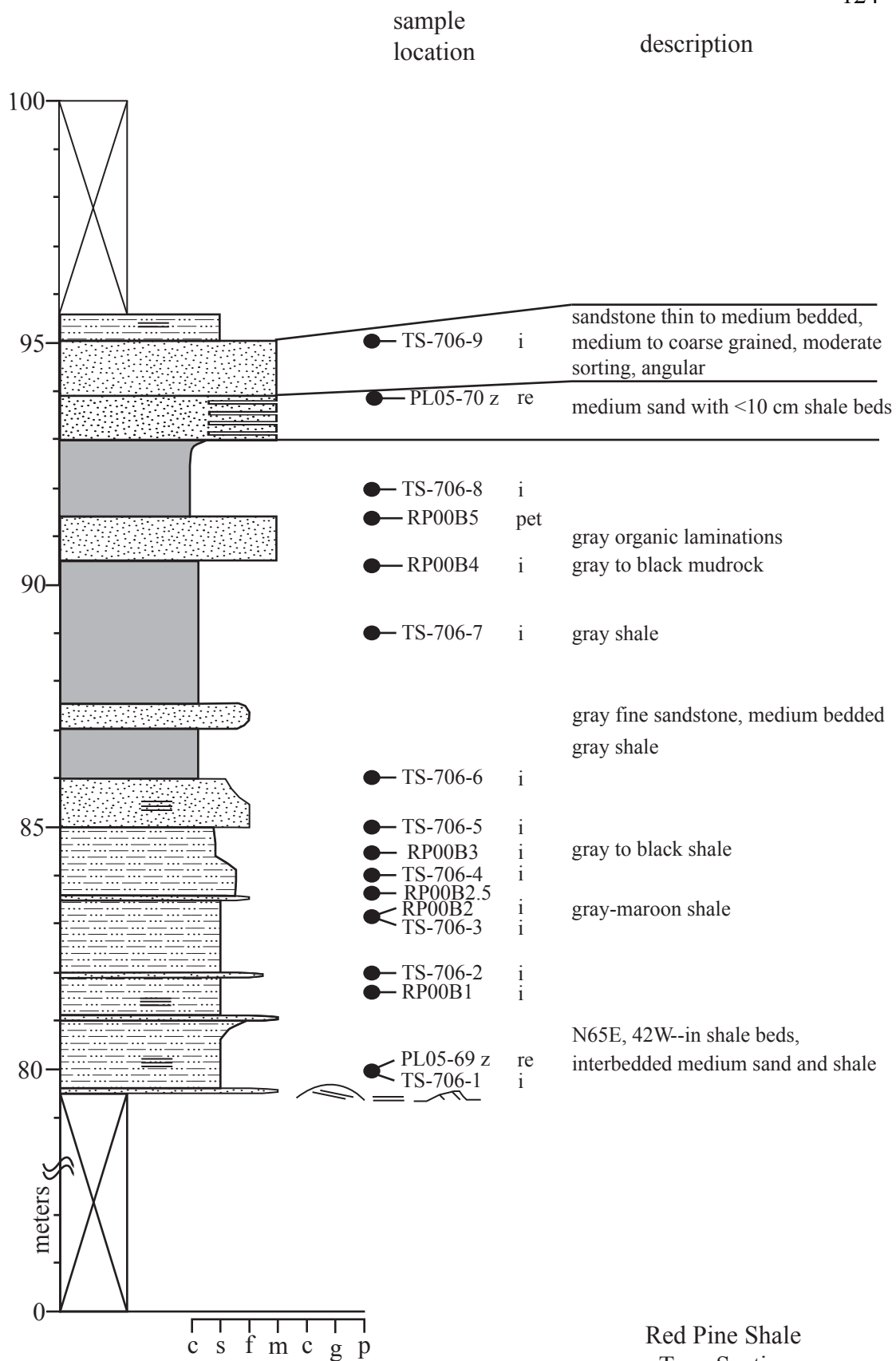
Appendix D: Other point count data tables

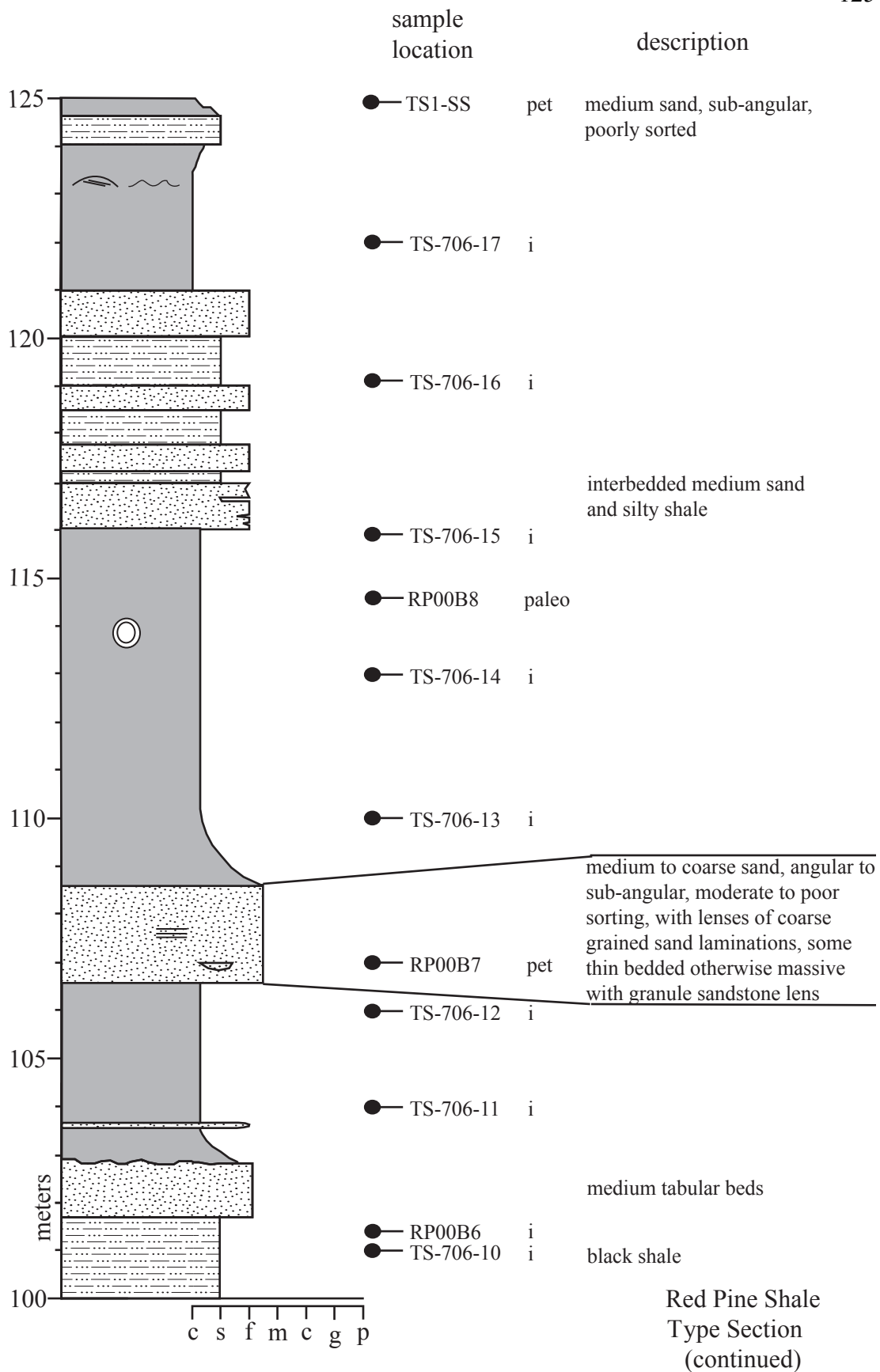
| Thin Section Textural Data |             |       |                  |                      |               |                             |
|----------------------------|-------------|-------|------------------|----------------------|---------------|-----------------------------|
| Locale                     | Sample      | Meter | Grain Size Range | Rounding             | Sorting       | Notes                       |
| Lower Hades                | LH06-1      | 0     | c. sand          | sub-rounded          | poor          |                             |
| Lower Hades                | LH03-14     | 44    | med. sand        | sub-rounded          | moderate      |                             |
| Hades B                    | RP03B-8     | 16    | f.-med. sand     | sub-ang. - sub-round | moderate-well |                             |
| Hades B                    | HadesB 06-1 | 36    | f. sand          | sub-ang. - sub-round | moderate-well |                             |
| Hades B                    | RP03B-27    | 92    | f. sand          | sub-rounded          | moderate      | small sample=denser pt. ct. |
| Hades A                    | RP01A-19.5  | 52    | v.f.- f. sand    | sub-ang. - sub-round | moderate      |                             |
| Hades A                    | RP01A-23    | 62    | f.-med. sand     | sub-rounded          | poor          |                             |
| Hades A                    | RP01A-26    | 65    | med. sand        | sub-ang. - sub-round | moderate      |                             |
| Hades A                    | RP01A-47A   | 129   | v.f.- f. sand    | sub-angular          | poor          | small sample=denser pt. ct. |
| Hades A                    | RP01A-72    | 204   | v.f.- f. sand    | sub-ang. - sub-round | moderate      |                             |
| Hades A                    | RP01A-74A   | 210   | med.-c. sand     | sub-angular          | moderate      |                             |
| Hades A                    | RP01A-76    | 213   | med. sand        | sub-angular          | poor          |                             |
| Hades A                    | RP01A-76A   | 213   | med. sand        | sub-ang. - sub-round | poor          |                             |
| Hades A                    | RP01A-77    | 213.5 | c. sand          | sub-angular          | poor          |                             |
| Hades A                    | RP01A-78    | 218   | c. sand          | sub-angular          | poor          |                             |
| Hades A                    | RP01A-79a   | 225   | med. sand        | v. angular           | moderate      |                             |
| Hades A                    | RP01A-80    | 240   | f. sand          | v. angular           | moderate      |                             |
| Hades A                    | Hades 02    | 292   | f.-med. sand     | v. angular           | moderate-poor |                             |
| Hades A                    | Hades 06-1  | 309   | med. sand        | sub-ang. - sub-round | poor          |                             |
| Hades A                    | Hades 10    | 336   | med. sand        | sub-rounded          | moderate      | lots of plucked grains      |
| Hades A                    | Hades 06-2  | 348   | med. sand        | angular              | poor          |                             |
| Hades A                    | Hades 15    | 351   | med.-c. sand     | sub-rounded          | poor          | lost of plucked grains      |
| Hades A                    | Hades 06-3  | 365   | f. sand          | sub-rounded          | moderate      |                             |
| Hades A                    | Hades 21    | 400   | f. sand          | sub-angular          | poor          |                             |
| Hades A                    | Hades 28    | 446   | v.f.- f. sand    | sub-angular          | moderate      |                             |
| Hades A                    | Hades 29    | 461   | c. sand          | sub-angular          | poor          |                             |
| Hades A                    | Hades 39    | 564   | med. sand        | sub-angular          | moderate      |                             |
| Hades A                    | Hades 56    | 627   | med. sand        | sub-angular          | moderate-poor |                             |
| Hades A                    | Hades 60    | 650   | med. sand        | sub-angular          | poor          |                             |
| Hades A                    | Hades 64    | 653   | c.-v.c. sand     | sub-ang. - sub-round | moderate      |                             |
| Hades A                    | Hades 61    | 654.5 | med. sand        | ang.-sub-angular     | poor          |                             |
|                            |             |       |                  |                      |               | <i>continued</i>            |

| Thin Section Textural Data ( <i>continued</i> ) |            |       |                  |                      |               |                             |
|-------------------------------------------------|------------|-------|------------------|----------------------|---------------|-----------------------------|
| Locale                                          | Sample     | Meter | Grain Size Range | Rounding             | Sorting       | Notes                       |
| Hades C                                         | HC06-1     | 20.5  | med.-c. sand     | ang.-sub-angular     | poor          |                             |
| Hades C                                         | RP01C-1    | 0.5   | c. sand          | sub-angular          | poor          |                             |
| Hades C                                         | RP01C-4    | 15    | c. sand          | angular              | poor          |                             |
| Hades C                                         | RP01C-8    | 25    | med.-c. sand     | sub-ang. - sub-round | moderate-poor |                             |
| Hades C                                         | HC06-2     | 33    | med.-c. sand     | sub-angular          | poor          |                             |
| Hades C                                         | HC06-3     | 63    | med.-c. sand     | ang.-sub-angular     | moderate-poor |                             |
| Hades C                                         | HC06-4     | 76    | med.-c. sand     | sub-angular          | poor          |                             |
| Type Section                                    | RP00B-2.5  | 43.5  | med. sand        | sub-angular          | moderate-well |                             |
| Type Section                                    | RP0B-5     | 45    | f.-med. sand     | sub-angular          | moderate-poor |                             |
| Type Section                                    | RP0B-7     | 49    | med.-c. sand     | ang.-sub-angular     | moderate-poor |                             |
| Type Section                                    | TS1-SS     | 86    | med. sand        | sub-angular          | poor          |                             |
| Type Section                                    | RP00B-10   | 91.5  | med.-c. sand     | sub-angular          | moderate-poor |                             |
| Type Section                                    | TS3-SS     | 103   | med. sand        | sub-angular          | moderate      |                             |
| Type Section                                    | RP0B-23    | 105   | med.-v.c. sand   | ang.-sub-angular     | poor          |                             |
| Type Section                                    | RP00B-12   | 112   | med. sand        | sub-rounded          | moderate-well |                             |
| Type Section                                    | TS5-SS     | 132   | c. sand          | ang.-sub-angular     | moderate      |                             |
| Type Section                                    | RP0B-30    | 135   | v.f.- f. sand    | ang.-sub-angular     | moderate      |                             |
| Type Section                                    | TS6-SS     | 172   | med. sand        | sub-angular          | moderate      |                             |
| Type Section                                    | RP00B-17.5 | 177.5 | med.-c. sand     | ang.-sub-angular     | moderate-poor |                             |
| Type Section                                    | RP00B-21   | 207   | f.-med. sand     | ang.-sub-angular     | moderate      |                             |
| Type Section                                    | RP00B-22a  | 218   | f.-c. sand       | sub-angular          | moderate-poor |                             |
| Type Section                                    | RP00B-22b  | 219   | f.-c. sand       | sub-rounded          | moderate-poor |                             |
| Type Section                                    | TS7-SS     | 265   | med.-c. sand     | angular              | moderate      |                             |
| Type Section                                    | RP00B-32   | 300   | f. sand          | sub-rounded          | well sorted   |                             |
| Type Section                                    | RP00B-40   | 360   | f. sand          | sub-rounded          | well sorted   |                             |
| Type Section                                    | RP00B-42a  | 387   | f.-c. sand       | sub-angular          | moderate-poor |                             |
| Type Section                                    | RP00B-44   | 413   | f. sand-pebble   | ang.-sub-angular     | poor          |                             |
| Ashley Creek                                    | AC04-7     | --    | med.-v.c. sand   | well rounded         | poor          |                             |
| Ashley Creek                                    | AC-3       | 67    | v.f. sand        | sub-rounded          | moderate-well | small sample=denser pt. ct. |
| Ashley Creek                                    | AC-10      | 124   | v.f.- f. sand    | sub-rounded          | well sorted   | small sample=denser pt. ct. |
| Ashley Creek                                    | AC-11      | 124   | v.f.- f. sand    | sub-ang. - sub-round | well sorted   |                             |
|                                                 |            |       |                  |                      |               | <i>continued</i>            |

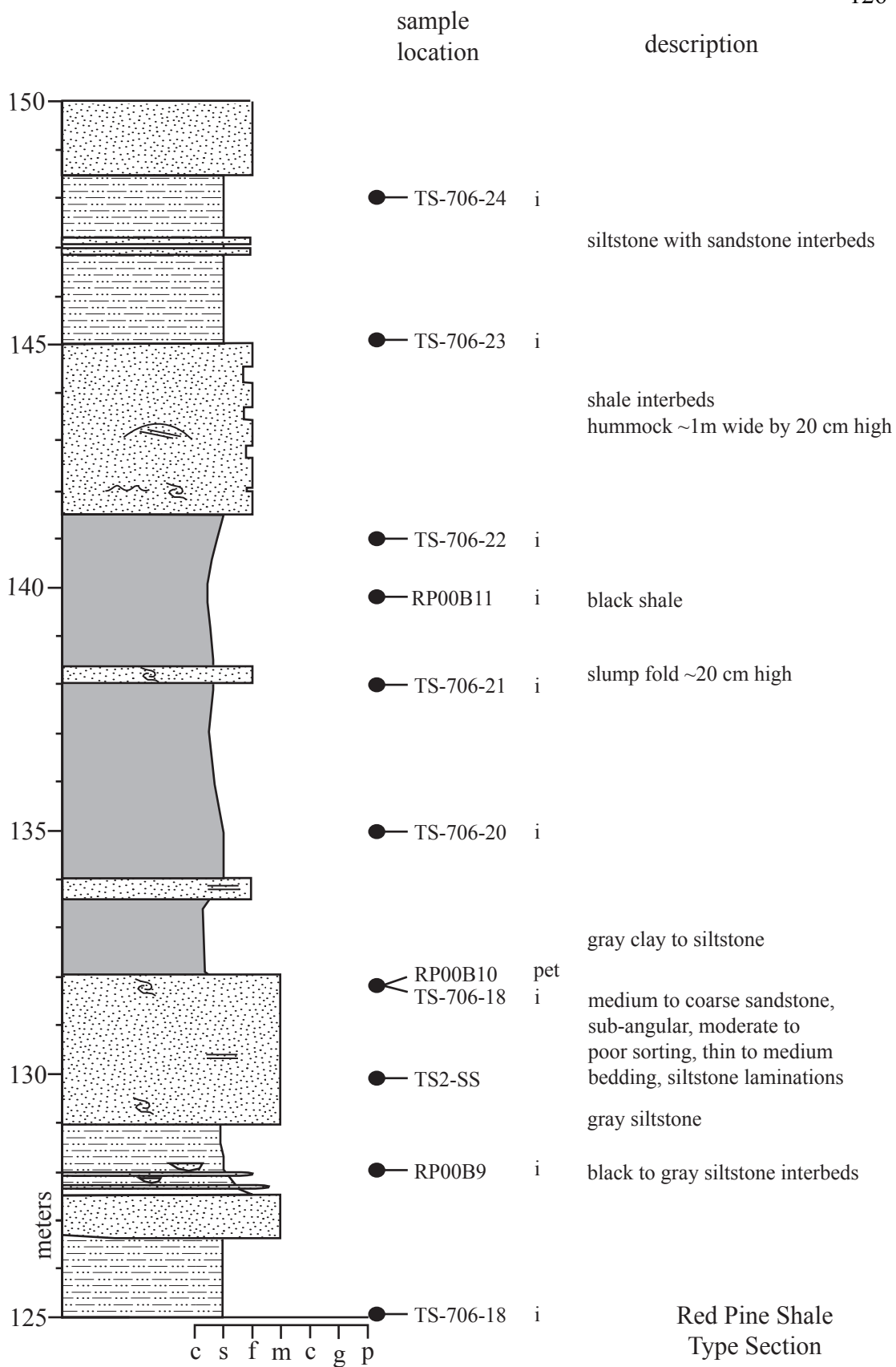
| Thin Section Textural Data ( <i>continued</i> ) |        |       |                         |                     |               |                             |
|-------------------------------------------------|--------|-------|-------------------------|---------------------|---------------|-----------------------------|
| Locale                                          | Sample | Meter | Grain Size Range        | Rounding            | Sorting       | Notes                       |
| Henry's Fork                                    | HF-1   | sub 0 | v.f.- f. sand           | sub-angular         | moderate      | Hades Quartzite sample      |
| Henry's Fork                                    | HF-5   | 126   | f. sand                 | sub-rounded         | well sorted   |                             |
| Henry's Fork                                    | HF-6   | 129   | v.f. sand               | sub-rounded         | well sorted   | small sample=denser pt. ct. |
| Henry's Fork                                    | HF-12  | 153.5 | med. sand -fine pebbles | angular             | poor          |                             |
| Henry's Fork                                    | HF-14  | 165   | f.-med. sand            | sub-round - rounded | well sorted   |                             |
| Henry's Fork                                    | HF-15  | 168   | f. sand                 | sub-round - rounded | well sorted   |                             |
| Henry's Fork                                    | HF-16  | 209   | f.-med. sand            | sub-rounded         | moderate-poor |                             |

Appendix E: Detailed stratigraphic columns

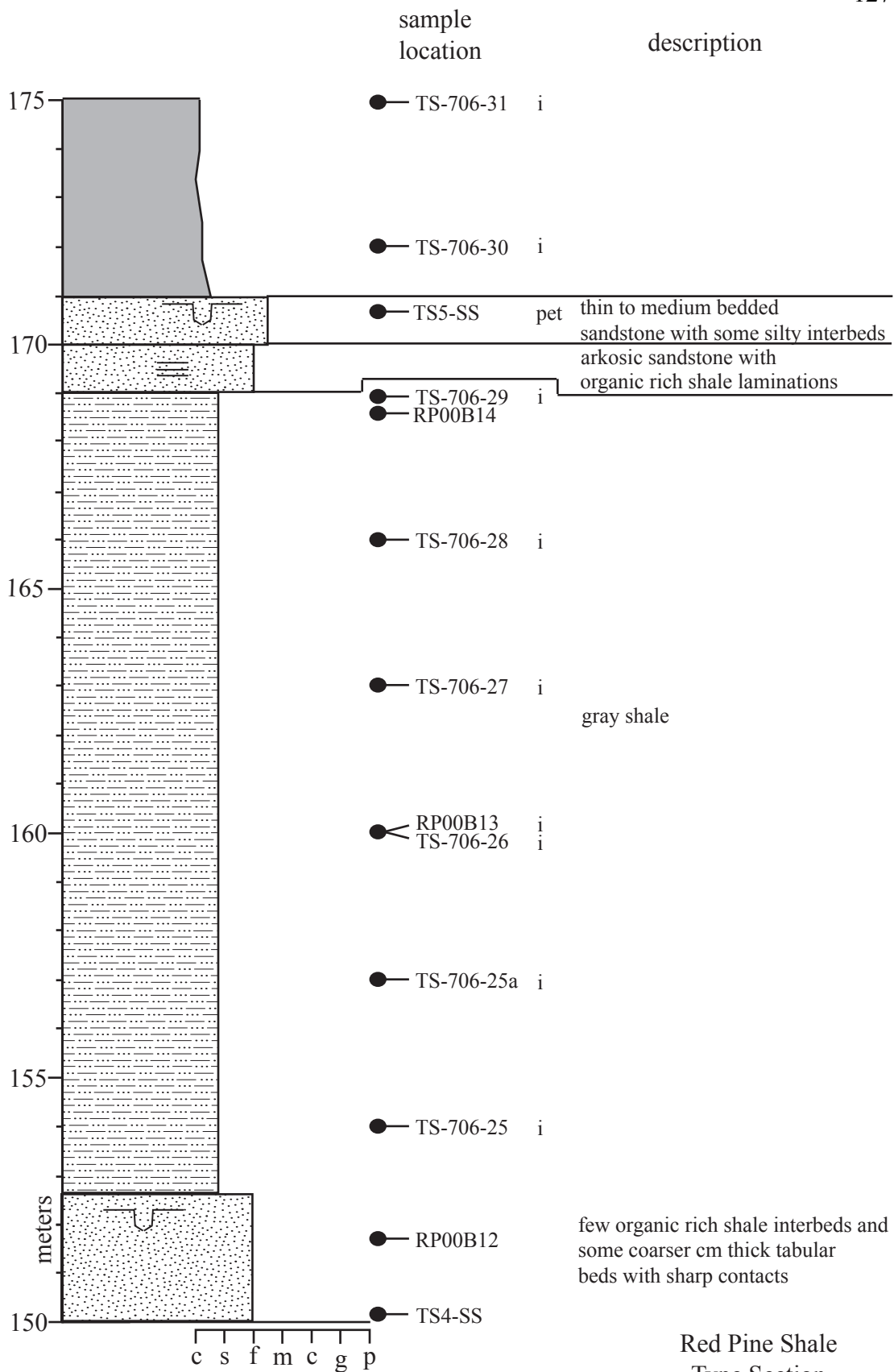




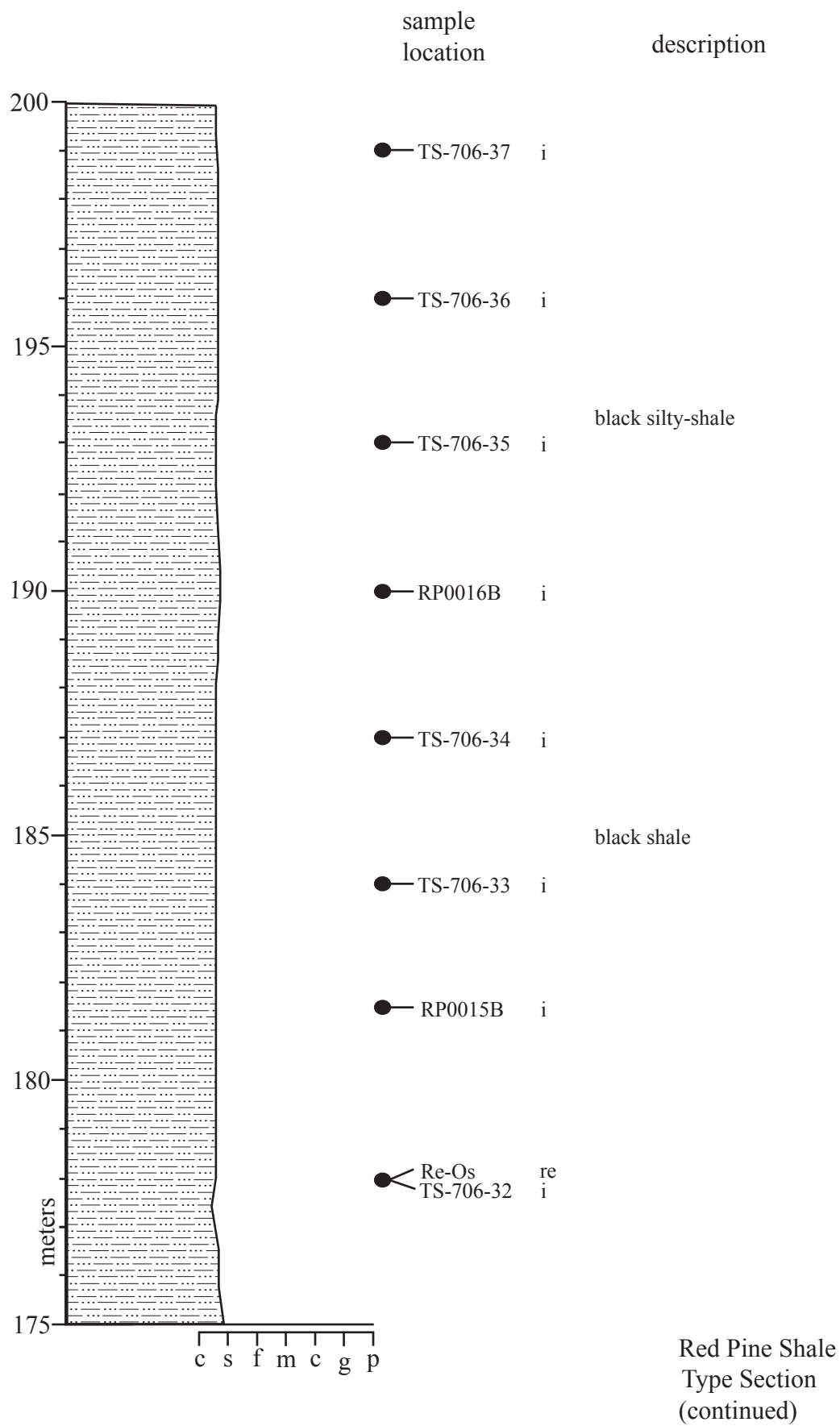


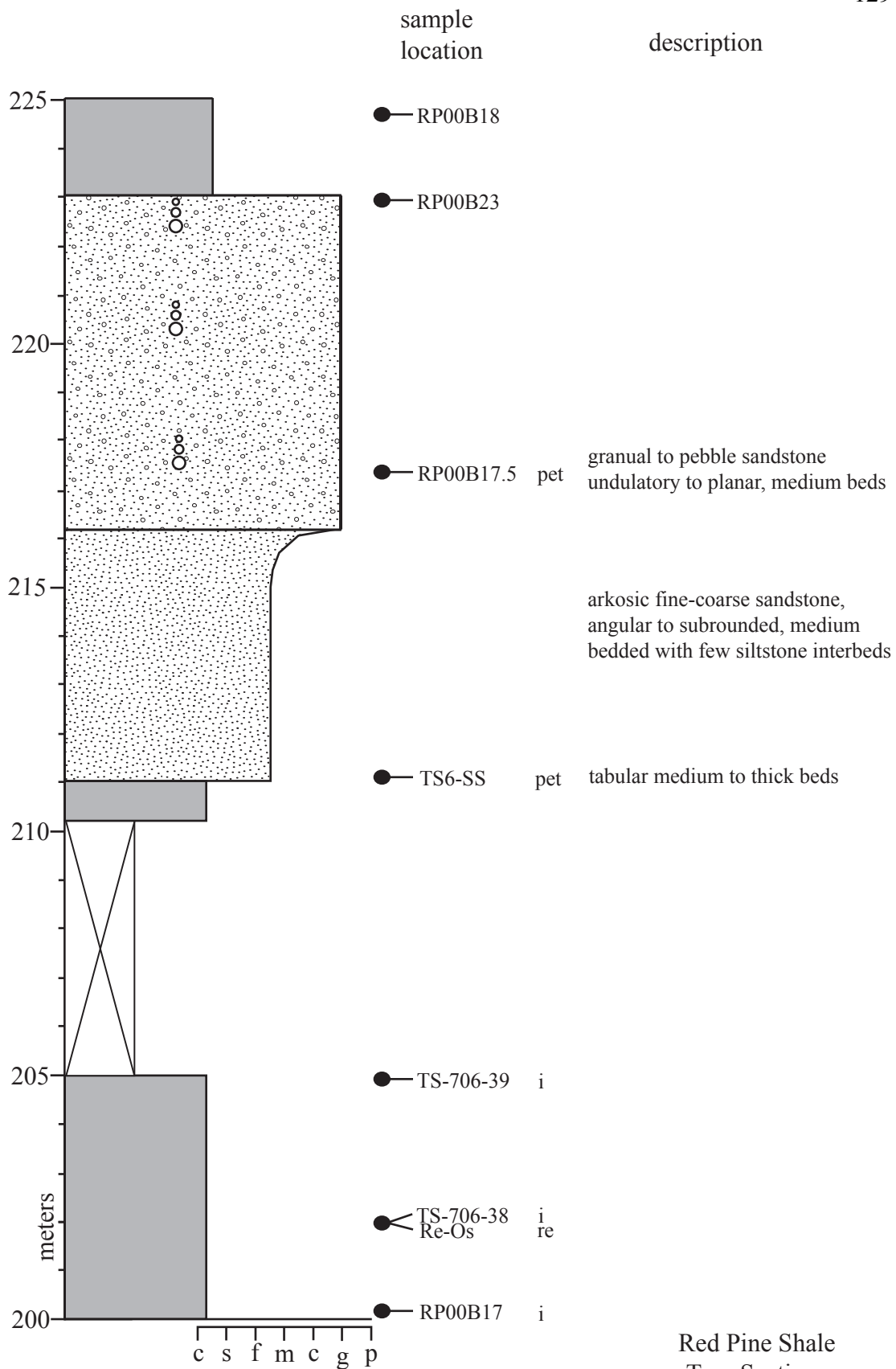


Red Pine Shale  
Type Section  
(continued)

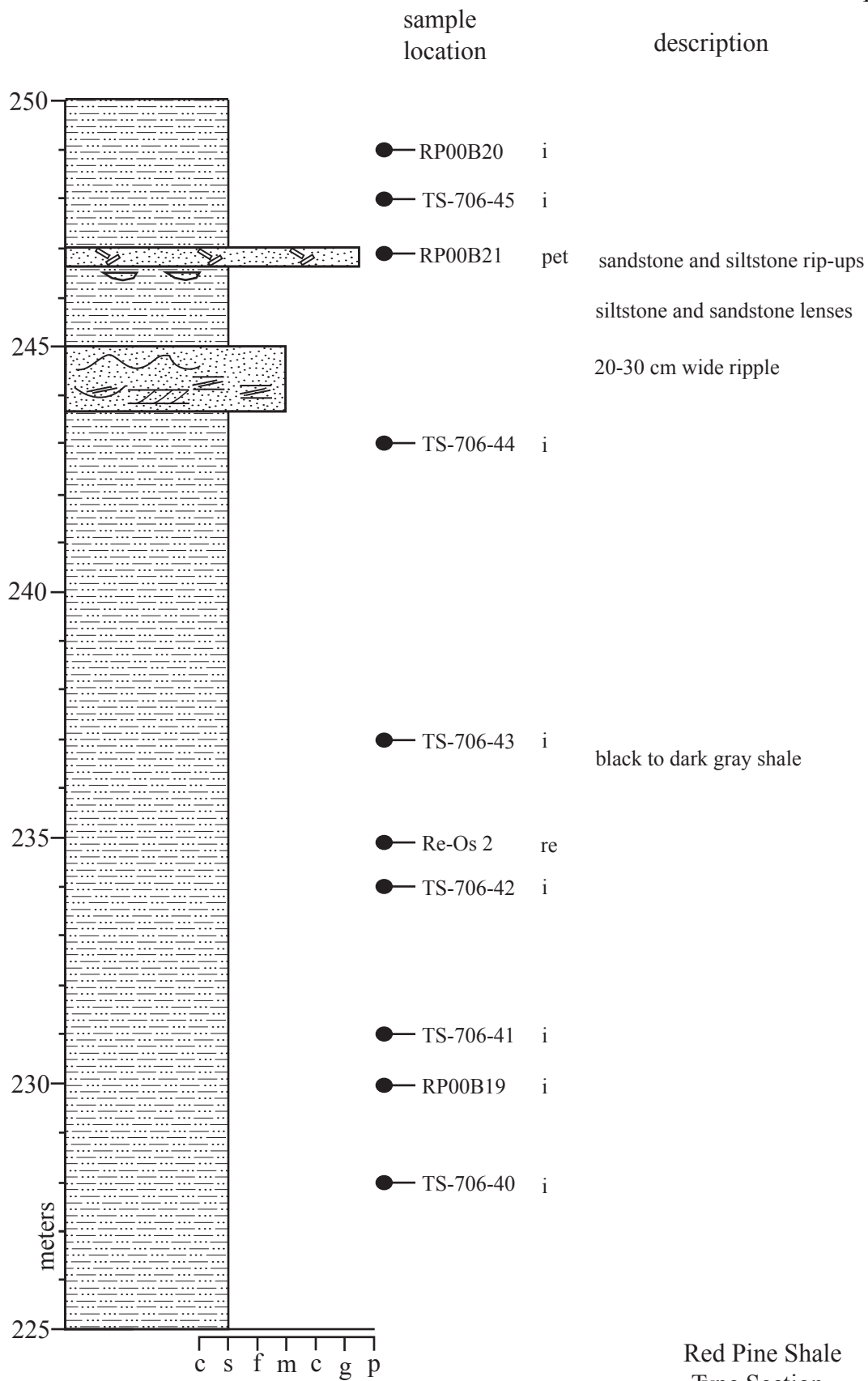


Red Pine Shale  
Type Section  
(continued)

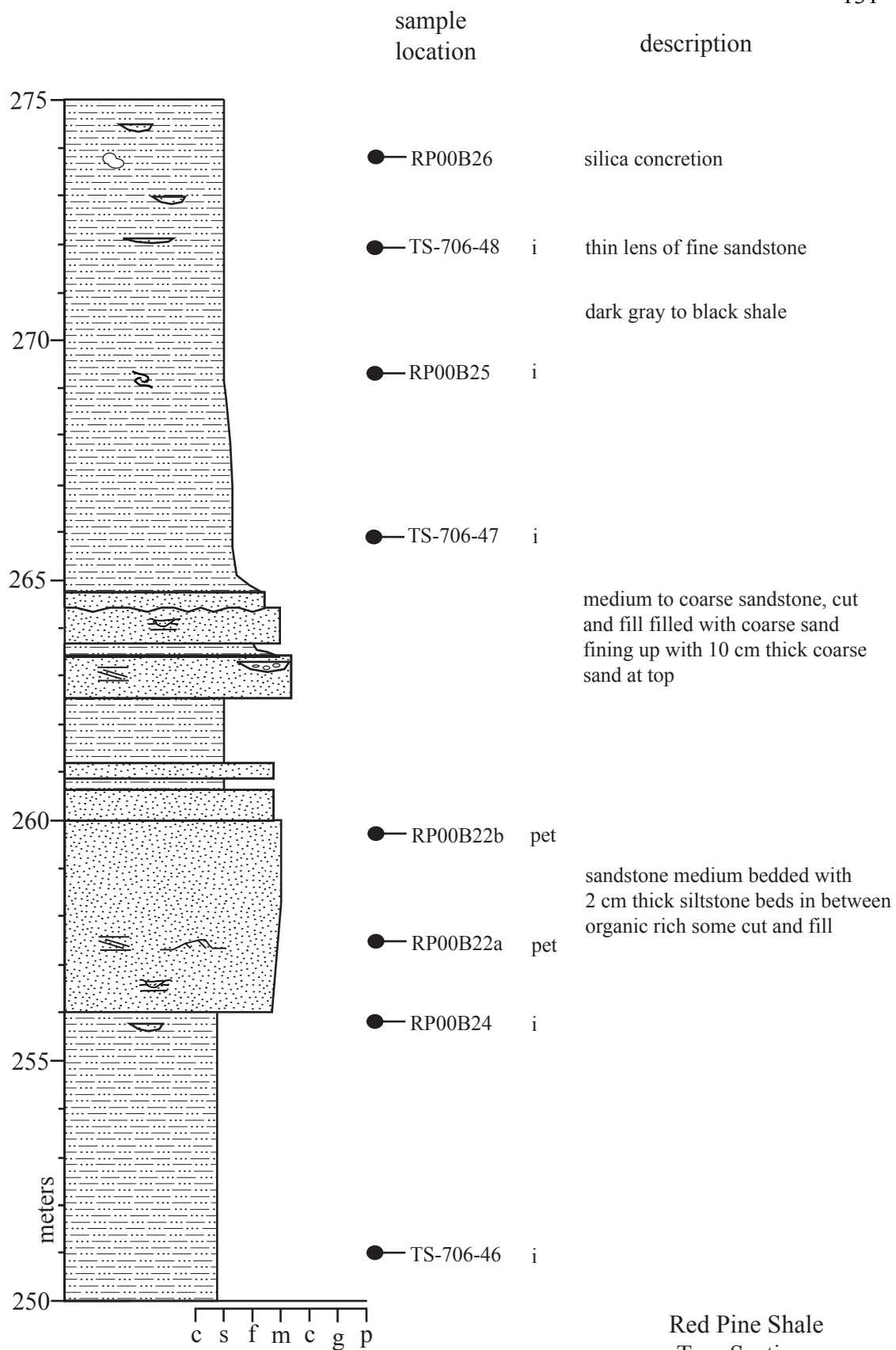




Red Pine Shale  
Type Section  
(continued)



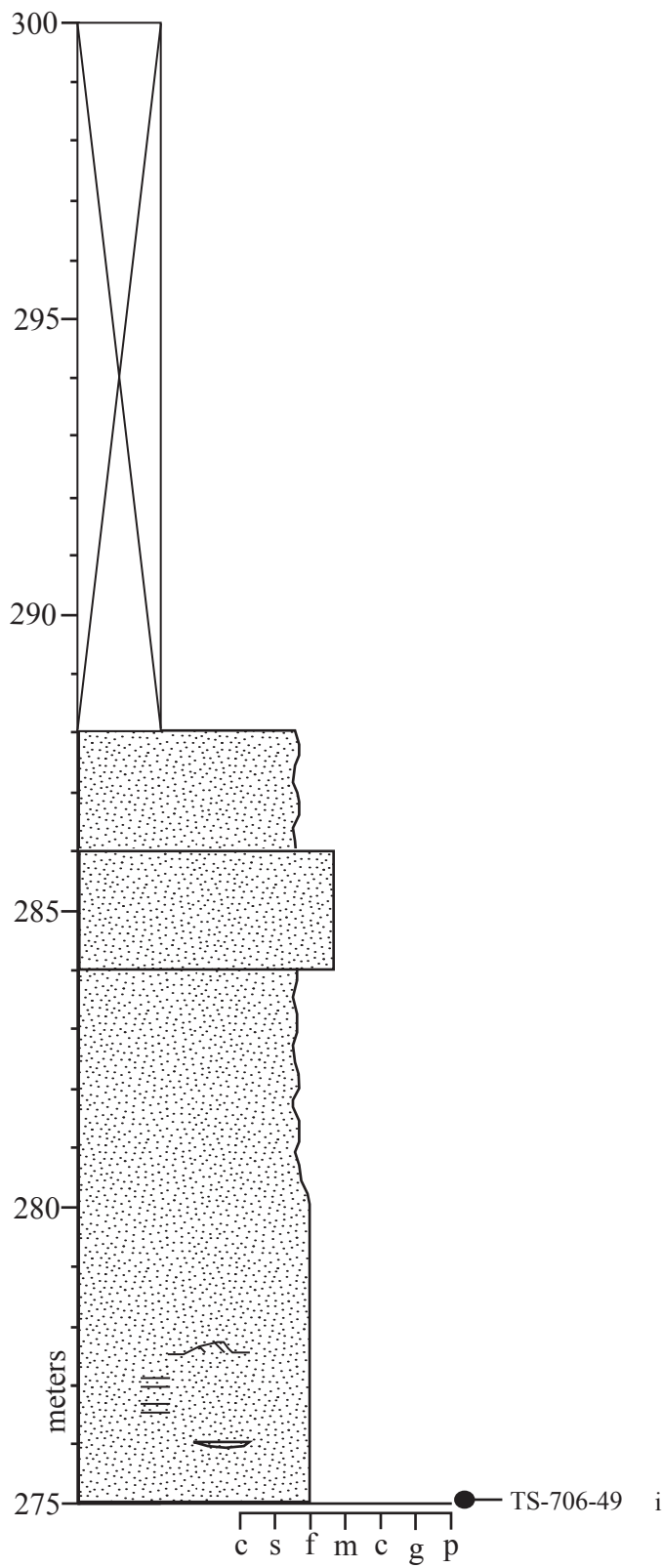
Red Pine Shale  
Type Section  
(continued)



Red Pine Shale  
Type Section  
(continued)

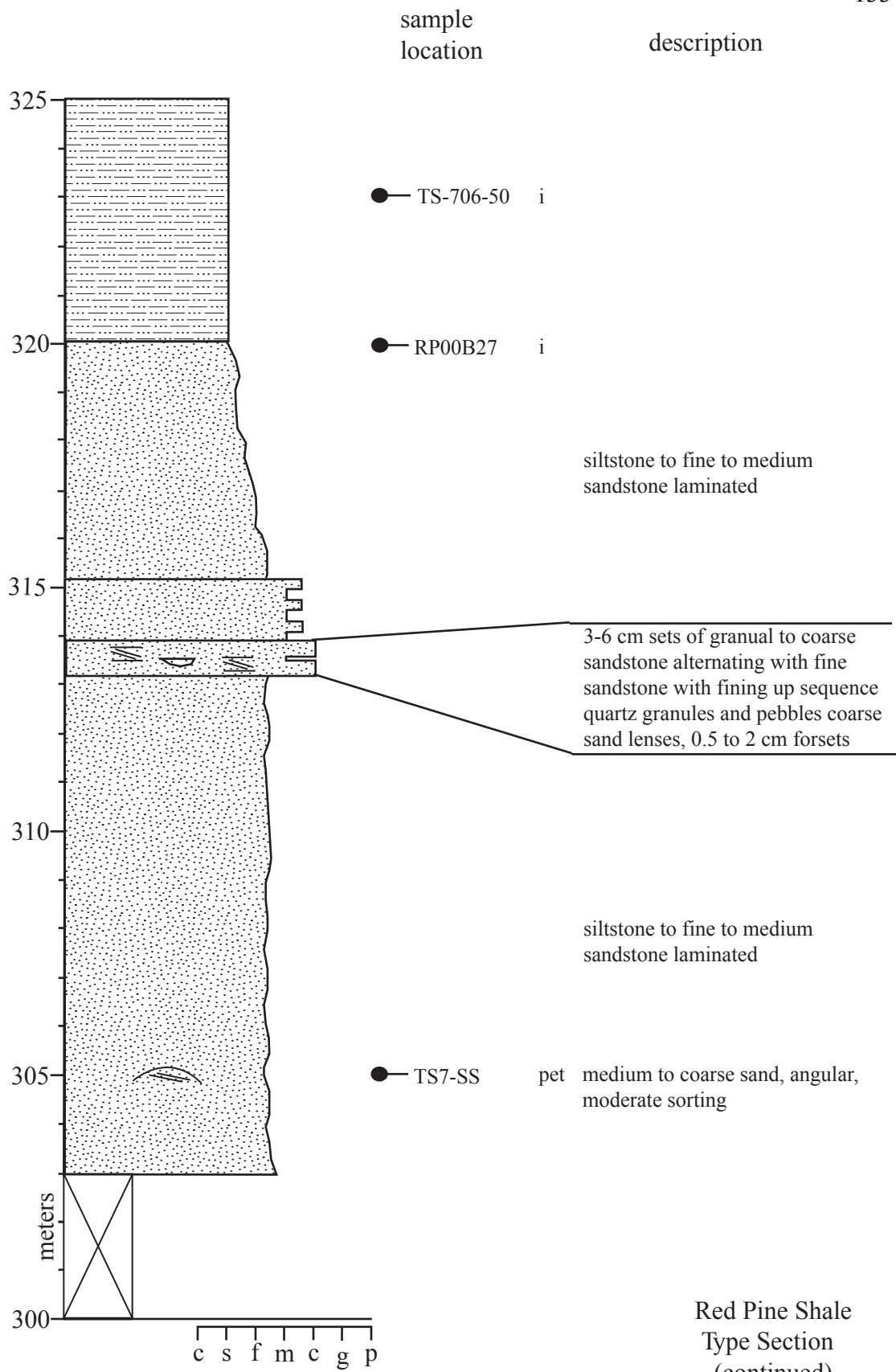
sample  
location

description

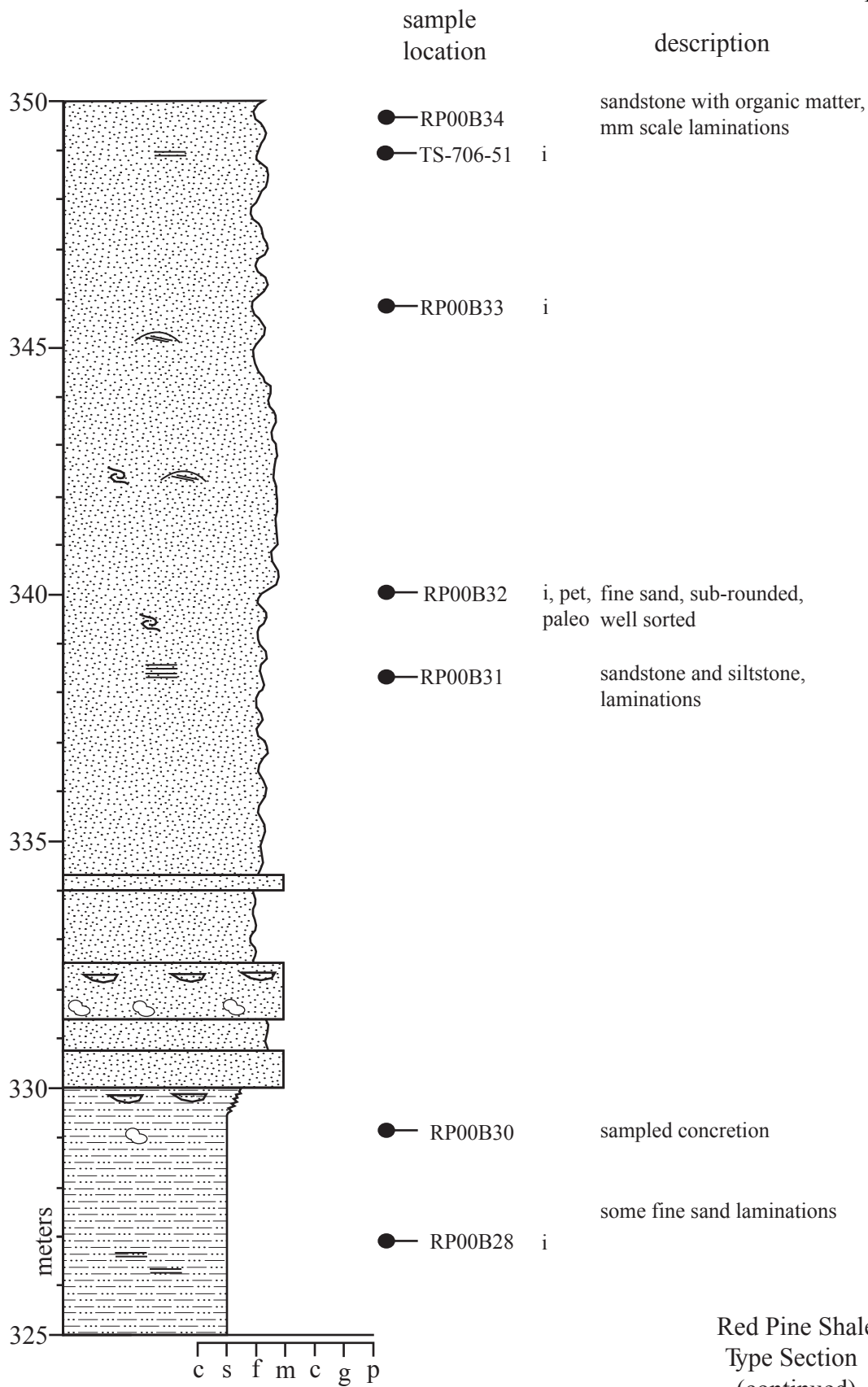


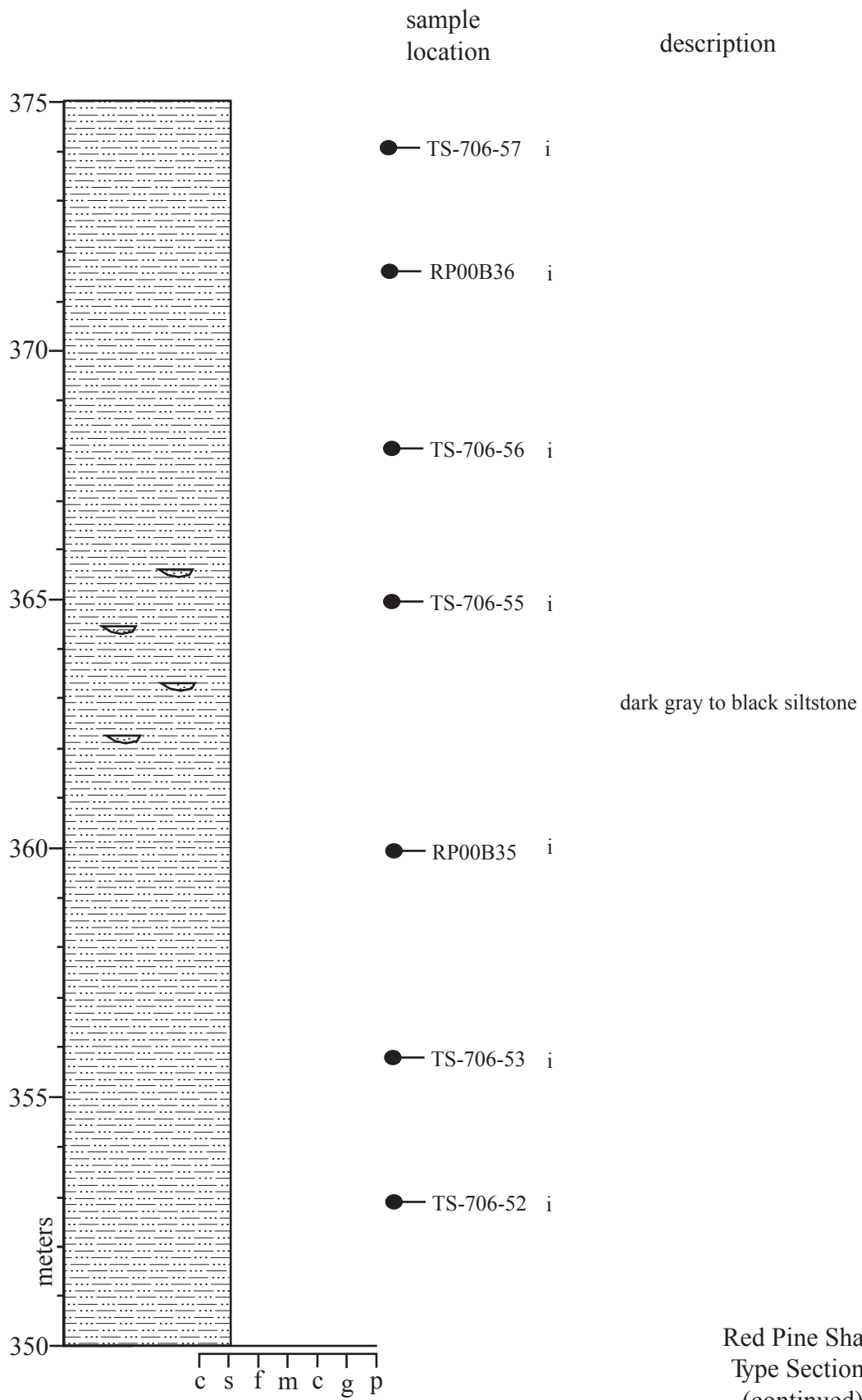
some shale laminations, organic rich

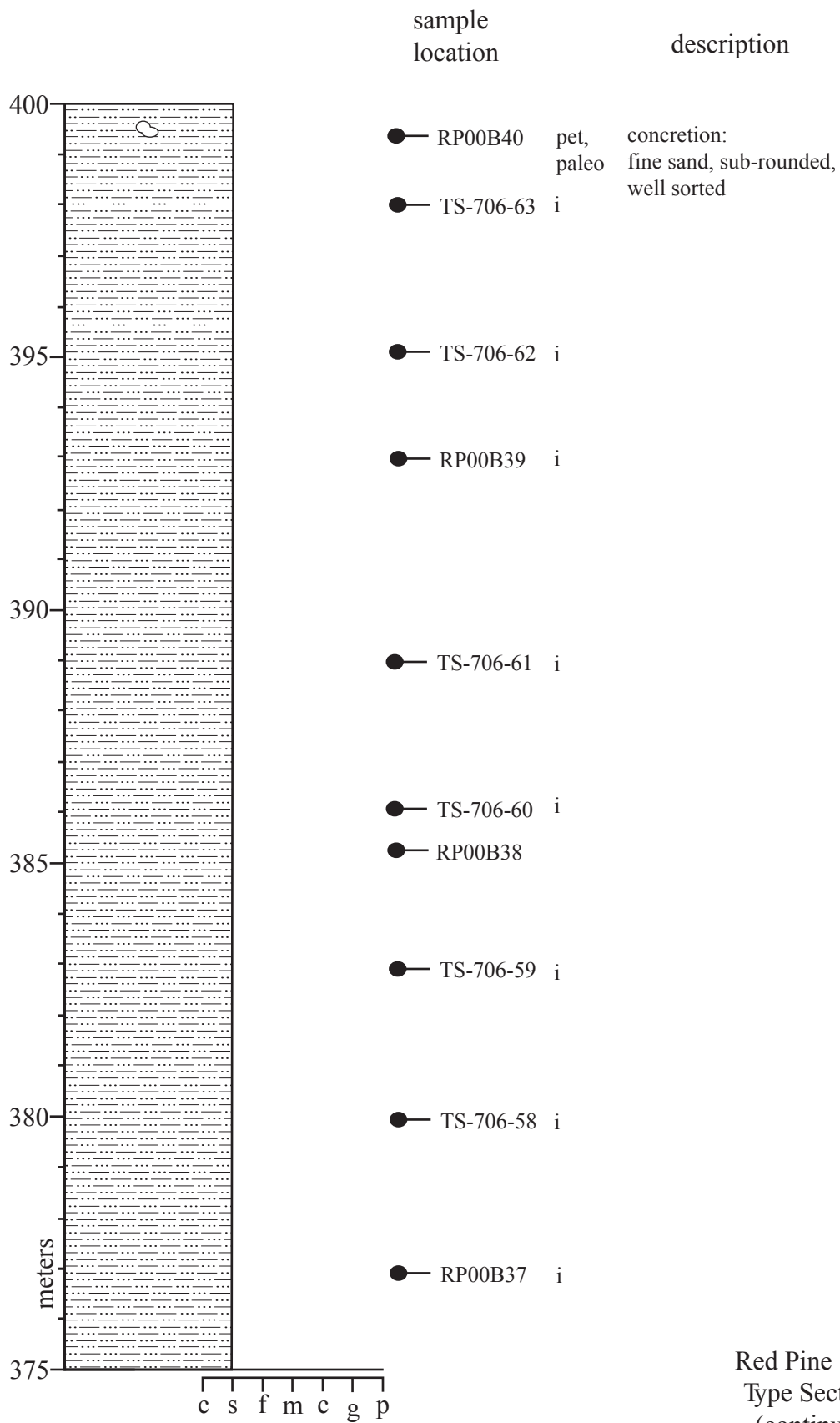
Red Pine Shale  
Type Section  
(continued)



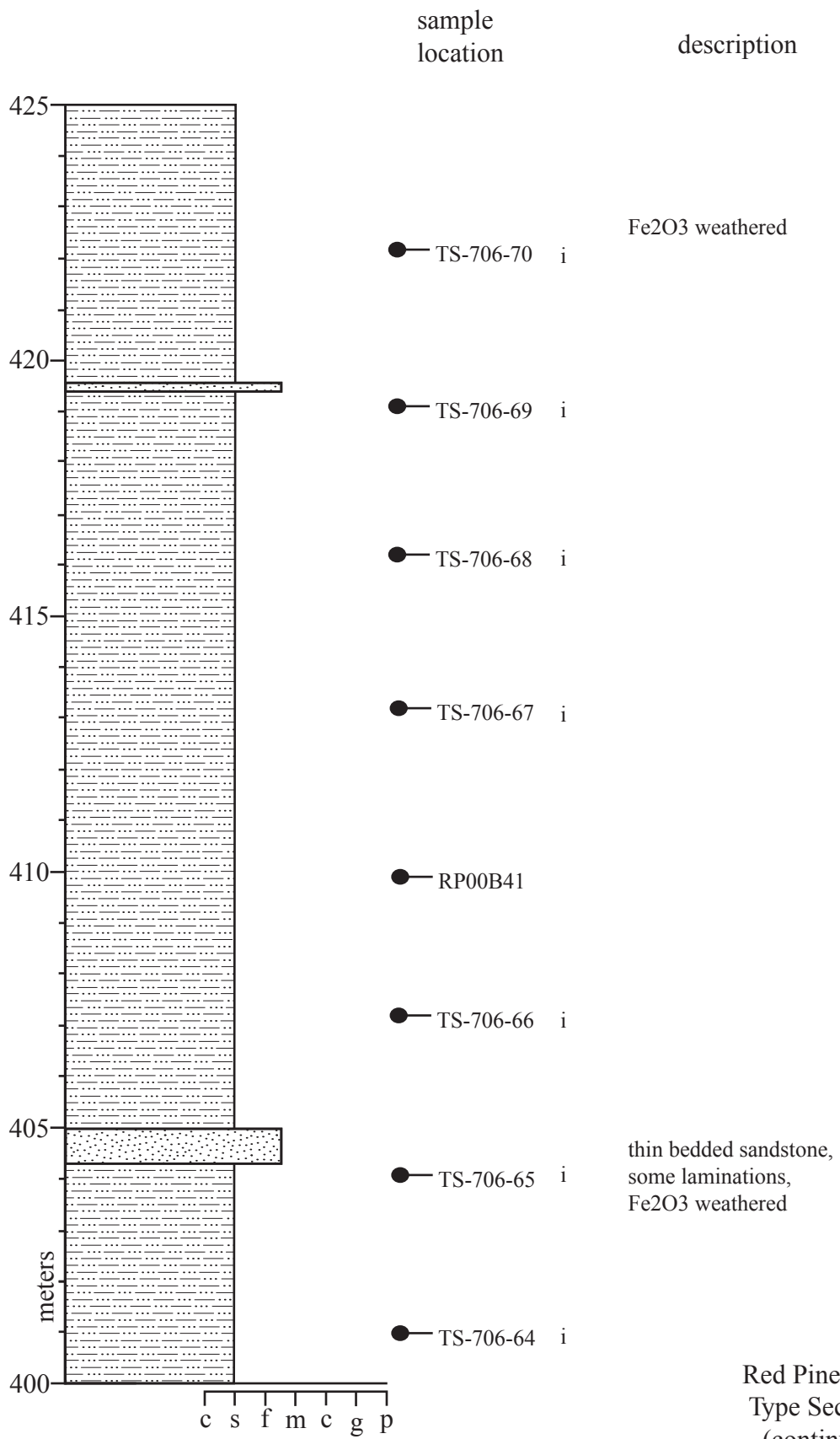




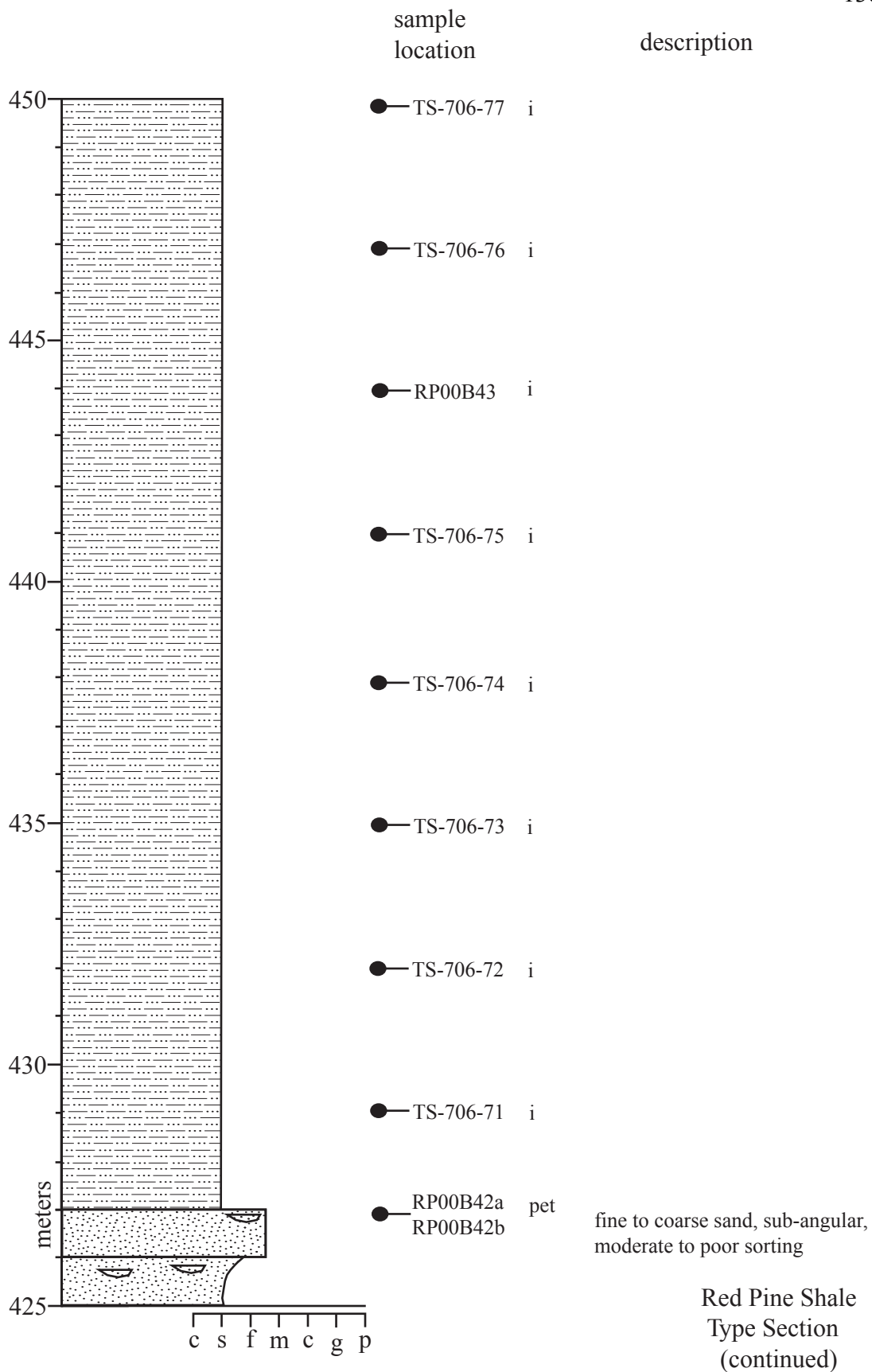


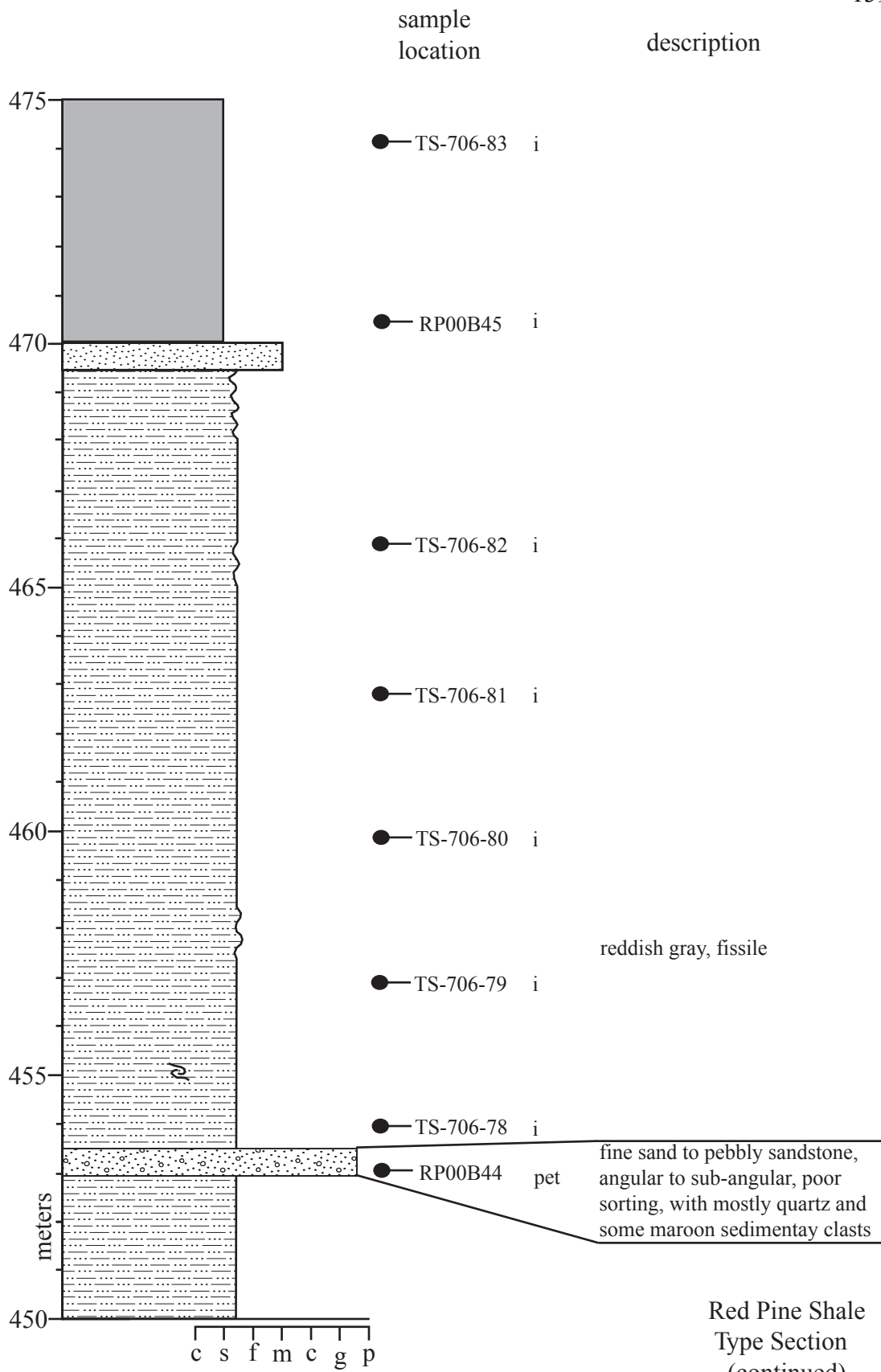


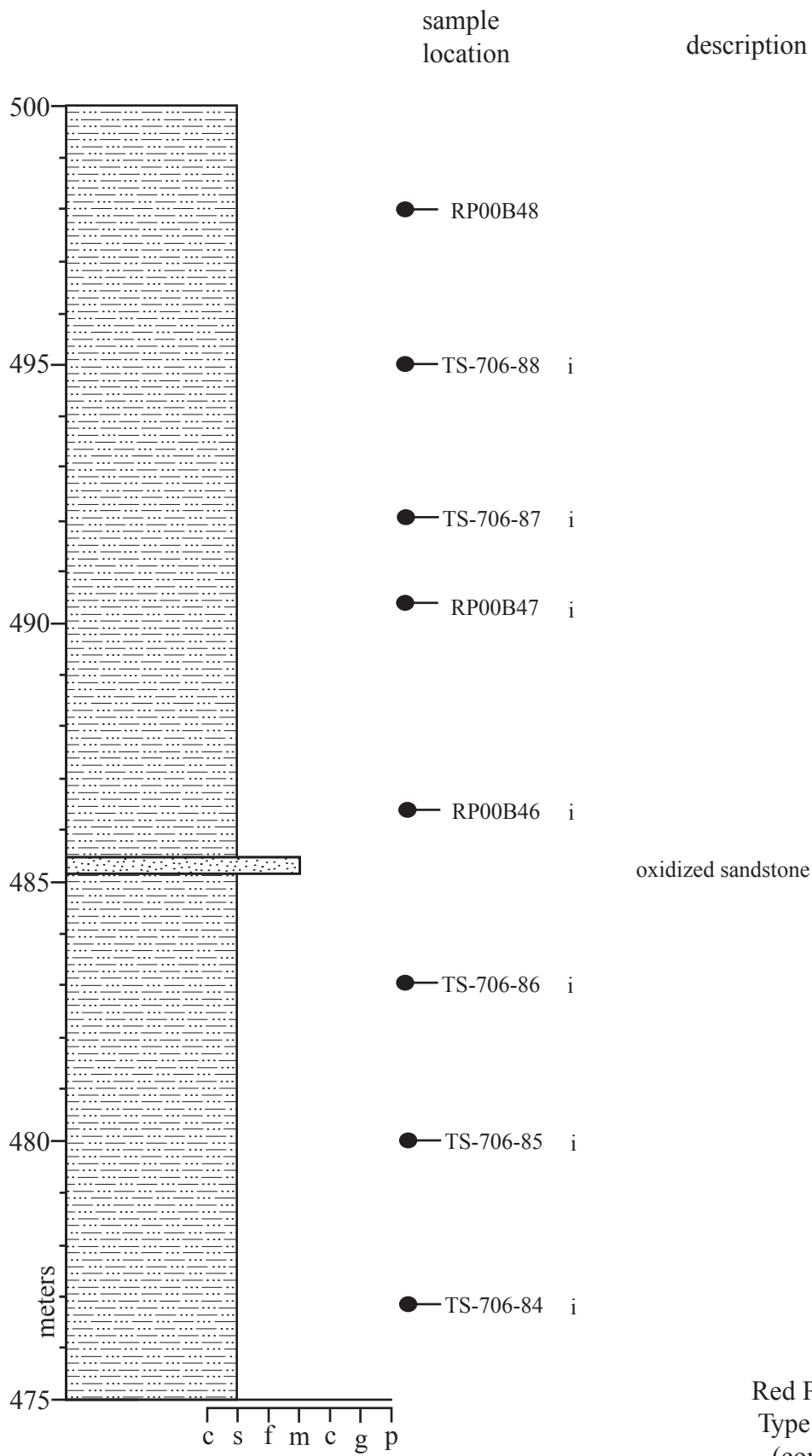
Red Pine Shale  
Type Section  
(continued)



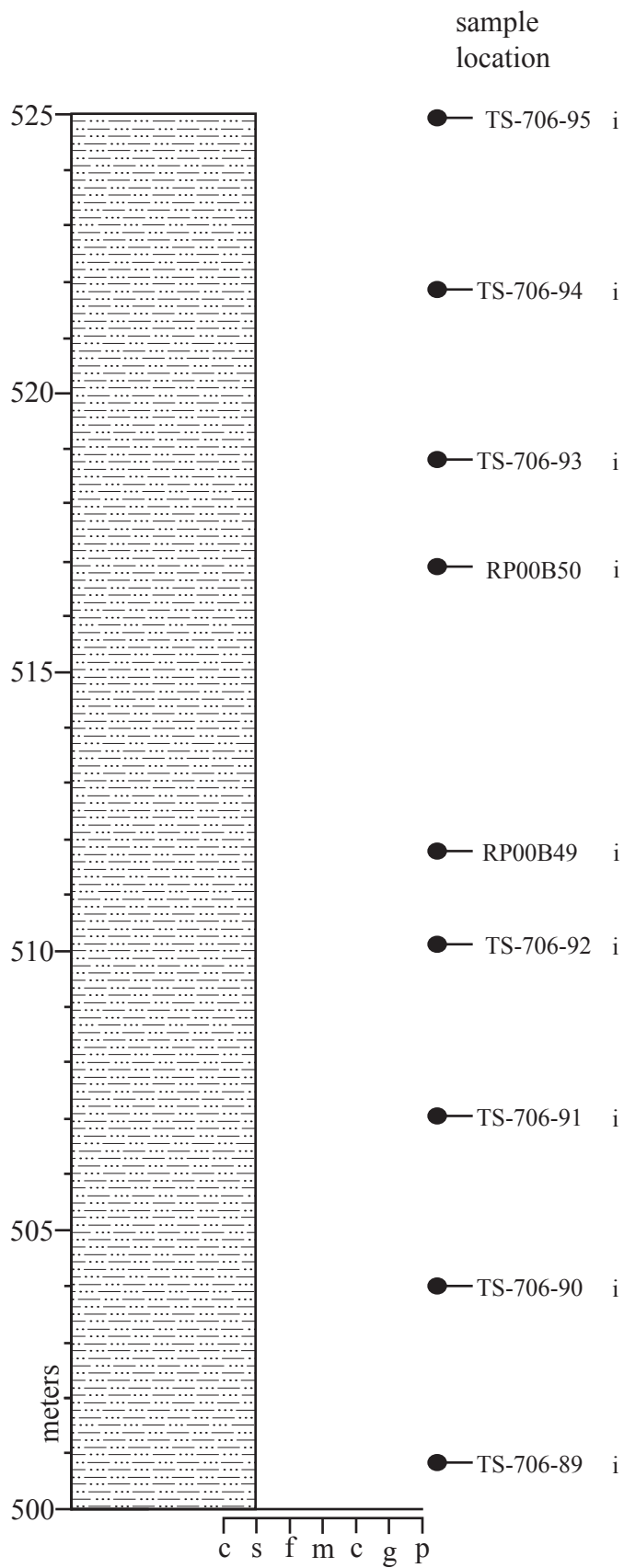
Red Pine Shale  
Type Section  
(continued)





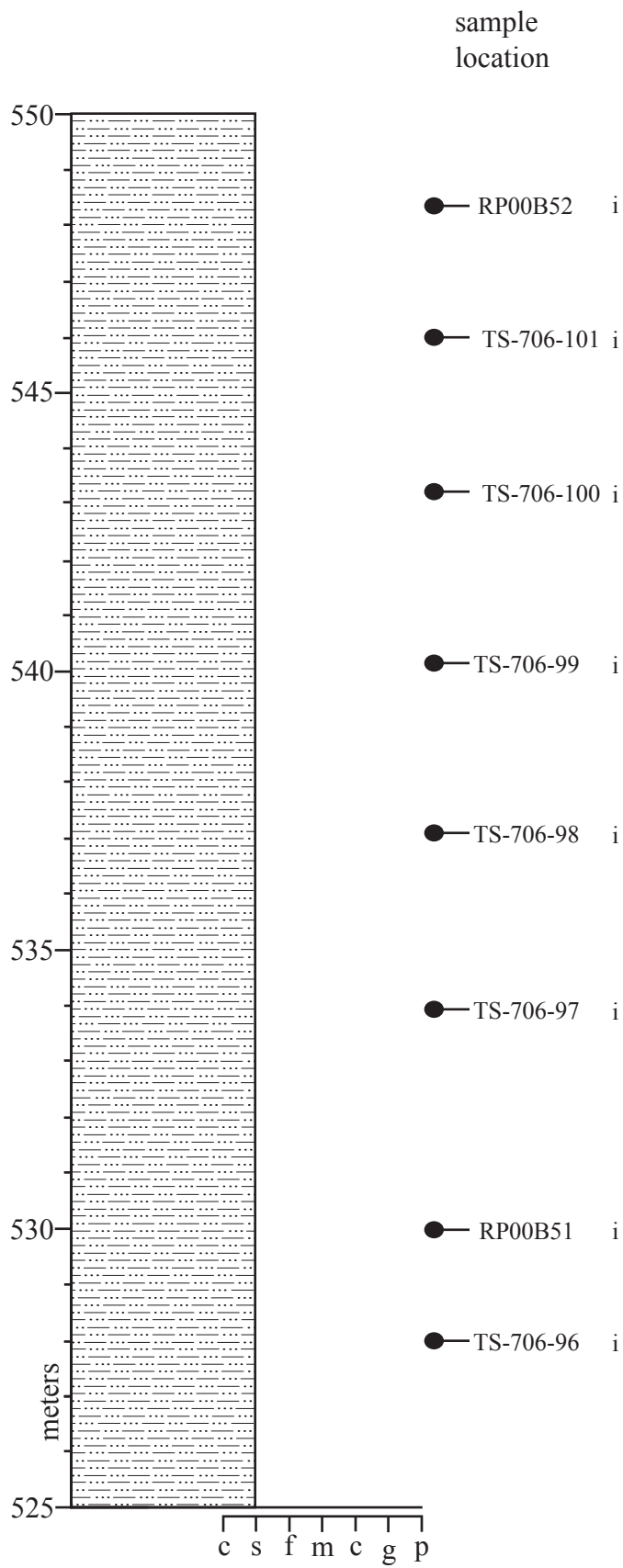


Red Pine Shale  
Type Section  
(continued)



Red Pine Shale  
Type Section  
(continued)



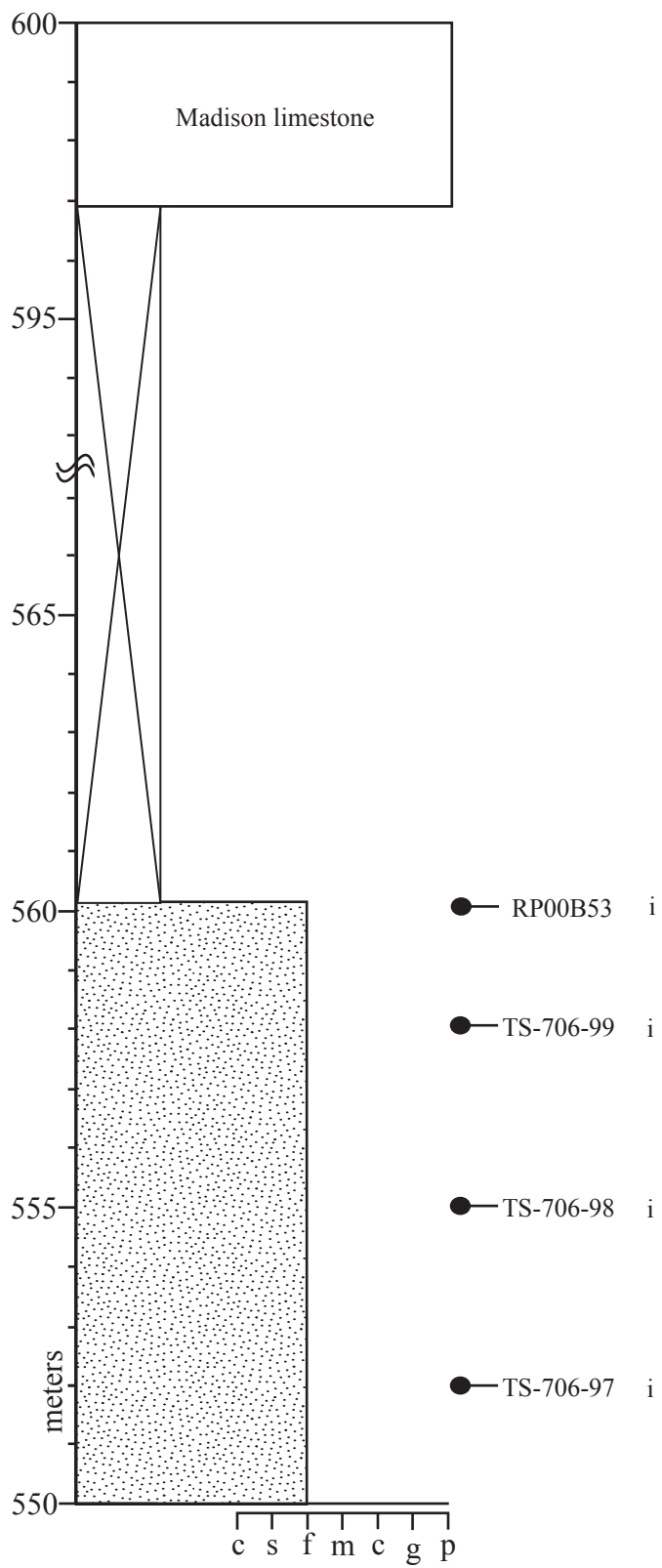


description

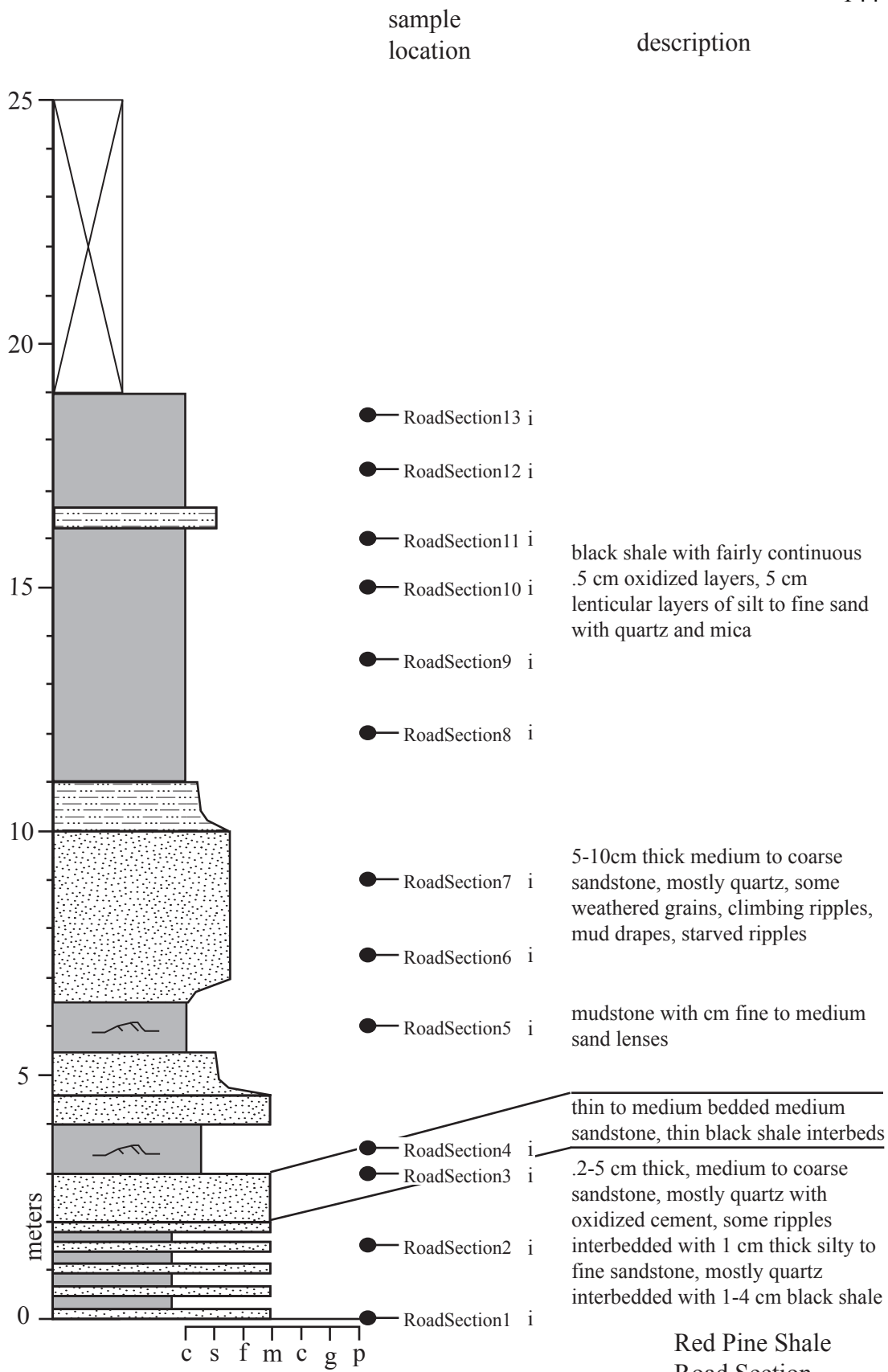
Red Pine Shale  
Type Section  
(continued)

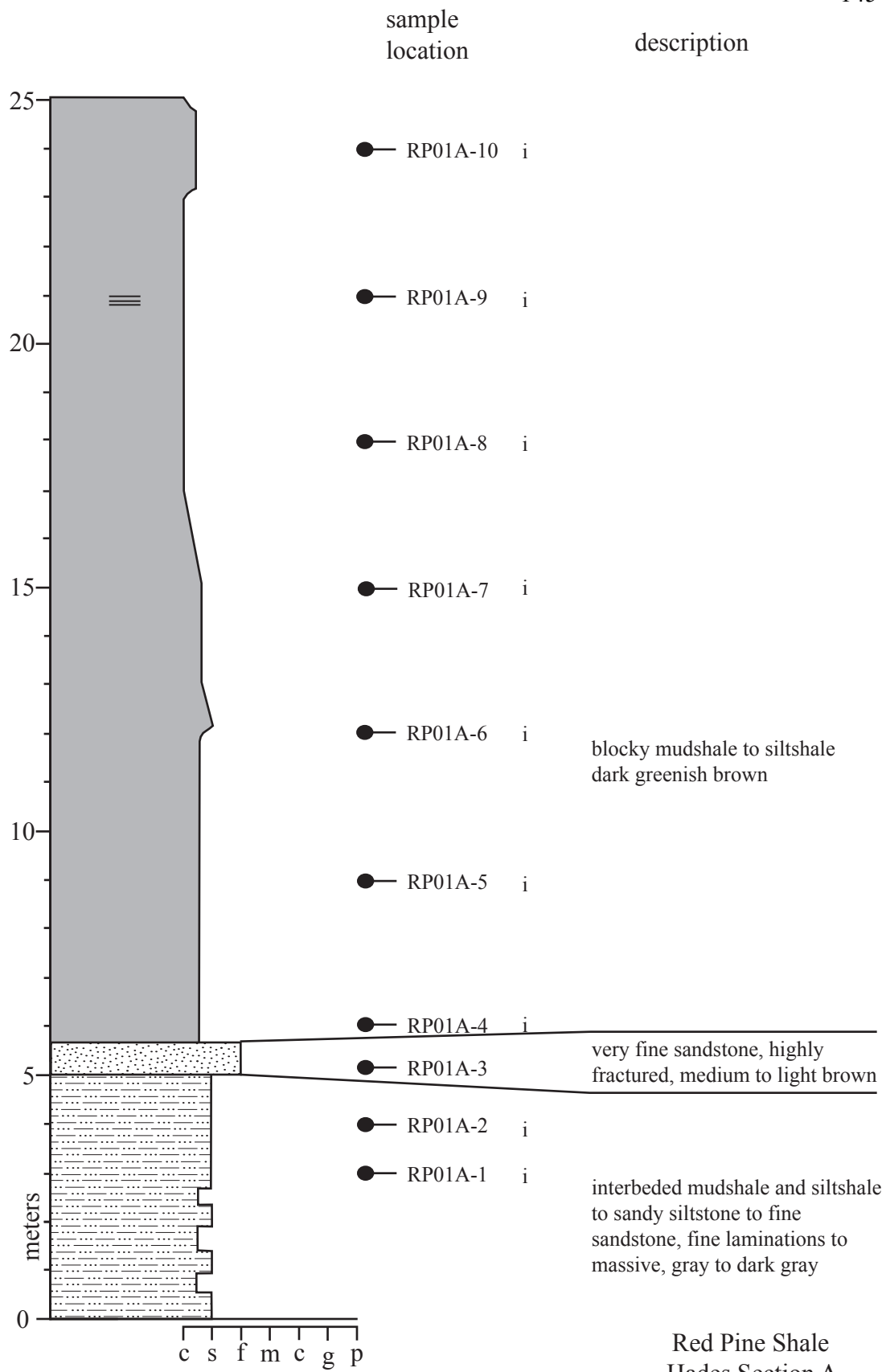
sample  
location

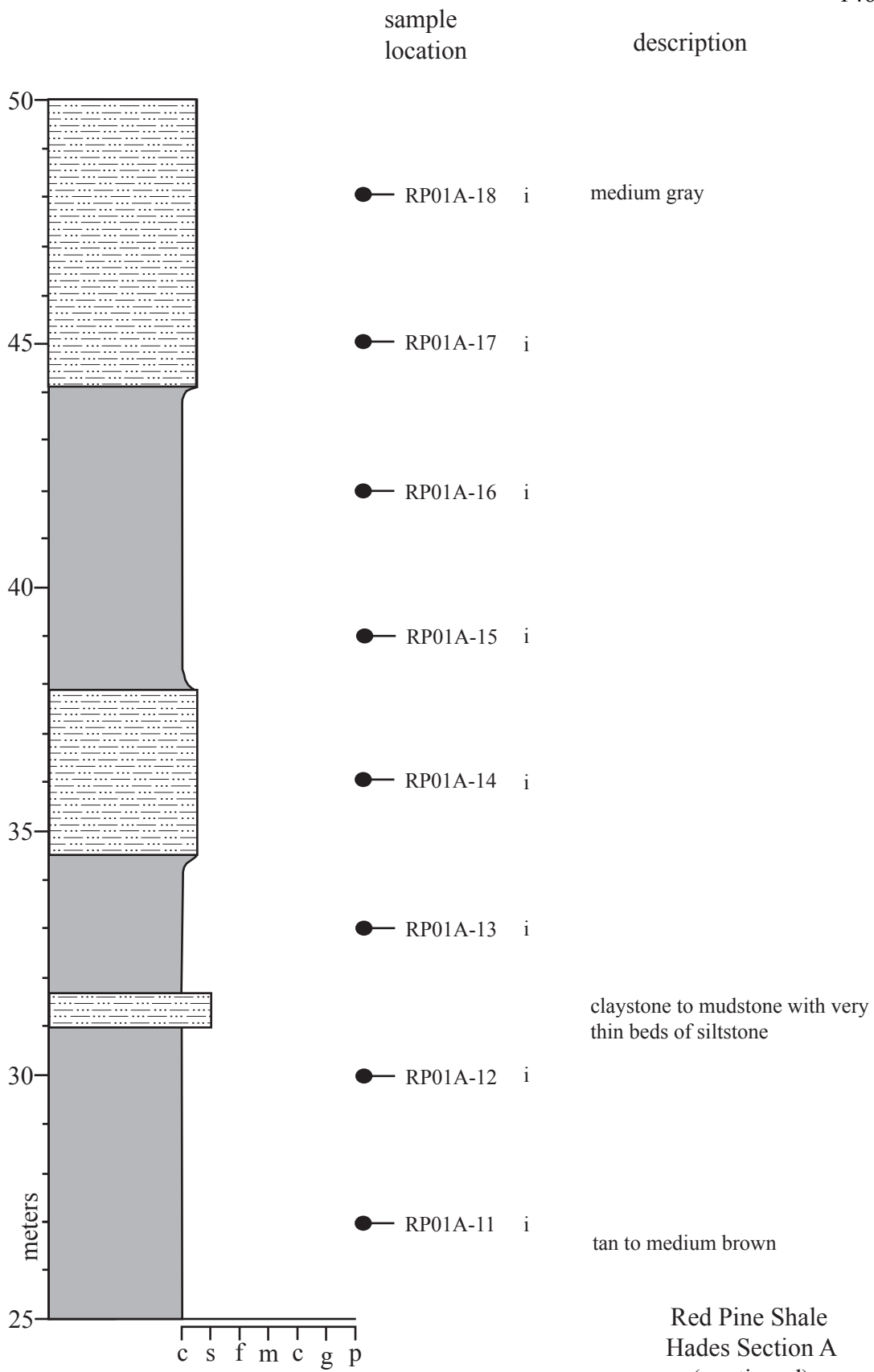
description

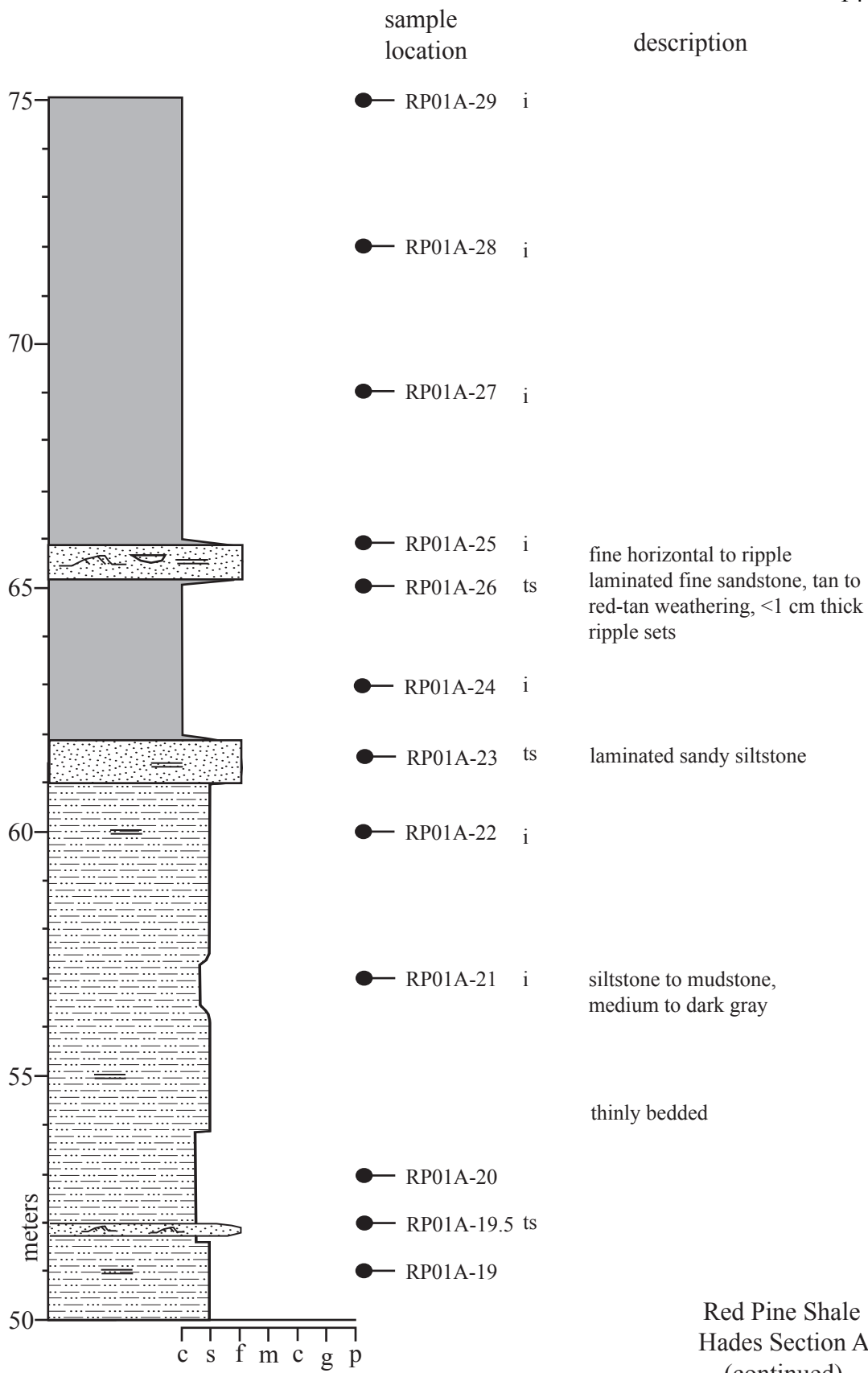


Red Pine Shale  
Type Section  
(continued)

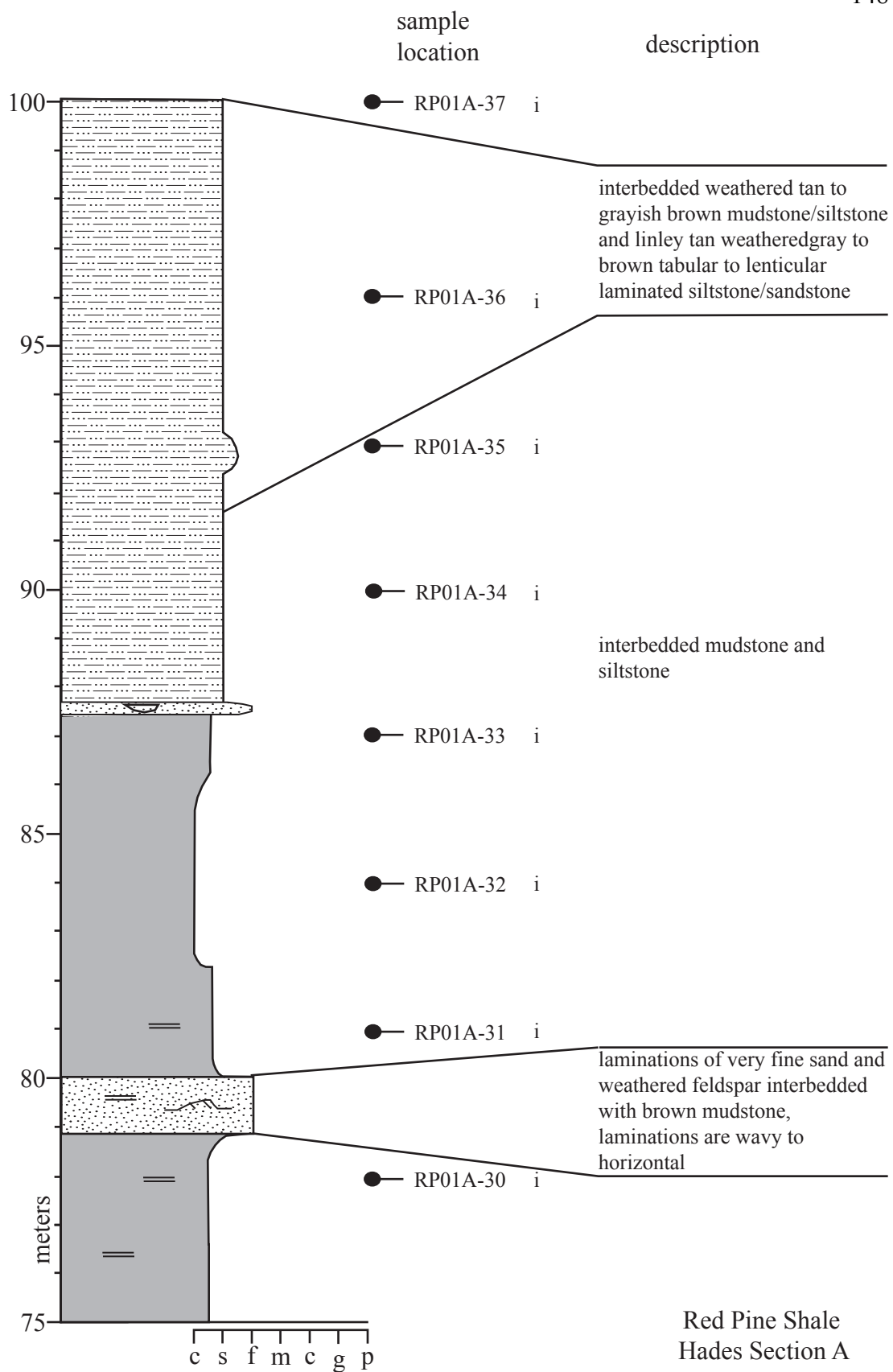


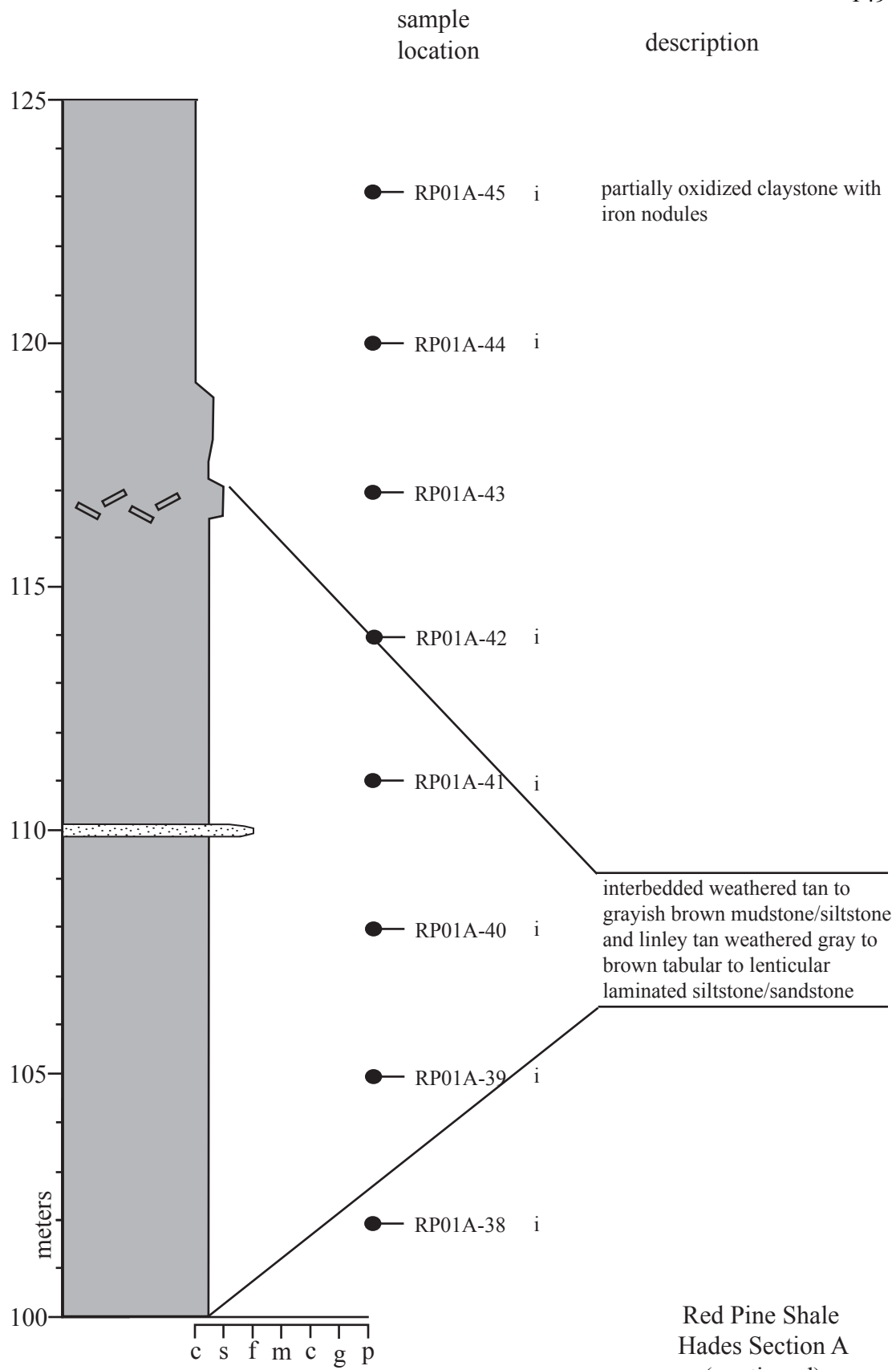




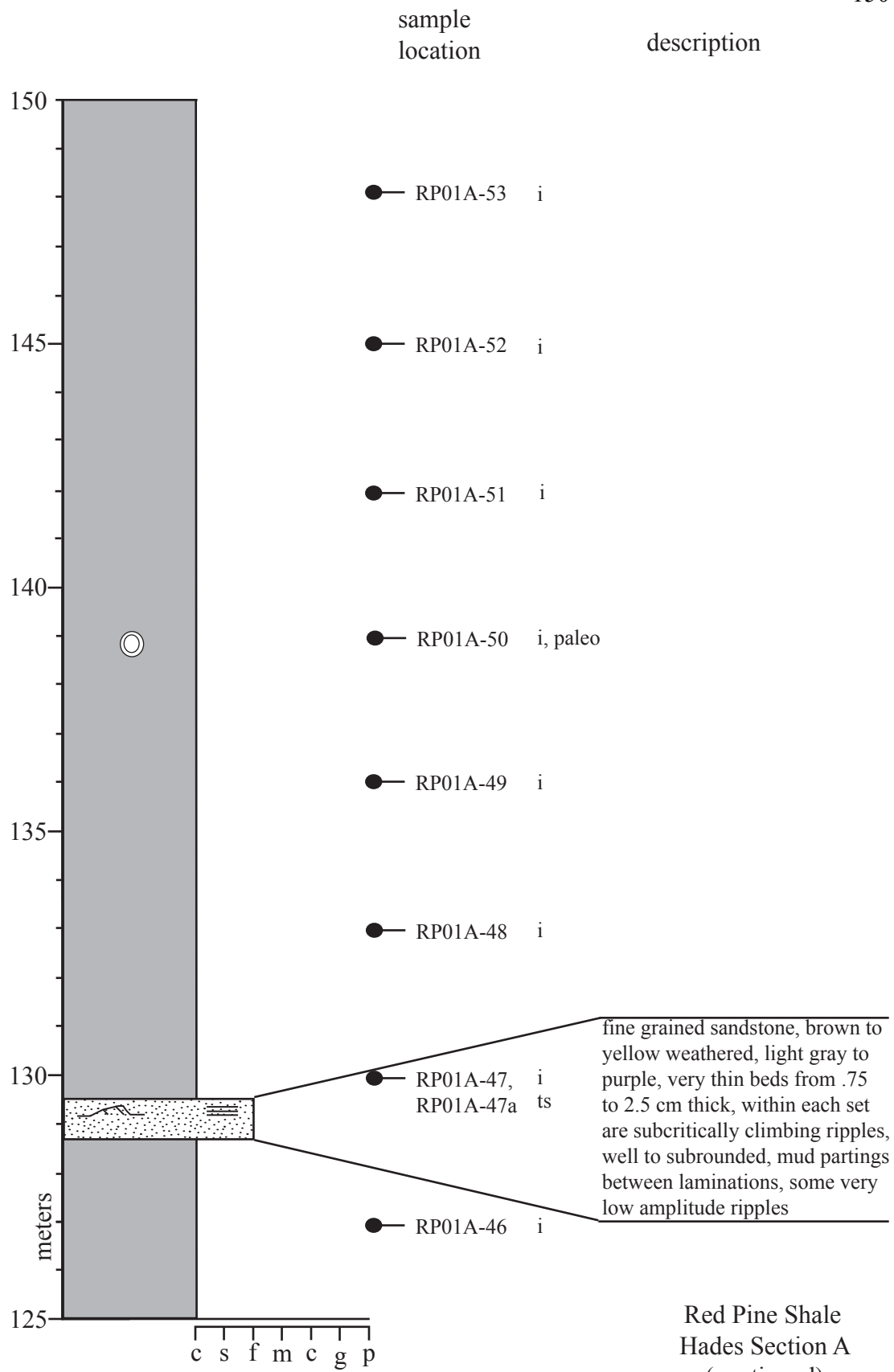


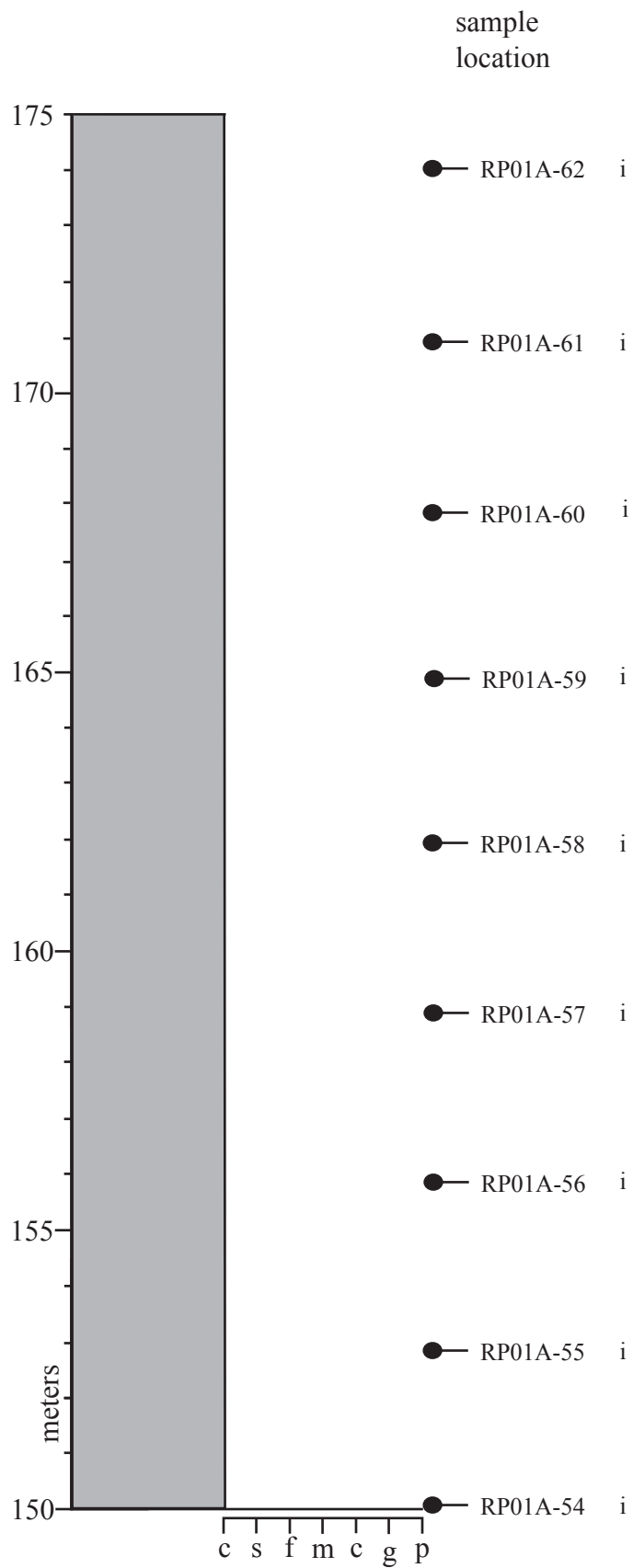
Red Pine Shale  
Hades Section A  
(continued)





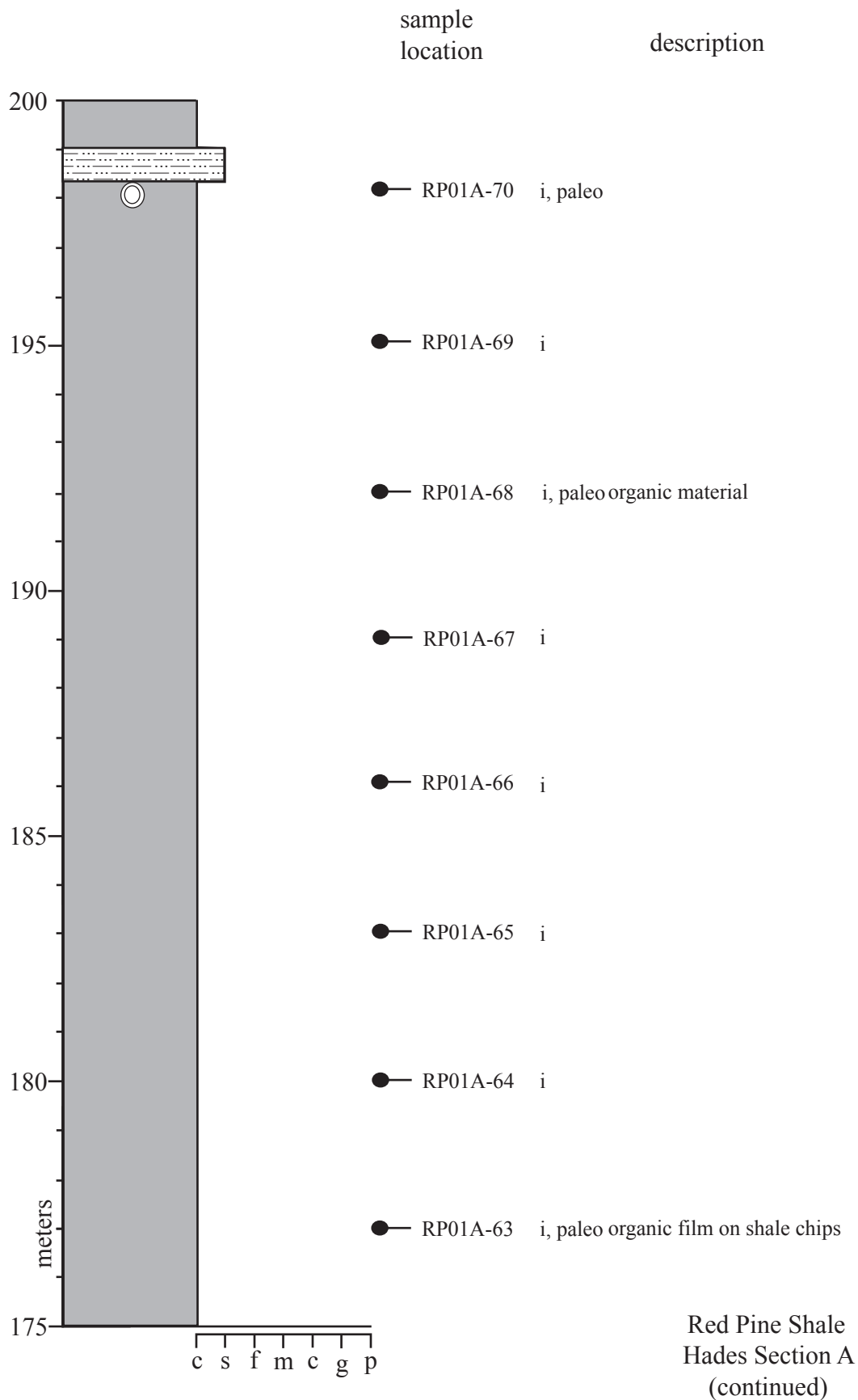


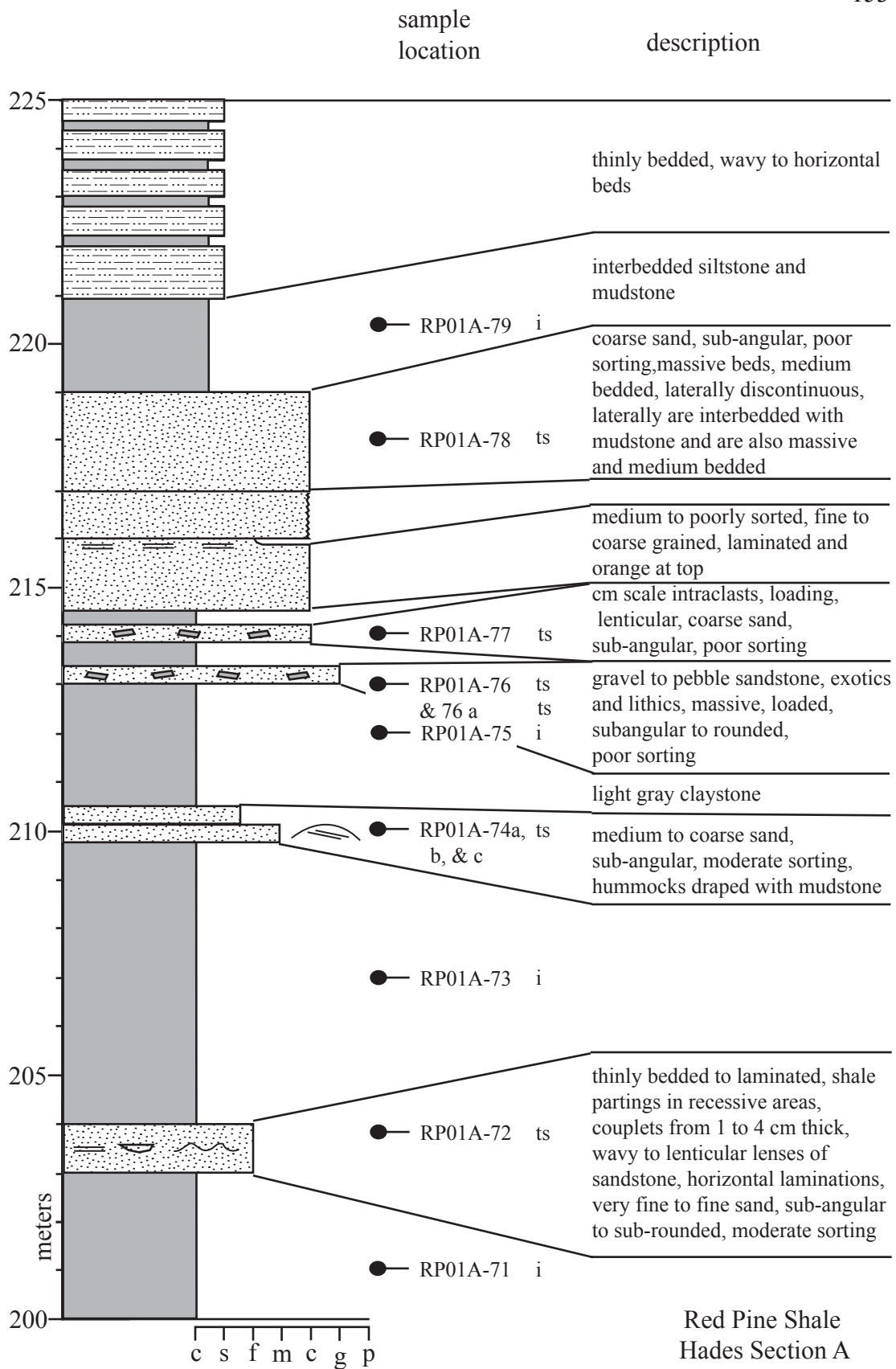




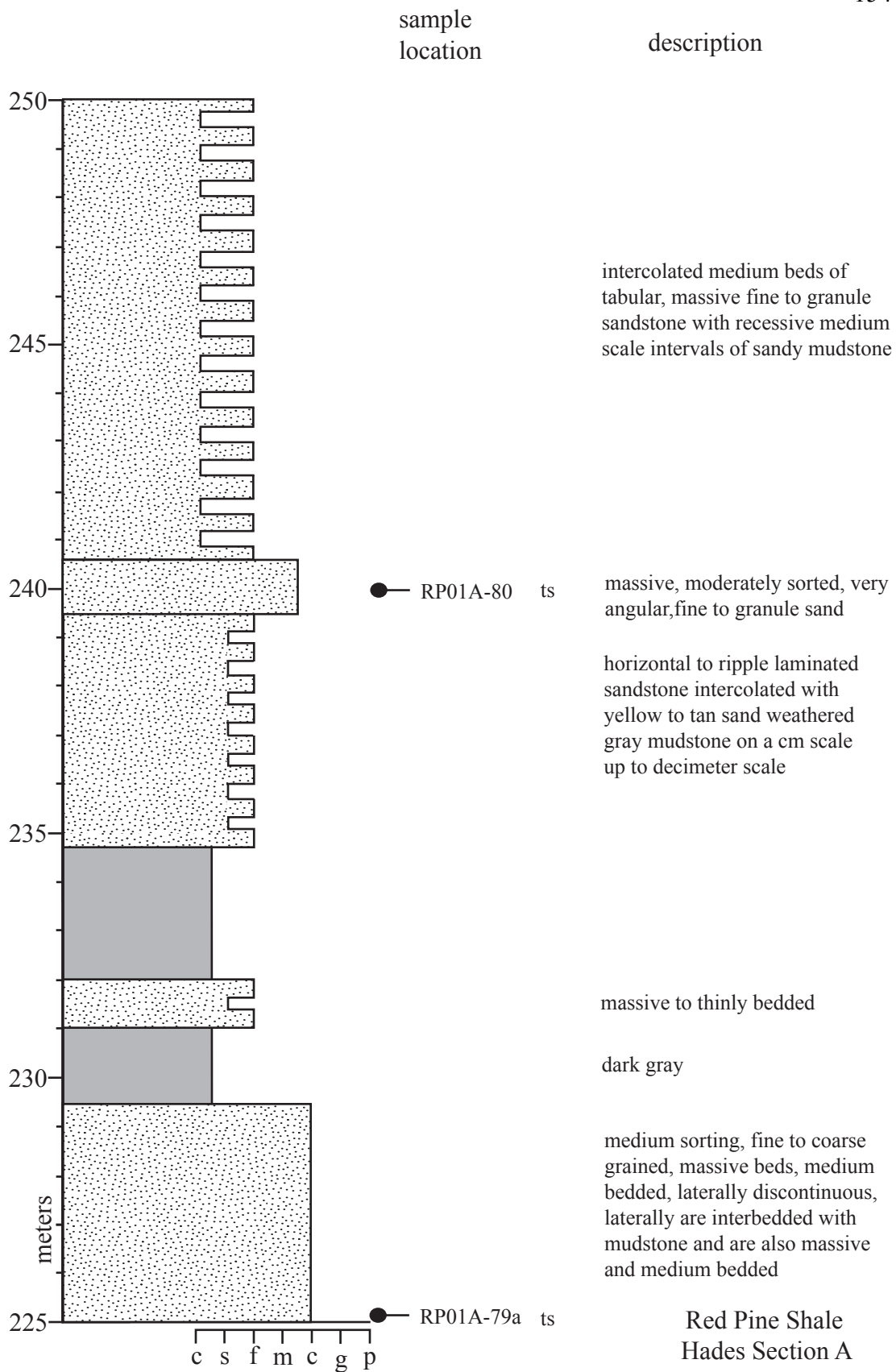
description

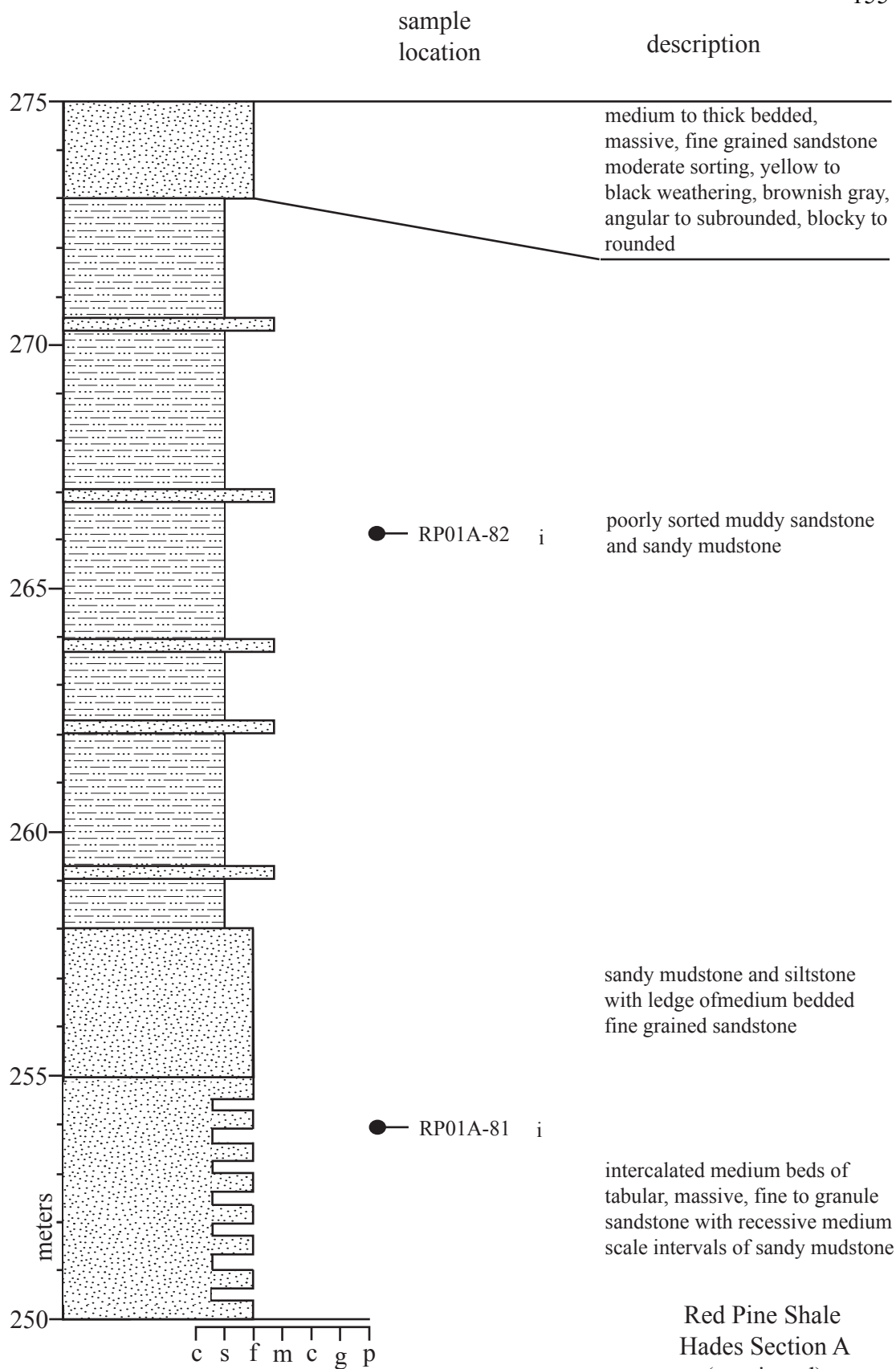
Red Pine Shale  
Hades Section A  
(continued)

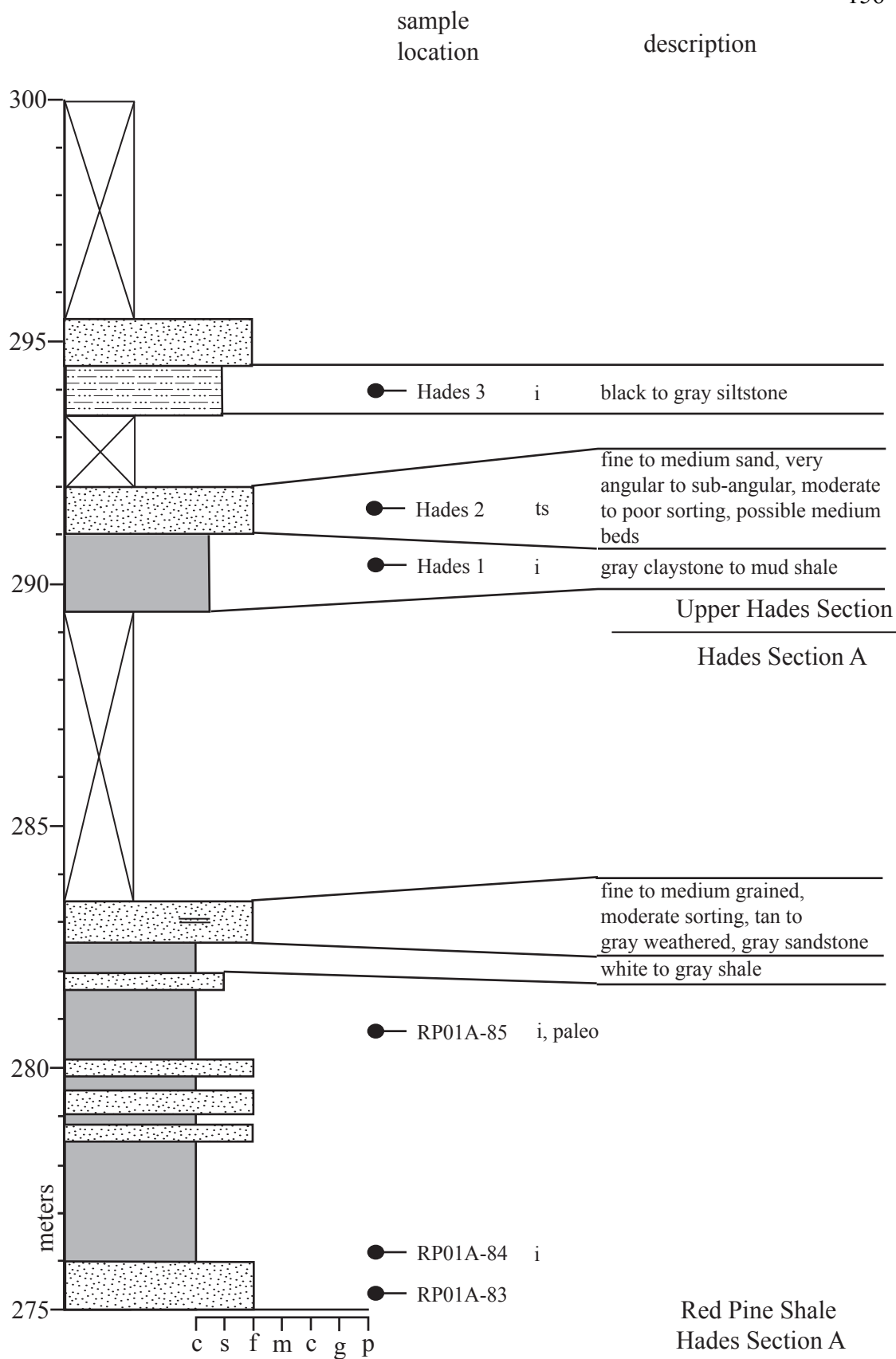




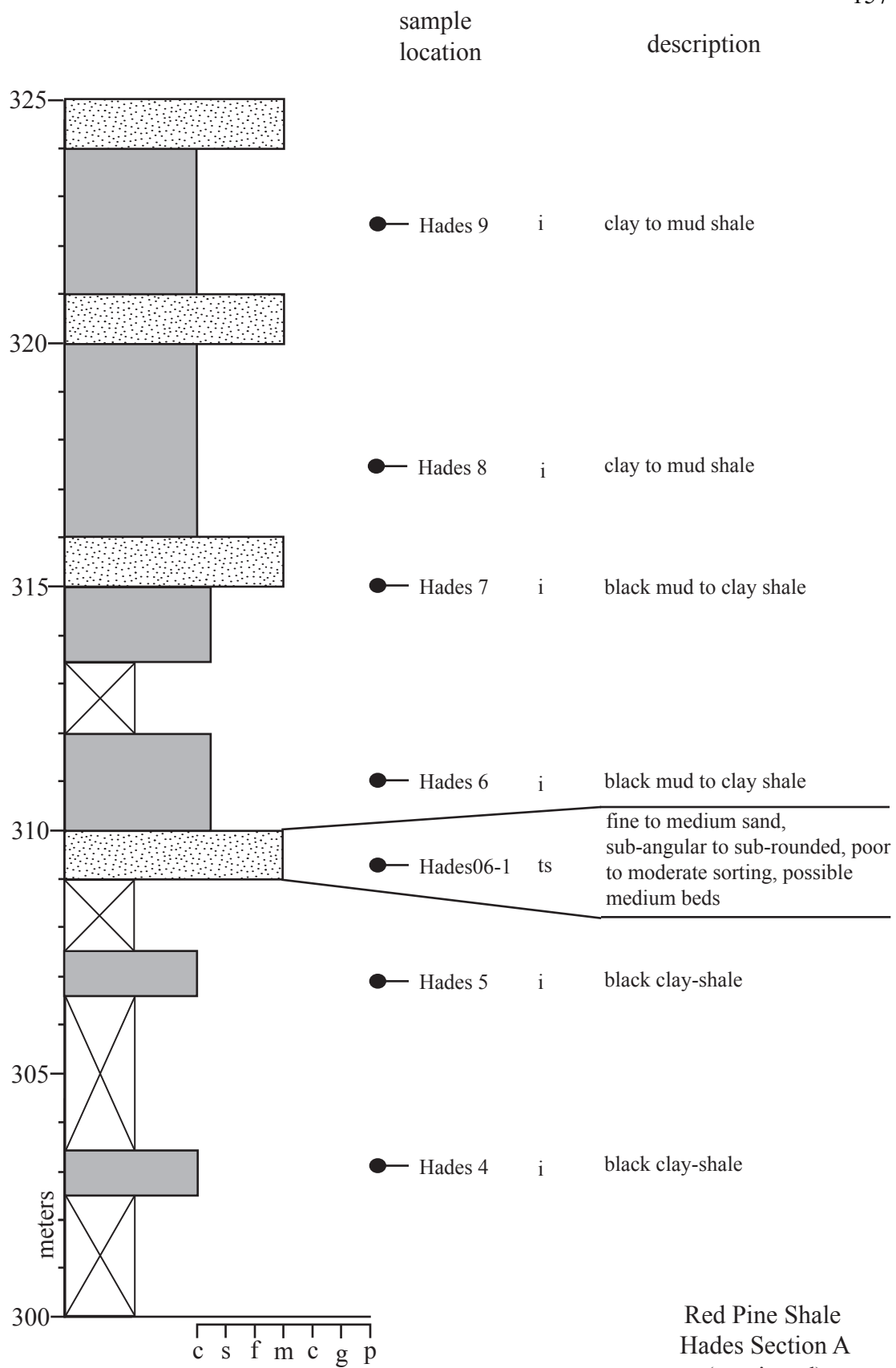
Red Pine Shale  
Hades Section A  
(continued)



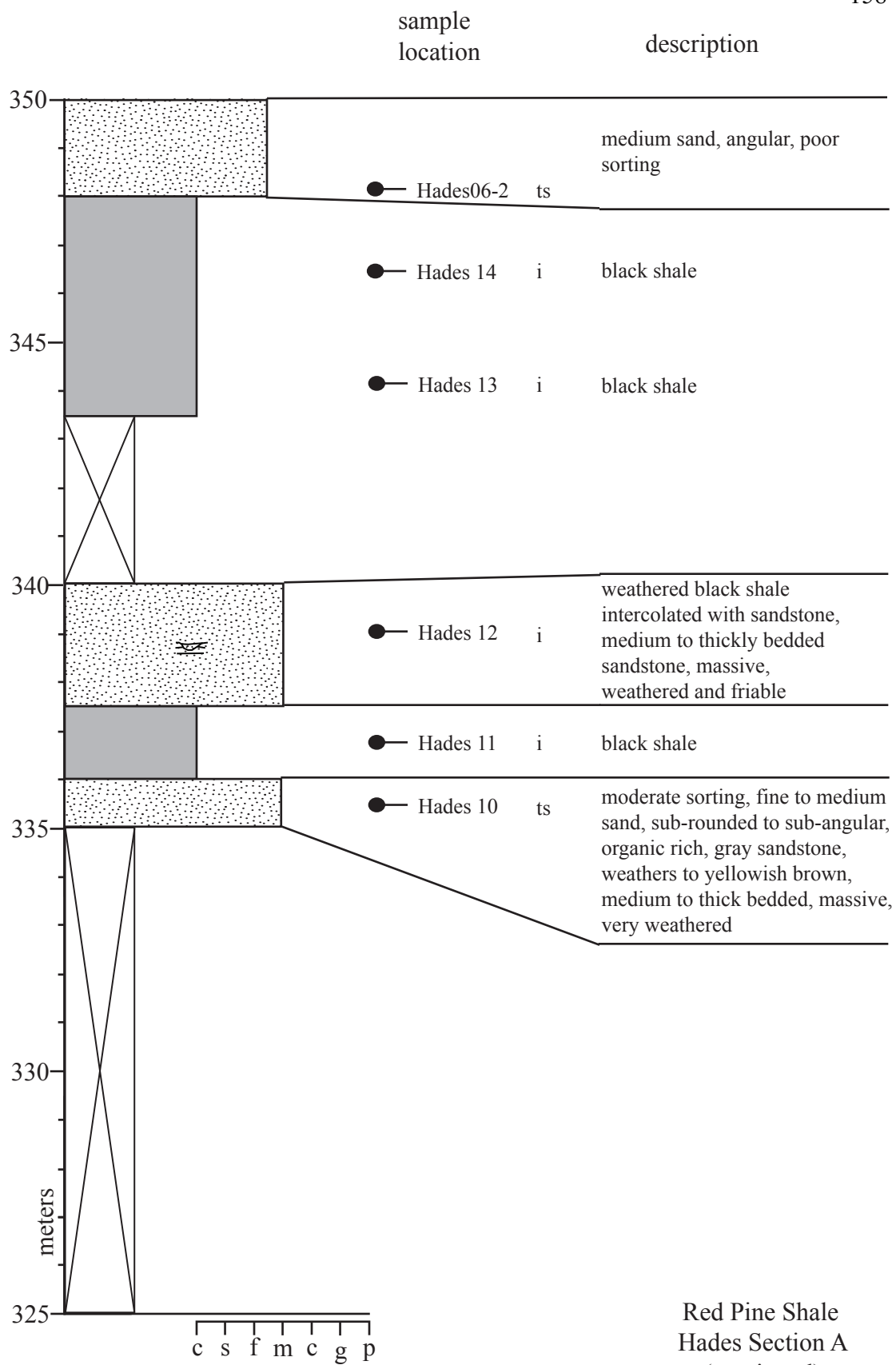




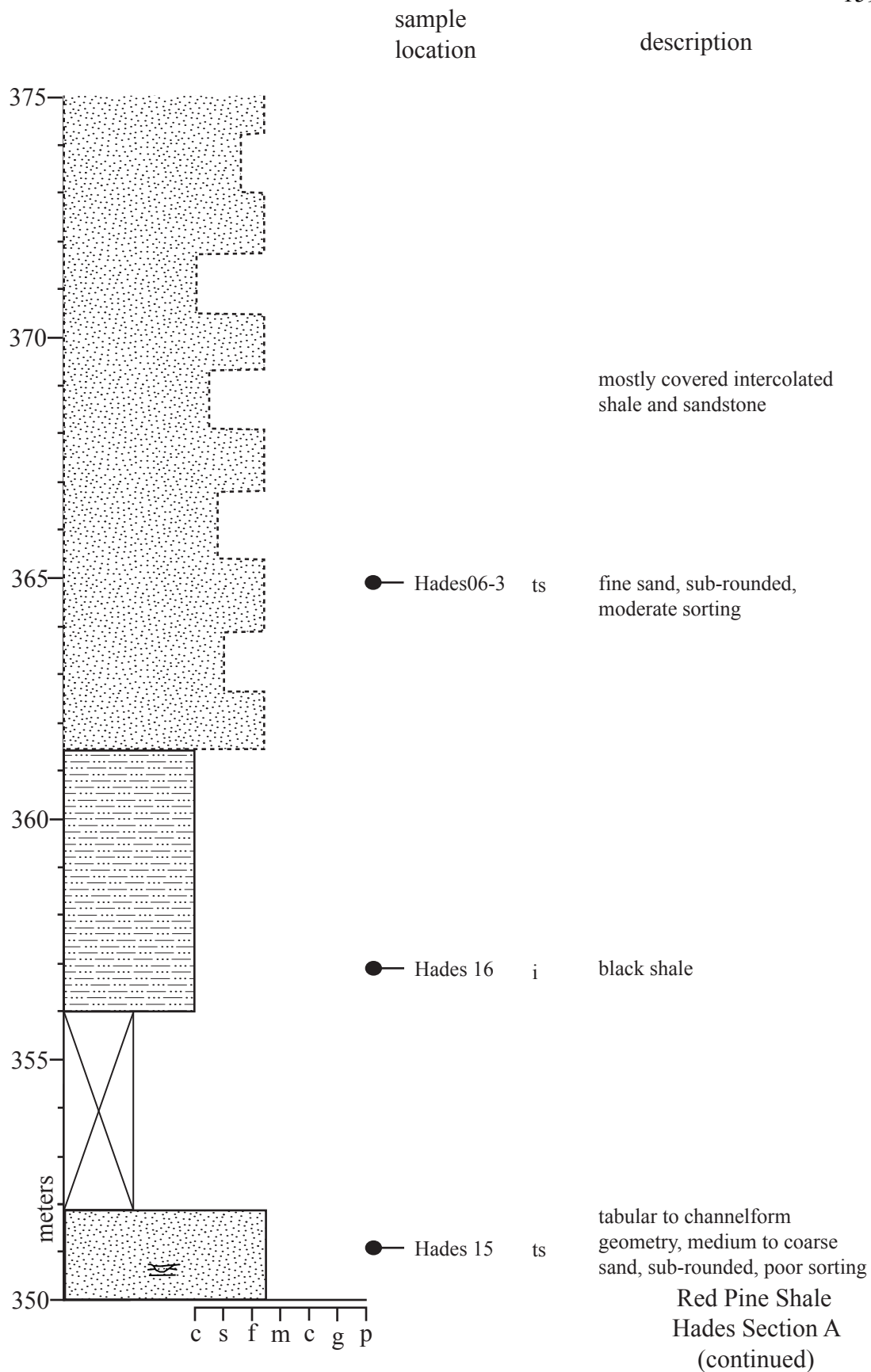
Red Pine Shale  
Hades Section A  
(continued)

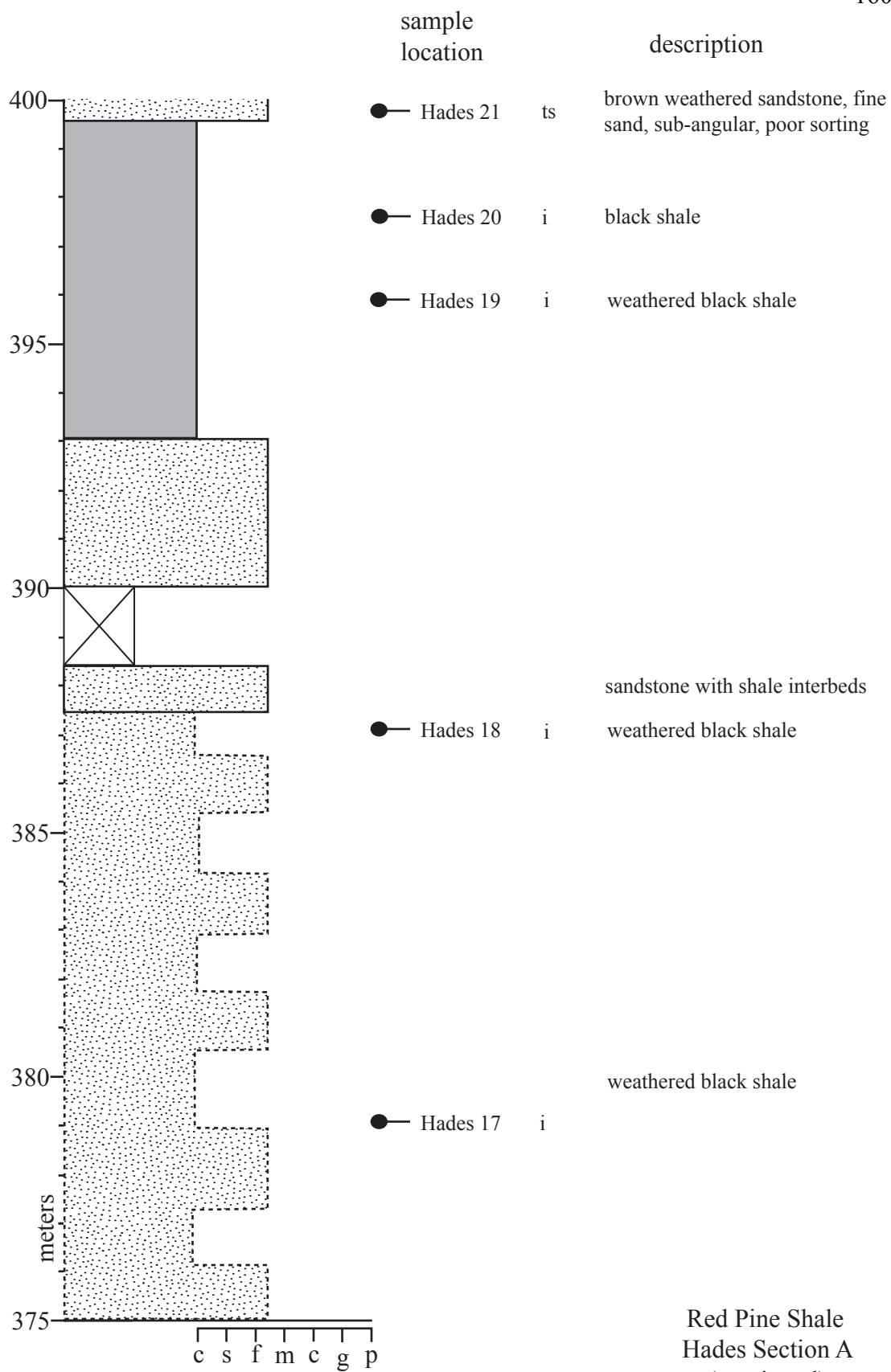


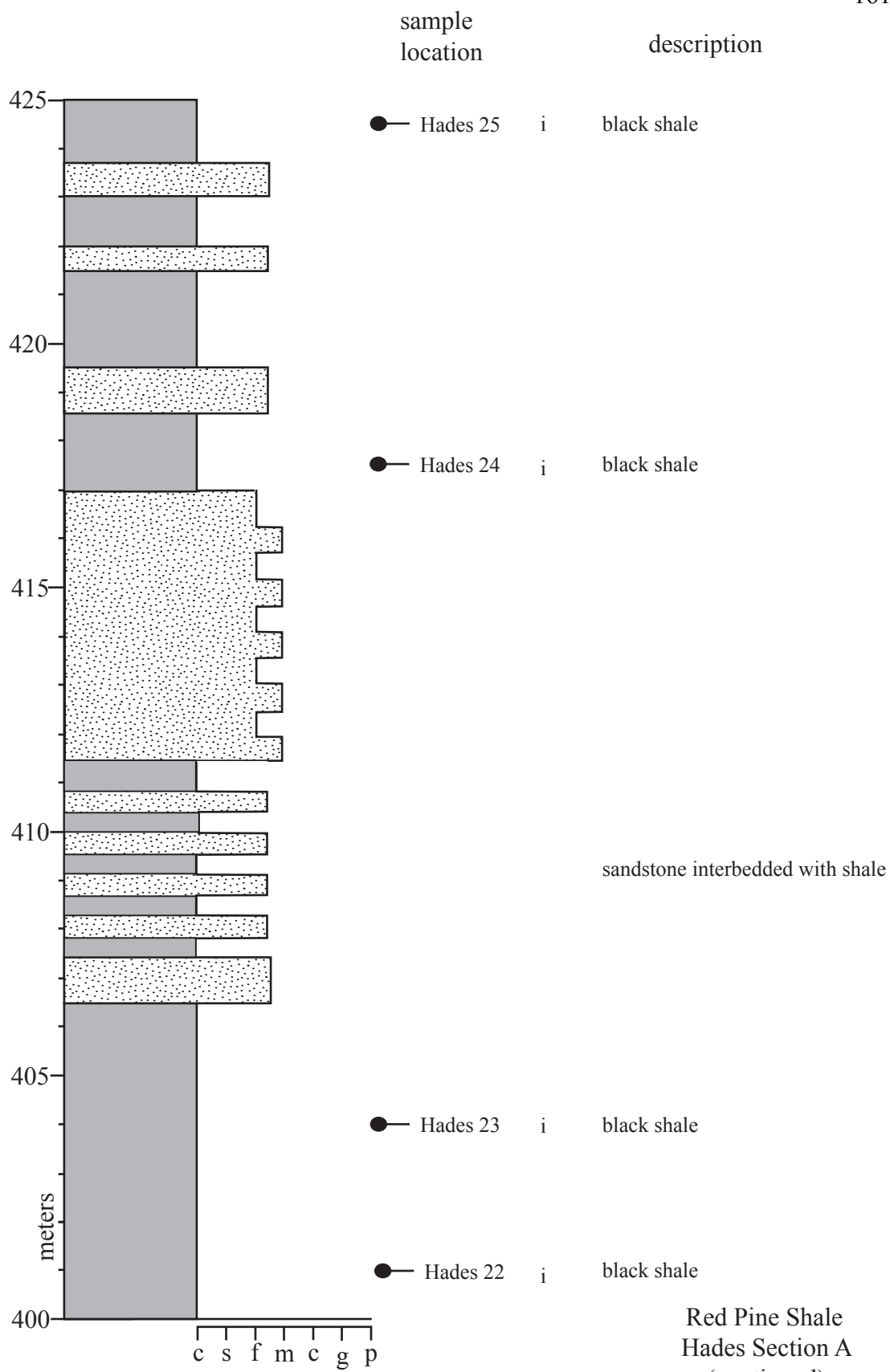


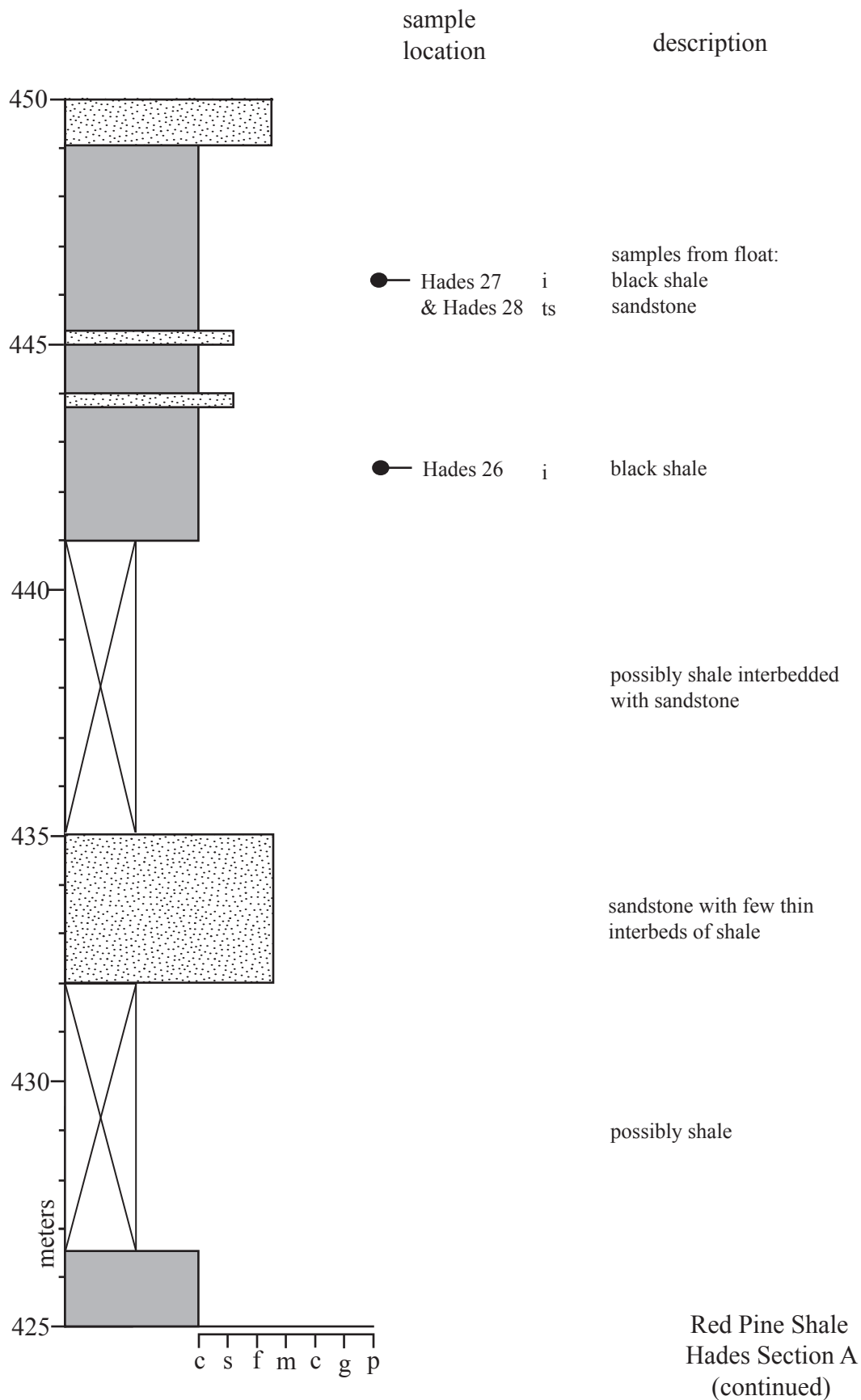


Red Pine Shale  
Hades Section A  
(continued)



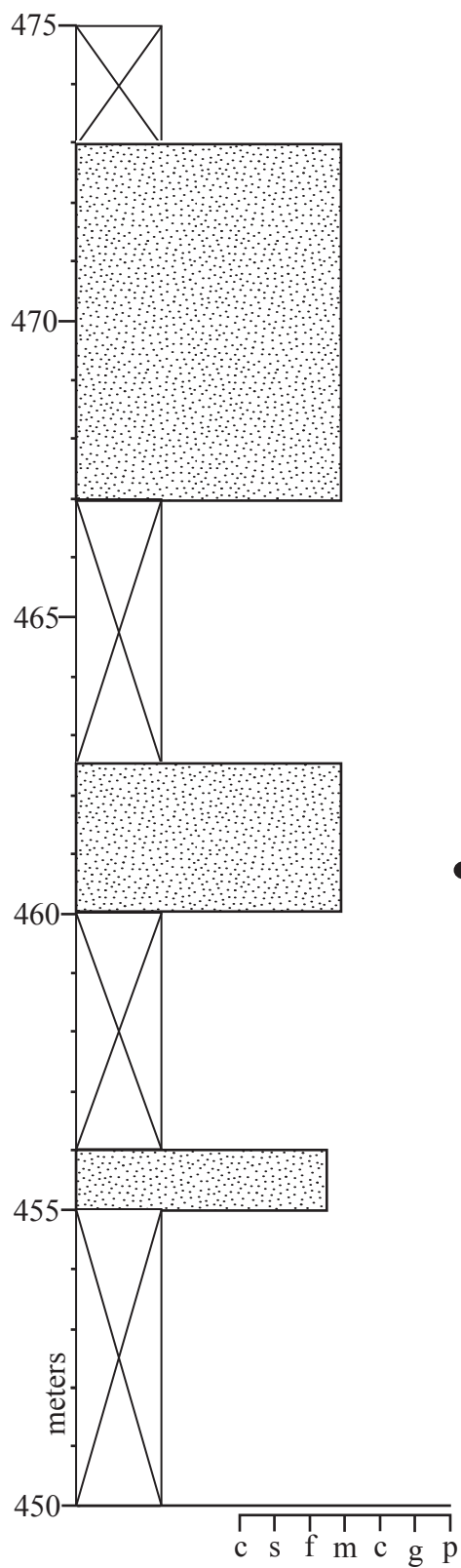






sample  
location

description

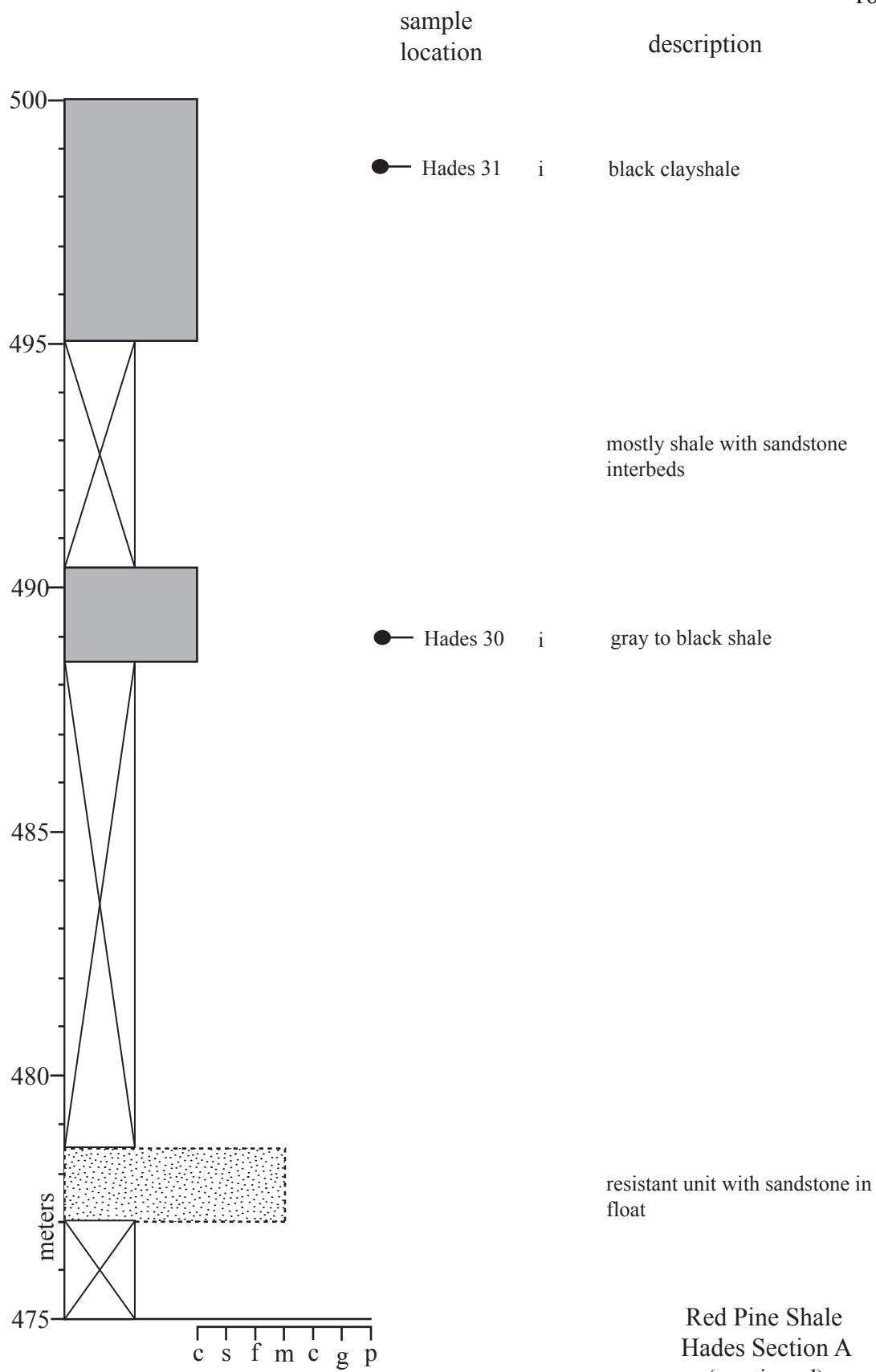


possible shale interbeds

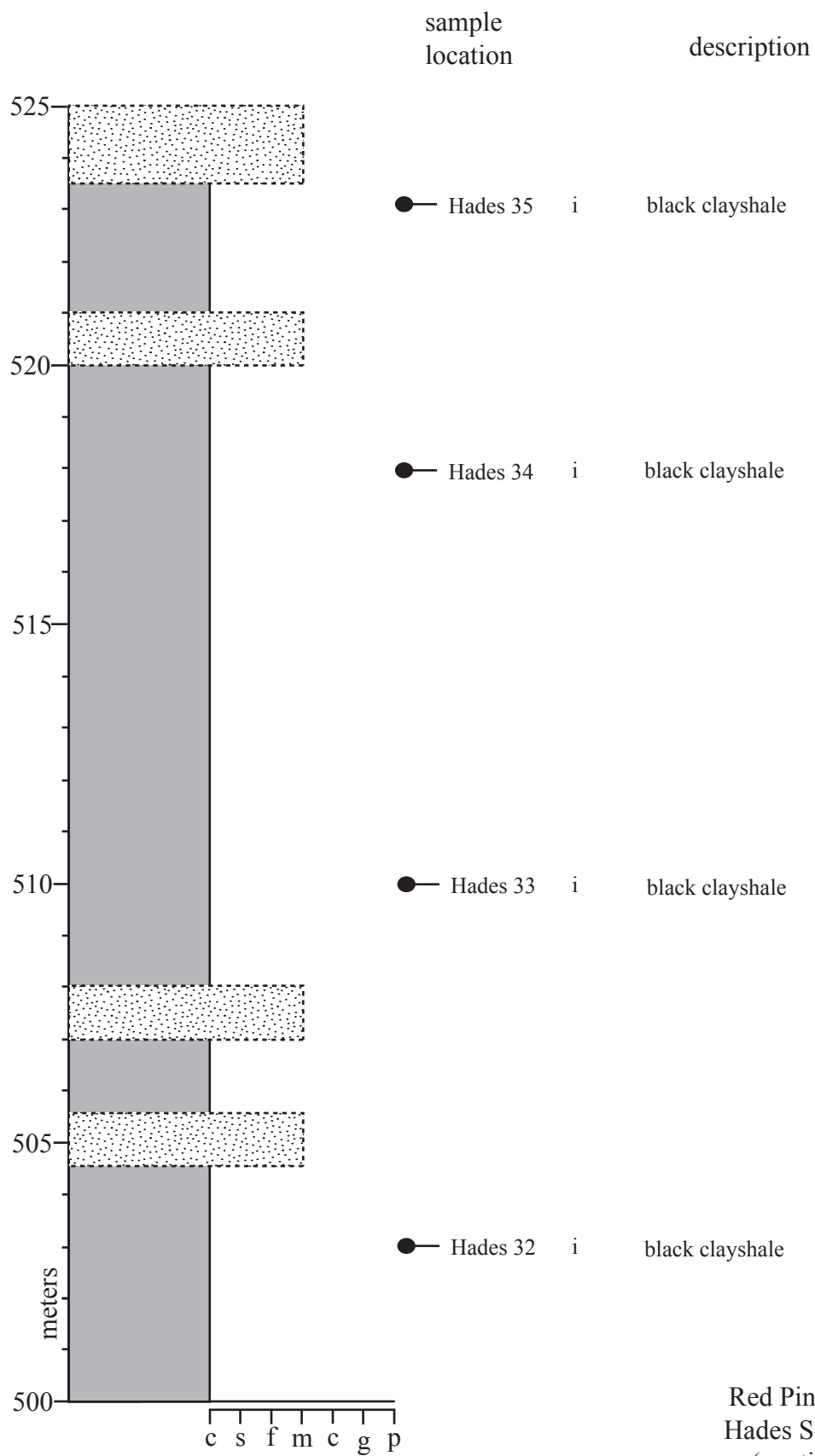
● Hades 29 ts

very weathered sandstone  
outcrop, gray, fine to coarse,  
angular to round with finer gray  
ground mass, poorly sorted

Red Pine Shale  
Hades Section A  
(continued)

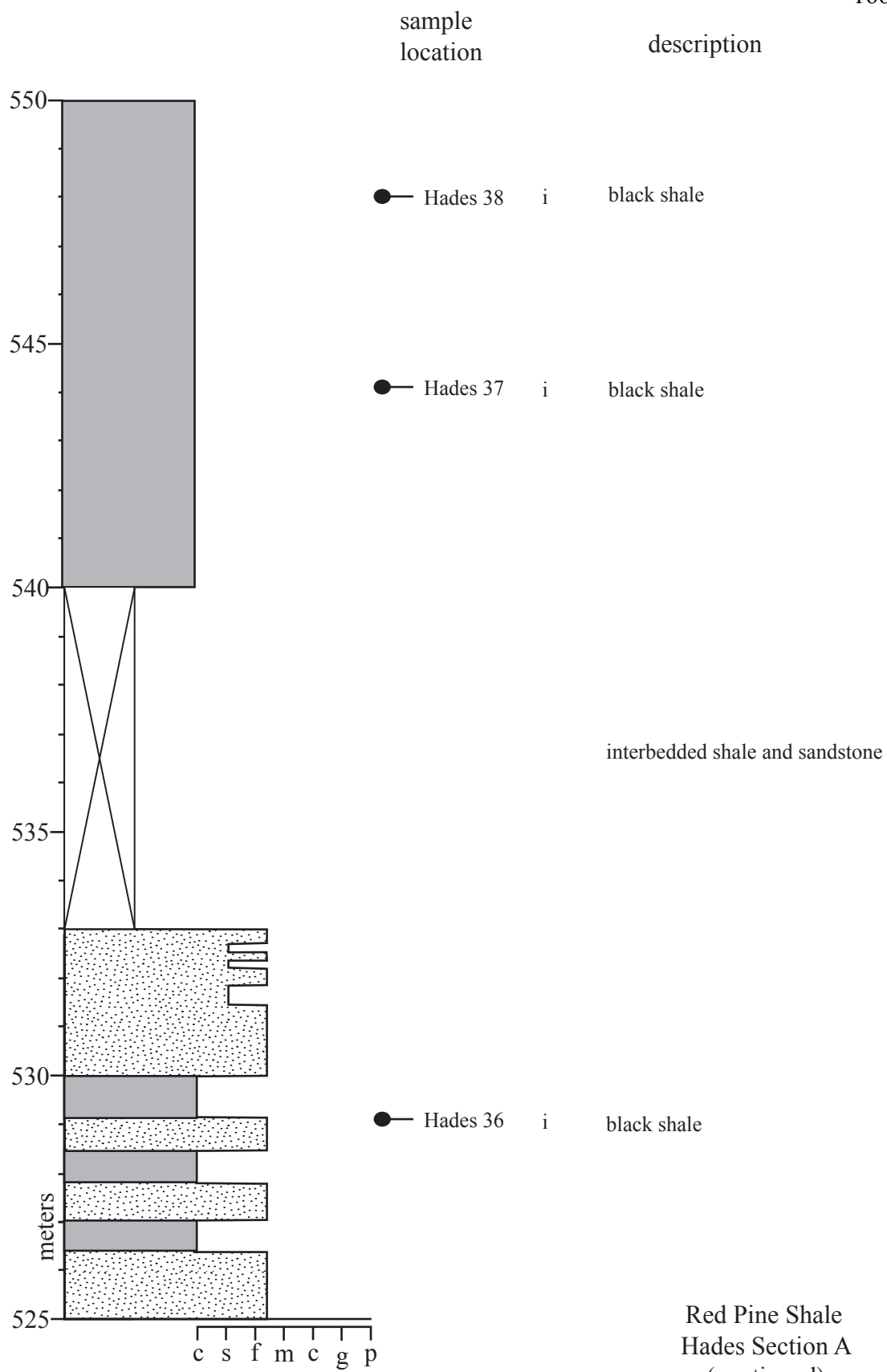


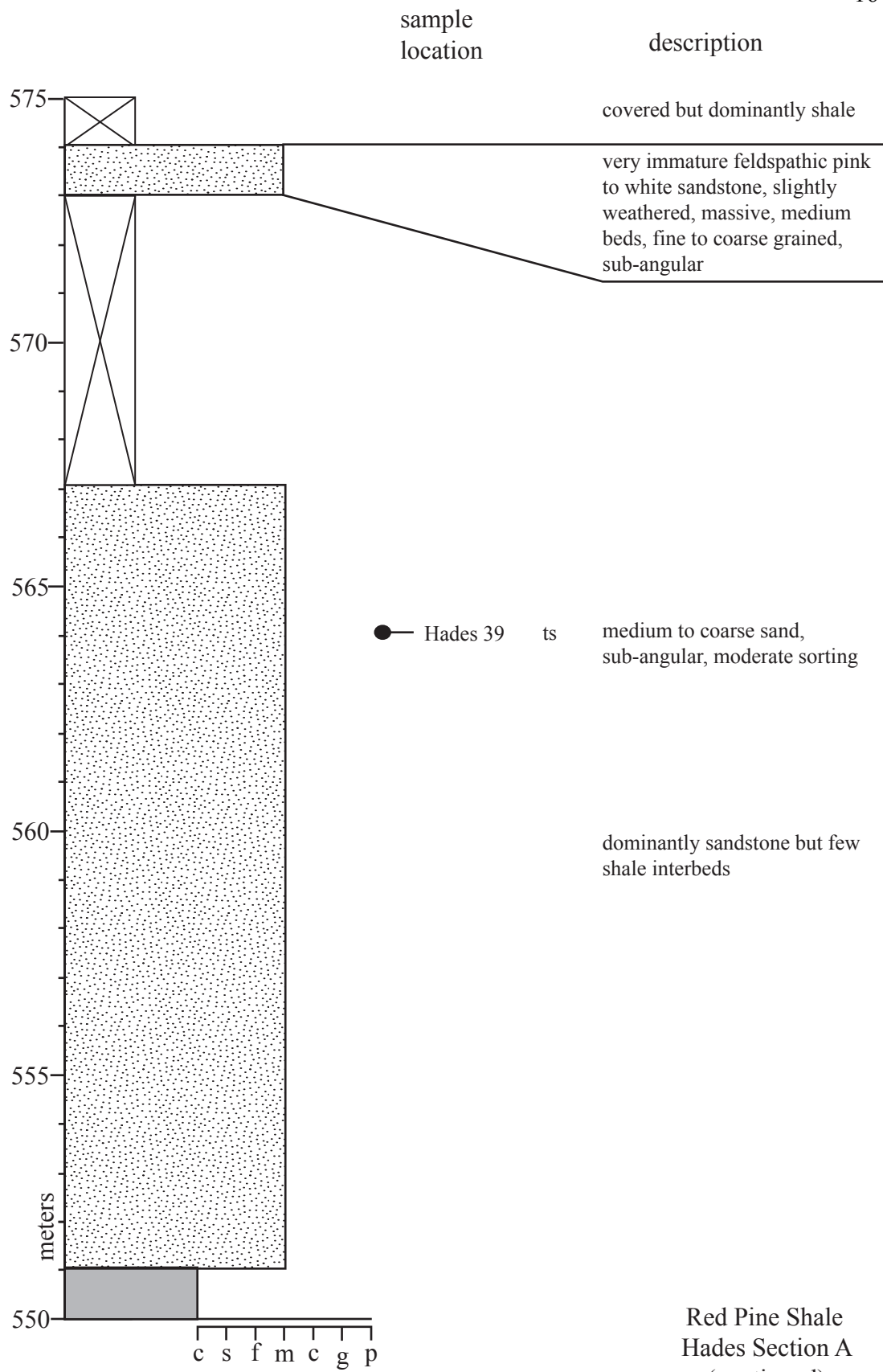
Red Pine Shale  
Hades Section A  
(continued)



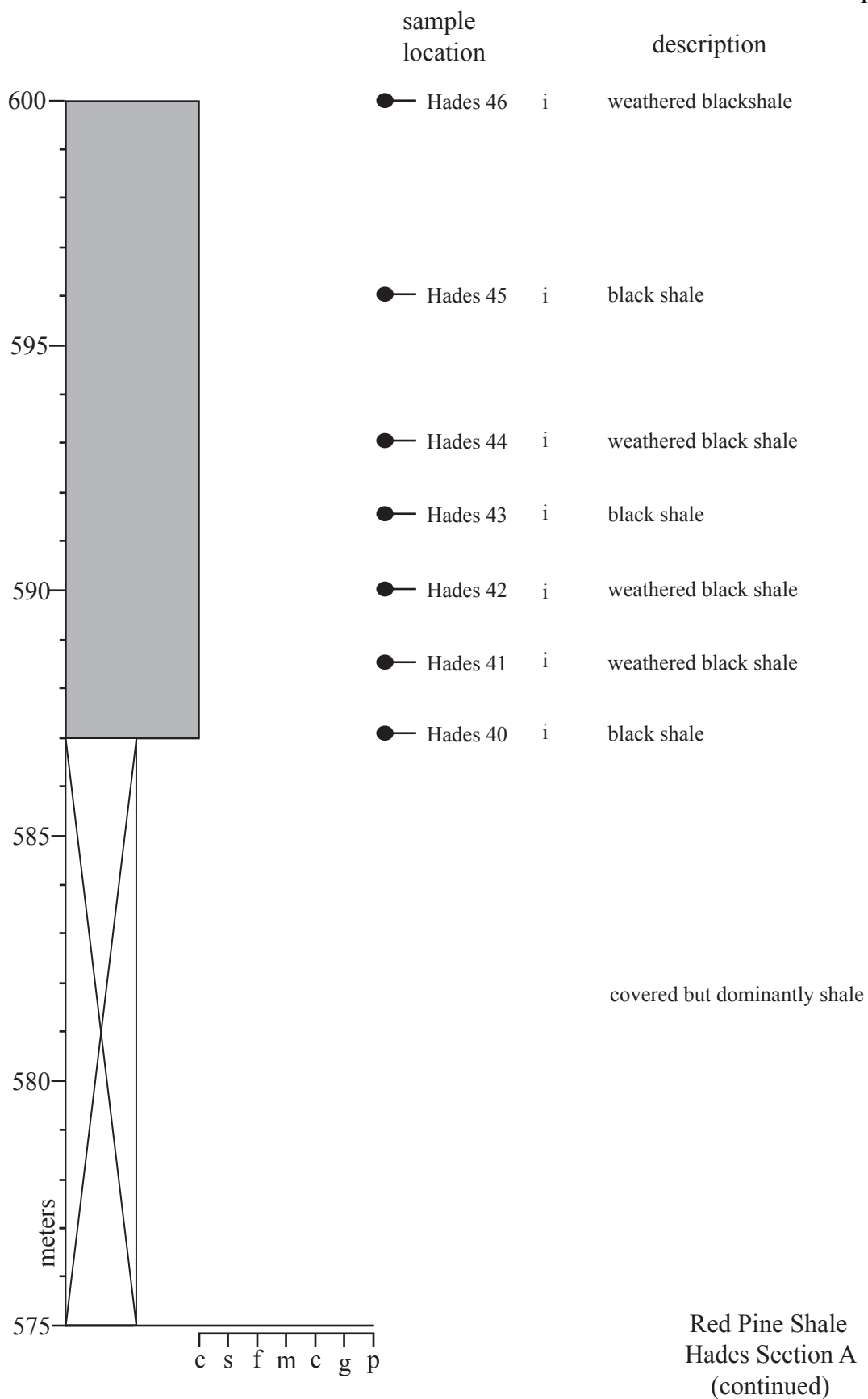
Red Pine Shale  
Hades Section A  
(continued)

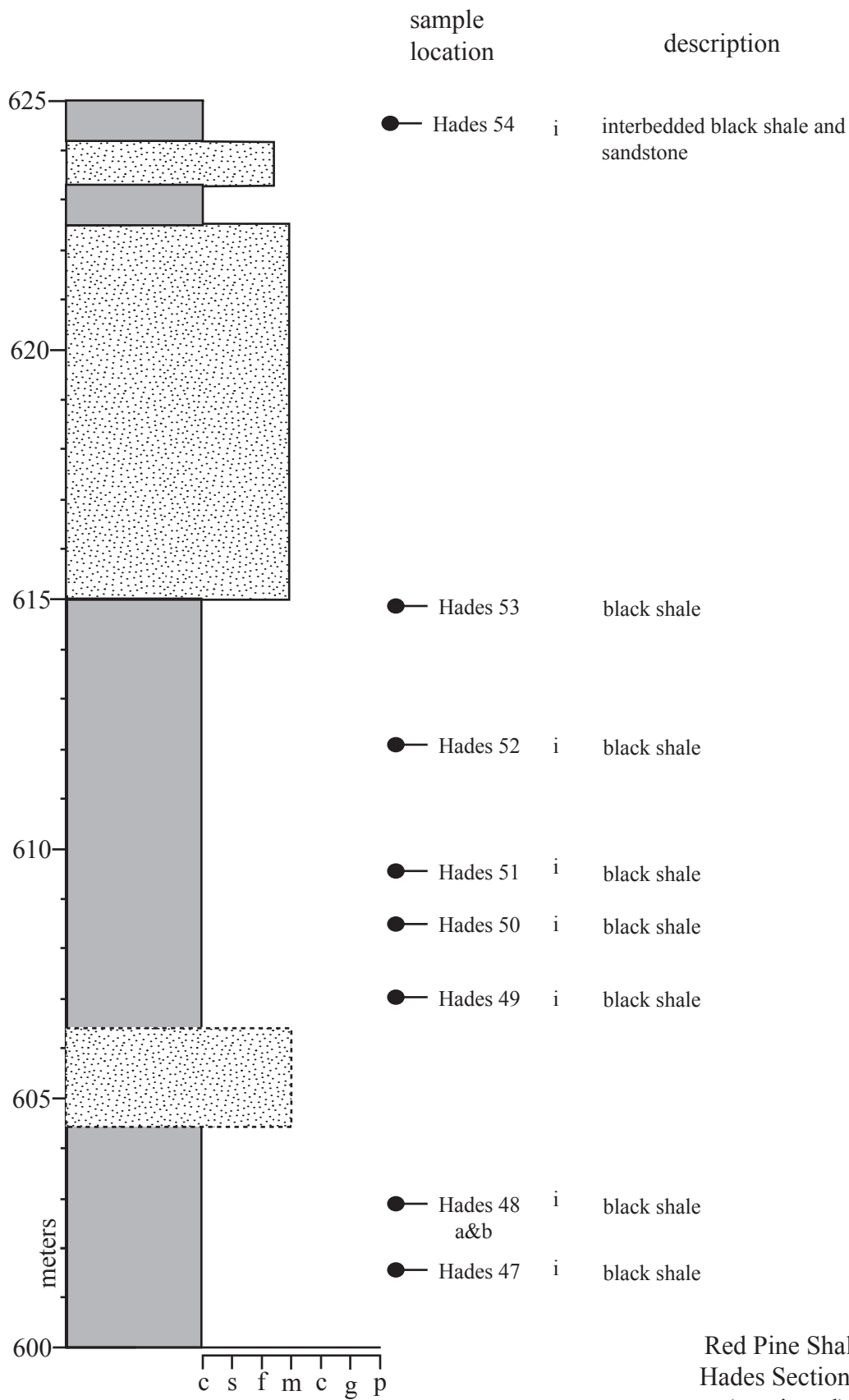




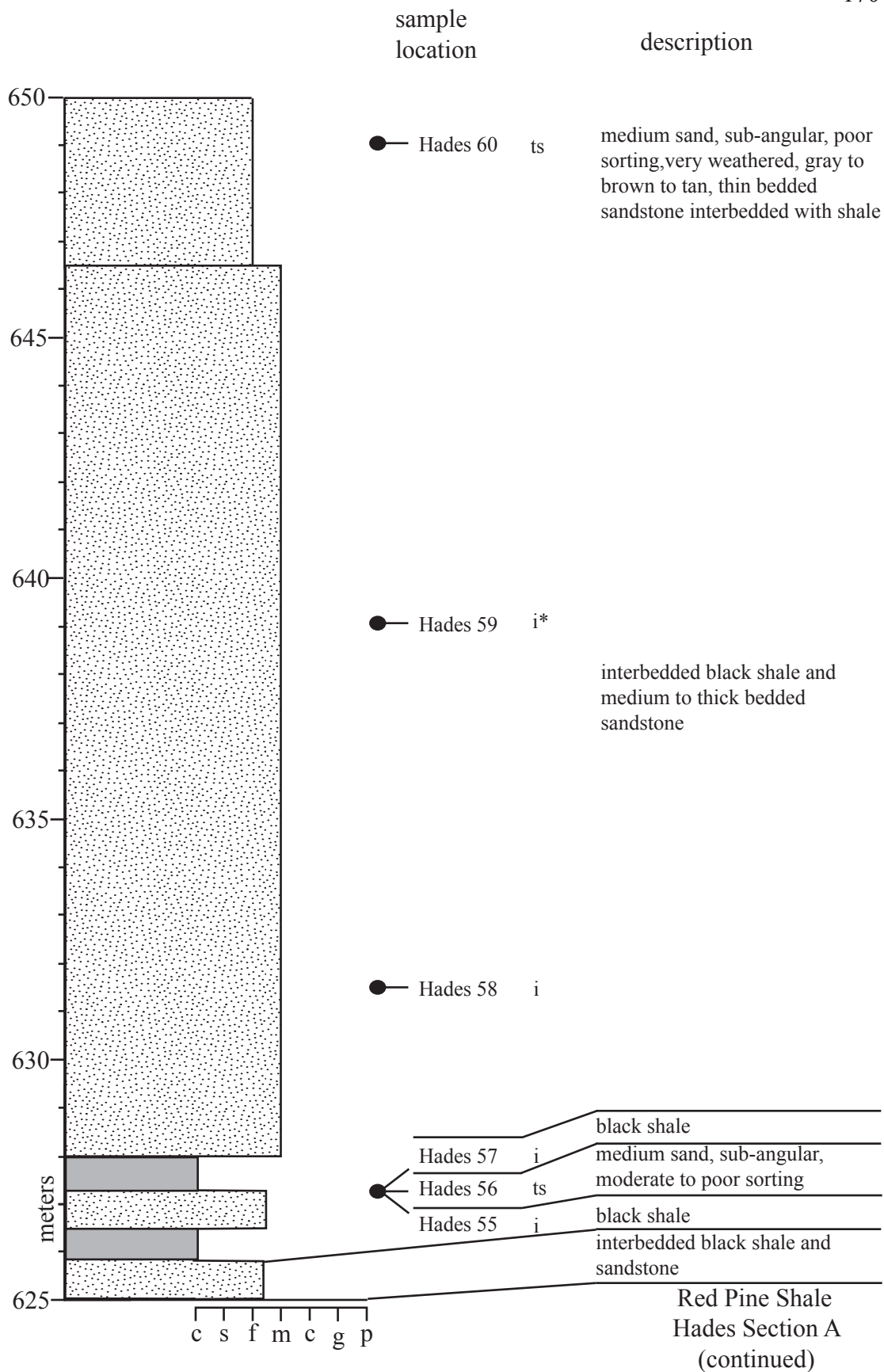


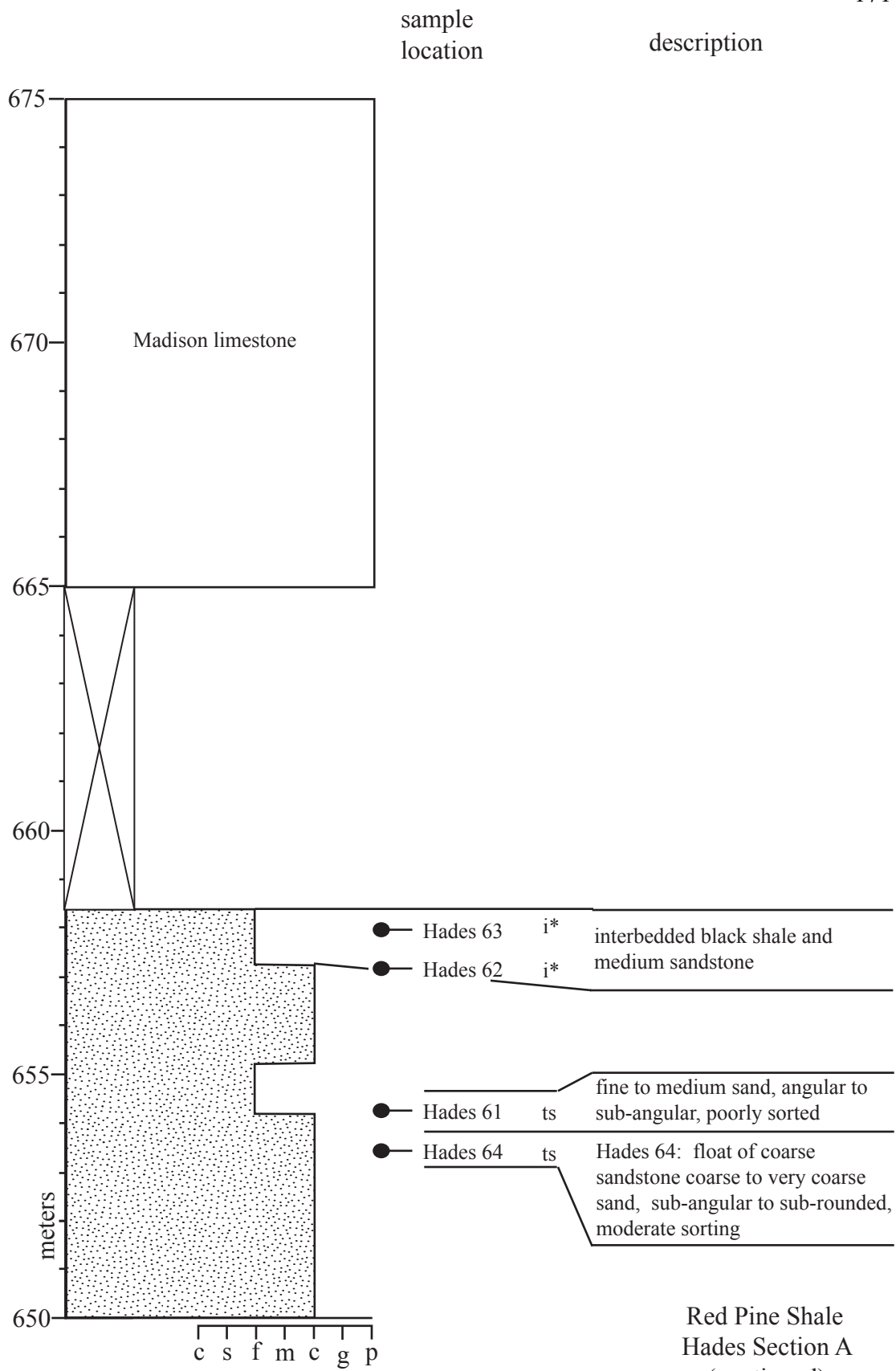
Red Pine Shale  
Hades Section A  
(continued)



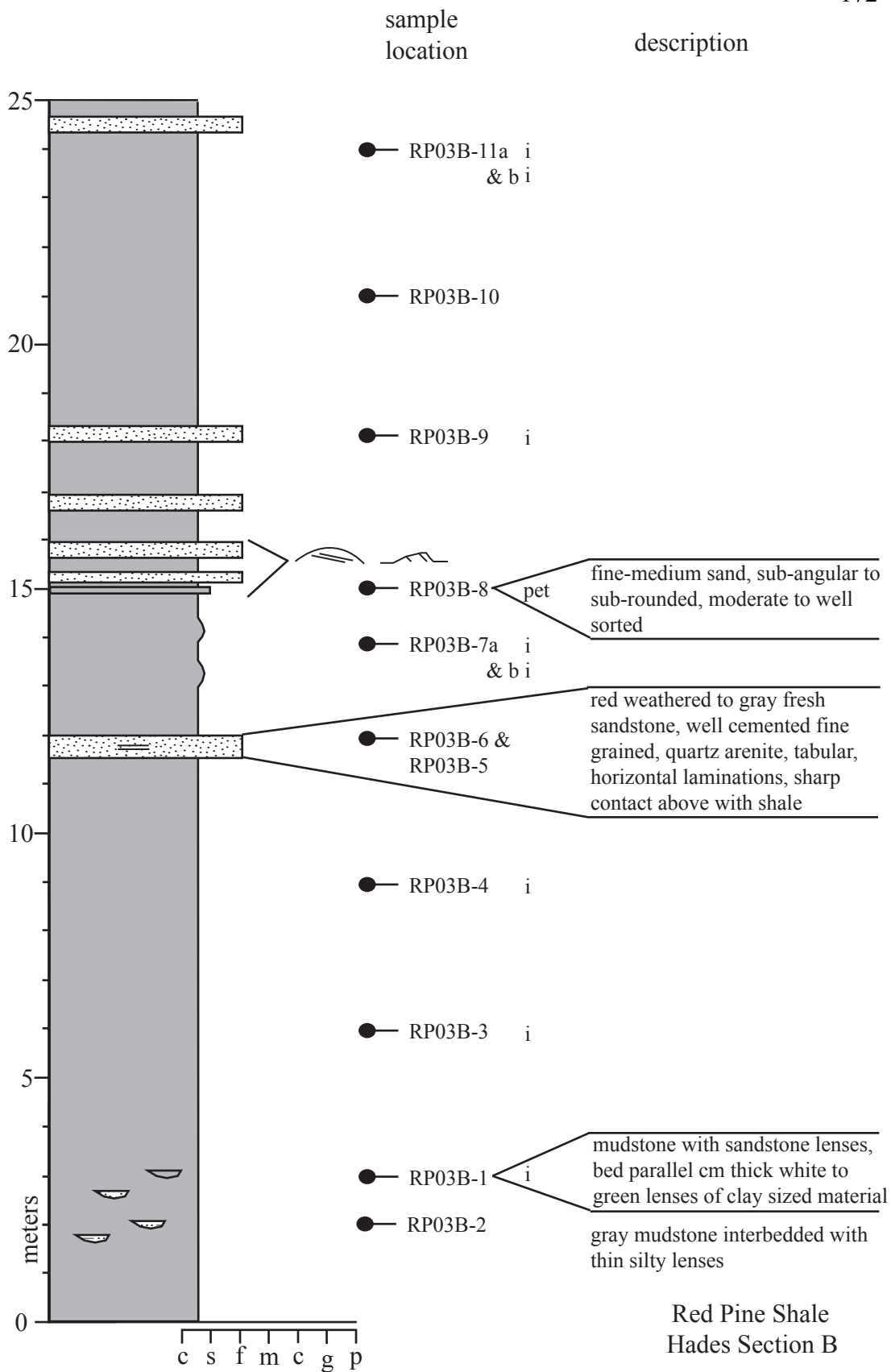


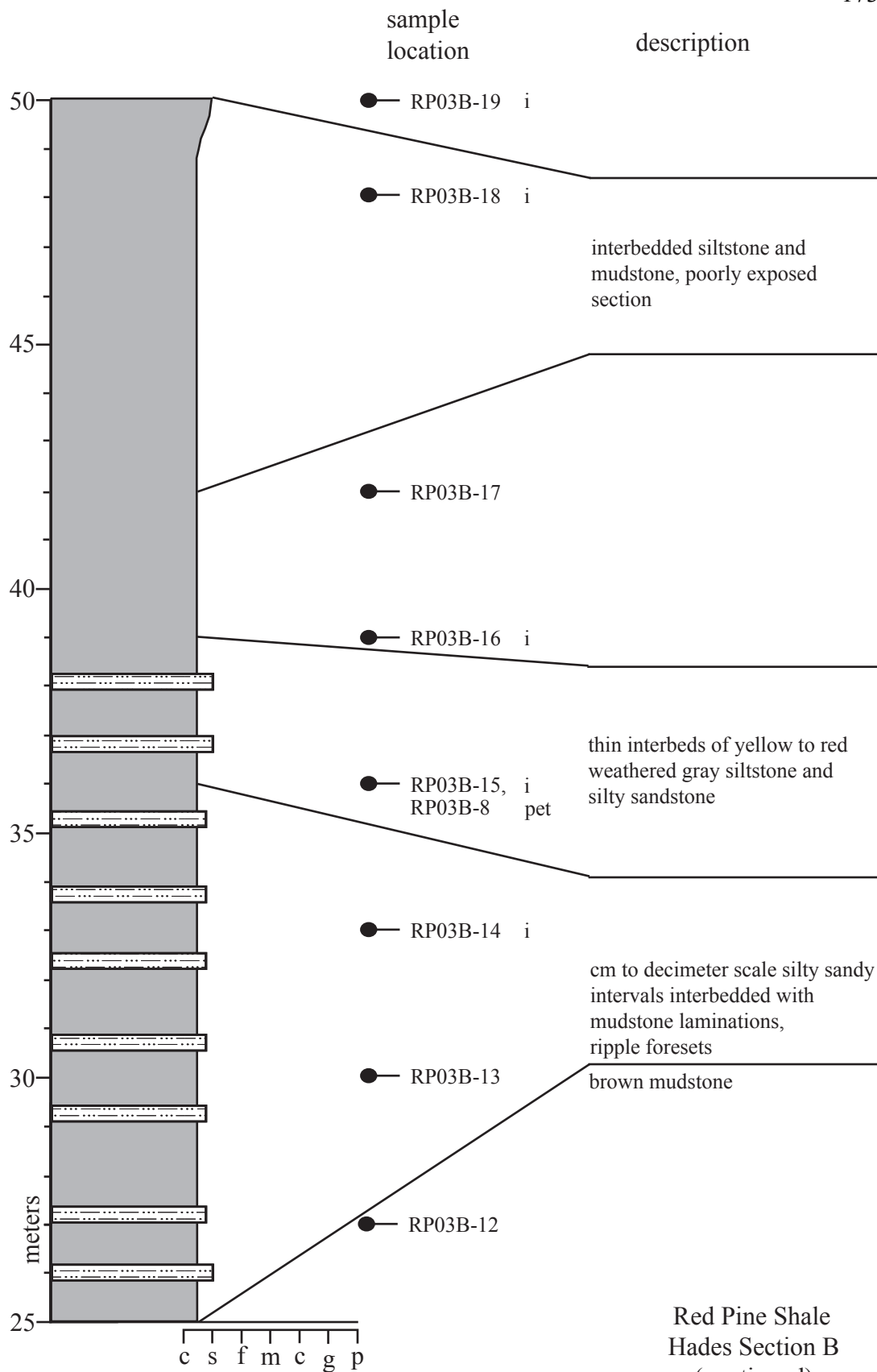
Red Pine Shale  
Hades Section A  
(continued)





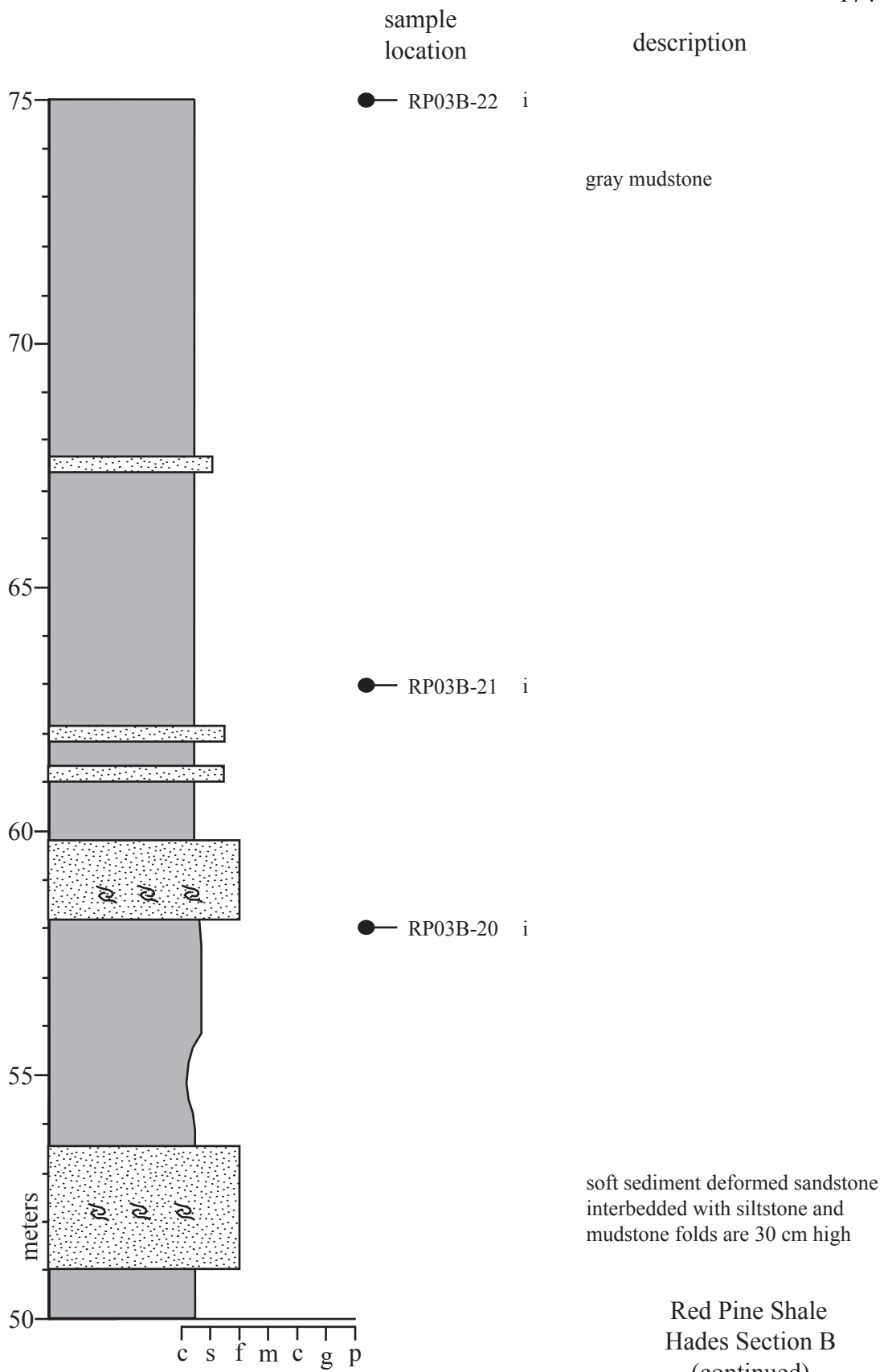
Red Pine Shale  
Hades Section A  
(continued)

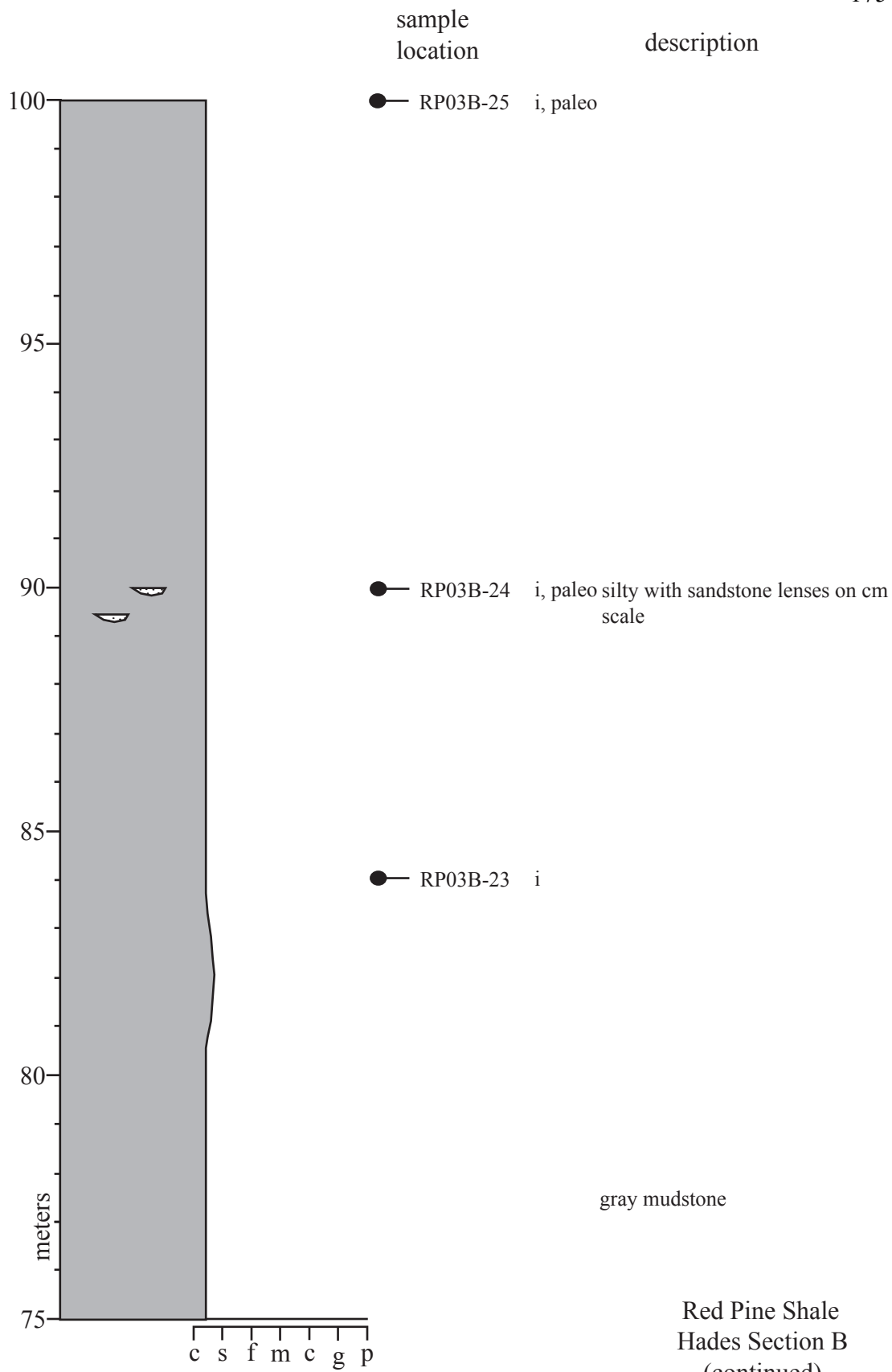




Red Pine Shale  
Hades Section B  
(continued)

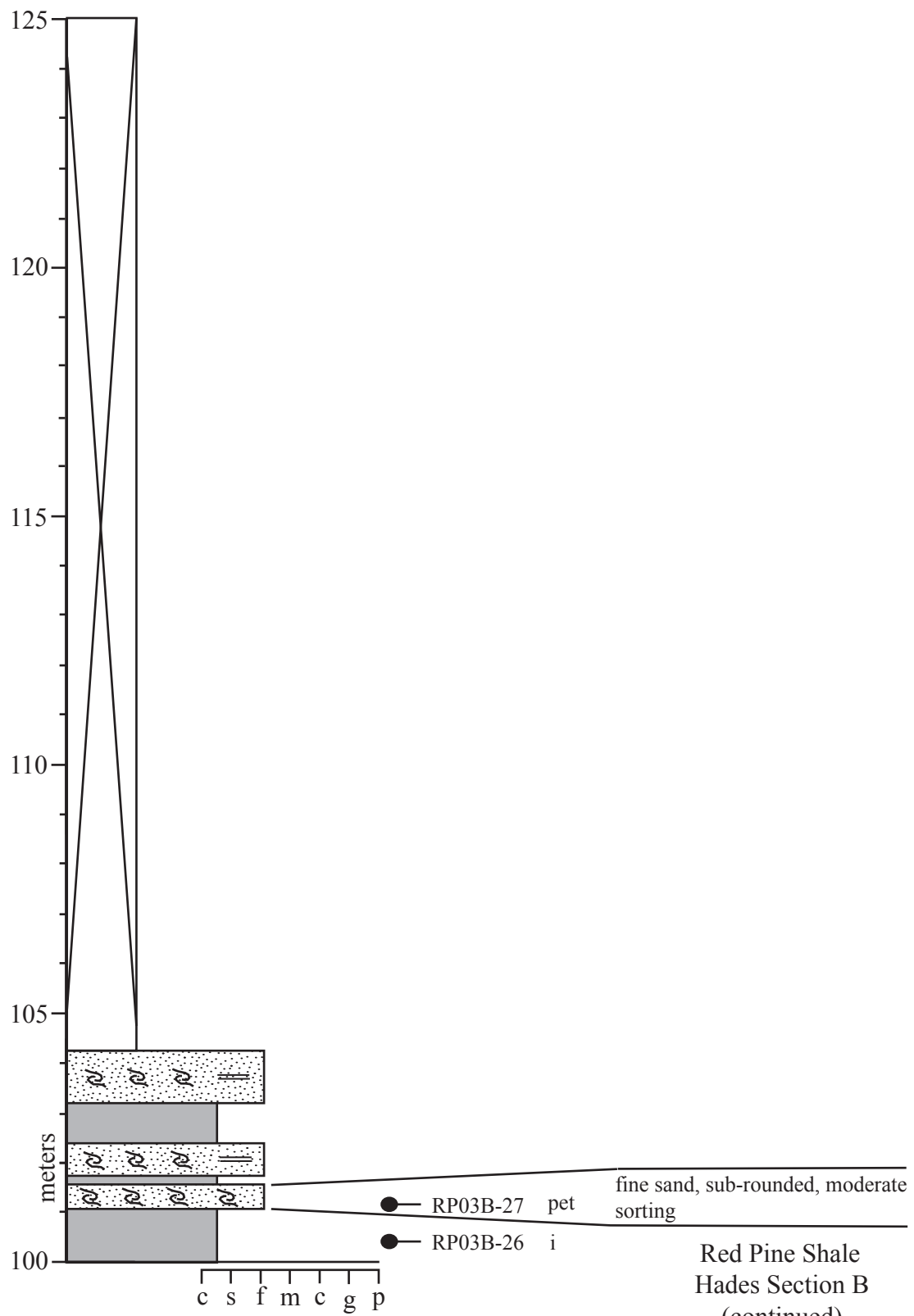




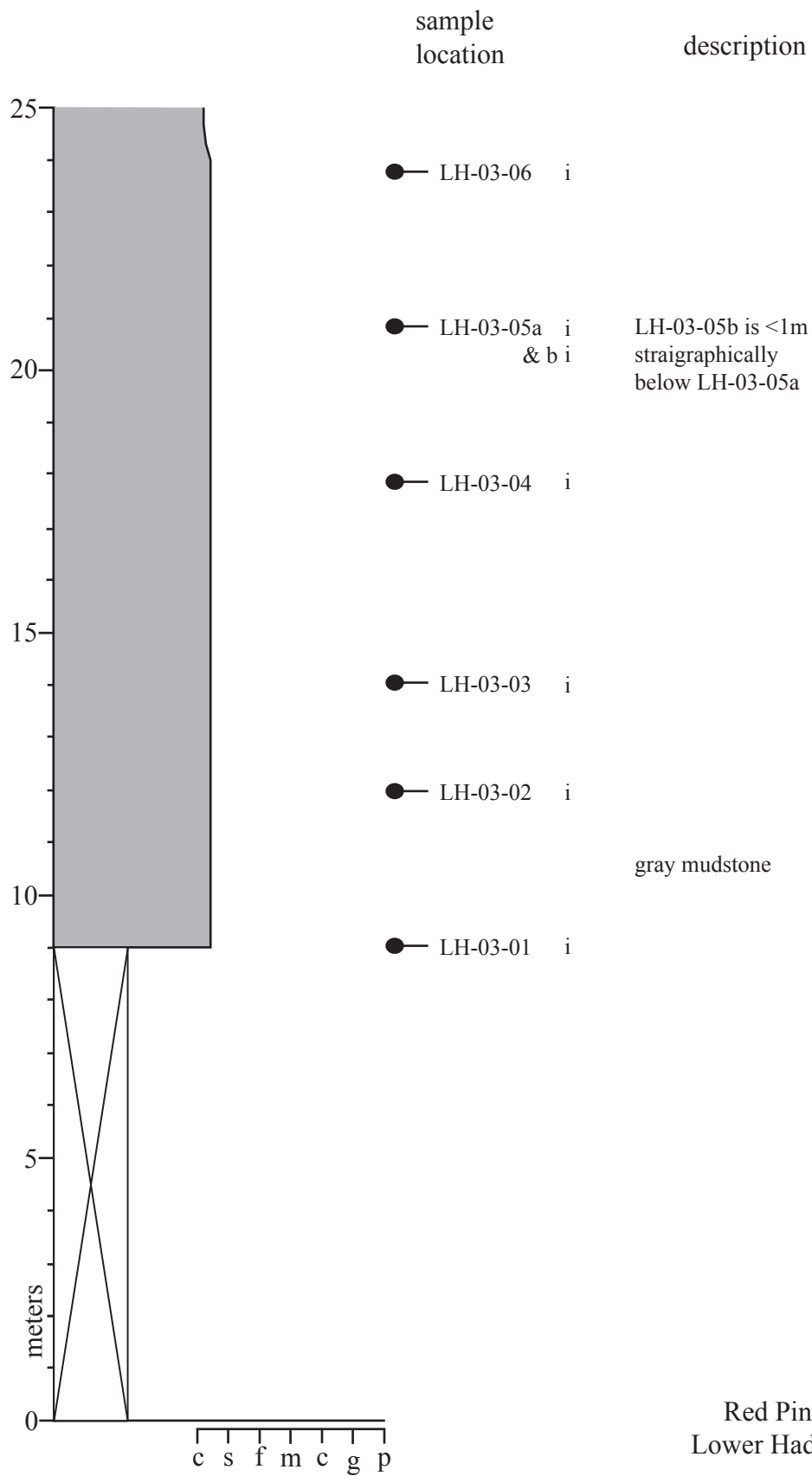


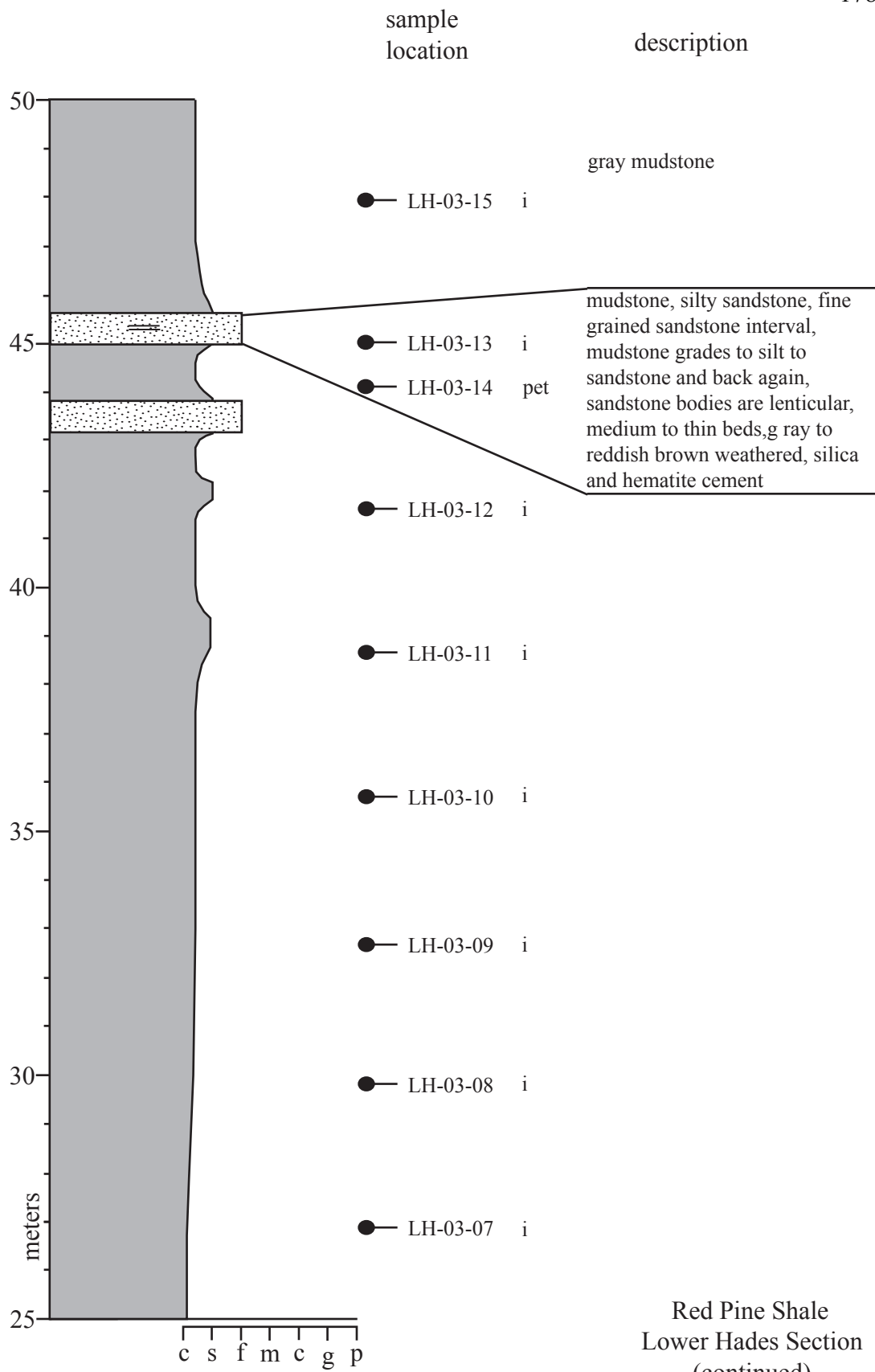
sample  
location

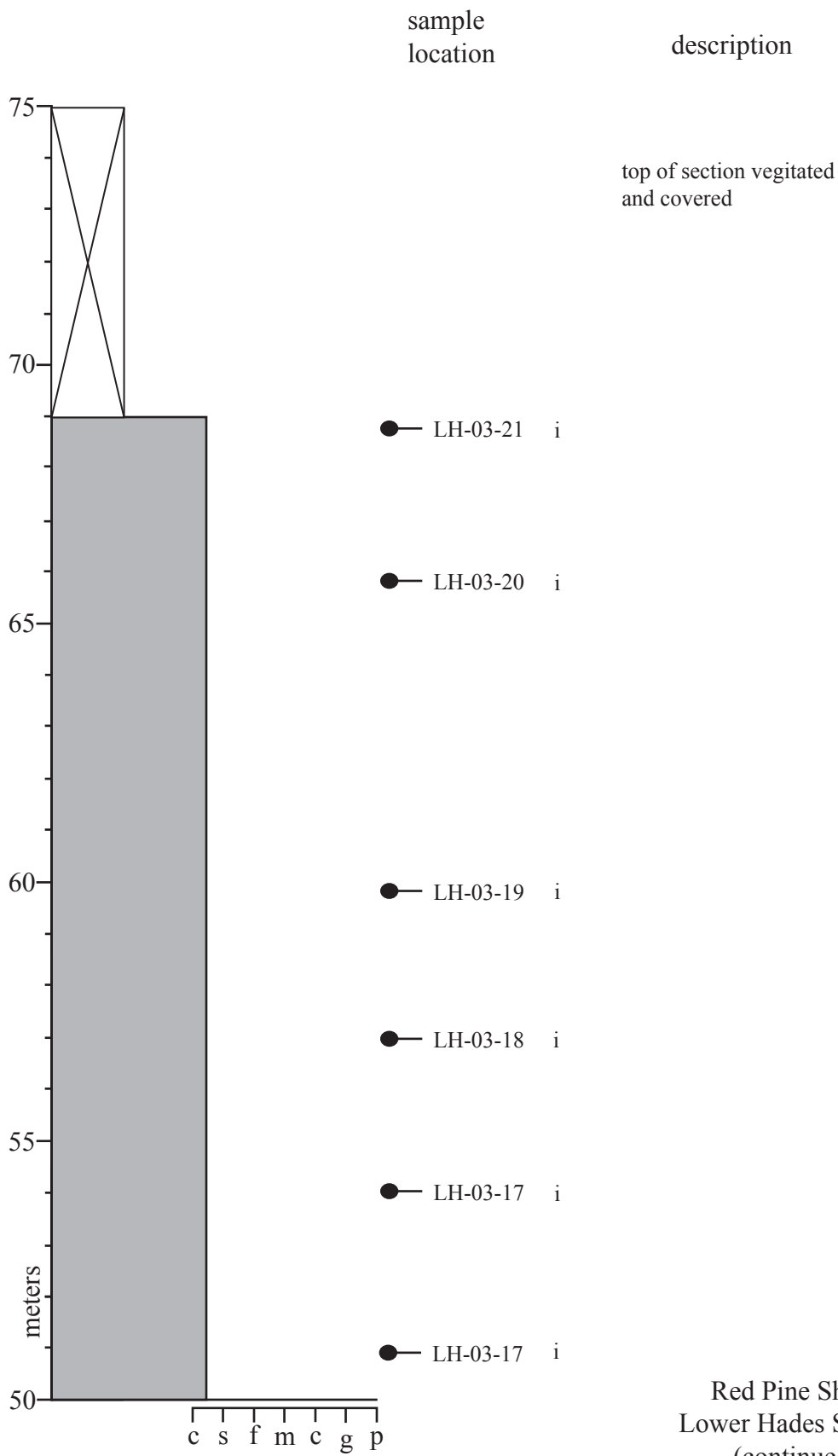
description



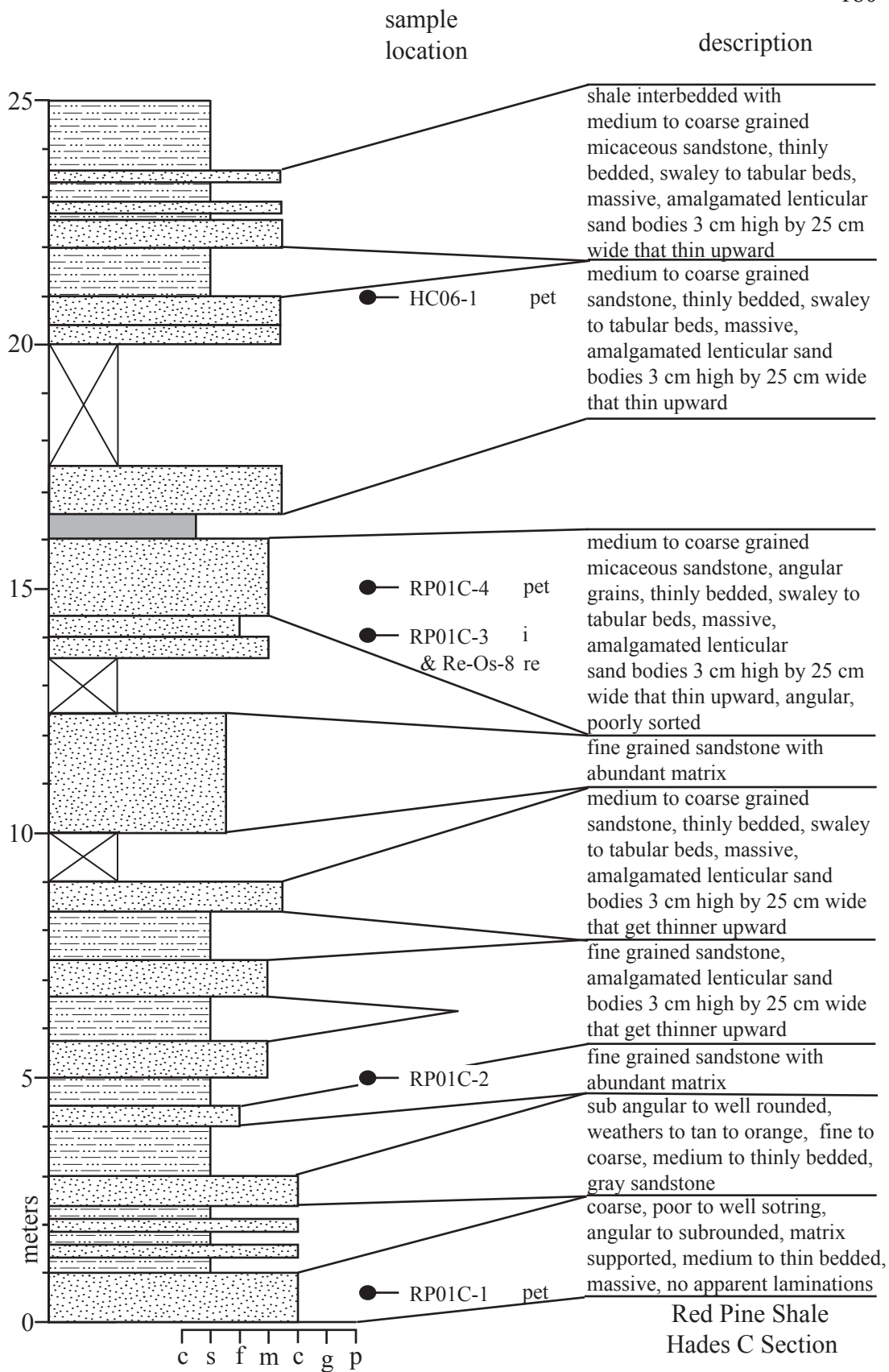
Red Pine Shale  
Hades Section B  
(continued)

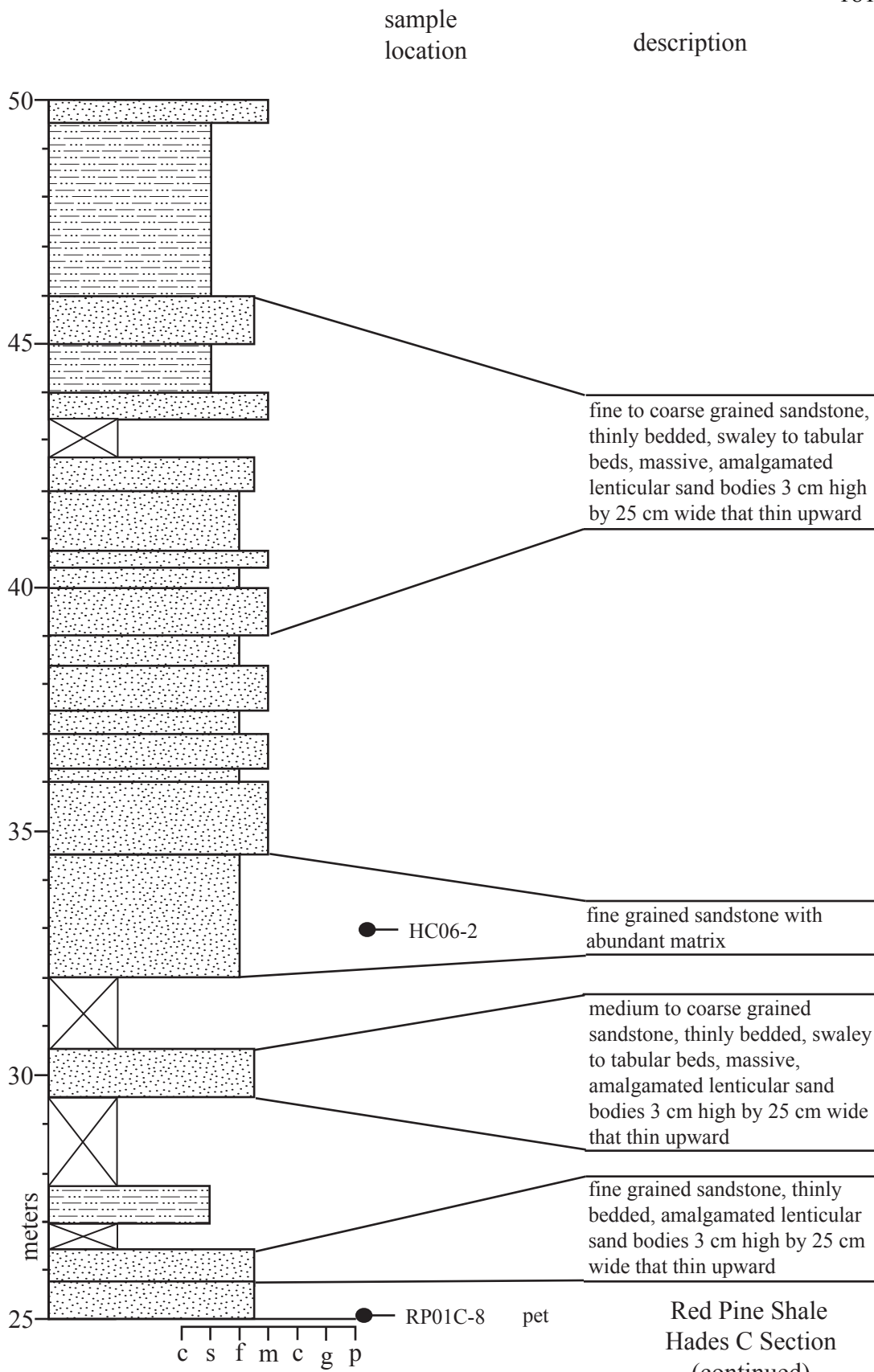




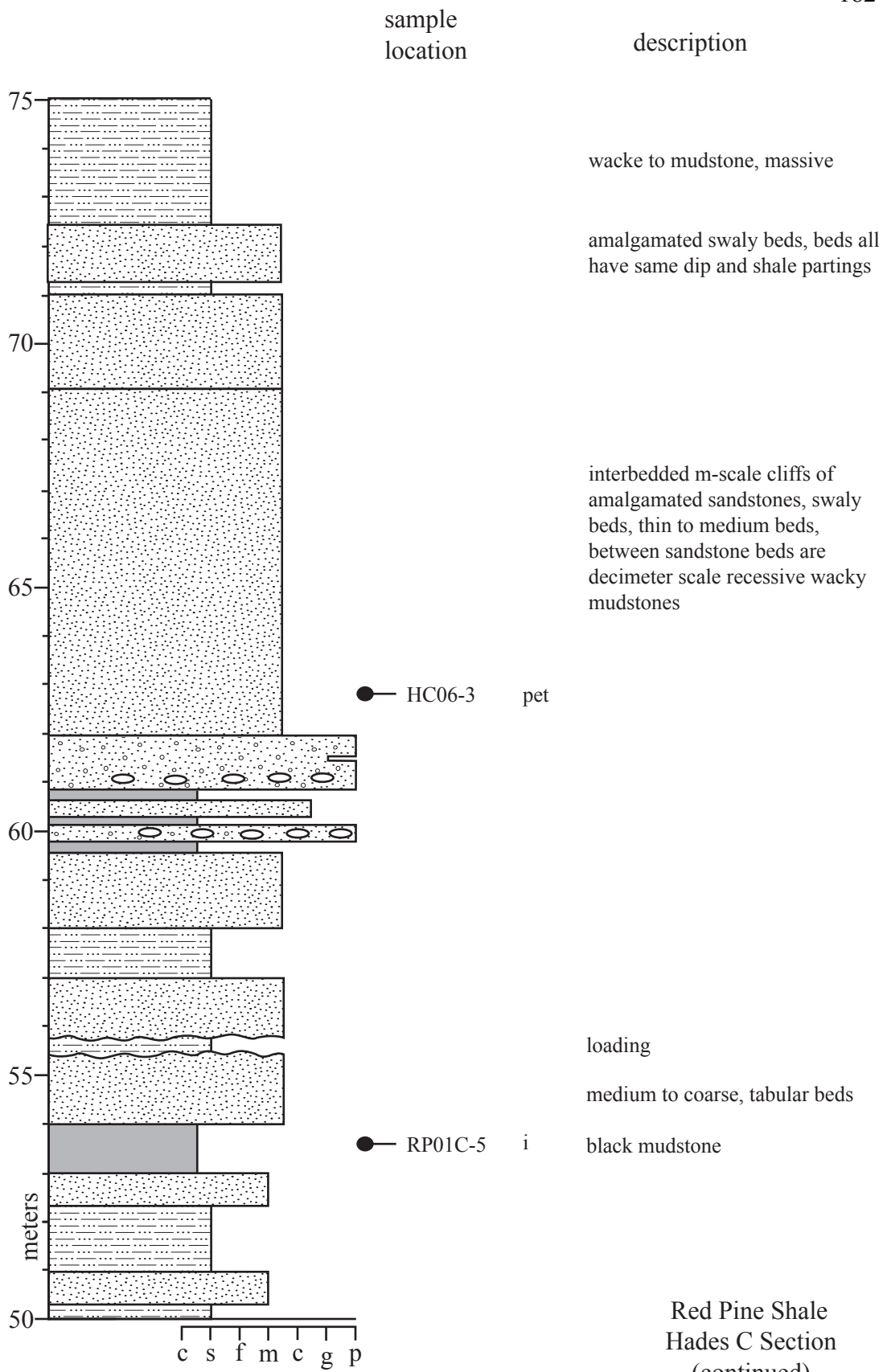


Red Pine Shale  
Lower Hades Section  
(continued)

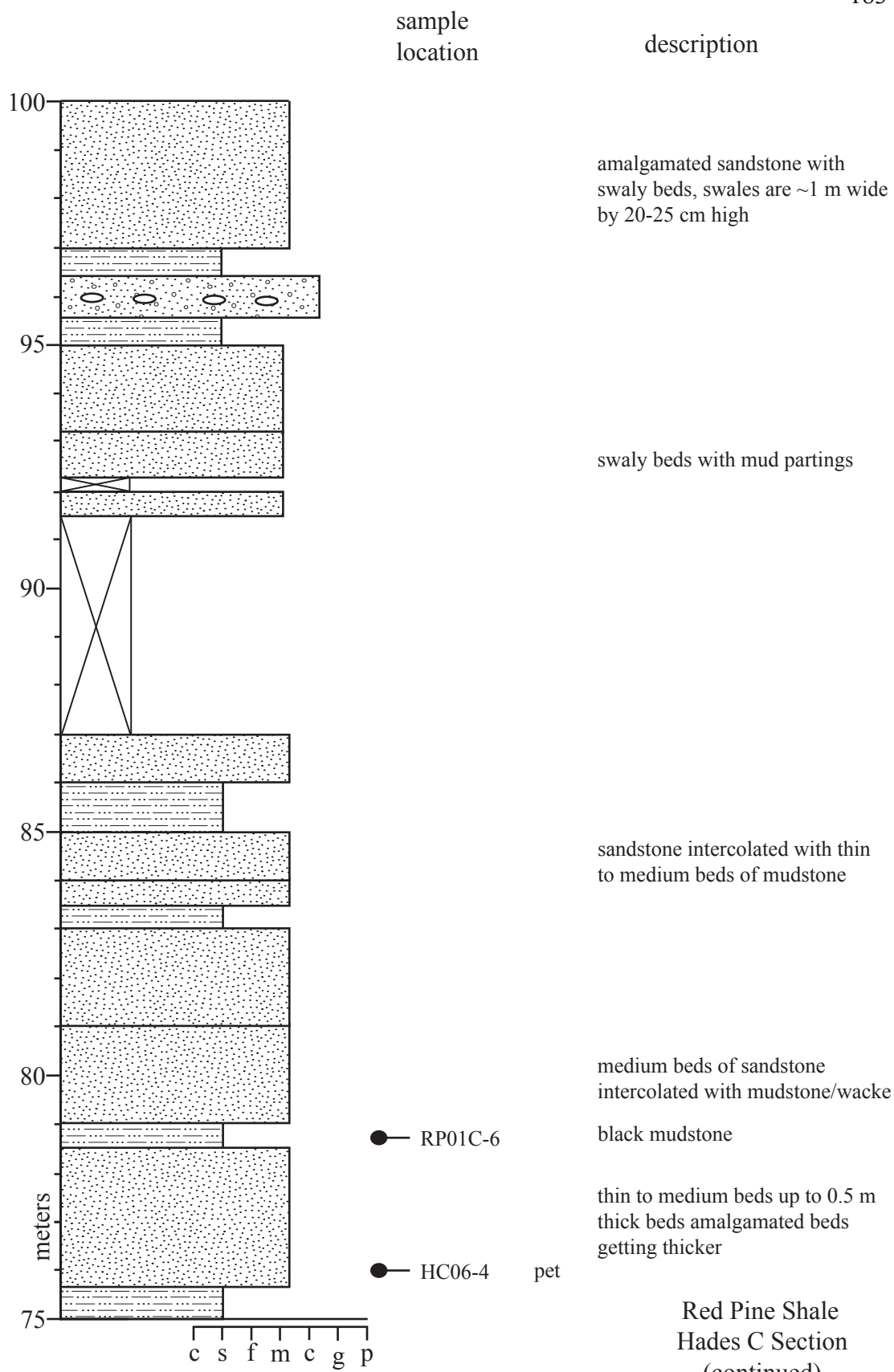






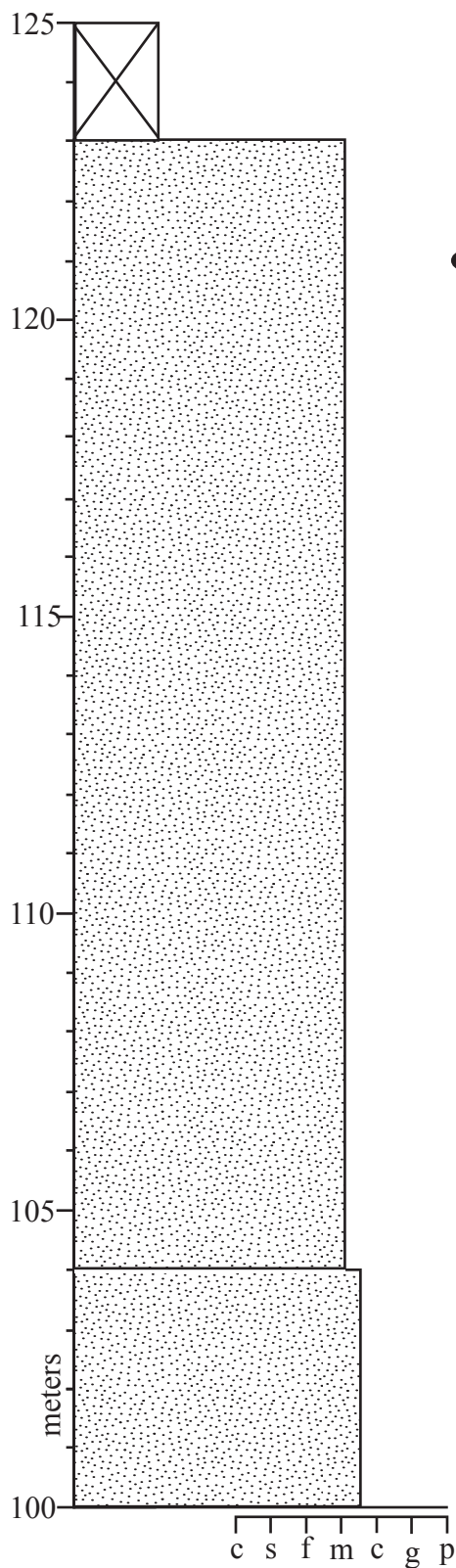


Red Pine Shale  
Hades C Section  
(continued)



sample  
location

description



fine to medium grained sandstone, micaceous, well sorted, thin recesses of mudstone/wacke, sampled mudstone and sandstone

● RP01C-7

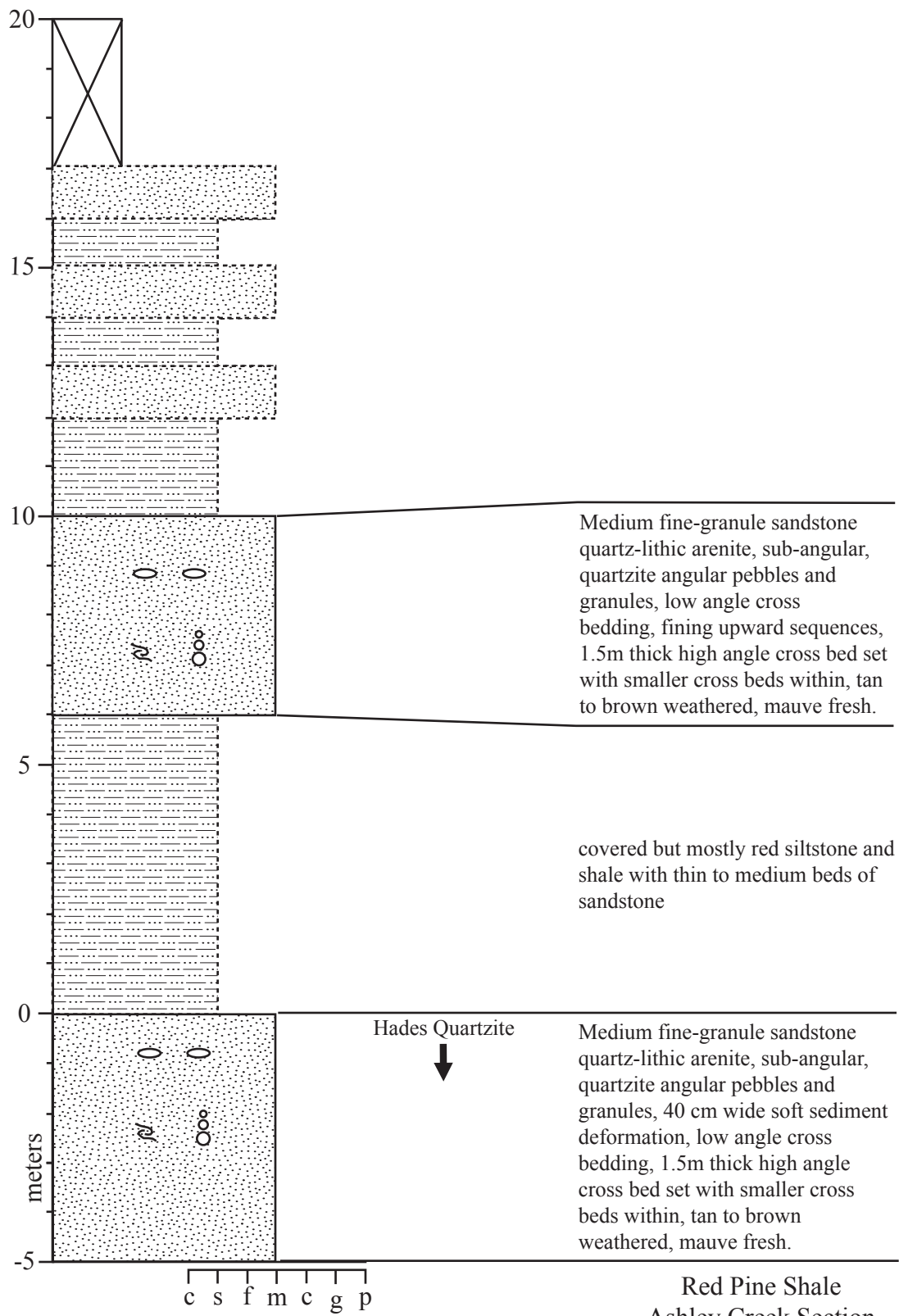
thin to medium swaly beds, 2-3m wide by 40 cm deep filled with amalgamated beds or hummocks

amalgamated sandstone with swaly beds, swales are ~1 m wide by 20-25 cm high

Red Pine Shale  
Hades C Section  
(continued)

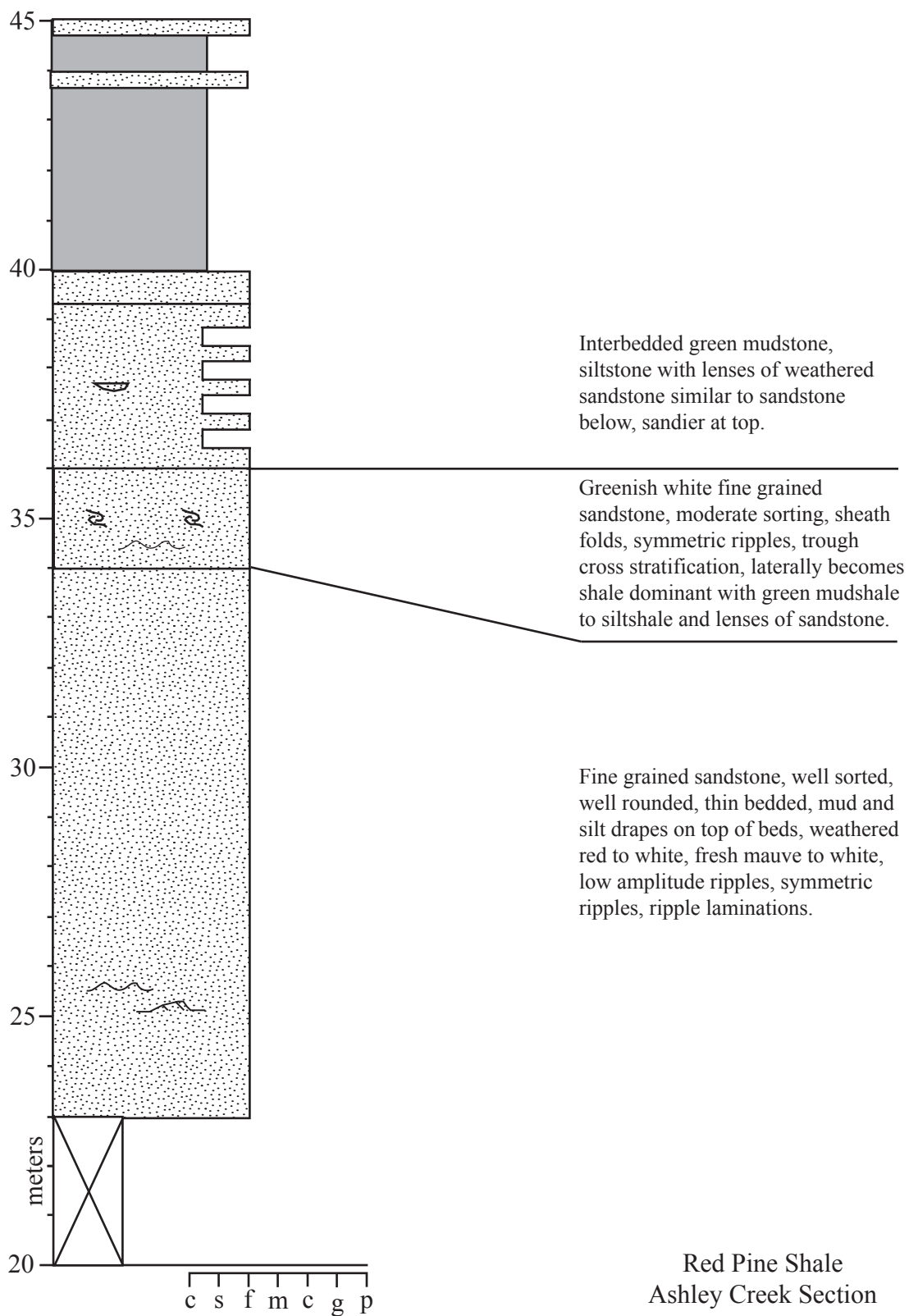
sample  
location

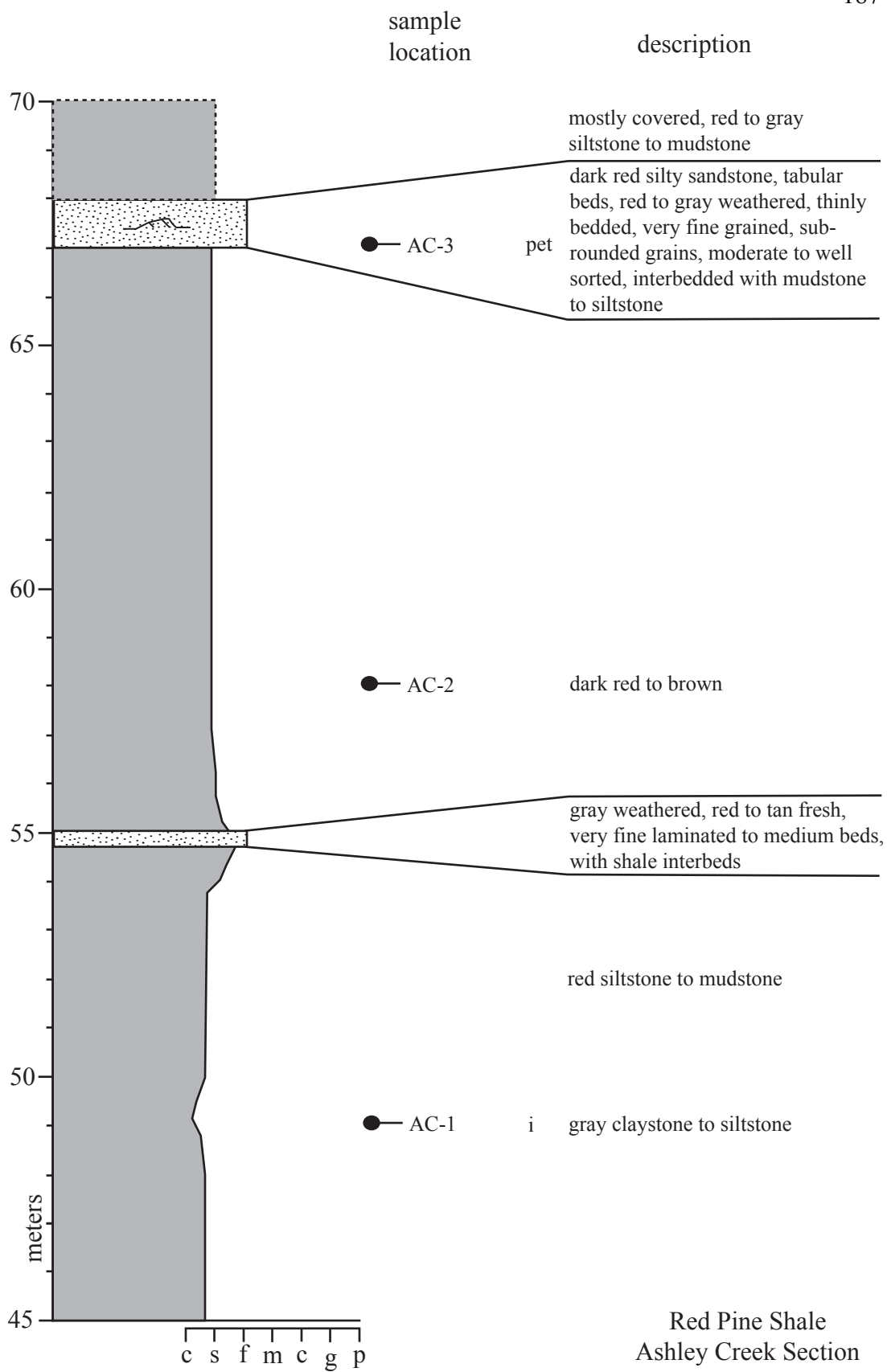
description



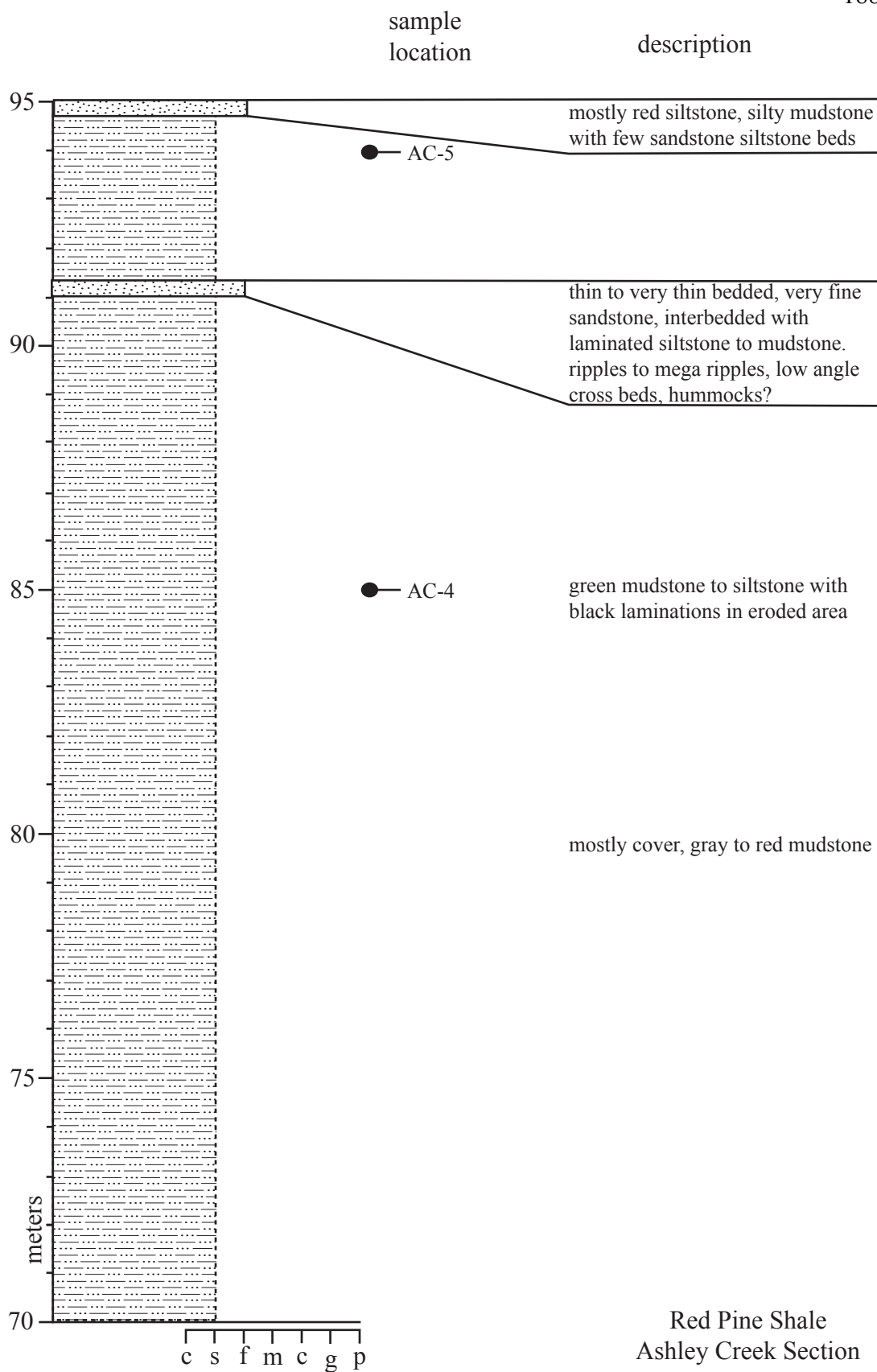
sample  
location

description

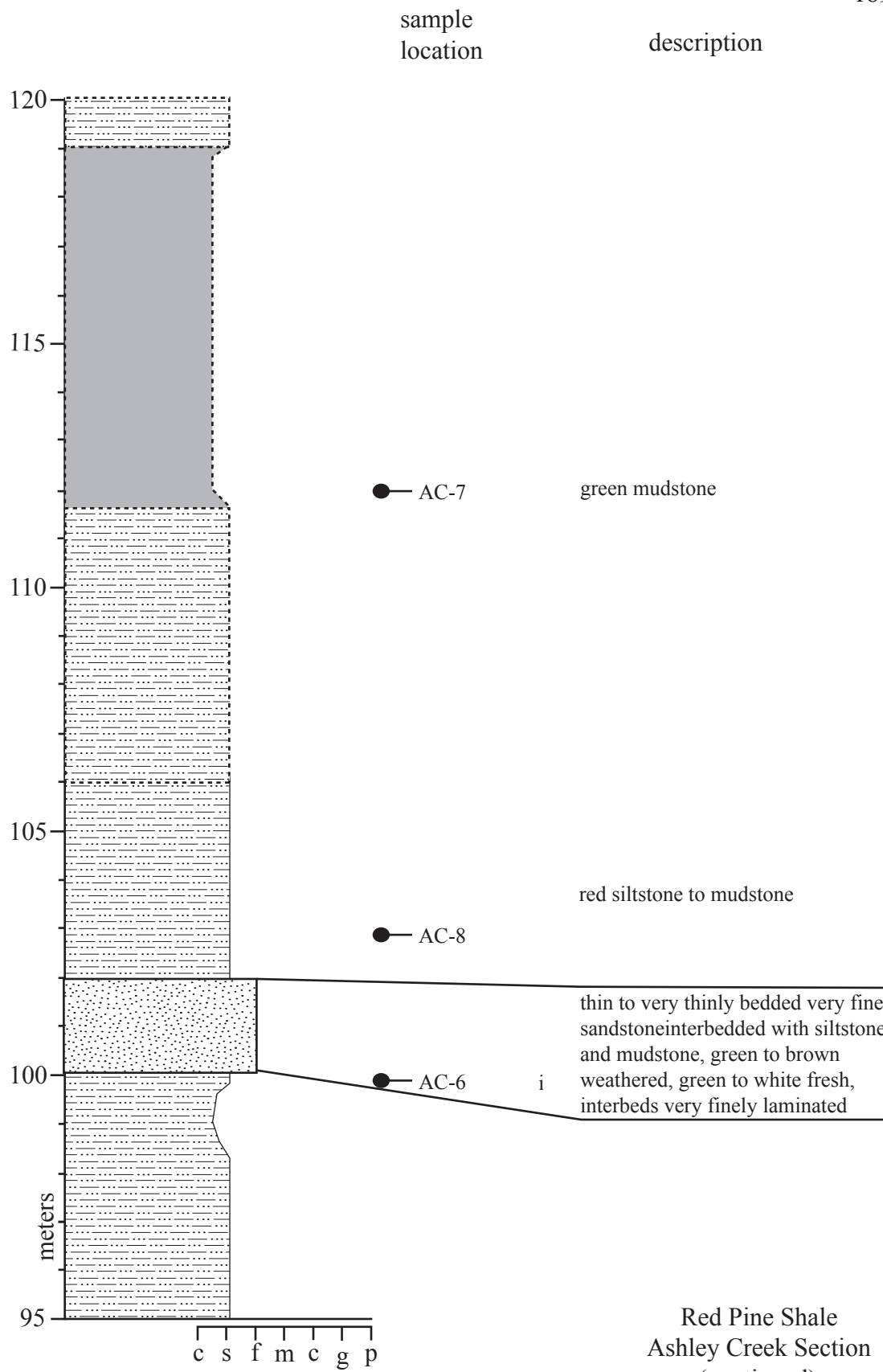




Red Pine Shale  
Ashley Creek Section  
(continued)



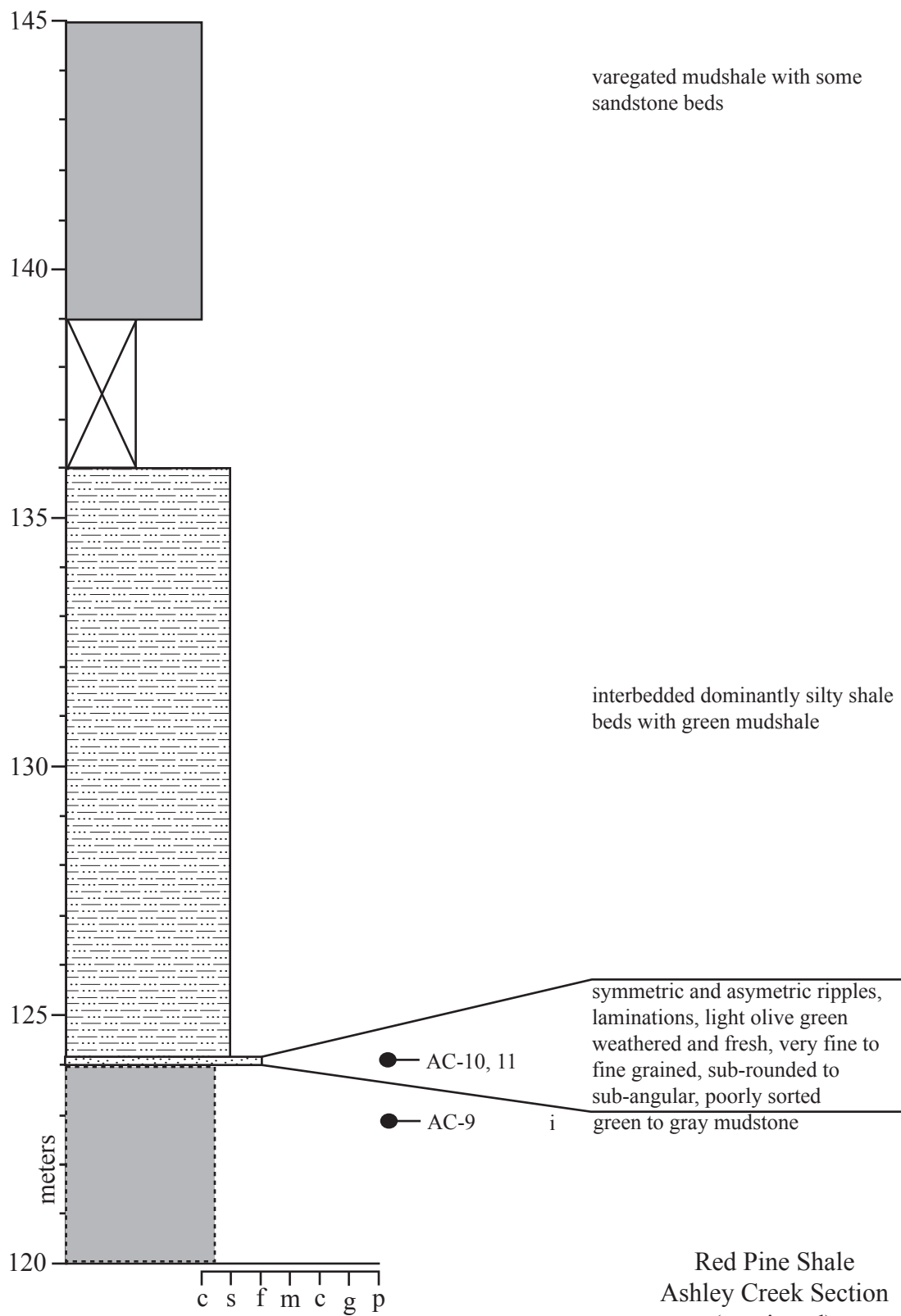
Red Pine Shale  
Ashley Creek Section  
(continued)



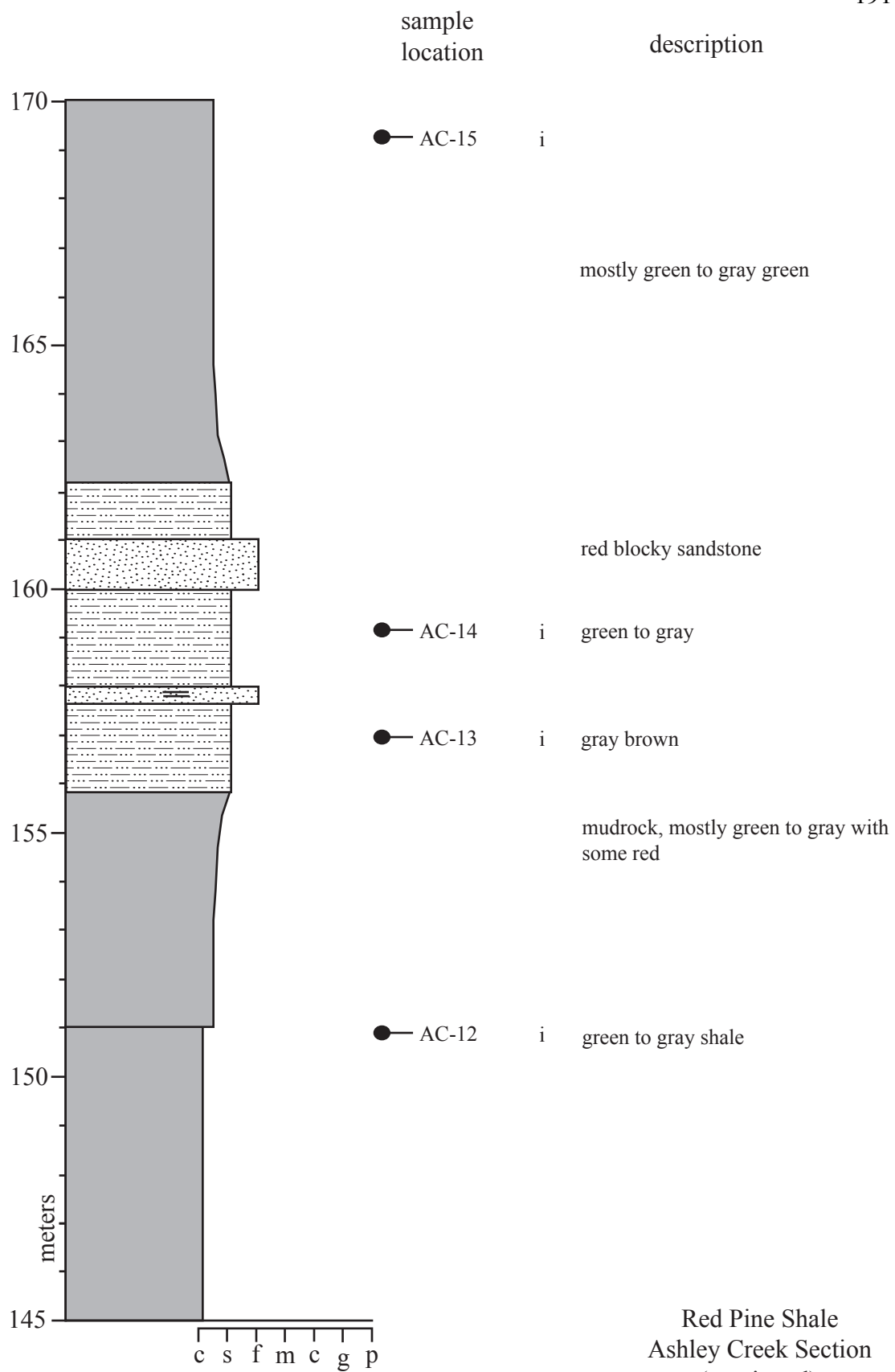


sample  
location

description

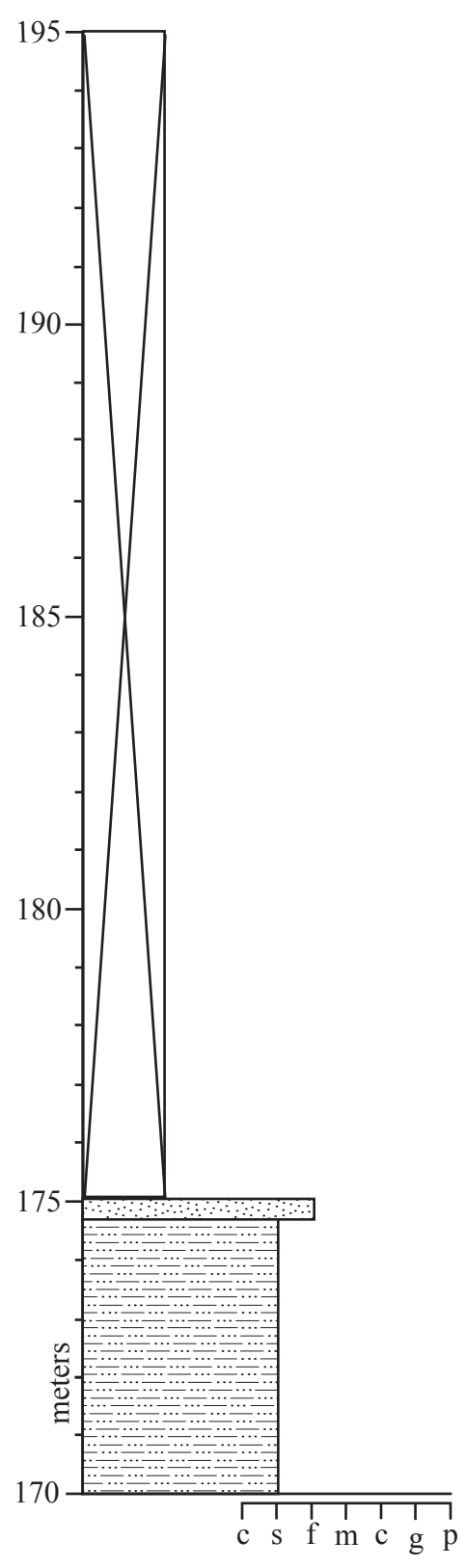


Red Pine Shale  
Ashley Creek Section  
(continued)



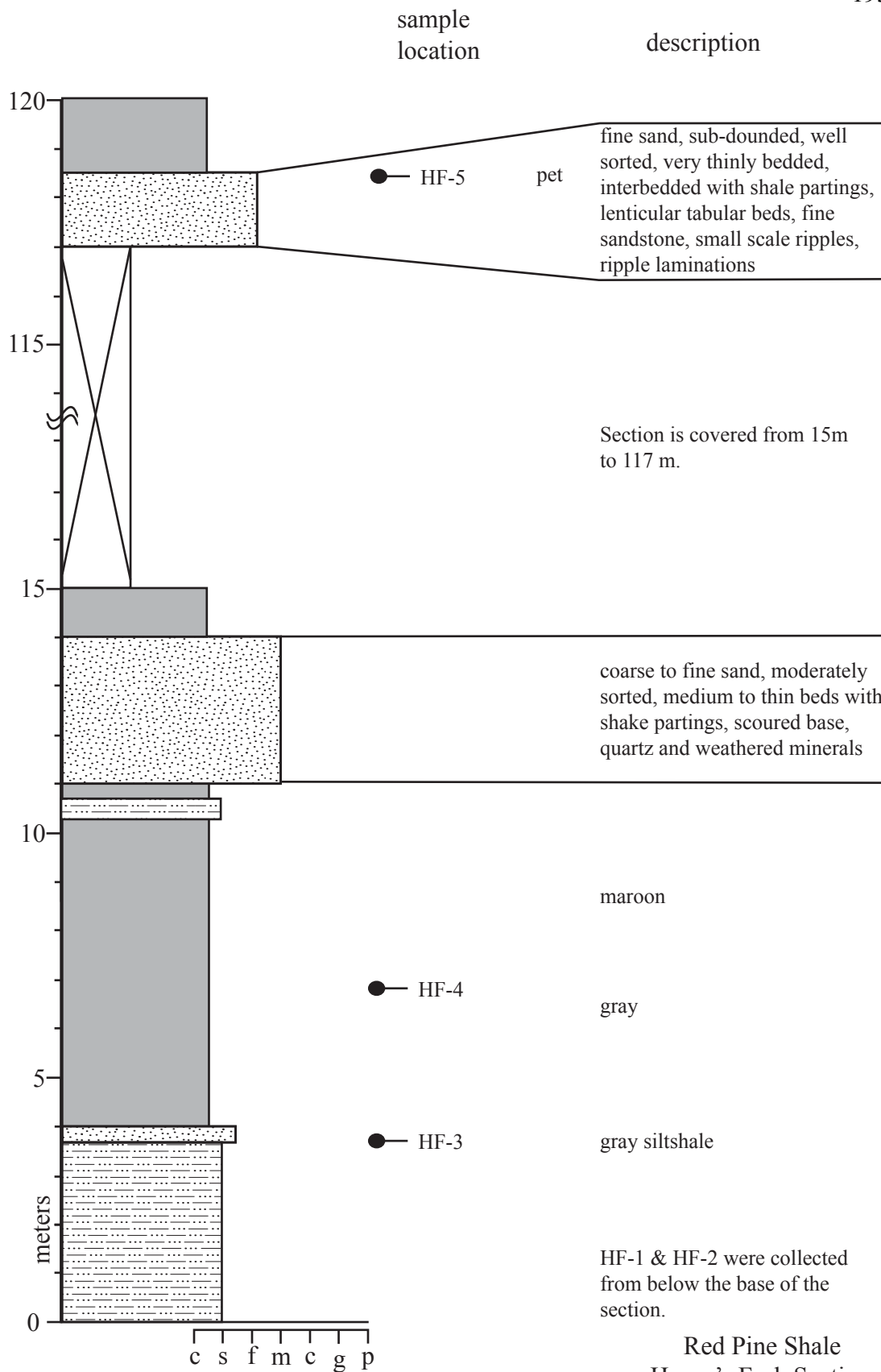
sample  
location

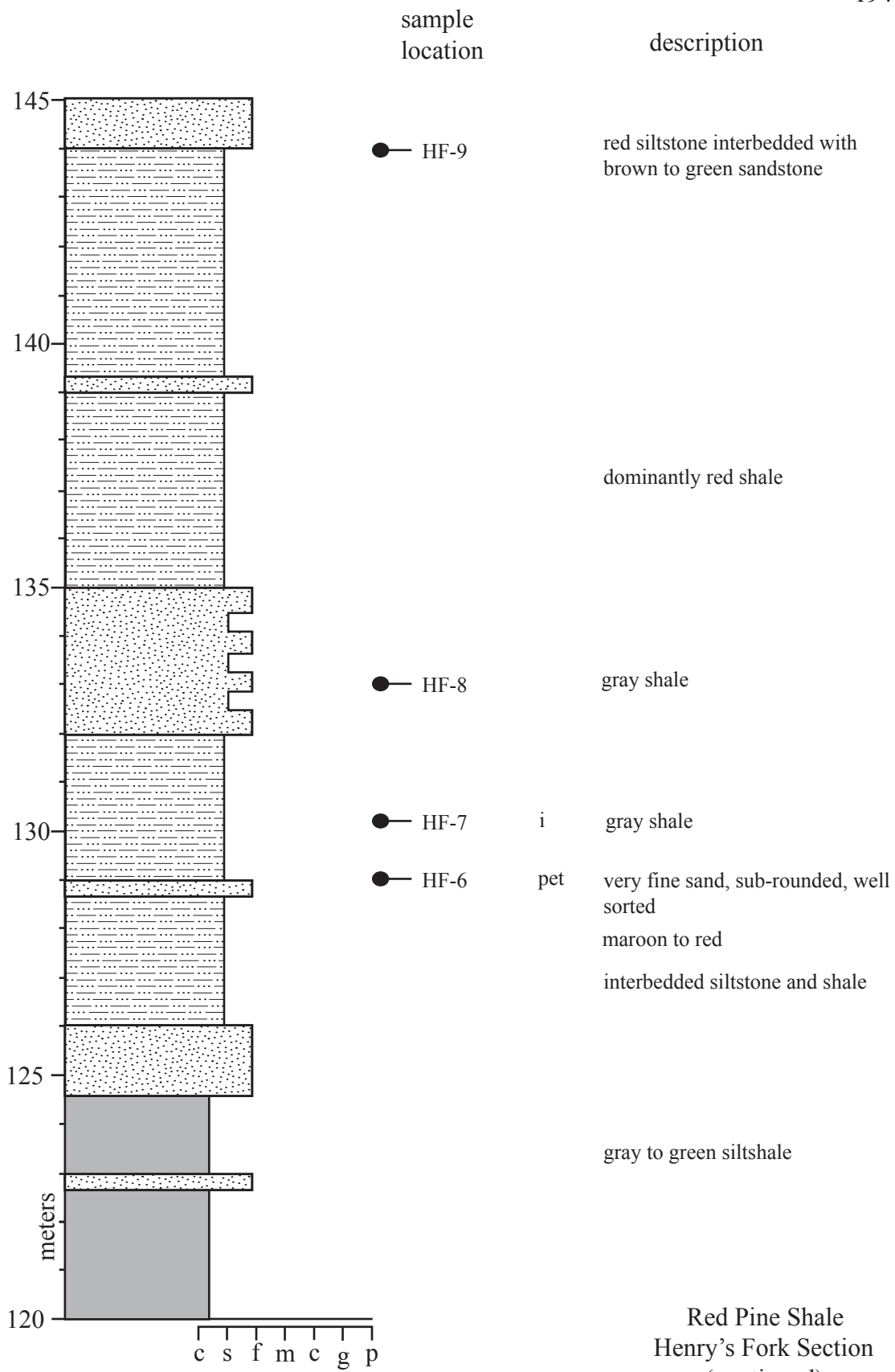
description

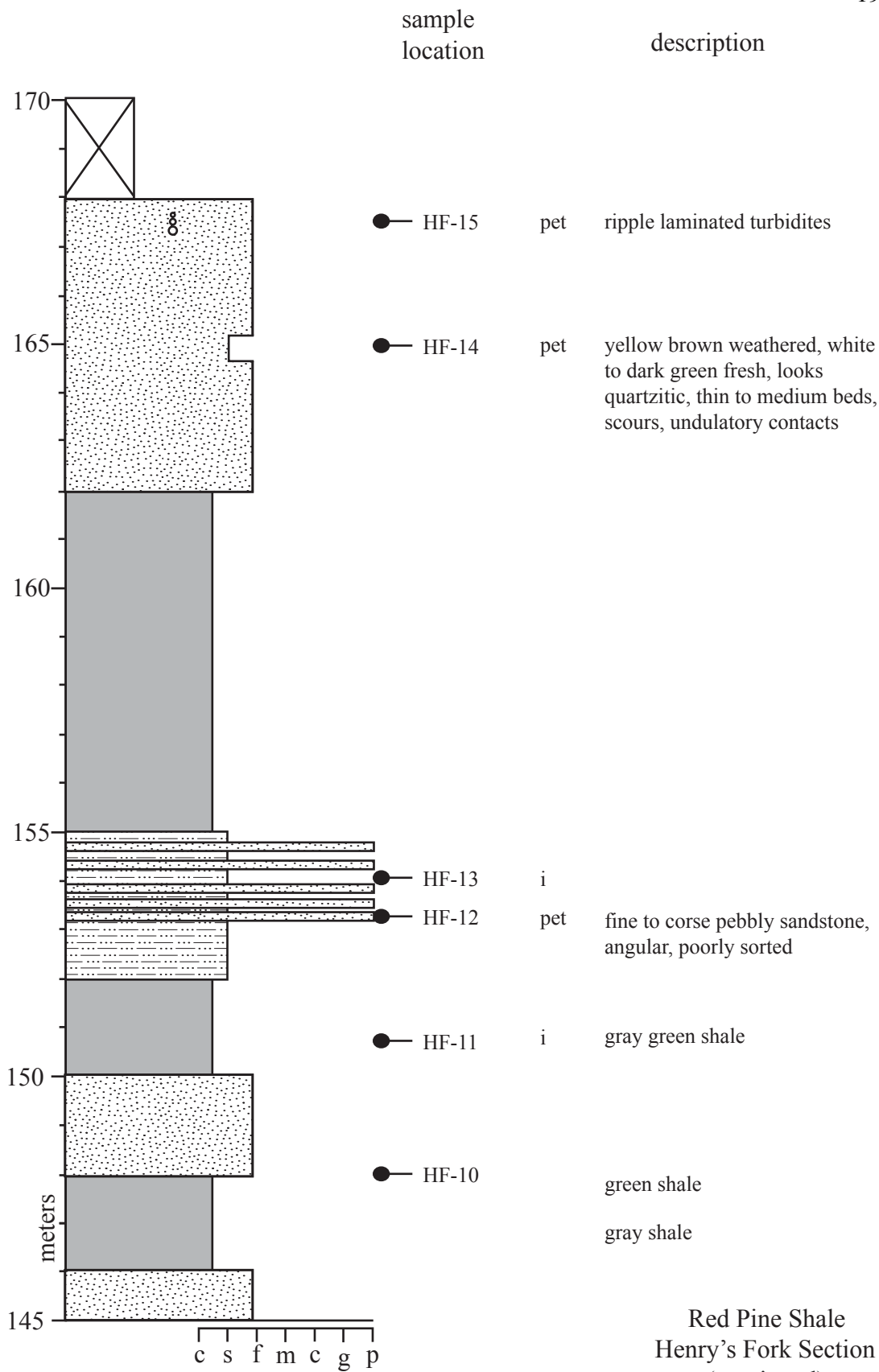


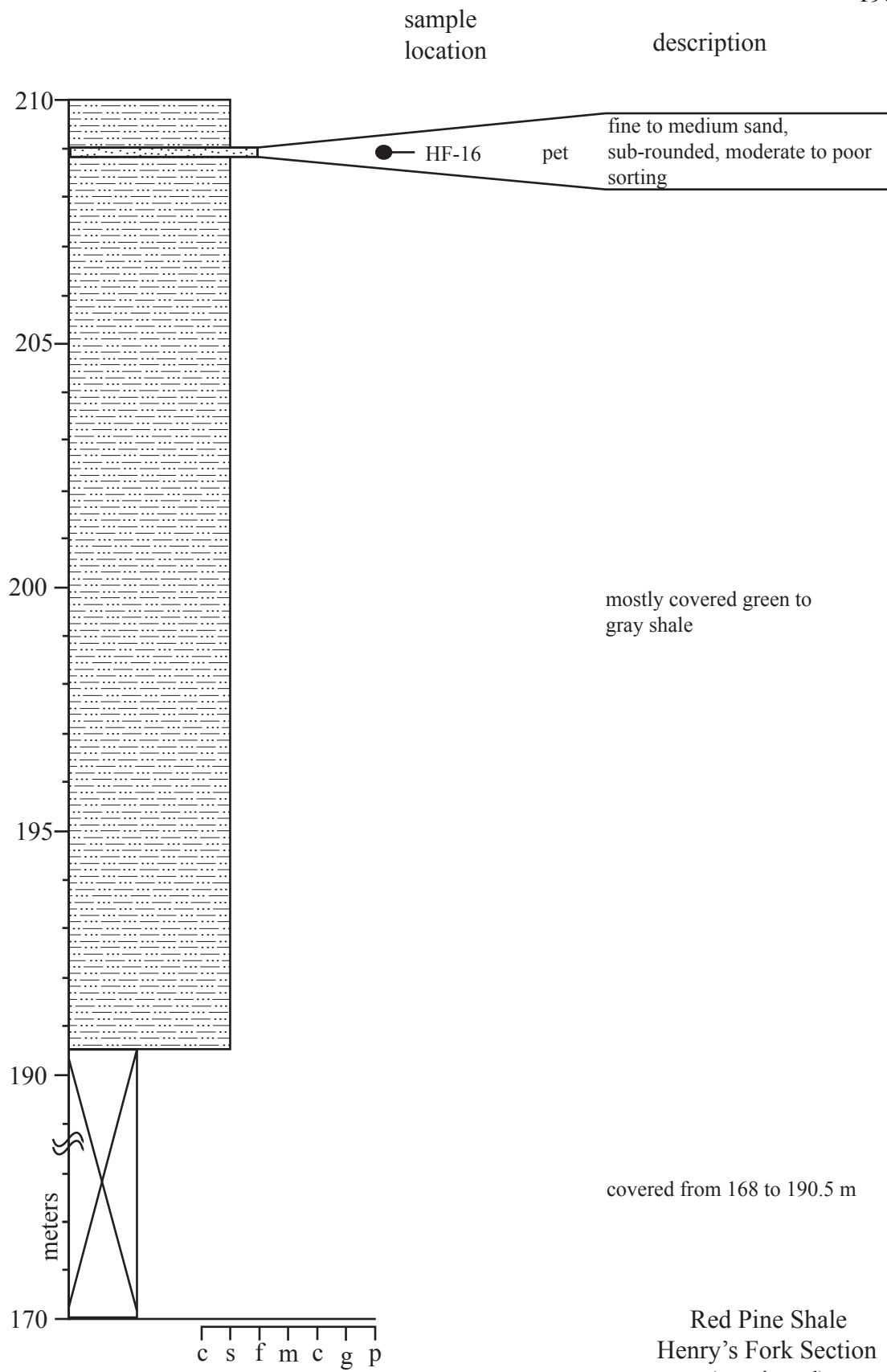
green to gray siltstone

Red Pine Shale  
Ashley Creek Section  
(continued)





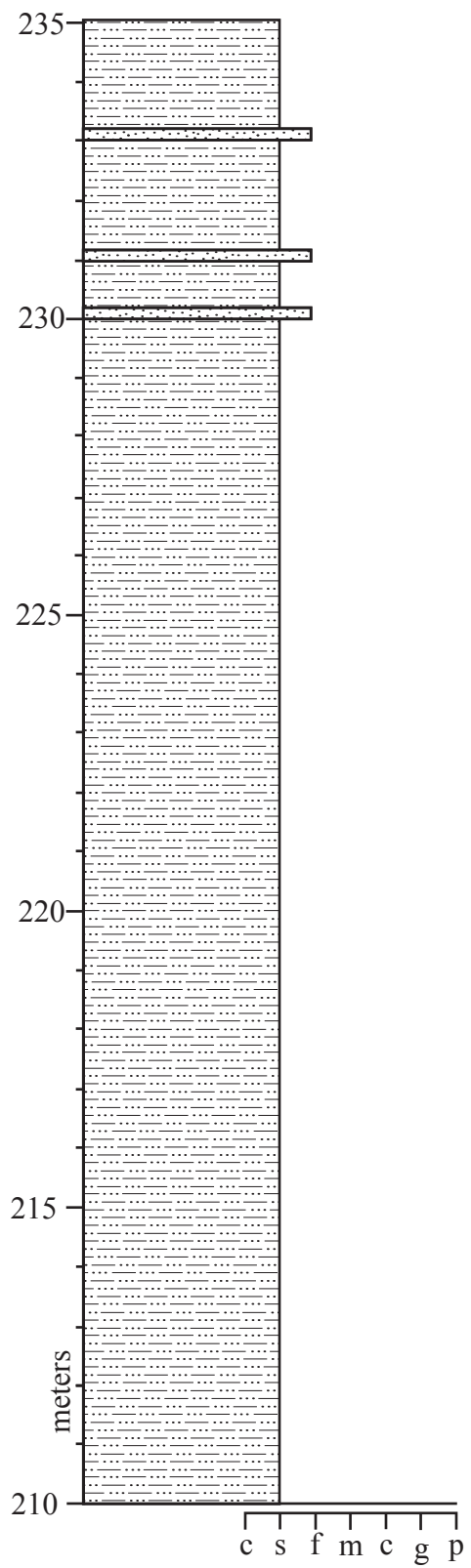




Red Pine Shale  
Henry's Fork Section  
(continued)

sample  
location

description



gray shale

gray shale

red shale

gray shale

gray to red shale

black to reddish shale

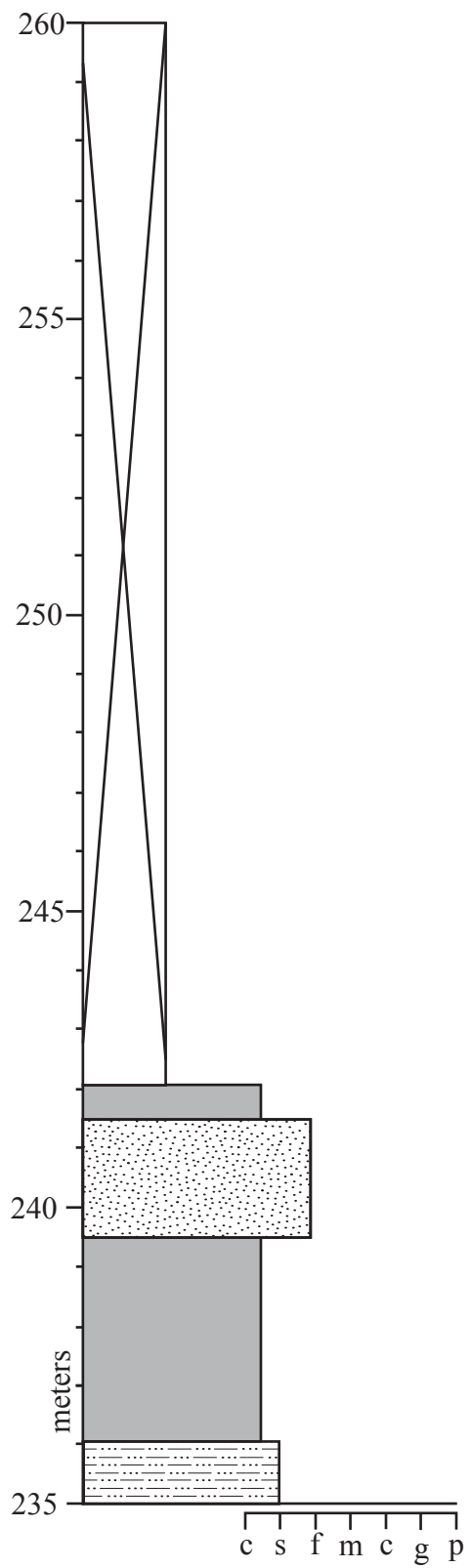
dark gray with some red shale

Red Pine Shale  
Henry's Fork Section  
(continued)



sample  
location

description



trail at 247.5 m

gray shale


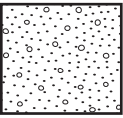

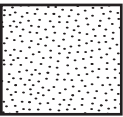

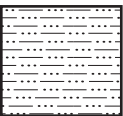















medium to thin beds, wavy  
contacts, massive

red shale

gray shale

Red Pine Shale  
Henry's Fork Section  
(continued)

## Key to measured sections

|                                                                                     |                                 |                                                                                     |                        |
|-------------------------------------------------------------------------------------|---------------------------------|-------------------------------------------------------------------------------------|------------------------|
|    | break in section                |   | sandstone with pebbles |
|    | sample location                 |   | sandstone              |
|    | acritarch                       |   | siltstone              |
|    | pebble                          |   | mudstone and claystone |
|    | laminations                     |  | covered section        |
|    | hummocky cross-stratification   |                                                                                     |                        |
|    | ripple cross-lamination         |                                                                                     |                        |
|    | asymmetric ripples              |                                                                                     |                        |
|    | symmetric ripples               |                                                                                     |                        |
|    | slump fold                      |                                                                                     |                        |
|    | concretion                      |                                                                                     |                        |
|  | fining upward sequence          |                                                                                     |                        |
|  | shale rip-ups                   |                                                                                     |                        |
|  | lens                            |                                                                                     |                        |
|  | channel                         |                                                                                     |                        |
|  | cut and fill                    |                                                                                     |                        |
| i                                                                                   | isotope and TOC sample          |                                                                                     |                        |
| i*                                                                                  | isotope sample but no TOC value |                                                                                     |                        |
| pet                                                                                 | petrography sample              |                                                                                     |                        |
| re                                                                                  | Re-O sample                     |                                                                                     |                        |
| paleo                                                                               | paleontology sample             |                                                                                     |                        |
| dz                                                                                  | detrital zircon sample          |                                                                                     |                        |
|                                                                                     |                                 | p                                                                                   | pebble sandstone       |
|                                                                                     |                                 | g                                                                                   | ganule sandstone       |
|                                                                                     |                                 | c                                                                                   | coarse sandstone       |
|                                                                                     |                                 | m                                                                                   | medium sandstone       |
|                                                                                     |                                 | f                                                                                   | fine sandstone         |
|                                                                                     |                                 | s                                                                                   | siltstone              |
|                                                                                     |                                 | c                                                                                   | claystone              |

## Appendix F: Measured section localities and descriptions

| Measured Section Localities and Descriptions |                                                                                                                                                                                                                                                                                                                                   |                                                                                                                                                                                                                                                                                                                                                                      |
|----------------------------------------------|-----------------------------------------------------------------------------------------------------------------------------------------------------------------------------------------------------------------------------------------------------------------------------------------------------------------------------------|----------------------------------------------------------------------------------------------------------------------------------------------------------------------------------------------------------------------------------------------------------------------------------------------------------------------------------------------------------------------|
| Section                                      | Location                                                                                                                                                                                                                                                                                                                          | Description                                                                                                                                                                                                                                                                                                                                                          |
| Type Section                                 | Located in northwestern part of the range along Red Pine Creek, a tributary to Smith and Moorehouse Creek (figs. 3a. and 4a.). The contact between the Red Pine Shale and the Hades Pass quartzite is UTM zone 12T 0490444 E, 4508422N in Red Pine Creek.                                                                         | Thickness: 662m ; The only measured section that exhibits all six facies; C-isotope range: -29.12‰ to -16.91‰ PDB; Average: -25.19‰ PDB; TOC range: 0.04% to 2.29%; Average: 0.46%; Complete section showing gradational basal contact with the Hades quartzite and erosional upper contact with the Mississippian Madison limestone; identified by Williams (1953). |
| Mud Lake Flat Road                           | Located in the northwestern part of range along Red Pine Creek, approximately 1mi. northeast on Mud Lake Flat Road from type section (figs. 3a. and 4a.) Section begins on road.                                                                                                                                                  | Thickness: 18.5 m; C-isotope range: -26.03‰ to -19.74‰ PDB; Average:-23.54‰ PDB. TOC range: 0.15% to 1.16 Average: 0.49%; partial section.                                                                                                                                                                                                                           |
| Hades A                                      | Located in the southwest part of range along Hades Creek, a tributary of north fork of the Duchesne River across from the USFS Hades campground and up National Forest Road 312 (figs. 3b. and 4b.). Section begins in the creek bed just west of "Hades Creek dam" on the north-facing slope at UTM zone 12T 0511871E, 4488004N. | Measured thickness: 290m; Facies present: shale, shale-and-sandstone, sandstone; C-isotope range: -29.46‰ to -23.90‰ PDB; Average: -26.52‰ PDB; TOC range: 3.7% to 0.1%; Average: 0.76%; base not exposed.                                                                                                                                                           |
| upper Hades                                  | Measured from the top of Hades A section to the Mississippian Madison limestone. The contact between Hades A and the upper Hades section is UTM zone 12T 0512276E, 4488166N and the upper contact of this section with the Madison limestone is UTM zone 12T 0513568E, 4488531N.                                                  | Thickness: 370m; Facies present: shale, shale-and-sandstone, sandstone; C-isotope range: -29.46‰ to -23.90‰ PDB; Average: -26.52‰ PDB; TOC range: 3.7% to 0.1%; Average: 0.76%; Erosional upper contact with Mississippian Madison limestone.                                                                                                                        |
|                                              |                                                                                                                                                                                                                                                                                                                                   | <i>continued</i>                                                                                                                                                                                                                                                                                                                                                     |

| Measured Section Localities and Descriptions ( <i>continued</i> ) |                                                                                                                                                                                                                                                                                                                                                       |                                                                                                                                                                                                               |
|-------------------------------------------------------------------|-------------------------------------------------------------------------------------------------------------------------------------------------------------------------------------------------------------------------------------------------------------------------------------------------------------------------------------------------------|---------------------------------------------------------------------------------------------------------------------------------------------------------------------------------------------------------------|
| Section                                                           | Location                                                                                                                                                                                                                                                                                                                                              | Description                                                                                                                                                                                                   |
| Hades B                                                           | Found by walking laterally southwest from the base of Hades A to the next exposed area of the Red Pine Shale. The base is ~70 m downstream from the "Hades dam" on the north-facing slope. Base of section is UTM zone 12T 0511795E, 4487901N in the creek bed. Top of section is UTM zone 12T 0511954E, 4487816N.                                    | Thickness: 104m; Facies present: shale, shale-and-sandstone, slump fold; C-isotope range: -24.65‰ to -27.10‰ PDB; Average: -25.84‰ PDB; TOC range: 0.29% to 0.06%; Average: 0.15%.; partial floating section. |
| Lower Hades                                                       | Located just downstream from Hades B at nose of the same ridge. Can be found by walking directly south from bend in National Forest road 312 and crossing Hades Creek. Section is measured from creek bed up the slope until Red Pine Shale is covered. Base of section is UTM zone 12T 0511442E, 487380N and top is UTM zone 12T 0511519E, 4487336N. | Thickness: 69m; Facies present: shale, shale-and-sandstone; C-isotope range: -23.99‰ to -24.87‰ PDB; Average: -24.38‰ PDB; TOC range: 0.54% to 0.20%; Average: 0.35%; partial floating section.               |
| Hades C                                                           | Located in the southwest part of the range west across the Duchesne River from Iron Mine Campground on unmarked road north of second switchback of National Forest high clearance road 180. Base of section is UTM zone 12T 05088220E, 4488240N.                                                                                                      | Thickness: 123m; Facies present: shale-and-sandstone, sandstone; C-isotope range: -27.37‰ to -29.26‰ PDB; Average: -28.21‰ PDB; TOC range: 5.91% to 1.33%; Average: 3.56%; partial floating section.          |
|                                                                   |                                                                                                                                                                                                                                                                                                                                                       | <i>continued</i>                                                                                                                                                                                              |

| Measured Section Localities and Descriptions ( <i>continued</i> ) |                                                                                                                                                                                                                |                                                                                                                                                                                                                                                                                                                                                                                                        |
|-------------------------------------------------------------------|----------------------------------------------------------------------------------------------------------------------------------------------------------------------------------------------------------------|--------------------------------------------------------------------------------------------------------------------------------------------------------------------------------------------------------------------------------------------------------------------------------------------------------------------------------------------------------------------------------------------------------|
| Section                                                           | Location                                                                                                                                                                                                       | Description                                                                                                                                                                                                                                                                                                                                                                                            |
| Ashley Creek                                                      | Located on south-central part of range on west side of Ashley Creek where Red Pine trail intersects Ashley Creek (figs 3c., and 4c.). Basal contact with Hades Pass quartzite is exposed near gauging station. | Measured thickness: 178.5m; Total thickness measured from Sprinkel (2002) geologic map: ~300m; Facies Present: shale, shale-and-sandstone, slump fold, sandstone; C-isotope range: -17.10‰ to -27.65‰ PDB; Average: -20.97‰ PDB; Sandstones are mostly very fine- to fine-grained well sorted and well to sub-rounded quartz arenite; measured from gradational contact with the Hades Pass quartzite. |
| Henry's Fork                                                      | Located on north flank of range and west side of Henry's Fork, ~0.75 mi up the trail that follows the creek (figs. 3d. and 4d.). The measured section begins in the creek bed.                                 | Measured thickness: 248m; Total thickness measured from Bryant (1995) geologic map: ~1800m; Facies present: shale, shale-and-sandstone, sandstone, pebbly sandstone; C-isotope range: 19.55‰ to -26.47‰ PDB; Average: -24.02‰ PDB; Sandstones are mostly fine- to medium-grained generally sub-rounded and well sorted quartz arenite; measured from gradational contact with Hades Pass quartzite.    |